Multicomponent Free Radical Polymerization Model Refinements and Extensions with Depropagation

by

David Dorschner

A thesis

presented to the University of Waterloo

in fulfillment of the

thesis requirement for the degree of

Master of Applied Science

in

Chemical Engineering

Waterloo, Ontario, Canada, 2010

Author's Declaration

I hereby declare that I am the sole author of this thesis. This is a true copy of the thesis, including any required final revisions, as accepted by my examiners.

I understand that my thesis may be made electronically available to the public.

David Dorschner

Abstract

This thesis is directed towards expanding and refining a free radical multi-component polymerization model. The model considers up to six monomers (unique in the literature), both in bulk and solution polymerization, for either batch or semi-batch reactor modes. As the simulator database contains 13 monomers, 5 initiators, 4 solvents, 3 chain transfer agents and 2 inhibitors, all tested over a wide range of polymerization conditions, from data in both academic and industrial laboratories, several hundred combinations of ingredients can be modeled. The many outputs generated by the model include conversion, molecular weight, polymer composition, branching indicators, sequence length, as well as many others polymerization characteristics related to both production rate and polymer quality. Although the only literature data found to-date contains a maximum of four monomers, model predictions for homo-, co-, ter- and tetra-polymerizations show reasonable agreement against the data at both regular and elevated temperatures. Recently, with the basic polymerization kinetics modeled sufficiently, several expansions to the simulation software have been added. Specifically, depropagation, multiple initiators, back-biting, and composition control have been incorporated and/or improved, each adding to the advancement of the polymerization simulation tool.

Depropagation is a vital mechanism that should be accounted for at elevated temperatures. Currently the software has the functionality to implement depropagation but requires further literature resources for improving the kinetic predictions for conversion and polymer composition. Consequently, depropagation research is ongoing.

Back-biting and beta-scission of butyl acrylate (BA) is a recent development in free radical polymerization. The completed extension can model BA under the same diverse conditions as the base model, in homo-, co- and ter-polymerizations with depropagation, if applicable.

The ability to generate a polymer with a constant (or controlled) composition throughout the reaction has several practical uses. Originally, three composition control scenarios were considered. At present, several methods as well as combinations of methods have been integrated into the model.

With these new expansions and the ability to simulate several initiators at the same time, this model is directed towards becoming a complete free radical polymerization tool for training and educational uses both in industry and academia.

Acknowledgements

My time in Waterloo has been wonderful. Not only have I completed another long-term goal but I've managed to gain many dear friends and fantastic memories in the process.

I would like to show gratitude to my wonderful supervisor, professor Penlidis, and to professor Duever for the patient support and encouragement they have given me over the past two years. They are incredible people and it was a privilege to work with them.

As patient and loving as ever, Irina Drehuta made the long-distance relationship seem effortless. What an amazing person she is and I am lucky to share so many magnificent years with her. I love you.

Finally, my absolute appreciation goes to my family. They have given me the motivation and determination to succeed in everything I do. I lead a blessed life because of you; thank you.

Dedication

To my mother and father, for the wonderful life they have given me.

Table of Contents

List of Figures x

List of Tables xxii

1. Introduction 1

1.1. Research Objectives 1

1.2. Outline 2

2. Polymerization Background Information 3

2.1. Reaction Kinetics 3

2.1.1. Initiation 3

2.1.2. Propagation 4

2.1.3. Termination 4

2.1.4. Chain Transfer to Small Molecules 5

2.1.5. Chain Transfer to Dead Polymer Chains 5

2.2. Assumptions Used for Model Development 7

2.3. Literature Review 8

2.3.1. Tetra-polymerization 8

2.3.2. Ter-polymerization 8

2.3.3. Co-polymerization 9

2.3.4. Homo-polymerization 14

3. Model Development and Features/Options 17

3.1. Reaction Balances 17

3.1.1. Monomer Balances 17

3.1.2. Radical Balances 17

3.1.3. Volume Shrinkage 18

3.1.4. Polymer Balances 18

3.1.5. Additional Balances 18

3.2. Additional Modeling Considerations 20
3.2.1. Initiation 20
3.2.2. Propagation 21
3.2.3. Termination 24
3.2.4. Chain Transfer Reactions 24
3.2.5. Depropagation 25
3.2.6. Diffusion-Control Kinetics 28
3.2.7. Backbiting and β-Scission of Butyl Acrylate 31
3.3. Reaction Outputs 37
3.3.1. Conversion 37
3.3.2. Polymer Composition 37
3.3.3. Molecular Weight and Branching 38
3.3.4. Sequence Length 39
3.3.5. Dyad/Triad Fractions 39
3.3.6. Extension to Pentad Fractions 40
3.4. Model Features/Options 42
3.5. Database Characteristics 43
4. Model Testing/Troubleshooting 45
4.1. Homo-polymerization of Ethyl Acrylate 46
4.2. Homo-polymerization of Butyl Methacrylate 48
4.3. Co-Polymerization of Styrene and Ethyl Acrylate 50
4.4. Co-Polymerization of Methyl Methacrylate and Butyl Acrylate 53
4.5. Co-polymerization of Styrene and Acrylonitrile 69
4.6. Co-polymerization of Methyl Methacrylate and Methyl Acrylate 71
4.7. Co-polymerization of Alpha Methyl Styrene and Methyl Methacrylate 73
5. Model Extensions/Refinements and Case Studies 75
5.1. Depropagation 75

5.1.1. Case Study 1: Homo-polymerization of Butyl Methacrylate....77
5.1.2. Case Study 2: Co-polymerization of Alpha Methyl Styrene and Styrene....82
5.1.3. Case Study 3: Co-polymerization of AMS and MMA....85
5.1.4. Case Study 4: Co-polymerization of Styrene and Glycidyl Methacrylate....94
5.1.5. Case Study 5: Ter-polymerization of AMS, MMA and BA....101
5.1.6. Case Study 6: Hexa-polymerization – Simulation Trends....104
5.2. Backbiting of Butyl Acrylate....121
5.2.1 Case Study 7: Homo-polymerization of Butyl Acrylate....128
5.2.2 Case Study 8: Co-polymerization of Butyl Acrylate and Butyl Methacrylate.132
5.2.3 Case Study 9: Co-polymerization of Styrene and Butyl Acrylate....136
5.2.4 Case Study 10: Ter-polymerization of Styrene, BMA and BA....142
5.3. Multiple Initiator Functionality....147
6. Composition Control....159
6.1. Policy 1....165
6.2. Policy 2....171
6.3. Policy 3....178
6.4. Combinations of Policies....182
6.5. Extensions to Multivariable Cases....190
6.6. Additional Considerations/Remarks....196
6.7. Practical Implementations....207
6.7.1. Modified Policy 1....207
6.7.2. Modified Policy 2....209
6.7.3. General Policy Considerations....210
6.7.4. Monomer Flowrate Constraints....212
7. Conclusions and Future Steps....219
References....221
Appendices....237

Appendix I. Implementing Initiation in a Simulation Model....237
Appendix II. Initiator Database....240
Appendix III. Monomer Database....243
Appendix IV. Chain Transfer Agent and Solvent Databases....257
Appendix V. Alternative Solution for Composition Control Policy 2....260
Appendix VI. User Manual Excerpt and Overall Summary....261

List of Figures

Figure 1.1: Simulation process for the hexa-polymerization model....1
Figure 3.1: Ter-polymerizations of Sty/BA/BMA by Li and Hutchinson (2007)....22
Figure 3.2: Simulation of the co-polymerizations of Sty/GMA at 100°C....23
Figure 3.3: Simulation of the co-polymerizations of Sty/GMA at 95°C....23
Figure 3.4: Simulation of the co-polymerization of MMA/BA T = 90°C $[dTBPO]_0$ = 0.045M f_{BA0} = 0.148 with T_{gpij} = 77°C....30
Figure 3.5: Simulation of the co-polymerization of MMA/BA T = 90°C $[dTBPO]_0$ = 0.045M f_{BA0} = 0.148 with T_{gpij} = 69°C....30
Figure 3.6: Backbiting of Butyl Acrylate....31
Figure 3.7: Concentration of midchain radicals over a range of temperatures....32
Figure 3.8: Simulation of the co-polymerization of Sty/AN at 60°C $[AIBN]_0$ = 0.05 M....41
Figure 4.1: Simulation of the batch homo-polymerization of EA $[AIBN]_0$ = 0.0008 M using Gao and Penlidis rate constant....47
Figure 4.2: Simulation of the batch homo-polymerization of EA $[AIBN]_0$ = 0.0008 M using Van Herk rate constant....47
Figure 4.3: Simulation of the homo-polymerization of BMA T = 60°C pre-correction....48
Figure 4.4: Simulation of the homo-polymerization of BMA T = 60°C post-correction....49
Figure 4.5: Simulation of the co-polymerization of Sty/EA T = 70°C $[BPO]_0$ = 0.045M....50
Figure 4.6: Simulation of the co-polymerization of Sty/EA T = 70°C $[BPO]_0$ = 0.045M....51
Figure 4.7: Simulation of the co-polymerization of Sty/EA T = 70°C $[BPO]_0$ = 0.045M f_{Sty0} = 0.1668....51
Figure 4.8: Simulation of the co-polymerization of Sty/EA T = 70°C $[BPO]_0$ = 0.047M f_{Sty0} = 0.548....52
Figure 4.9: Simulation of the co-polymerization of MMA/BA T = 90°C $[dTBPO]_0$ = 0.044M toluene = 30wt% f_{MMA0} = 0.852....55
Figure 4.10: Simulation of the co-polymerization of MMA/BA T = 90°C $[dTBPO]_0$ = 0.045M toluene = 30wt% f_{MMA0} = 0.561....55
Figure 4.11: Simulation of the co-polymerization of MMA/BA T = 90°C $[dTBPO]_0$ = 0.045M toluene = 23wt% f_{MMA0} = 0.851....56
Figure 4.12: Simulation of the co-polymerization of MMA/BA T = 90°C $[dTBPO]_0$ = 0.045M toluene = 23wt% f_{MMA0} = 0.561....56
Figure 4.13: Simulation of the co-polymerization of MMA/BA T = 90°C $[dTBPO]_0$ = 0.045M toluene = 0wt% f_{MMA0} = 0.852....57

Figure 4.14: Simulation of the co-polymerization of MMA/BA T = 115°C $[dTBPO]_0$ = 0.0062M toluene = 30wt% f_{MMA0} = 0.852 57
Figure 4.15: Simulation of the co-polymerization of MMA/BA T = 115°C $[dTBPO]_0$ = 0.045M toluene = 30wt% f_{MMA0} = 0.852 58
Figure 4.16: Simulation of the co-polymerization of MMA/BA T = 115°C $[dTBPO]_0$ = 0.0058M toluene = 23wt% f_{MMA0} = 0.852 58
Figure 4.17: Simulation of the co-polymerization of MMA/BA T = 115°C $[dTBPO]_0$ = 0.0063M toluene = 0wt% f_{MMA0} = 0.561 59
Figure 4.18: Simulation of the co-polymerization of MMA/BA T = 140°C $[dTBPO]_0$ = 0.0005M toluene = 30wt% f_{MMA0} = 0.852 59
Figure 4.19: Simulation of the co-polymerization of MMA/BA T = 140°C $[dTBPO]_0$ = 0.00049M toluene = 0wt% f_{MMA0} = 0.852.....60
Figure 4.20: Simulation of the co-polymerization of MMA/BA T = 140°C $[dTBPO]_0$ = 0.00012M toluene = 0wt% f_{MMA0} = 0.852.....60
Figure 4.21: Simulation of the co-polymerization of MMA/BA T = 90°C $[dTBPO]_0$ = 0.045M toluene = 30wt% f_{MMA0} = 0.852 61
Figure 4.22: Simulation of the co-polymerization of MMA/BA T = 90°C $[dTBPO]_0$ = 0.045M toluene = 30wt% f_{MMA0} = 0.561 61
Figure 4.23: Simulation of the co-polymerization of MMA/BA T = 90°C $[dTBPO]_0$ = 0.045M toluene = 23wt% f_{MMA0} = 0.851 62
Figure 4.24: Simulation of the co-polymerization of MMA/BA T = 90°C $[dTBPO]_0$ = 0.045M toluene = 23wt% f_{MMA0} = 0.561 62
Figure 4.25: Simulation of the co-polymerization of MMA/BA T = 90°C $[dTBPO]_0$ = 0.047M toluene = 0wt% f_{MMA0} = 0.852 63
Figure 4.26: Simulation of the co-polymerization of MMA/BA T = 90°C $[dTBPO]_0$ = 0.046M toluene = 0wt% f_{MMA0} = 0.745 63
Figure 4.27: Simulation of the co-polymerization of MMA/BA T = 115°C $[dTBPO]_0$ = 0.0062M toluene = 30wt% f_{MMA0} = 0.852 64
Figure 4.28: Simulation of the co-polymerization of MMA/BA T = 115°C $[dTBPO]_0$ = 0.045M toluene = 30wt% f_{MMA0} = 0.851 64
Figure 4.29: Simulation of the co-polymerization of MMA/BA T = 115°C $[dTBPO]_0$ = 0.0058M toluene = 23wt% f_{MMA0} = 0.852 65
Figure 4.30: Simulation of the co-polymerization of MMA/BA T = 115°C $[dTBPO]_0$ = 0.0063M toluene = 0wt% f_{MMA0} = 0.561 65
Figure 4.31: Simulation of the co-polymerization of MMA/BA T = 140°C $[dTBPO]_0$ = 0.00047M toluene = 30wt% f_{MMA0} = 0.852.....66

Figure 4.32: Simulation of the co-polymerization of MMA/BA T = 140°C $[dTBPO]_0$ = 0.00049M toluene = 0wt% f_{MMA0} = 0.852 66
Figure 4.33: Simulation of the co-polymerization of MMA/BA T = 140°C $[dTBPO]_0$ = 0.00045M toluene = 0wt% f_{MMA0} = 0.745 67
Figure 4.34: Simulation of the co-polymerization of MMA/BA T = 90°C $[dTBPO]_0$ = 0.045M toluene = 30wt% f_{MMA0} = 0.852 67
Figure 4.35: Simulation of the co-polymerization of MMA/BA T = 90°C $[dTBPO]_0$ = 0.045M toluene = 23wt% f_{MMA0} = 0.561 68
Figure 4.36: Simulation of the co-polymerization of MMA/BA T = 90°C $[dTBPO]_0$ = 0.046M toluene = 0wt% f_{MMA0} = 0.745 68
Figure 4.37: Simulation of the batch co-polymerization of Sty/AN T = 60°C 69
Figure 4.38: Simulation of the batch co-polymerization of Sty/AN T = 60°C 70
Figure 4.39: Simulation of the co-polymerization of MMA/MA T = 50°C 71
Figure 4.40: Simulation of the co-polymerization of MMA/MA T = 50°C 72
Figure 4.41: Simulation of the co-polymerization of AMS/MMA at 60°C 73
Figure 4.42: Simulation of the co-polymerization of AMS/MMA at 80°C 74
Figure 5.1: Simulation of the co-polymerization of MMA/BA T = 140°C $[dTBPO]_0$ = 0.0005M toluene = 30 wt% f_{BA0} = 0.148 75
Figure 5.2: Simulation of the co-polymerization of MMA/BA T = 140°C $[dTBPO]_0$ = 0.0005M toluene = 30 wt% f_{BA0} = 0.148 76
Figure 5.3: Simulation of the homo-polymerization of BMA T = 132°C $[dTBPO]_0$ = 0.09 wt% xylene = 91 wt% k_{dp} from Li *et al.* (2005) 77
Figure 5.4: Simulation of the homo-polymerization of BMA T = 132°C $[dTBPO]_0$ = 0.09 wt% xylene = 91 wt% k_{dp} from Wang *et al.* (2009a) 78
Figure 5.5: Simulation of the homo-polymerization of BMA T = 110°C $[dTBPO]_0$ = 0.17 wt% xylene = 83 wt% 79
Figure 5.6: Simulation of the homo-polymerization of BMA T = 132°C $[dTBPO]_0$ = 0.17 wt% xylene = 83 wt% 79
Figure 5.7: Simulation of the homo-polymerization of BMA T = 132°C $[dTBPO]_0$ = 0.34 wt% xylene = 66 wt% 80
Figure 5.8: Simulation of the homo-polymerization of BMA T = 132°C $[dTBPO]_0$ = 0.09 wt% xylene = 91 wt% 80
Figure 5.9: Simulation of the homo-polymerization of BMA T = 132°C $[dTBPO]_0$ = 0.17 wt% xylene = 83 wt% 81
Figure 5.10: Simulation of the homo-polymerization of BMA T = 132°C $[dTBPO]_0$ = 0.34 wt% xylene = 66 wt% 81

Figure 5.11: Simulation of the co-polymerization of AMS/Sty T = 60°C 83
Figure 5.12: Simulation of the co-polymerization of AMS/Sty T = 90°C 83
Figure 5.13: Simulation of the co-polymerization of AMS/Sty T = 110°C 84
Figure 5.14: Simulation of the co-polymerization of AMS/Sty T = 150°C 84
Figure 5.15: Simulation of the bulk co-polymerization of AMS/MMA T = 140°C $[dTBPO]_0$ = 2 wt% f_{AMS0} = 45 wt% 86
Figure 5.16: Simulation of the bulk co-polymerization of AMS/MMA T = 140°C $[dTBPO]_0$ = 2 wt% f_{AMS0} = 45 wt% 87
Figure 5.17: Simulation of the bulk co-polymerization of AMS/MMA T = 140°C $[dTBPO]_0$ = 2 wt% f_{AMS0} = 45 wt% 87
Figure 5.18: Simulation of the bulk co-polymerization of AMS/MMA T = 140°C $[dTBPO]_0$ = 0.5 wt% f_{AMS0} = 45 wt% 88
Figure 5.19: Simulation of the bulk co-polymerization of AMS/MMA T = 140°C $[dTBPO]_0$ = 0.5 wt% f_{AMS0} = 45 wt% 88
Figure 5.20: Simulation of the bulk co-polymerization of AMS/MMA T = 140°C $[dTBPO]_0$ = 0.5 wt% f_{AMS0} = 45 wt% 89
Figure 5.21: Simulation of the bulk co-polymerization of AMS/MMA T = 140°C $[dTBPO]_0$ = 1 wt% f_{AMS0} = 29 wt% 89
Figure 5.22: Simulation of the bulk co-polymerization of AMS/MMA T = 140°C $[dTBPO]_0$ = 1 wt% f_{AMS0} = 29 wt% 90
Figure 5.23: Simulation of the bulk co-polymerization of AMS/MMA T = 140°C $[dTBPO]_0$ = 1 wt% f_{AMS0} = 29 wt% 90
Figure 5.24: Simulation of the bulk co-polymerization of AMS/MMA T = 115°C $[dTBPO]_0$ = 8 wt% f_{AMS0} = 45 wt% 91
Figure 5.25: Simulation of the bulk co-polymerization of AMS/MMA T = 115°C $[dTBPO]_0$ = 8 wt% f_{AMS0} = 45 wt% 91
Figure 5.26: Simulation of the bulk co-polymerization of AMS/MMA T = 115°C $[dTBPO]_0$ = 8 wt% f_{AMS0} = 45 wt% 92
Figure 5.27: Simulation of the bulk co-polymerization of AMS/MMA T = 115°C $[dTBPO]_0$ = 2 wt% f_{AMS0} = 45 wt% 92
Figure 5.28: Simulation of the bulk co-polymerization of AMS/MMA T = 115°C $[dTBPO]_0$ = 2 wt% f_{AMS0} = 45 wt% 93
Figure 5.29: Simulation of the bulk co-polymerization of AMS/MMA T = 115°C $[dTBPO]_0$ = 2 wt% f_{AMS0} = 45 wt% 93
Figure 5.30: Simulation of the co-polymerization of Sty/GMA T = 170°C f_{Sty0} = 0.732 95
Figure 5.31: Simulation of the co-polymerization of Sty/GMA T = 190°C f_{Sty0} = 0.732 95

Figure 5.32: Simulation of the co-polymerization of Sty/GMA T = 190°C f_{Sty0} = 0.509 96
Figure 5.33: Simulation of the co-polymerization of Sty/GMA T = 190°C f_{Sty0} = 0.303 96
Figure 5.34: Simulation of the co-polymerization of Sty/GMA T = 190°C xylene = 30wt% f_{Sty0} = 0.726 97
Figure 5.35: Simulation of the co-polymerization of Sty/GMA T = 190°C xylene = 30wt% f_{Sty0} = 0.506 97
Figure 5.36: Simulation of the co-polymerization of Sty/GMA T = 190°C xylene = 30wt% f_{Sty0} = 0.303 98
Figure 5.37: Simulation of the co-polymerization of Sty/GMA T = 230°C f_{Sty0} = 0.732 98
Figure 5.38: Simulation of the co-polymerization of Sty/GMA T = 138°C $[TBPA]_0$ = 2 wt% xylene = 30 wt%.....99
Figure 5.39: Simulation of the co-polymerization of Sty/GMA T = 138°C $[TBPA]_0$ = 2 wt% xylene = 30 wt%.....100
Figure 5.40: Simulation of the bulk ter-polymerization of AMS/MMA/BA T = 140°C $[dTBPO]_0$ = 0.5 wt%.....102
Figure 5.41: Simulation of the bulk ter-polymerization of AMS/MMA/BA T = 140°C $[dTBPO]_0$ = 0.5 wt%.....103
Figure 5.42: Simulation of the bulk ter-polymerization of AMS/MMA/BA T = 140°C $[dTBPO]_0$ = 0.5 wt% f_{AMS0} = f_{MMA0} = 45 wt% 103
Figure 5.43: Simulation trends of bulk hexa-polymerization with and without depropagation 105
Figure 5.44: Simulation trends of bulk hexa-polymerization with and without depropagation 106
Figure 5.45: Simulation trends of bulk hexa-polymerization with and without depropagation 106
Figure 5.46: Simulation trends of bulk hexa-polymerization with and without depropagation 107
Figure 5.47: Simulation trends of bulk hexa-polymerization with and without depropagation 108
Figure 5.48: Simulation trends of bulk hexa-polymerization with and without depropagation 109
Figure 5.49: Simulation trends of bulk hexa-polymerization with and without depropagation 109
Figure 5.50: Simulation trends of bulk hexa-polymerization with and without depropagation 110

Figure 5.51: Simulation trends of bulk hexa-polymerization with and without depropagation 110
Figure 5.52: Simulation trends of bulk hexa-polymerization without depropagation 111
Figure 5.53: Simulation trends of bulk hexa-polymerization with depropagation 111
Figure 5.54: Simulation trends of bulk hexa-polymerization with depropagation 112
Figure 5.55: Simulation trends of bulk hexa-polymerization without depropagation 113
Figure 5.56: Simulation trends of bulk hexa-polymerization with depropagation 114
Figure 5.57: Simulation trends of bulk hexa-polymerization with depropagation 114
Figure 5.58: Simulation trends of bulk hexa-polymerization with depropagation 115
Figure 5.59: Simulation trends of bulk hexa-polymerization with and without depropagation 116
Figure 5.60: Simulation trends of bulk hexa-polymerization with depropagation 116
Figure 5.61: Simulation trends of bulk hexa-polymerization with depropagation 117
Figure 5.62: Simulation trends of bulk hexa-polymerization with depropagation 117
Figure 5.63: Simulation trends of bulk hexa-polymerization with and without depropagation 118
Figure 5.64: Simulation of the homo-polymerization of BA at 160°C with no initiator and 60 wt% xylene 122
Figure 5.65: Simulation of the homo-polymerization of BA at 180°C with no initiator and 60 wt% xylene 123
Figure 5.66: Simulation of the homo-polymerization of BA at 160°C with no initiator and 60 wt% xylene 123
Figure 5.67: Simulation of the homo-polymerization of BA at 180°C with no initiator and 60 wt% xylene 124
Figure 5.68: Simulation of the homo-polymerization of BA at 160°C with no initiator and 60 wt% xylene 124
Figure 5.69: Simulation of the homo-polymerization of BA at 180°C with no initiator and 60 wt% xylene 125
Figure 5.70: Simulation of the homo-polymerization of BA at 160°C with no initiator and 60 wt% xylene 125
Figure 5.71: Simulation of the homo-polymerization of BA at 180°C with no initiator and 60 wt% xylene 126
Figure 5.72: Simulation of the homo-polymerization of BA at 140°C 127
Figure 5.73: Simulation of the homo-polymerization of BA T = 138°C $[dTBPO]_0$ = 2 wt% xylene = 35wt% constant feed time = 360 min 129

Figure 5.74: Simulation of the homo-polymerization of BA T = 138°C $[dTBPO]_0$ = 2 wt% xylene = 35wt% constant feed time = 360 min 129
Figure 5.75: Simulation of the homo-polymerization of BA T = 138°C $[dTBPO]_0$ = 2 wt% xylene = 35wt% constant feed time = 360 min 130
Figure 5.76: Simulation of the homo-polymerization of BA T = 138°C $[dTBPO]_0$ = 2 wt% xylene = 35wt% constant feed time = 360 min 130
Figure 5.77: Simulation of the homo-polymerization of BA T = 138°C $[dTBPO]_0$ = 2 wt% xylene = 35wt% constant feed time = 180 min 131
Figure 5.78: Simulation of the homo-polymerization of BA T = 138°C $[dTBPO]_0$ = 2 wt% xylene = 35wt% constant feed time = 180 min 131
Figure 5.79: Simulation of the co-polymerizations of BMA/BA T = 138°C $[dTBPO]_0$ = 1.7 wt% xylene = 30wt%.....133
Figure 5.80: Simulation of the co-polymerizations of BMA/BA T = 138°C $[dTBPO]_0$ = 1.7 wt% xylene = 30wt%.....134
Figure 5.81: Simulation of the co-polymerizations of BMA/BA T = 138°C $[dTBPO]_0$ = 1.7 wt% xylene = 30wt%.....134
Figure 5.82: Simulation of the co-polymerizations of BMA/BA T = 138°C $[dTBPO]_0$ = 1.7 wt% xylene = 30wt%.....135
Figure 5.83: Simulation of the co-polymerization of BMA/BA T = 138°C $[dTBPO]_0$ = 1.7 wt% xylene = 30wt% f_{BA0} = 50 wt%.....135
Figure 5.84: Simulation of the semi-batch co-polymerization of Sty/BA T = 138°C $[TBPA]_0$ = 2 wt% xylene = 30wt% f_{Sty0} = 75 wt%.....137
Figure 5.85: Simulation of the semi-batch co-polymerization of Sty/BA T = 138°C $[TBPA]_0$ = 2 wt% xylene = 30wt% f_{Sty0} = 75 wt%.....137
Figure 5.86: Simulation of the semi-batch co-polymerization of Sty/BA T = 138°C $[TBPA]_0$ = 2 wt% xylene = 30wt% f_{Sty0} = 75 wt%.....138
Figure 5.87: Simulation of the semi-batch co-polymerization of Sty/BA T = 138°C $[TBPA]_0$ = 2 wt% xylene = 30wt% f_{Sty0} = 50 wt%.....138
Figure 5.88: Simulation of the semi-batch co-polymerization of Sty/BA T = 138°C $[TBPA]_0$ = 2 wt% xylene = 30wt% f_{Sty0} = 50 wt%.....139
Figure 5.89: Simulation of the semi-batch co-polymerization of Sty/BA T = 138°C $[TBPA]_0$ = 2 wt% xylene = 30wt% f_{Sty0} = 50 wt%.....139
Figure 5.90: Simulation of the semi-batch co-polymerization of Sty/BA T = 138°C $[TBPA]_0$ = 2 wt% xylene = 30wt% f_{Sty0} = 25 wt%.....140
Figure 5.91: Simulation of the semi-batch co-polymerization of Sty/BA T = 138°C $[TBPA]_0$ = 2 wt% xylene = 30wt% f_{Sty0} = 25 wt%.....140

Figure 5.92: Simulation of the semi-batch co-polymerization of Sty/BA T = 138°C $[TBPA]_0$ = 2 wt% xylene = 30wt% f_{Sty0} = 25 wt% 141
Figure 5.93: Simulation of the semi-batch ter-polymerization of Sty/BMA/BA T = 138°C $[TBPA]_0$ = 2 wt% xylene = 30wt% f_{Sty0} = f_{BMA0} = 33 wt% 143
Figure 5.94: Simulation of the semi-batch ter-polymerization of Sty/BMA/BA T = 138°C $[TBPA]_0$ = 2 wt% xylene = 30wt% f_{Sty0} = f_{BA0} = 25 wt% 143
Figure 5.95: Simulation of the semi-batch ter-polymerization of Sty/BMA/BA T = 138°C $[TBPA]_0$ = 2 wt% xylene = 30wt% f_{Sty0} = f_{BA0} = 15 wt% 144
Figure 5.96: Simulation of the semi-batch ter-polymerization of Sty/BMA/BA T = 138°C $[TBPA]_0$ = 2 wt% xylene = 30wt% f_{Sty0} = f_{BMA0} = 15 wt% 144
Figure 5.97: Simulation of the semi-batch ter-polymerization of Sty/BMA/BA T = 138°C $[TBPA]_0$ = 2 wt% xylene = 30wt% 145
Figure 5.98: Simulation of the semi-batch ter-polymerization of Sty/BMA/BA T = 138°C $[TBPA]_0$ = 2 wt% xylene = 30wt% 145
Figure 5.99: Simulation of the semi-batch ter-polymerization of Sty/BMA/BA T = 138°C $[TBPA]_0$ = 2 wt% xylene = 30wt% 146
Figure 5.100: Simulation of batch co-polymerization of Sty/BA at 80°C $[AIBN]_0$ = $[BPO]_0$ = $[Fict]_0$ = 0.33 wt% f_{Sty0} = 50 wt% 148
Figure 5.101: Simulation of batch co-polymerization of Sty/BA at 80°C $[AIBN]_0$ = $[BPO]_0$ = $[Fict]_0$ = 0.33 wt% f_{Sty0} = 50 wt% 148
Figure 5.102: Simulation of batch co-polymerization of Sty/BA at 80°C $[AIBN]_0$ = $[BPO]_0$ = $[Fict]_0$ = 0.33 wt% f_{Sty0} = 50 wt% 149
Figure 5.103: Simulation of batch co-polymerization of Sty/BA at 80°C $[AIBN]_0$ = $[BPO]_0$ = $[Fict]_0$ = 0.33 wt% f_{Sty0} = 50 wt% 149
Figure 5.104: Simulation of batch co-polymerization of Sty/BA at 80°C $[AIBN]_0$ = $[BPO]_0$ = $[Fict]_0$ = 0.33 wt% f_{Sty0} = 50 wt% 150
Figure 5.105: Simulation of batch co-polymerization of Sty/BA at 80°C $[AIBN]_0$ = $[BPO]_0$ = $[Fict]_0$ = 0.33 wt% f_{Sty0} = 50 wt% 150
Figure 5.106: Simulation of semi-batch co-polymerization of Sty/BA at 80°C $[AIBN]_0$ = $[BPO]_0$ = $[Fict]_0$ = 0.33 wt% f_{Sty0} = 50 wt% 152
Figure 5.107: Simulation of semi-batch co-polymerization of Sty/BA at 80°C $[AIBN]_0$ = $[BPO]_0$ = $[Fict]_0$ = 0.33 wt% f_{Sty0} = 50 wt% 152
Figure 5.108: Simulation of semi-batch co-polymerization of Sty/BA at 80°C $[AIBN]_0$ = $[BPO]_0$ = $[Fict]_0$ = 0.33 wt% f_{Sty0} = 50 wt% 153
Figure 5.109: Simulation of semi-batch co-polymerization of Sty/BA at 80°C $[AIBN]_0$ = $[BPO]_0$ = $[Fict]_0$ = 0.33 wt% f_{Sty0} = 50 wt% 153

Figure 5.110: Simulation of semi-batch co-polymerization of Sty/BA at 80°C $[AIBN]_0$ = $[BPO]_0$ = $[Fict]_0$ = 0.33 wt% f_{Sty0} = 50 wt% 154
Figure 5.111: Simulation of semi-batch co-polymerization of Sty/BA at 80°C $[AIBN]_0$ = $[BPO]_0$ = $[Fict]_0$ = 0.33 wt% f_{Sty0} = 50 wt% 154
Figure 5.112: Simulation of semi-batch co-polymerization of Sty/BA at 80°C $[AIBN]_0$ = $[BPO]_0$ = $[Fict]_0$ = 0.33 wt% f_{Sty0} = 50 wt% 155
Figure 5.113: Simulation of semi-batch co-polymerization of Sty/BA at 80°C $[AIBN]_0$ = $[BPO]_0$ = $[Fict]_0$ = 0.33 wt% f_{Sty0} = 50 wt% 155
Figure 5.114: Simulation of batch/semi-batch co-polymerization of Sty/BA at 80°C using AIBN, BPO, and Fict f_{Sty0} = 50 wt% 157
Figure 5.115: Simulation of batch/semi-batch co-polymerization of Sty/BA at 80°C using AIBN, BPO, and Fict f_{Sty0} = 50 wt% 157
Figure 5.116: Simulation of batch/semi-batch co-polymerization of Sty/BA at 80°C using AIBN, BPO, and Fict f_{Sty0} = 50 wt% 158
Figure 5.117: Simulation of batch/semi-batch co-polymerization of Sty/BA at 80°C using AIBN, BPO, and Fict f_{Sty0} = 50 wt% 158
Figure 6.1: Simulation of the co-polymerization of Sty/BA at 50°C with iterations to reach a constant polymer composition....164
Figure 6.2: Simulation of composition control policy 1, Sty/BA at 50°C $[AIBN]_0$ = 0.05M....166
Figure 6.3: Simulation of composition control policy 1, Sty/BA at 50°C $[AIBN]_0$ = 0.05M....168
Figure 6.4: Simulation of composition control policy 1, Sty/BA at 50°C $[AIBN]_0$ = 0.05M....169
Figure 6.5: Simulation of composition control policy 1, Sty/BA at 50°C $[AIBN]_0$ = 0.05M....169
Figure 6.6: Simulation of composition control policy 1, Sty/BA at 50°C $[AIBN]_0$ = 0.05M....170
Figure 6.7: Simulation of composition control policy 1, Sty/BA at 50°C $[AIBN]_0$ = 0.05M....170
Figure 6.8: Simulation of composition control policy 2, Sty/BA at 60°C $[AIBN]_0$ = 0.05M....172
Figure 6.9: Simulation of composition control policy 2, Sty/BA at 60°C $[AIBN]_0$ = 0.05M....175
Figure 6.10: Simulation of composition control policy 2, Sty/BA at 60°C $[AIBN]_0$ = 0.05M..175
Figure 6.11: Simulation of composition control policy 2, Sty/BA at 60°C $[AIBN]_0$ = 0.05M..176
Figure 6.12: Simulation of composition control policy 2, Sty/BA at 60°C $[AIBN]_0$ = 0.05M..176
Figure 6.13: Simulation of composition control policy 2, Sty/BA at 60°C $[AIBN]_0$ = 0.05M..177
Figure 6.14: Simulation of composition control policy 3, Sty/BA at 50°C $[AIBN]_0$ = 0.05M..179
Figure 6.15: Simulation of composition control policy 3, Sty/BA at 50°C $[AIBN]_0$ = 0.05M..180
Figure 6.16: Simulation of composition control policy 3, Sty/BA at 50°C $[AIBN]_0$ = 0.05M..180
Figure 6.17: Simulation of composition control policy 3, Sty/BA at 50°C $[AIBN]_0$ = 0.05M..181
Figure 6.18: Simulation of composition control policy 3, Sty/BA at 50°C $[AIBN]_0$ = 0.05M..181

Figure 6.19: Simulation of composition control policy 2 with policy 1 finish, Sty/BA at 60°C $[AIBN]_0$ = 0.05M 183
Figure 6.20: Simulation of composition control policy 2 with policy 1 finish, Sty/BA at 60°C $[AIBN]_0$ = 0.05M 183
Figure 6.21: Simulation of composition control policy 2 with policy 1 finish, Sty/BA at 60°C $[AIBN]_0$ = 0.05M 184
Figure 6.22: Simulation of composition control policy 2 with policy 1 finish, Sty/BA at 60°C $[AIBN]_0$ = 0.05M 184
Figure 6.23: Simulation of composition control policy 2 with policy 1 finish, Sty/BA at 60°C $[AIBN]_0$ = 0.05M CTA = 0.3g.....185
Figure 6.24: Simulation of composition control policy 1 with batch temperature finish, Sty/BA at 50°C $[AIBN]_0$ = 0.05M 186
Figure 6.25: Simulation of composition control policy 1 with batch temperature finish, Sty/BA at 50°C $[AIBN]_0$ = 0.05M 187
Figure 6.26: Simulation of composition control policy 1 with batch temperature finish, Sty/BA at 50°C $[AIBN]_0$ = 0.05M 187
Figure 6.27: Simulation of composition control policy 1 with batch temperature finish, Sty/BA at 50°C $[AIBN]_0$ = 0.05M 188
Figure 6.28: Simulation of composition control policy 1 with batch temperature finish, Sty/BA at 50°C $[AIBN]_0$ = 0.05M 188
Figure 6.29: Simulation of composition control policy 1 with batch temperature finish, Sty/BA at 50°C $[AIBN]_0$ = 0.05M 189
Figure 6.30: Simulation of composition control policy 1 with batch temperature finish, Sty/BA at 50°C $[AIBN]_0$ = 0.05M 189
Figure 6.31: Simulation of composition control policy 2, Sty/BA/EA/BMA at 60°C $[AIBN]_0$ = 0.4 wt% 191
Figure 6.32: Simulation of composition control policy 3, Sty/BA/EA/BMA at 60°C $[AIBN]_0$ = 0.4 wt% 192
Figure 6.33: Simulation of composition control policy 2, Sty/BA/EA/BMA at 60°C $[AIBN]_0$ = 0.4 wt% 192
Figure 6.34: Simulation of composition control policy 3, Sty/BA/EA/BMA at 60°C $[AIBN]_0$ = 0.4 wt% 193
Figure 6.35: Simulation of composition control policy 2, Sty/BA/EA/BMA at 60°C $[AIBN]_0$ = 0.4 wt% 193
Figure 6.36: Simulation of composition control policy 3, Sty/BA/EA/BMA at 60°C $[AIBN]_0$ = 0.4 wt% 194

Figure 6.37: Simulation of composition control policy 2, Sty/BA/EA/BMA at 60°C $[AIBN]_0$ = 0.4 wt% 194
Figure 6.38: Simulation of composition control policy 3, Sty/BA/EA/BMA at 60°C $[AIBN]_0$ = 0.4 wt% 195
Figure 6.39: Mayo-Lewis co-polymer composition curve of styrene and butyl methacrylate 197
Figure 6.40: Simulation of composition control policy 1, Sty/BMA at 50°C $[AIBN]_0$ = 0.05M f_{Sty0} = 0.13 198
Figure 6.41: Simulation of composition control policy 1, Sty/BMA at 50°C $[AIBN]_0$ = 0.05M f_{Sty0} = 0.925 198
Figure 6.42: Mayo-Lewis co-polymer composition curve of ethyl acrylate and butyl methacrylate 199
Figure 6.43: Simulation of composition control policy 2, EA/BMA at 60°C $[AIBN]_0$ = 0.05M f_{EA0} = 0.26 200
Figure 6.44: Simulation of composition control policy 2, EA/BMA at 60°C $[AIBN]_0$ = 0.05M f_{EA0} = 0.26 200
Figure 6.45: Simulation of composition control policy 2, EA/BMA at 60°C $[AIBN]_0$ = 0.05M f_{EA0} = 0.26 201
Figure 6.46: Simulation of composition control policy 2, EA/BMA at 60°C $[AIBN]_0$ = 0.05M f_{EA0} = 0.26 201
Figure 6.47: Simulation of composition control policy 2, Sty/BA at 50°C $[AIBN]_0$ = 0.05M 202
Figure 6.48: Simulation of composition control policy 2, Sty/BA at 50°C $[AIBN]_0$ = 0.05M CTA = 1g 203
Figure 6.49: Semi-batch Co-polymerization Operating Conditions for Policy 2 203
Figure 6.50: Simulation of composition control policy 3, Sty/BA at 50°C $[AIBN]_0$ = 0.05M 205
Figure 6.51: Simulation of composition control policy 3, Sty/BA at 50°C $[AIBN]_0$ = 0.05M 205
Figure 6.52: Manual simulation attempt for the co-polymerization of Sty/BA at 50°C $[AIBN]_0$ = 0.05M 206
Figure 6.53: Manual simulation attempt for the co-polymerization of Sty/BA at 50°C $[AIBN]_0$ = 0.05M 206
Figure 6.54: Simulation of composition control policy 3, Sty/BA at 50°C $[AIBN]_0$ = 0.05M 211
Figure 6.55: Simulation of composition control policy 1, EA/BMA at 60°C $[AIBN]_0$ = 0.05M 212
Figure 6.56: Simulation of composition control policy 1, EA/BMA at 60°C $[AIBN]_0$ = 0.05M 213

Figure 6.57: Simulation of composition control policy 1, EA/BMA at 60°C $[AIBN]_0$ = 0.05M 213
Figure 6.58: Simulation of the sub-optimal monomer flowrate used in the co-polymerization of EA/BMA.....214
Figure 6.59: Simulation of the sub-optimal monomer flowrate used in the co-polymerization of EA/BMA.....215
Figure 6.60: Simulation of the sub-optimal monomer flowrate with constraints.....215
Figure 6.61: Simulation of the sub-optimal monomer flowrate with constraints.....216
Figure 6.62: Simulation of the sub-optimal monomer flowrate with constraints.....216
Figure 6.63: Simulation of the sub-optimal monomer flowrate with constraints.....217
Figure 6.64: Simulation of the sub-optimal monomer flowrate with constraints.....217
Figure 6.65: Simulation of the sub-optimal monomer flowrate with constraints.....218

List of Tables

Table 2-1: Reference List for Tetra- and Ter-polymerizations 9
Table 2-2: Reference List for Co-polymerizations 11
Table 2-3: Reference List for Homo-polymerizations 15
Table 4-1: Previous Model Simulations from Jung (2008) 45
Table 4-2: Propagation Rate Constants of Acrylates from Van Herk (2009) 46
Table 4-3: Propagation Rate Constants of Acrylates from Database 46
Table 4-4: Co-polymerization of MMA/BA with dTBPO as initiator and n-dodecyl mercaptan as CTA (Dubé *et al.*, 2002) 53
Table 5-1: Kinetic Data for the Co-polymerizations of AMS and Styrene 82
Table 5-2: Reaction Conditions for the Co-polymerizations of AMS and MMA 85
Table 5-3: Reaction Conditions and Kinetic Data Used for the Co-polymerization of Styrene and GMA 94
Table 5-4: Reactivity and Depropagation Ratios for the Ter-polymerization of AMS, MMA and BA at 140°C 101
Table 5-5: Reactivity Ratios for Hexa-polymerization Simulation Trends 120
Table 5-6: Reactivity Ratios for the Ter-polymerization of Styrene, Butyl Methacrylate and Butyl Acrylate at 138°C 142
Table 6-1: Reactivity Ratios Used for the Tetra-polymerization of Styrene, BA, EA and BMA 190
Table A-1: Kinetic Database for AIBN 240
Table A-2: Kinetic Database for BPO 241
Table A-3: Kinetic Database for TBPA (tert-butyl peroxyacetate) 241
Table A-4: Kinetic Database for TBPB (tert-butyl peroxybenzoate) 242
Table A-5: Kinetic Database for dTBPO (di-tert-butyl peroxide) 242
Table A-6: Kinetic Database for the Fictitious Initiator 242
Table A-7: Kinetic Database for Acrylic Acid 244
Table A-8: Kinetic Database for Acrylonitrile 245
Table A-9: Kinetic Database for Butyl Acrylate 246
Table A-10: Kinetic Database for Butyl Methacrylate 247
Table A-11: Kinetic Database for Ethyl Acrylate 248
Table A-12: Kinetic Database for Glycidyl Methacrylate 249
Table A-13: Kinetic Database for Hydroxyethyl Acrylate 250
Table A-14: Kinetic Database for Hydroxyethyl Methacrylate 251
Table A-15: Kinetic Database for Methacrylic Acid 252

Table A-16: Kinetic Database for Methyl Methacrylate 253
Table A-17: Kinetic Database for α-methyl Styrene.....254
Table A-18: Kinetic Database for Styrene 255
Table A-19: Kinetic Database for Vinyl Acetate 256
Table A-20: Kinetic Database for Xylene 257
Table A-21: Kinetic Database for Toluene 257
Table A-22: Kinetic Database for Benzene.....258
Table A-23: Kinetic Database for Ethyl Acetate.....258
Table A-24: Kinetic Database for Carbon Tetra-chloride 258
Table A-25: Kinetic Database for Octanethiol.....259
Table A-26: Kinetic Database for Dodecanethiol.....259

1. Introduction

1.1. Research Objectives

Mathematical modeling of free radical polymerization has become desired in both academia and industry for its economic and time-saving benefits. With an increasing number of monomers, the complexity of the system grows. The polymerizations observed herein are from one monomer (homo-) to six monomers (hexa-) inclusive and show a variety of reaction outputs.

The objectives of this thesis are to contribute to the enhancement of the hexa-polymerization model database and to increase the versatility of the simulator by creating several advantageous extensions. To enhance the model, several hours went towards searching the literature for kinetic parameters and experimental data. A previously created depropagation option was improved the most from these efforts. The first extension created within this project was multiple initiator functionality. Back-biting and beta-scission of butyl acrylate and composition control were designed and tested afterward with great success. In the original model (Jung, 2008) and also with the mentioned extensions, the model can predict with great accuracy any of the rates of reaction or polymer quality outputs (molecular weight, polymer composition, sequence length, conversion). The model has the ability to simulate batch and semi-batch, bulk or solution, isothermal or nonisothermal, ideal or diffusion-limited kinetics and depropagation or no depropagation when determining these predictive yields (see Figure 1.1).

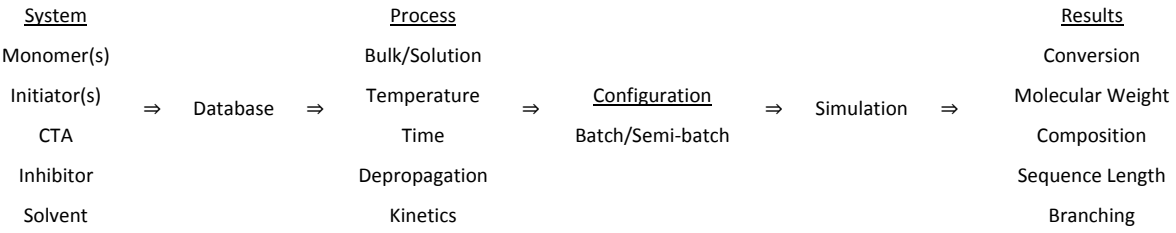

Figure 1.1: Simulation process for the hexa-polymerization model

1.2. Outline

Chapter 1 discusses the project objectives and model capabilities. It also provides the thesis outline.

Chapter 2 introduces some free radical polymerization background, discussing initiation, propagation, termination and chain transfer. The assumptions used to develop a mechanistic model are then mentioned, followed by a comprehensive literature review.

Chapter 3 deals with model development. The same polymerization steps from chapter 2 will be converted into model equations. Several other considerations and balances will also be included to explain the entire inner workings of the prediction software. Many reaction outputs are discussed, as well as additional model features and database characteristics.

Chapter 4 shows the bulk of the model testing and refinements. It is in this section that the kinetic parameters or experimental data found are critically examined.

Chapter 5 looks at the depropagation, back-biting and multiple initiator extensions. Ten case studies are analyzed in this section, including hexa-polymerization trends with depropagation.

Chapter 6 is the constant polymer composition control section. It first explains how composition control works, then derives each of the three policies and finally, works with additional considerations such as higher component extensions, combinations of policies and practical implementation.

Chapter 7 concludes the report with notes on future steps for the simulation model.

Chapter 8 includes the thesis appendices. In this section, interpolation of certain parameters due to the complexity of multi-component systems is first explained. The entire kinetic database is then tabulated, including initiators, chain transfer agents, solvents and monomers. The appendices also present possible alternative derivations for the composition control section. Finally, the user manual for the model is mentioned and an excerpt included.

2. Polymerization Background Information

2.1. Reaction Kinetics

There are several types of polymerization processes available and each is quite useful depending on the final product desired. Fundamentally, there are two major polymerization methods: step-growth polymerization and chain-growth polymerization.

Step-growth polymerization consists of two molecules with sufficient energy reacting to form a larger one. This is repeated several thousand times until the only molecules left are very long polymer chains. As such, it requires a very long time to reach high molecular weights with rates typical of any regular chemical reaction.

Chain-growth polymerization occurs when a double-bond is broken through various forms of initiation, whether by a free radical or an external energy source. Laser, ultra-violet radiation and heat are all examples of external initiation mechanisms. Depending on the external circumstances and ingredients used, there are several different chain-growth polymerizations: free radical, ionic, emulsion, graft, atom transfer and living. The polymerization analyzed in this report is regular free radical polymerization.

A free radical polymerization cycle is quite quick. Once the vinyl-bond of a monomer is opened by bonding with a free radical, it quickly reacts with another monomer's double-bond. This continues very rapidly until the chain terminates. As large polymer chains are created in quick bursts, the molecular weights obtained are already high at the start of the reaction and remain relatively constant until completion (Odian, 1970).

Another major contributor to the polymer's final properties is the number of monomers used. Depending on whether the polymerization in question is a homo-polymerization (one monomer), a co-polymerization (two monomers) or a multi-component polymerization (three or more monomers), the application of the final product can change quite dramatically. The modeling software developed and referred to throughout this thesis can simulate multi-component free radical polymerization of up to six monomers.

2.1.1. Initiation

The onset of free radical polymerization occurs when a free radical reacts with a vinyl-bond. These free radicals are created by splitting molecules with an external energy source. Most common initiators are peroxides as the oxygen-oxygen single bond is quite easy to split.

Another type is with the initiator azobisisobutyronitrile (AIBN), where the splitting of the molecule occurs by removing nitrogen gas (N_2).

In reaction 2.1, homolytic fission occurs and the initiator is split into two radicals. The second part of initiation occurs when the radicals react with a monomer and give rise to a radical of chain length unity (denoted by the subscript 1).

$$I \longrightarrow 2R_0^* \qquad 2.1.$$

$$R_0^* + M \longrightarrow R_1^* \qquad 2.2.$$

However, not all radicals react with monomers. They can also recombine or react with impurities and solvent molecules. This is accounted for by the initiator efficiency, *f*, whereas an efficiency of 0.5 means only half of the primary radicals will initiate polymerization.

Some monomers, mainly styrenics, can also undergo self-initiation. This phenomenon only becomes relevant at elevated temperatures and is generally assumed negligible during regular reaction conditions when a chemical initiator is included in the reaction.

2.1.2. Propagation

Upon initiation the polymer chain continues to grow via individual monomer addition. This is demonstrated in reaction 2.3 below:

$$R_r^* + M \longrightarrow R_{r+1}^* \qquad 2.3.$$

When more than one type of monomer is present, the reactivity of each monomer determines which is more likely to be added. Under the terminal model, the likelihood of a specific monomer reacting with the propagating radical chain depends only on the final unit of the growing chain. At high enough temperatures, the reverse reaction, where the recently added monomer depropagates, can occur. This is explained in further detail in Depropagation (section 3.2.5).

2.1.3. Termination

In this step, the growing radical chain terminates with another radical, thus stopping propagation. The two methods in which this can happen are combination (2.4) and disproportionation (2.5). The product(s) yielded are one or two dead polymer chains, respectively.

$$R_r^* + R_s^* \longrightarrow P_{r+s} \qquad 2.4.$$

$$R_r^* + R_s^* \longrightarrow P_r + P_s \qquad 2.5.$$

As shown, combination consists of the two radicals forming a bond and combining whereas disproportionation involves the transfer of a hydrogen atom in the *beta* position to the other radical forming a terminal double bond in the process. The likelihood of each termination method depends on the stereochemistry and functionality of the monomers involved.

2.1.4. Chain Transfer to Small Molecules

Another phenomenon that occurs in free radical polymerization is chain transfer. Radical chains have the ability to react with anything. As discussed previously, the chain terminates when radicals react with each other and increases when they react and bond with monomers. As an alternative, radicals can transfer to another molecule by accepting a hydrogen atom and creating a charge on the donating molecule. The donating molecule may be a monomer, solvent molecule, impurity or chain transfer agent. After chain transfer, the previously growing chain is terminated and the newly formed radical continues to propagate as before. Chain transfer has a large impact on molecular weight as the chains are terminated quite prematurely but has no dramatic effect on conversion or composition as the radicals continue to propagate unaffected.

$$R_r^* + X \longrightarrow P_r + R_1^* \qquad 2.6.$$

There are some special considerations that should be mentioned. The purpose of the solvent is to lower the viscosity of the polymerization mixture. Primarily, this occurs by dissolving the contents of the reaction mixture; however, this is also achieved through chain transfer reactions. When solvent is present in large amounts, the reaction, although much slower, occurs at a rate that allows for viscosity reduction and minor diffusion control limitations. Chain transfer to a chain transfer agent, however, happens more readily.

A chain transfer agent is a molecule designed to initiate chain transfer. It is specifically added into the reaction mixture to reduce the final molecular weight. As the chain transfer rate constant is relatively high, even a small amount will have a dramatic effect on molecular weight. A final reaction to discuss is chain transfer to dead polymer molecules.

2.1.5. Chain Transfer to Dead Polymer Chains

Long chain branching occurs when a radical attacks a dead polymer chain. If a hydrogen atom is taken from the backbone of the chain, the resulting “internal” radical will begin to

propagate away from the original chain creating a third arm or branch. This significantly affects polydispersity and weight-averaged molecular weight.

Branching will also occur when the growing radical reacts with a terminal double bond of a dead polymer chain. These terminal double bond units are formed in termination by disproportionation and especially by chain transfer to a small molecule, usually a monomer unit. Each monomer unit of free radical polymerization contains a vinyl bond. In chain transfer, the radical removes a hydrogen and leaves the double bond intact. Upon termination of this new chain, the double bond remains situated at the first monomer unit (in the terminal position). Re-initiation of this double bond with a growing radical chain will create a long chain branch.

Tetra-functional branching, which leads to cross-linking, occurs when a radical chain combines with an internal double bond. These bonds are inherent only to specific types of monomers (di-vinyl) and as such, it is known when cross-linking will be expected.

2.2. Assumptions Used for Model Development

Five general assumptions have been used to create this model. Each is quite common in polymerization modeling software.

1. Perfect Mixing
2. Reaction Kinetics follow the Terminal Model
3. Steady-State Hypothesis is valid
4. Long-Chain Approximation (LCA-I) is valid
5. Long-Chain Approximation (LCA-II) is valid

Perfect mixing assumes that every point in the reaction mixture is under the same conditions. There is no variability in temperature or concentration at any point.

The terminal model assumes that the reactivity of the propagating chain is independent of chain length and only depends on the final monomer unit of the chain. A contrasting theory is the penultimate model which assumes that reactivity of the radical chain depends on the last two monomer additions.

The Steady-State Hypothesis appropriately assumes that the radical concentration is at steady-state. This implies that the initiation and termination reactions are equal to each other and much larger than radical accumulation. This has widely been accepted as a valid method for modeling free radical polymerization.

The first long-chain approximation assumes that monomer consumption is only as a result of propagation. In theory, monomers are also consumed in the initiation step but due to the large chain lengths, the majority of monomer consumption is through propagation. Therefore, LCA-I assumes that monomer consumption due to initiation or transfer reactions is negligible.

The second long-chain approximation assumes that the cross-propagation rates are equal. This is a device used to calculate the radical fractions throughout the multi-component polymerization. Quite simply, this implies that for every monomer *i* consumed, a radical of monomer *i* will react. As a result, the number of times monomer *i* follows monomer *j* in a polymer chain is equal to the number of times monomer *j* follows unit *i*.

2.3. Literature Review

The thesis completed Jung (2008) was focused primarily on the extension of co-polymerization software to hexa-polymerization. This required many references to refine and improve the software kinetics. Jung (2008) had previously collected over 100 different sources for the specific monomer system in question, covering all aspects of kinetic modeling. As the basic free radical polymerization modeling was covered in quite some detail, this literature review will touch on certain important papers mentioned in Jung (2008) but focus more on recent additions and on the modeling expansions completed in this thesis. All literature used in the development of the model, added recently or in the past, are included in the reference tables. In general, the papers will be addressed chronologically and by the number of monomers.

2.3.1. Tetra-polymerization

Sahloul (2004) conducted tetra-polymerizations of styrene, ethyl acrylate (EA), hydroxyethyl acrylate (HEA) and methacrylic acid (MAA) measuring conversion, polymer composition, and molecular weights at elevated temperature. The reactivity ratios for each co-monomer pair were also calculated from the composition data. A simulation against the experimental data can be found in Jung (2008). Due to the scarcity of multi-component systems, no new tetra-polymerization experiments have been found.

2.3.2. Ter-polymerization

Pseudo-rate constants and free volume theory, both of which are implemented in the model, were originally proposed by Hamielec *et al.* (1987a, 1987b) and extended by Dubé *et al.* (1997). Composition equations followed the work by Alfrey and Goldfinger (1944) and Walling and Briggs (1945).

For model testing, alpha-methyl styrene (AMS), butyl acrylate (BA) and methyl methacrylate (MMA) were examined by both McManus *et al.* (2004) and Leamen *et al.* (2006). The experimental data obtained from McManus *et al.* (2004) are simulated using the reactivity ratios proposed by Leamen *et al.* (2006). With two independent studies on the same system, decent results are not unexpected.

Li and Hutchinson (2007) also worked on a ter-polymerization system, determining the propagation rate constant for styrene, BA and butyl methacrylate (BMA) over a range of temperatures. Their results are discussed in section 3.2.2.

Very few references of ter-polymerizations have been published in the last couple of years. Of the ones pertaining to our system, Wang (2010) was the most important. He conducted

several ter-polymerizations of styrene, butyl acrylate (BA) and butyl methacrylate (BMA), recording monomer concentration, polymer composition, molecular weight and polymer content at elevated temperatures. His objective was to show the importance of modeling additional reaction mechanisms of acrylates and methacrylates at elevated temperatures (depropagation, back-biting, beta-scission). The results of the simulations are discussed in section 5.2.4. Table 2-1 lists all the references found for ter- and tetra-polymerizations.

Table 2-1: Reference List for Tetra- and Ter-polymerizations

Monomer System	Reference	Focus
Tetra	Sahloul (2004)	Data Generation
Ter	Alfrey and Goldfinger (1944,1946)	Polymer Composition
	Walling and Briggs (1945)	Polymer Composition
	Valvassori and Sartori (1967)	Polymer Composition
	Galbraith *et al.* (1987)	Reactivity Ratios
	Hamielec *et al.* (1987a, 1987b)	Comprehensive
	Dubé and Penlidis (1995)	Model Testing
	Hocking and Klimchuk (1996)	Polymer Composition
	Dubé and Penlidis (1996)	Data Generation
	Dubé *et al.* (1997)	Comprehensive
	McManus *et al.* (1998)	Model Testing
	Gao and Penlidis (2000)	Model Testing
	Keramopoulos and Kiparissides (2003)	Model Testing
	McManus *et al.* (2004)	Data Generation/Deprop.
	Leamen *et al.* (2005)	Depropagation
	Li and Hutchinson (2007)	Reaction Kinetics
	Wang (2010)	Depropagation/Back-biting

2.3.3. Co-polymerization

Free radical co-polymerization has been extensively researched. It is also the foundation for multi-component polymerizations as all larger systems use co-polymer reactivity ratios and reaction kinetic extensions from the two monomer system. As such, it is a very important part of free radical polymerization modeling and was covered in quite some detail by Jung (2008).

Co-polymer composition was first approached in 1944 by Alfrey and Goldfinger, Mayo and Lewis, and Wall. Since then, Skeist (1946) and Meyer and Lowry (1965) have improved

upon it, the latter creating an analytical solution for the co-polymer composition equation as a function of conversion. Sequence length determination was first attempted by Merz *et al.* (1946). Merz *et al.* (1946) also began to look at the penultimate monomer unit and its effect on co-polymer composition.

In 1954, Bradbury and Melville investigated the effect of the polymerization environment, more specifically the addition of a solvent, on the reactivity ratios of styrene and BA. Further reactivity ratio estimates were conducted by Gaddam *et al.* (1977). They used the Intersection method and the Fineman Ross method to determine the co-polymer reactivity ratios of hydroxypropyl methacrylate (HPMA) against methyl acrylate (MA), BA, ethyl acrylate (EA) and MMA. Kapur and Brar (1992) determined the initial triad fraction composition of vinyl acetate (VAc) and BMA using quaternary and carbonyl carbon resonances. They also postulated that the quaternary resonance estimations were more accurate due to an overlap in the carbonyl resonances and proposed a method of improving the carbonyl resonance readings.

Depropagation was first realized once McCormick (1957) discovered that AMS does not polymerize above its ceiling temperature of 61°C. Several developments occurred thereafter, with a major approach to modeling depropagation arising in Krüger *et al.* (1987). Their probabilistic approach, also found in Jung (2008), was considered more stable and produced better convergence than previous models by Lowry (1960) and Wittmer (1971). Palmer *et al.* (2000, 2001) discussed this same idea while analyzing the co-polymerization of AMS and MMA. A penultimate depropagation model has been proposed to be more accurate than the terminal model by Grady *et al.* (2002) and Li *et al.* (2005, 2006) and more recently by Wang and Hutchinson (2008a, 2008b) and Wang (2010).

Glycidyl methacrylate (GMA) is a recent monomer addition to the modeling software and substantial kinetic information was required to model it accurately. Liu *et al.* (1995) conducted several co-polymerizations of MMA and GMA in bulk and in solution to determine the reactivity ratios using a non-linear least squares method. Brar and Dutta (1998) analyzed the reactivity ratios between acrylonitrile (AN) and GMA using low and full conversion experiments. Their results were later confirmed in-house using RREVM, a computer program using the advanced Error-in-Variables-Model estimation method created by Dubé *et al.* (1991). Polic *et al.* (1998) later improved on the software and published an extensive reactivity ratio literature review. The co-polymerization of styrene and GMA was also analyzed by Wolf *et al.* (2002) at elevated temperatures. Reactivity ratios were determined at low conversions and tested against full conversion experiments.

Depropagation was not accounted for in the reactivity ratio determination even though GMA has been shown to depropagate in Wang (2010). The systems of styrene/GMA and styrene/BA, studied by Wang (2010), are used as model testing case studies in sections 5.1.4 and 5.2.3.

Additional reactivity ratios were published in 2001, by Buback *et al.* They analyzed several acrylate/methacrylate systems for the determination of reactivity ratios and co-polymer propagation rate constants. An important part of their work was comparing the terminal model against the implicit and explicit penultimate effect models.

Dubé *et al.* (2002) conducted several elevated temperature co-polymerizations of BA and MMA to observe the effect that monomer, initiator, solvent and chain transfer agent feed concentrations have on conversion, polymer composition, and molecular weight. The experimental data and simulation results are discussed later in Chapter 4.

Sahloul *et al.* (2005) were the first to find Arrhenius expressions for the reactivity ratios of EA-Hydroxyethyl acrylate (HEA) and HEA-MA using EVM. Abdollahi *et al.* (2007) also worked with EA by determining the reactivity ratios of the co-polymerization with styrene at 70°C. In the paper, they compared their results to several other accepted methods. Experimental data of conversion and polymer composition was also published which can be found in Chapter 4 (see section 4.3).

Constant co-polymer composition is a large addition to the modeling software with most of its base coming from Fujisawa and Penlidis (2008). They proposed modeling strategies for maintaining a uniform polymer composition throughout polymerization. These three different methods were then compared with simulations using molecular weight, conversion, rate of reaction, branching and sequence length.

On a general note, free radical polymerization was recently compared to nitroxide-mediated polymerization by Popescu *et al.* (2010) using bisacrylate content in the final polymer. The reference list for all the co-polymerizations found in the literature can be found in Table 2-2.

Table 2-2: Reference List for Co-polymerizations

Reference	Focus
Branson and Simha (1943)	Modeling
Alfrey and Goldfinger (1944)	Polymer Composition
Mayo and Lewis (1944)	Polymer Composition
Simha and Branson (1944)	Modeling

Wall (1944)	Polymer Composition
Stockmayer (1945)	Composition Distribution
Merz *et al.* (1946)	Polymer Composition
Skeist (1946)	Polymer Composition
Walling (1949)	Modeling
Fineman and Ross (1950)	Reactivity Ratios
Mayo and Walling (1950)	Reaction Kinetics
Bradbury and Melville (1954)	Reactivity Ratios
Lowry (1960)	Depropagation
Harwood and Ritchey (1964)	Sequence Length
Meyer and Lowry (1965)	Polymer Composition
Otsu *et al.* (1965, 1966)	Reactivity Ratios
Cameron and Kerr (1967)	Reactivity Ratios
Chan and Meyer (1968)	Polymer Composition
Harwood (1968)	Sequence Length
Howell *et al.* (1970)	Depropagation
Izu and O'Driscoll (1970)	Depropagation
Wittmer (1971)	Depropagation
Fischer (1972)	Depropagation
Johnston (1973)	Modeling
Chow (1975)	Reactivity Ratios
Gaddam *et al.* (1977)	Reactivity Ratios
Johnson *et al.* (1978)	Modeling
Dionisio and O'Driscoll (1979)	Modeling
Patino-Leal *et al.* (1980)	Reactivity Ratios
Reilly and Patino-Leal (1981)	Reactivity Ratios
Borchardt (1982)	Reactivity Ratios
Hill *et al.* (1982)	Sequence Length
Duever *et al.* (1983)	Reactivity Ratios
Lord (1984)	Model Testing
Teramachi *et al.* (1984)	Composition Distribution
Borchardt (1985)	Reactivity Ratios
Garcia-Rubio *et al.* (1985)	Reactivity Ratios/Model Testing
Balaraman *et al.* (1986)	Composition and Sequence Length Distribution
Catala *et al.* (1986)	Reactivity Ratios
Krüger *et al.* (1987)	Depropagation
Tacx *et al.* (1988)	Composition Distribution
Dubé (1989)	Reactivity Ratios/Model Testing
O'Driscoll and Huang (1989, 1990)	Modeling

Davis *et al.*(1990)	Reaction Kinetics
Dubé *et al.* (1990)	Reactivity Ratios/Model Testing
Dubé *et al.* (1991)	Reactivity Ratios
Kapur and Brar (1992)	Modeling
Engelmann and Schmidt-Naake (1993)	Composition Distribution
Reilly *et al.* (1993)	Reactivity Ratios
Switata-Zeliazkow (1993)	Modeling
Xie and Hamielec (1993)	Modeling
Kim (1994)	Reactivity Ratios/Model Testing
Vivaldo-Lima *et al.* (1994)	Modeling
Dubé and Penlidis (1995)	Reactivity Ratios/Model Testing
Liu *et al.* (1995)	Reactivity Ratios
Rossignoli and Duever (1995)	Reactivity Ratios
McManus and Penlidis (1996)	Reactivity Ratios/Model Testing
Brar and Dutta (1998)	Reactivity Ratios
Gao and Penlidis (1998)	Model Testing
Polic *et al.* (1998)	Reactivity Ratios
Brandrup *et al.* (1999)	Reaction Kinetics and Reactivity Ratios
Chambard *et al.* (1999)	Reactivity Ratios
Martinet and Guillot (1999)	Depropagation
McManus *et al.* (1999)	Reactivity Ratios
Hakim *et al.* (2000)	Reactivity Ratios
Palmer *et al.* (2000, 2001)	Depropagation
Buback *et al.* (2001)	Reactivity Ratios
Scholtens *et al.* (2001)	Composition Distribution
Dubé *et al.* (2002)	Depropagation
Grady *et al.* (2002)	Depropagation
Kim and Harwood (2002)	Sequence Length
Wolf *et al.* (2002)	Reactivity Ratios
Fernandez-Garcia *et al.* (2003)	Modeling
Cheong and Penlidis (2004)	Depropagation
Sahloul and Penlidis (2004, 2005)	Reactivity Ratios
Sahloul *et al.* (2005)	Reactivity Ratios
Leamen *et al.* (2005)	Depropagation
Li *et al.* (2005)	Depropagation
Jianying *et al.* (2006)	Reactivity Ratios
Li *et al.* (2006)	Depropagation
Abdollahi *et al.* (2007)	Reactivity Ratios

Mun *et al.* (2007)	Reactivity Ratios
Fujisawa and Penlidis (2008)	Modeling
Wang and Hutchinson (2008a, b)	Depropagation
Popescu *et al.* (2010)	Modeling
Wang (2010)	Depropagation/Back-biting

2.3.4. Homo-polymerization

Most homo-propagation cases were simulated in Jung (2008). Very few new papers have been published on a topic as old as free radical homo-polymerization and as such, the previous work of Jung (2008) will not be reiterated. Acrylates, however, have recently been found to take part in back-biting and beta-scission reactions under certain conditions. As such, there have been many recent papers on the homo-polymerization of BA and acrylates in general.

Van Herk (2009) gave a complete history of the development of acrylate propagation kinetics beginning with the origin of the PLP technique. His account finishes with the accepted rate constants for various acrylates, all in the form of Arrhenius expressions. Castignolles (2009) suggested that the standard technique for determining propagation rate constants, pulsed-laser polymerization-size exclusion chromatography (PLP-SEC), has a high degree of uncertainty in acrylate monomers due to the large amounts of long chain branching. This suggests that there is a large degree of error in past acrylate propagation papers.

The original mechanism for back-biting and beta-scission of BA was formulated by Peck and Hutchinson (2004). The required parameters for their model were estimated through the homo-polymerization of BA in xylene. Barth *et al.* (2009) also focused on the homo-polymerization of BA. They determined the fraction of mid-chain radicals to regular secondary propagating radicals at very low temperatures, proving the existence of back-biting regardless of the temperature level. Nikitin and Hutchinson (2009) proposed a penultimate model when modeling the back-biting phenomenon of BA with all model equations and kinetic references. An extension to this model was published shortly thereafter by Wang *et al.* (2009b), accounting for the presence of macromonomers with proposed rate constants. Zorn *et al.* (2009) produced conversion data and homo-propagation rate constants for both BA and EA with and without initiator. The idea that acrylates might self-initiate by decomposition of impurities at high temperatures was revisited by Rantow *et al.* (2006).

Ahmad *et al.* (2009) analyzed the homo-polymerization of BA in order to determine the reason for the difference in branching between free radical and controlled polymerizations. The reason seemed to be a result of the increased presence of short chain radicals in free radical polymerization. Table 2-3 is the reference list for all the homo-polymerization papers used.

Table 2-3: Reference List for Homo-polymerizations

Reference	Focus
Bywater (1955)	Depropagation
McCormick (1957)	Depropagation
Nair and Muthana (1961)	Reaction Kinetics
Carlsson *et al.* (1966)	Reaction Kinetics
Raghuram and Nandi (1967, 1970)	Reaction Kinetics
Hui and Hamielec (1972)	Reaction Kinetics/Modeling
Friis and Nyhagen (1973)	Reaction Kinetics
Arai and Saito (1976)	Modeling
Husain and Hamielec (1978)	Modeling
Garcia-Rubio *et al.*(1979)	Modeling
Marten and Hamielec (1982)	Modeling
Stickler (1983)	Modeling
Stickler *et al.* (1984)	Modeling
Buback *et al.* (1989)	Reaction Kinetics
Buback (1990)	Reaction Kinetics/Modeling
Dubé *et al.* (1991)	Reaction Kinetics/Modeling
Kumar and Gupta (1991)	Reaction Kinetics
Kuindersma (1992)	Model Testing
Gao (1992)	Model Testing
Buback *et al.* (1995)	Reaction Kinetics
Hutchinson *et al.* (1995)	Reaction Kinetics
Beuermann *et al.* (1996)	Reaction Kinetics
Gao and Penlidis (1996)	Model Testing
Lyons *et al.* (1996)	Reaction Kinetics
Gao *et al.* (1997)	Model Testing
Beuermann *et al.* (1997)	Reaction Kinetics
Hutchinson *et al.* (1997)	Reaction Kinetics
Buback *et al.* (1998)	Reaction Kinetics
Maeder and Gilbert (1998)	Reaction Kinetics
Beuermann *et al.* (1999)	Reaction Kinetics
Buback *et al.* (1999)	Reaction Kinetics

McKenna *et al.* (1999)	Reaction Kinetics
Dhib *et al.* (2000)	Model Testing
Asua *et al.* (2004)	Reaction Kinetics
Nising and Meyer (2004)	Reaction Kinetics
Peck and Hutchinson (2004)	Reaction Kinetics/Modeling
Gao *et al.* (2004)	Modeling
Quan *et al.* (2005)	Reaction Kinetics
Vargun and Usanmaz (2005)	Reaction Kinetics
Willemse *et al.* (2005)	Back-biting
Buback and Junkers (2006)	Reaction Kinetics
Rantow *et al.* (2006)	Modeling
Matthews *et al.* (2007)	Molecular Weights
Nikitin *et al.* (2007)	Back-biting
Chen *et al.* (2007)	Reaction Kinetics
Ahmad *et al.* (2009)	Modeling
Barth *et al.* (2009)	Back-biting
Castignolles (2009)	Modeling
Nikitin and Hutchinson (2009)	Back-biting
Van Herk (2009)	Modeling
Wang *et al.* (2009a)	Depropagation
Wang *et al.* (2009b)	Back-biting
Zorn *et al.* (2009)	Reaction Kinetics

3. Model Development and Features/Options

3.1. Reaction Balances

The modeling software uses numerical methods to solve reaction balances every minute of the reaction simulation. All of the balances shown below are for a semi-batch reactor case. For the case of a batch simulation, simply remove the input flowrate term.

3.1.1. Monomer Balances

Monomer consumption is assumed to only occur in the propagation step (see LCA-I, section 2.2), therefore the following balance is used.

$$\frac{dN_i}{dt} = F_{i,in} - R_{pi}V \qquad 3.1.$$

where N_i, $F_{i,in}$, R_{pi}, and V represent the number of moles of species i, the molar input flowrate of species i, the rate of consumption of species i and the total volume of the reaction mixture, respectively.

With all six monomers present, there will be six monomer consumption balances and 36 propagation reactions (six for each monomer).

$$R_{pi} = \sum_{j=1}^{6} R_{ji} = \sum_{j=1}^{6} k_{pji}\left[R_j^*\right][M_i] \qquad 3.2.$$

Also note: $[M] = \sum_{i=1}^{6}[M_i]$ $[R^*] = \sum_{i=1}^{6}[R_i^*]$ $f_i = \frac{[M_i]}{[M]}$ $\phi_j = \frac{[R_j^*]}{[R^*]}$

where k_{pji}, $[R^*]$, $[M]$, f_i, and ϕ_j are the propagation rate constant, total radical concentration, total monomer concentration, mole fraction of monomer species i and mole fraction of radical species j, respectively.

3.1.2. Radical Balances

As a homo-propagation reaction does not change the number of radicals present, only the cross-propagation reactions are considered. Using LCA-II (section 2.2), the following balance for a six monomer system is generated.

$$\frac{dR_i^*}{dt} = \sum_{j=1}^{6} R_{ji} - \sum_{j=1}^{6} R_{ij} = \sum_{j=1}^{6} k_{pji}\left[R_j^*\right][M_i] - \sum_{j=1}^{6} k_{pij}[R_i^*][M_j] \approx 0 \qquad 3.3.$$

Both sides of the equation are then divided by the total monomer and radical concentrations and rearranged into a matrix form of M · r = b for an analytical solution. 'r' can then be solved for by simple matrix inversion: $r = M^{-1} \cdot b$. To calculate the individual radical concentrations, these radical fractions are multiplied against the total radical concentration (see section 3.1.5). For the complete derivation and solution of the radical balance, see Jung (2008).

3.1.3. Volume Shrinkage

As the reaction proceeds, more and more monomer will be consumed by the reaction leaving only polymer chains remaining. These polymer chains, quite naturally, occupy more space than the monomers before them; hence, there is a reduction in the reaction volume. The reaction volume term has a major influence as most of the reaction balances and outputs are expressed in terms of concentration (moles divided by volume).

$$\frac{dV}{dt} = \sum_{i=1}^{6} \left[\frac{F_{i,in} Mw_i}{\rho_{i,m}} - R_{pi} Mw_i \left(\frac{1}{\rho_{i,m}} - \frac{1}{\rho_p} \right) V \right] \qquad 3.4.$$

where Mw_i, $\rho_{i,m}$, and ρ_p represent the molecular weight of monomer species *i*, the density of monomer species *i* and the density of the polymer, respectively.

3.1.4. Polymer Balances

The amount of monomer species *i* incorporated into polymer chains is simply the amount of monomer consumed (using LCA-I) as well as the amount entering in a semi-batch feed.

$$\frac{dP_i}{dt} = F_{pi,in} + R_{pi} V \qquad 3.5.$$

where $F_{pi,in}$ is the inlet molar flowrate of monomer *i* already incorporated into polymer chains.

3.1.5. Additional Balances

Reaction balances are also required for the remaining four inputs: initiators, impurities, chain transfer agents and solvents. An initiator simply decomposes over time whereas an impurity, a chain transfer agent or a solvent molecule are only consumed if they react with a radical. As such, the following four balances are created:

$$\frac{dN_I}{dt} = F_{I,in} - k_d N_I \qquad 3.6.$$

$$\frac{dN_Z}{dt} = F_{Z,in} - k_{fz}N_Z[R^*] \tag{3.7.}$$

$$\frac{dN_C}{dt} = F_{C,in} - k_{fC}N_C[R^*] \tag{3.8.}$$

$$\frac{N_S}{dt} = F_{S,in} - k_{fS}N_S[R^*] \tag{3.9.}$$

where k_d, k_{fZ}, k_{fC} and k_{fS} are the initiator decomposition rate constant, and the transfer to impurity, chain transfer agent and solvent rate constants, respectively.

In terms of radical concentration, only the initiator, impurity and termination reactions have any affect. Therefore the total radical concentration balance is shown below for up to *m* initiators.

$$\frac{d(V[R^*])}{dt} = 2\sum_{k=1}^{m} f_{eff,k}k_{d,k}N_{I,k} - k_{fZ}N_Z[R^*] - k_t[R^*]^2V \tag{3.10.}$$

where $f_{eff,k}$ and k_t are the initiator efficiencies and the overall termination rate constant, respectively. Also note that k_t is simply the summation of the combination and disproportionation rate constants.

Using the total radical concentration balance and assuming the steady-state hypothesis is valid, we can find the total radical concentration is dependent only on the concentration of impurities and initiators in the reaction mixture.

$$[R^*] = \frac{1}{2}\left\{\left[\left(\frac{k_{fZ}[Z]}{k_t}\right)^2 + \frac{8}{k_t}\sum_{k=1}^{m} f_{eff,k}k_{d,k}[I_k]\right]^{1/2} - \frac{k_{fZ}[Z]}{k_t}\right\} \tag{3.11.}$$

If no impurities are present and only one initiator is used, this equation simplifies to the more recognizable version for the total radical concentration.

$$[R^*] = \left(2\frac{f_{eff}k_d}{k_t}[I]\right)^{1/2} \tag{3.12.}$$

3.2. Additional Modeling Considerations

In a homo-polymerization, each of the following equations can be derived directly from polymerization reaction kinetics (see section 2.1). In order to account for the variability among the different monomers in multi-component cases, the so-called pseudo-rate constant method has been employed. This allows for the appropriate weighing of the individual rate constants. In general, in each of the following sections the rate constant of each monomer is multiplied by the amount of that monomer in the system and the appropriate radical fraction.

3.2.1. Initiation

The rate of initiation in a free radical homo-polymerization is shown below.

$$R_I = 2f_{eff}k_d[I] \tag{3.13.}$$

Consequently, for multiple initiators the rate of initiation would be the summation of the effects from each initiator. Or, in equation form,

$$R_I = 2\sum_{k=1}^{m} f_{eff,k}k_{d,k}[I_k] \tag{3.14.}$$

where m is the number of initiators.

Upon adding additional types of monomers into the system, the initiator efficiency is affected as it depends on the monomer-initiator pair and not the initiator alone. As such,

$$R_I = 2\sum_{k=1}^{m} f_{eff,pseudo,k}k_{d,k}[I_k] \tag{3.15.}$$

$$f_{eff,pseudo,k} = \sum_{i=1}^{6} f_{eff,k,i}f_i \tag{3.16.}$$

where $f_{eff,pseudo,k}$ is the pseudo-initiator efficiency for initiator k.

However, difficulties may arise upon implementing this in modeling software. Slight differences in the decomposition rate constant for each monomer are present and affect the initiator likewise. Thus, the complete rate of initiation implemented for a multiple-initiator free radical multi-component polymerization is as follows:

$$R_I = 2\sum_{k=1}^{m} f_{eff,pseudo,k} k_{d,k,pseudo}[I_k] \quad 3.17.$$

$$f_{eff,pseudo,k} = \sum_{i=1}^{6} f_{eff,k,i} f_i \quad 3.16.$$

$$k_{d,pseudo,k} = \sum_{i=1}^{6} k_{d,k,i} f_i \quad 3.18.$$

where $k_{d,pseudo,k}$ is the pseudo-initiator decomposition rate constant for initiator k.

For a complete discussion on the implementation of the pseudo-initiator decomposition rate constant, see Appendix I.

A final addition to the rate of initiation is taken into account as styrene is known to self-initiate at elevated temperatures. The thermal initiation rate, based on a Diels-Alder mechanism, is known to follow a 3rd order reaction mechanism.

$$R_{th} = 2k_{th}\left[M_{Sty}\right]^3 \quad 3.19.$$

$$R_{I,total} = R_I + R_{th} \quad 3.20.$$

3.2.2. Propagation

Propagation is simply the rate of disappearance of monomer species within the reaction mixture. Although the amount of monomer consumed is accounted for by each species in the monomer balances, the overall rate of propagation is nonetheless required elsewhere for calculating other reaction output variables.

$$R_p = -\frac{d\left(\sum_{i=1}^{6}[M_i]\right)}{dt} = k_{p,pseudo}[M][R^*] \quad 3.21.$$

$$k_{p,pseudo} = \sum_{i=1}^{6}\sum_{j=1}^{6} k_{pij}\phi_i^* f_j \quad 3.22.$$

where $k_{p,pseudo}$ is the pseudo-propagation rate constant.

Performance of our model's pseudo-propagation rate constants can be seen in the following examples. Li and Hutchinson (2007) conducted several ter-polymerizations of styrene, butyl acrylate and butyl methacrylate over a range of temperatures, shown in Figure 3.1. The stars represent their experimental data; the dashed line with square points is their simulation of the terminal model under the same conditions; the dotted line with triangle points is their simulation of the penultimate model; and the solid line is our model's simulation (terminal model). This paper was trying to show the inadequacy of the terminal model in ter-polymerizations. These results, however, show that a terminal model can accurately predict ter-polymerizations if the correct kinetic parameters are used. Simulating a ter-polymerization with data refined for the penultimate model might not be the best method to judge effectiveness.

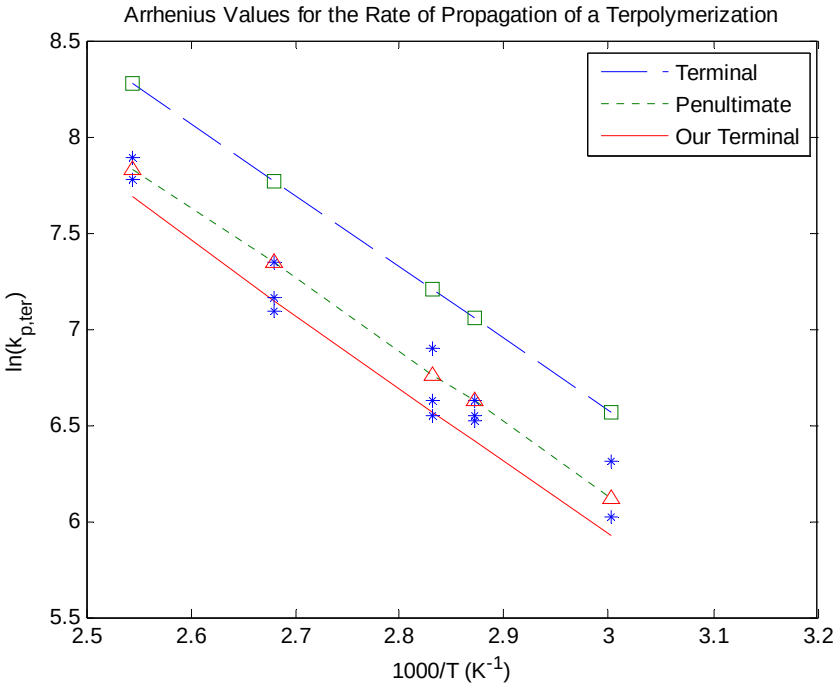

Figure 3.1: Ter-polymerizations of Sty/BA/BMA by Li and Hutchinson (2007)

Wang (2010) determined $k_{p,co}$ in a co-polymerization of styrene and glycidyl methacrylate at 100°C over a range of monomer feed ratios. Figure 3.2 shows the model's simulation under the same operating conditions. With only a 5°C decrease employed, our simulation in Figure 3.3 is much more accurate. These figures confirm that $k_{p,pseudo}$ produces acceptable results when modeling multi-component polymerizations. They also show how sensitive k_p is to changes in temperature. A system with poorly maintained reactor cooling would be subject to large amounts of error.

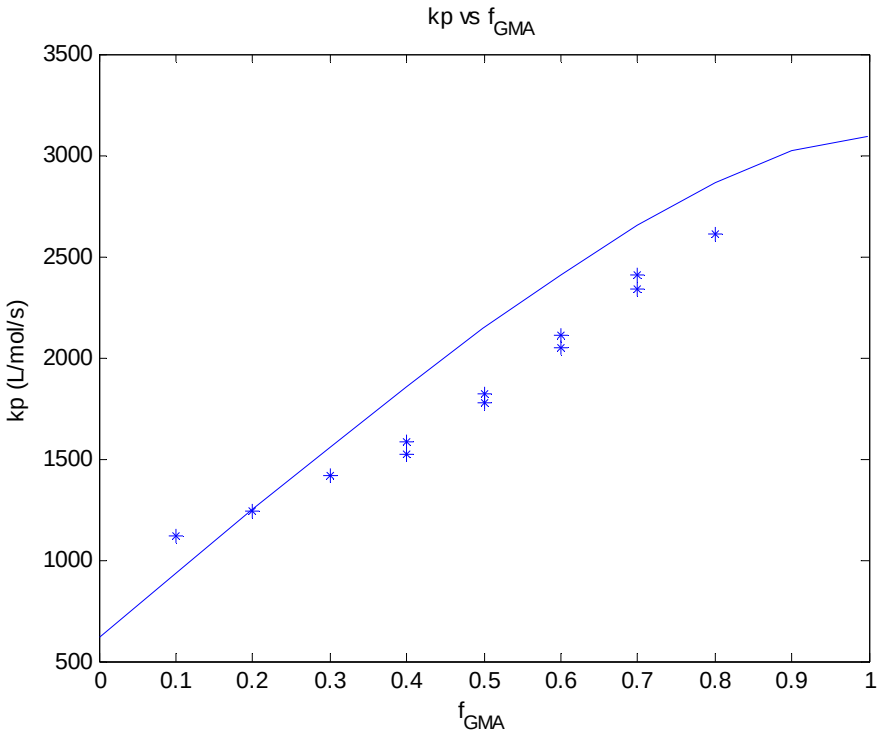

Figure 3.2: Simulation of the co-polymerizations of Sty/GMA at 100°C

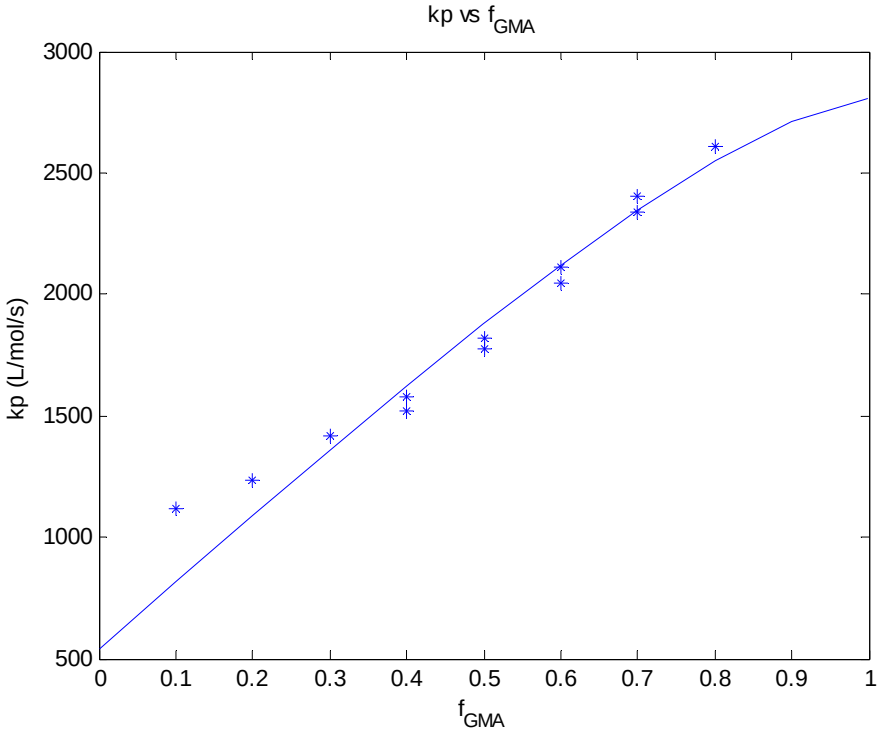

Figure 3.3: Simulation of the co-polymerizations of Sty/GMA at 95°C

3.2.3. Termination

Termination occurs by two mechanisms: disproportionation or combination of two growing radical chains. A pseudo-termination rate constant is also required in a multi-component polymerization.

$$R_t = k_{t,pseudo}[R^*]^2 = \sum_{i=1}^{6}\sum_{j=1}^{6} k_{tij}[R_i^*][R_j^*] = \sum_{i=1}^{6} k_{tii}\,[R_i^*]^2 + \sum_{i=1}^{6}\sum_{\substack{j=2 \\ (i\neq j)}}^{6} 2k_{tij}[R_i^*][R_j^*] \qquad 3.23.$$

where k_{tii} is the homo-termination rate constant and k_{tij}, $i \neq j$, is the cross-termination rate constant. Note $k_{tij} = k_{tji}$.

Of the two conventions available, the British and not the American, is used throughout. In the American convention, R_t would be multiplied by a factor of 2 and the k_t value halved accordingly. As long as one convention is used throughout, no differences in the final conclusions arise.

$$k_{t,pseudo} = \sum_{i=1}^{6}\sum_{j=1}^{6} k_{tij}\phi_i^*\phi_j^* \qquad 3.24.$$

A common representation of the cross-termination rate constant uses Walling's φ factor. This term has little physical meaning and therefore can be modified (as a parameter) in a relatively new system to achieve adequate results (Jung, 2008).

$$k_{tij} = \varphi\sqrt{k_{tii}k_{tjj}} \qquad 3.25.$$

3.2.4. Chain Transfer Reactions

Pseudo-rate constants are also required for each of the chain transfer reactions to account for differences between monomers. These reactions only have an effect on molecular weight as the reactivity of the growing radical and hence, the rate of propagation, is not affected by the length of the chain.

$$k_{fm,pseudo} = \sum_{i=1}^{6}\sum_{j=1}^{6} k_{fmij}\phi_i^* f_j \quad 3.26.$$

$$k_{fp,pseudo} = \sum_{i=1}^{6}\sum_{j=1}^{6} k_{fpij}\phi_i^* \bar{F}_j \quad 3.27.$$

$$k_{fCTA,pseudo} = \sum_{i=1}^{6} k_{fCTAi}\phi_i^* \quad 3.28.$$

$$k_{fS,pseudo} = \sum_{i=1}^{6} k_{fSi}\phi_i^* \quad 3.29.$$

$$k_{fZ,pseudo} = \sum_{i=1}^{6} k_{fZi}\phi_i^* \quad 3.30.$$

where $\bar{F}_j$ is the accumulated polymer composition of monomer species *j*.

As data is quite scarce for the cross-chain transfer rate constants to monomers and polymer, the model uses straightforward estimations. As such, the following approximations employed are reasonable.

$$k_{fmij} = \frac{k_{fmii}}{r_{ij}} \quad 3.31.$$

$$k_{fpij} = k_{fpii} \quad 3.32.$$

3.2.5. Depropagation

Depropagation is the reverse propagation reaction. It only occurs in significant amounts at elevated temperatures and is considered negligible elsewhere. This can be depicted by explaining Gibbs free energy throughout a polymerization reaction

$$\Delta G_p = \Delta H_p - T\Delta S_p \quad 3.33.$$

where ΔH_p and ΔS_p are the change in enthalpy and entropy, respectively.

Propagation occurs when ΔG_p is negative. This is generally easy enough to obtain as a polymerization (propagation) reaction is highly exothermic and therefore has a large negative enthalpy. The change in entropy is also negative as each propagation reaction removes degrees of freedom. With both enthalpy and entropy negative, the reaction is only spontaneous depending on the temperature of the system. An approximation of the ceiling temperature, the point of equilibrium where $\Delta G_p = 0$, can be reached by using order of magnitudes (Jung, 2008).

The reversible propagation reaction is shown in equation 3.34 and the modified rate of polymerization is as follows:

$$R_r^* + M \leftrightarrow R_{r+1}^* \tag{3.34.}$$

$$R_p = k_p[R^*][M] - \overline{k_p}[R^*] = k_p^{eff}[R^*][M] \tag{3.35.}$$

$$k_p^{eff} = k_p - \frac{\overline{k_p}}{[M]} \tag{3.36.}$$

where $\overline{k_p}$ and k_p^{eff} are the depropagation rate constant and the effective propagation rate constant, respectively.

As can be seen, at high monomer concentrations k_p^{eff} will approach k_p. This is intuitive as an increase in the amount of monomers would shift the balance to the right side of the reaction, acting as a driving force for propagation. Equilibrium occurs at a specific monomer concentration forcing $k_p^{eff} = 0$.

$$K_{eq} = \frac{k_p}{\overline{k_p}} = \frac{1}{[M]_{eq}} \tag{3.37.}$$

The fact that equilibrium occurs at a finite monomer concentration implies that a system where depropagation is present in every monomer never reaches full conversion.

The method used to model this phenomenon is Krüger's probabilistic approach (Krüger *et al.*, 1987 and Leamen, 2005). Through material balances and reaction probabilities, it can describe depropagation of any or all monomers in the system.

In a six monomer system, 72 reactions now take place: the original 36 propagation reactions as well as the 36 depropagation reactions.

$$\begin{array}{cccc} R_1^* + M_1 \leftrightarrow R_{11}^* & R_2^* + M_1 \leftrightarrow R_{21}^* & \dots & R_6^* + M_1 \leftrightarrow R_{61}^* \\ R_1^* + M_2 \leftrightarrow R_{12}^* & R_2^* + M_2 \leftrightarrow R_{22}^* & \dots & R_6^* + M_2 \leftrightarrow R_{62}^* \\ \vdots & \vdots & \dots & \vdots \\ R_1^* + M_6 \leftrightarrow R_{16}^* & R_2^* + M_6 \leftrightarrow R_{26}^* & \dots & R_6^* + M_6 \leftrightarrow R_{66}^* \end{array}$$

The amended monomer and radical balances are shown following.

$$R_{pj} = -\frac{d[M_j]}{dt} = \sum_{i=1}^{6} k_{pij}[R_i^*][M_j] - \sum_{i=1}^{6} \bar{k}_{pij}[R_{ij}^*] \qquad 3.38.$$

$$\frac{d[R_j^*]}{dt} = \sum_{\substack{i=1 \\ i\neq j}}^{6} \left(k_{pij}[R_i^*][M_j] + \bar{k}_{pji}[R_{ji}^*]\right) - \sum_{\substack{i=1 \\ i\neq j}}^{6} \left(k_{pji}[R_j^*][M_i] + \bar{k}_{pij}[R_{ij}^*]\right) \qquad 3.39.$$

Although the earlier terminal model assumption only required the final monomer unit on the chain, now we require knowledge of the penultimate unit as well. As deduced from the name of the approach, Krüger's method uses reaction probabilities to determine the penultimate unit. In other words, the likelihood of the radical concentration of type *j*, $[R_j^*]$, being attached to a monomer of type *i* (in the penultimate unit), $[R_{ij}^*]$, is P_{ij}.

$$P_{ij} = \frac{[R_{ij}^*]}{[R_j^*]} \qquad 3.40.$$

where $[R_j^*] = \sum_{i=1}^{6}[R_{ij}^*]$.

Therefore, the earlier balances can now be rewritten replacing $[R_{ij}^*]$, with $P_{ij}[R_j^*]$.

$$R_{pj} = -\frac{d[M_j]}{dt} = \sum_{i=1}^{6} k_{pij}[R_i^*][M_j] - \sum_{i=1}^{6} \bar{k}_{pij}P_{ij}[R_j^*] \qquad 3.41.$$

$$\frac{d[R_j^*]}{dt} = \sum_{\substack{i=1 \\ i\neq j}}^{6} \left(k_{pij}[R_i^*][M_j] + \bar{k}_{pji}P_{ji}[R_i^*]\right) - \sum_{\substack{i=1 \\ i\neq j}}^{6} \left(k_{pji}[R_j^*][M_i] + \bar{k}_{pij}P_{ij}[R_j^*]\right) \qquad 3.42.$$

Again, under the LCA-II, $\frac{d[R_j^*]}{dt} \approx 0$. With some rearranging, P_{ij} can be shown to be as follows (for a more extensive derivation of the entire depropagation section, see Jung, 2008).

$$P_{ij} = \frac{k_{pij}[R_i^*][M_j] - \bar{k}_{pij}P_{ij}[R_j^*]}{\sum_{l=1}^{6} k_{plj}[R_l^*][M_j] - \sum_{l=1}^{6} \bar{k}_{plj}P_{lj}[R_j^*]} \quad 3.43.$$

Matrix algebra is used again to solve for the radical fractions where $M \cdot r = b$. Numerical methods are thus required to solve $M \cdot r = b$ and determine the radical fractions throughout each step of the reaction simulation. With the radical fractions and penultimate unit probabilities determined, the monomer balances as well as output calculations (conversion, polymer composition, etc.) can be solved as before. The cross-depropagation rate constants used above are estimated from co-polymerization data or are taken from literature quite similarly to the method of obtaining propagation rate constants (Jung, 2008).

3.2.6. Diffusion-Control Kinetics

It is evident that in many polymerization reactors a distinct point occurs where the speed of polymerization increases significantly. This is generally known as auto-acceleration but also goes by several other names. Some polymerizations also exhibit a phenomenon where the reaction hits a limiting conversion plateau and propagation stops altogether. This is known as the glass-transition effect. These occur because of diffusion limitations within the reaction mixture.

As the reaction proceeds, the viscosity of the mixture increases due to the increasing number of polymer chains until a point where the chains are limited in movement, consequently decreasing termination. Small molecules like monomers are still mobile and propagation proceeds as normal. With fewer radicals being terminated, the rate of polymerization increases. These events describe auto-acceleration. If diffusion limitations become so great that even monomers and initiators have trouble moving around, then propagation will cease and one can observe the glass-transition effect.

The method selected to describe diffusion within polymerization reactors is the free volume approach. It defines a free volume for each species in the reaction (monomer, polymer and solvent) and determines the total free volume for the reaction. It then uses critical free volumes to determine the onset of diffusion.

$$V_f = \sum_{i=1}^{n} \left[V_{f,i}^0 + \propto_i (T - T_{g,i})\right] \frac{V_i}{V} \quad 3.44.$$

where i is the component explained, $V_{f,i}^0$ is the free volume of component i, $\propto_i$ is the thermal expansion coefficient, T is the reaction temperature, $T_{g,i}$ is the glass transition temperature of component i, V_i is the volume of component i, and V is the total reaction volume. The accepted values for $V_{f,i}^0$and $\propto_i$ where adequate data do not exist are 0.025 and 0.001 for both monomers and solvents, respectively. $V_{f,i}^0$and $\propto_i$ are both 0.00048 for polymer chains.

The glass transition temperature of the monomer and solvent are usually well known. To determine the glass transition temperature of the polymer, Johnston's method is employed.

$$\frac{1}{T_{g,poly}} = \sum_{i=1}^{6} \frac{w_i p_{ii}}{T_{gpi}} + \sum_{i=1}^{6} \sum_{\substack{j=1 \\ i \neq j}}^{6} \frac{w_i p_{ij} + w_j p_{ji}}{T_{gpij}} \qquad 3.45.$$

where T_{gpi} is the glass transition temperature for the homo-polymer of i (known), T_{gpij} is the glass transition temperature of a perfectly alternating co-polymer of i and j, w_i is the weight fraction of monomer i bound to polymer chains and p_{ij} is the probability of forming a dyad of monomers *i and j*. The probability of forming a dyad is explained in the sequence length distribution section (section 3.3.4).

Although seemingly only a minor part of a larger diffusion control scheme, the glass transition temperature of the alternating co-polymer can have a considerable impact on the model. Using experimental data from Dubé *et al.* (2002), Figure 3.4 shows the simulation with the original 77°C for the glass transition temperature of the alternating co-polymer of MMA/BA, whereas Figure 3.5 shows the simulation with a slightly decreased T_{gpij} of 69°C. One can see the relative importance the glass transition temperature can have on the model and on producing accurate simulations.

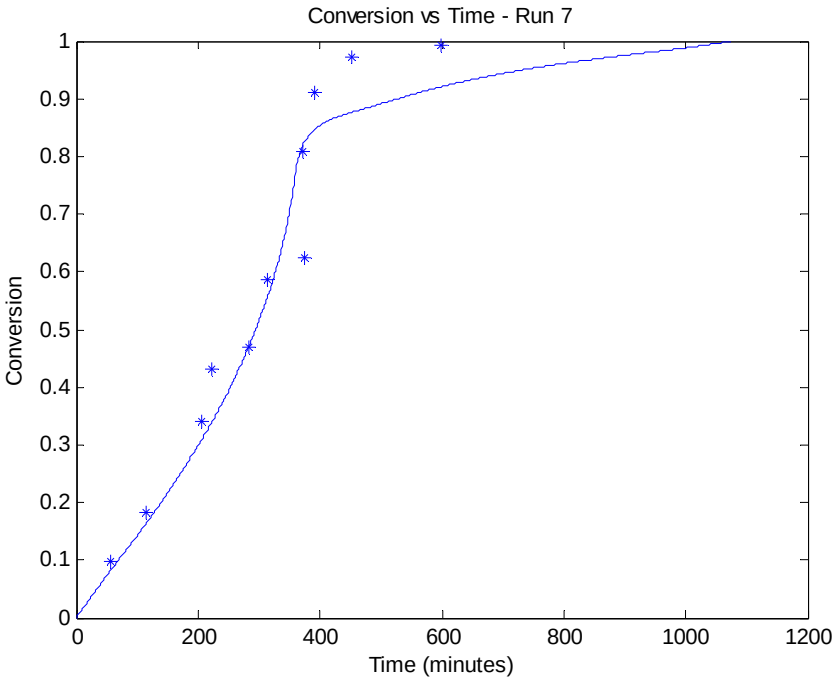

Figure 3.4: Simulation of the co-polymerization of MMA/BA T = 90°C $[dTBPO]_0$ = 0.045M f_{BA0} = 0.148 with T_{gpij} = 77°C

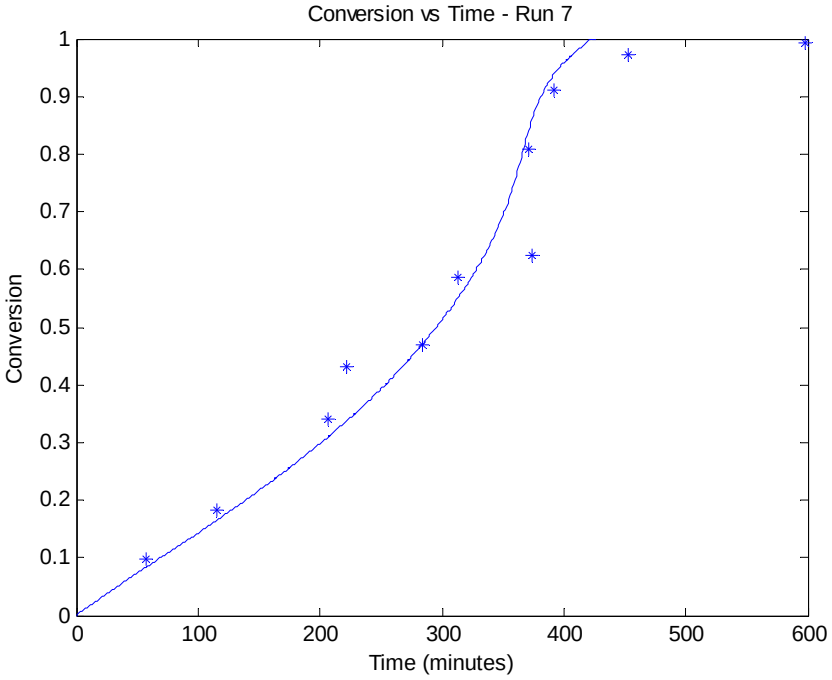

Figure 3.5: Simulation of the co-polymerization of MMA/BA T = 90°C $[dTBPO]_0$ = 0.045M f_{BA0} = 0.148 with T_{gpij} = 69°C

A complete discussion of the modeling of diffusion-control kinetics can be found in section 3.3 in Jung (2008).

3.2.7. Backbiting and β-Scission of Butyl Acrylate

Backbiting and beta-scission is a relatively new addition to the software; as such, this section will be completed in quite some detail. Backbiting occurs when the propagating secondary radical extracts a hydrogen atom from the pen-penultimate position. This is depicted in Figure 3.6. A tertiary or midchain radical, Q_r*, remains to continue propagating at a slower rate.

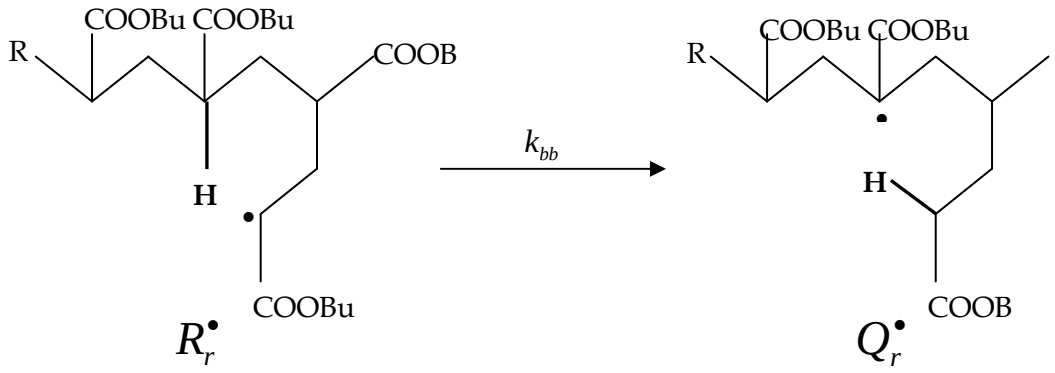

Figure 3.6: Backbiting of Butyl Acrylate

$$R_{bb} = k_{bb}[R^*] \qquad 3.46.$$

The driving force for backbiting is that the tertiary radical formed is more stable even at ambient temperatures (Willemse *et al.*, 2005 and Nikitin *et al.*, 2007). Barth *et al.* (2009) determined the concentration of midchain radicals (MCR) at ambient temperatures taken at very low conversion, shown in Figure 3.7.

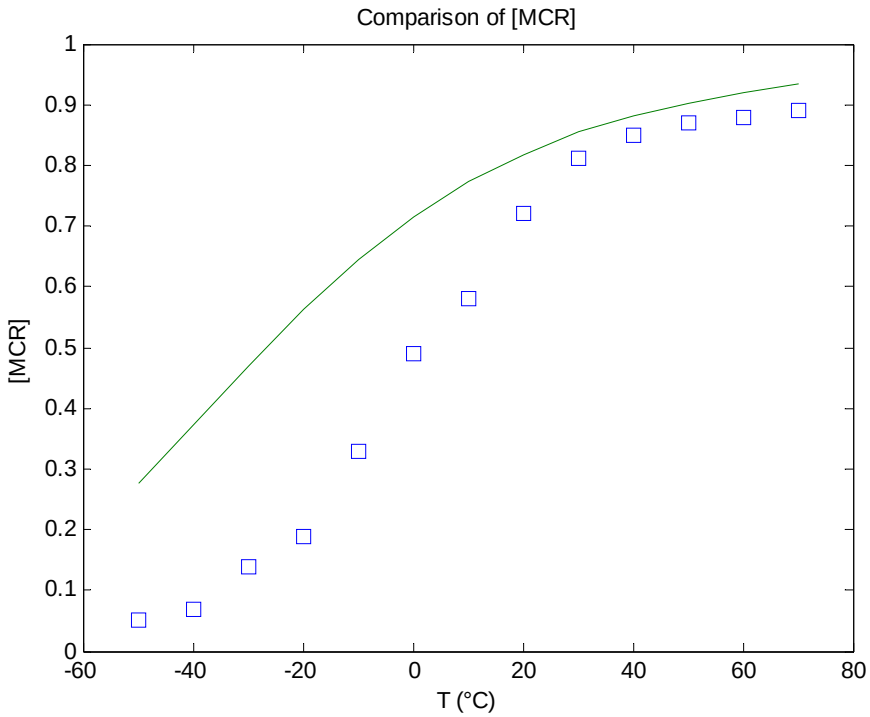

Figure 3.7: Concentration of midchain radicals over a range of temperatures

The simulation performs very well at temperatures above 20°C, which is the most common temperature range. From Figure 3.7, it is evident that backbiting is ever present and very important at all polymerization temperatures.

The midchain radical formed via backbiting can combine with a monomer, beta-fragment or terminate; chain transfer is assumed negligible because of the lack of kinetic parameters and as a means to simplify the model.

Propagation of the tertiary radical creates a new backbone leaving the existing chain portion as a short-chain branch (SCB). The propagating radical after reacting with a monomer is now assumed to exhibit secondary radical kinetics, hence using R^* instead of Q^*.

$$Q_r^* + M \xrightarrow{k_p^{tert}} R_{r+1}^* \qquad 3.47.$$

$$R_p^{tert} = k_p^{tert}[Q^*][M] \qquad 3.48.$$

Beta-scission usually occurs at 140°C and above (Rantow *et al.*, 2006). This is when the tertiary radical splits at the beta position leaving a dead polymer chain with a terminal bond and a radical of length two. This phenomenon significantly affects the molecular weight of

the polymer. The reverse scenario, where a dead trimer and a long chain radical is formed, is deemed nonexistant due to lack of short-chained species detected by ESI-FTMS spectral analysis (Grady *et al.*, 2002).

$$Q_r^* \xrightarrow{k_\beta} P_{r-2} + R_2^* \tag{3.49.}$$

$$R_{beta} = k_{beta}[Q^*] \tag{3.50.}$$

The tertiary radical might also undergo termination, either with a fellow tertiary radical or with the more common secondary radical. Disproportionation and combination are both possible but unlike secondary radicals, tertiary radicals are more likely to terminate via disproportionation (Moad and Solomon, 1995). The termination by combination ratios (to overall termination) for secondary-secondary, secondary-tertiary, and tertiary-tertiary radicals are assumed as 0.9, 0.3, and 0.1, respectively, following suggestions by Peck and Hutchinson (2004).

$$Q_r^* + R_s^* \xrightarrow{k_{tc}^{tert-sec}} P_{r+s} \; \boldsymbol{or} \; \xrightarrow{k_{td}^{tert-sec}} P_r + P_s \tag{3.51.}$$

$$Q_r^* + Q_s^* \xrightarrow{k_{tc}^{tert-tert}} P_{r+s} \; \boldsymbol{or} \; \xrightarrow{k_{td}^{tert-tert}} P_r + P_s \tag{3.52.}$$

$$R_t^{tert} = k_t^{tert-sec}[Q^*][R^*] + k_t^{tert-tert}[Q^*]^2 \tag{3.53.}$$

An extended mechanistic model for BA solution homo-polymerization in a batch/semi-batch reactor at elevated temperatures was developed following Rantow *et al.* (2006). The i^{th} moment equations of secondary/tertiary radicals (λ_i and δ_i, respectively) and dead polymer molecules (μ_i) are defined as:

$$\lambda_i = \sum_{r=3}^{\infty} r^i [R_r^*] \tag{3.54.}$$

$$\delta_i = \sum_{r=3}^{\infty} r^i [Q_r^*] \tag{3.55.}$$

$$\mu_i = \sum_{r=3}^{\infty} r^i [P_r] \tag{3.56.}$$

where *r* represents the chain length, starting at three.

The secondary and tertiary radicals exist as distinguishable entities in the system because of different reactivities. Radical balances with short chain lengths (0, 1, and 2) will also be included separately for determining other microstructure features, such as the number of short chain branches per chain (SCB) and the number of terminal double bonds per chain (TDB). This is why chain lengths start at three in the moment equations above. An additional feature is the assumption that BA self-initiates. Without any direct evidence, Rantow *et al.* (2006) assumed the thermal initiation of butyl acrylate at elevated temperatures and produced favorable results, thus it is included in the model. This was more recently confirmed by Zorn *et al.* (2009). With the additional complexity arising from the backbiting and beta-scission reactions, the monomer and radical balances are revisited below:

$$\frac{dN_{BA}}{dt} = F_{BA,in} - 2k_{th}[M]^2V - k_p([R_0^*] + [R_1^*] + [R_1^*]^{TDB} + [R_2^*] + \lambda_0)N_{BA} - k_p^{tert}\delta_0 N_{BA} - k_{fm}\lambda_0 N_{BA} \quad 3.57.$$

$$\frac{d[R_0^*]}{dt} = 2fk_d[I] + k_{fs}\lambda_0[S] - k_p[R_0^*][M] \quad 3.58.$$

$$\frac{d[R_1^*]}{dt} = 2k_{th}[M]^2 + k_p[R_0^*][M] - k_p[R_1^*][M] \quad 3.59.$$

$$\frac{d[R_2^*]}{dt} = k_p[R_1^*][M] + k_\beta\delta_0 + k_p[R_1^*]^{TDB}[M] - k_p[R_2^*][M] \quad 3.60.$$

$$\frac{d[R_1^*]^{TDB}}{dt} = k_{fm}\lambda_0[M] - k_p[R_1^*]^{TDB}[M] \quad 3.61.$$

$$\frac{d[TDB]}{dt} = k_\beta\delta_0 + k_p[R_1^*]^{TDB}[M] \quad 3.62.$$

$$\frac{d[SCB]}{dt} = k_p^{tert}\delta_0[M] \quad 3.63.$$

where:

N_{BA} moles of butyl acrylate monomer

$F_{BA,in}$ molar flowrate of BA in a semi-batch reactor

k_{th}	spontaneous initiation rate constant of BA
$[R_0^*]$	molar concentration of radicals of chain length zero (initiator decomposition)
$[R_1^*]$	molar concentration of radicals of chain length one
$[R_1^*]^{TDB}$	molar concentration of radicals of chain length one with a terminal double bond
$[R_2^*]$	molar concentration of radicals of chain length two
[TDB]	molar concentration of molecules with terminal double bonds
[SCB]	molar concentration of molecules with short chain branches

Additionally, the zeroth, first and second moments of secondary radicals, tertiary radicals and dead polymer molecules are shown following:

$$\frac{d\lambda_0}{dt} = k_p[R_2^*][M] + k_p^{tert}\delta_0[M] - \left(k_{bb} + k_{fm}[M] + k_{fS}[S]\right)\lambda_0 - (k_{tc} + k_{td}){\lambda_0}^2 - (k_{tc}^{tert-sec} + k_{td}^{tert-sec})\delta_0\lambda_0 \quad 3.64.$$

$$\frac{d\lambda_1}{dt} = 2fk_d[I] + k_p([R_2^*] + \lambda_0)[M] + k_p^{tert}\delta_1[M] - \left(k_{bb} + k_{fm}[M] + k_{fS}[S]\right)\lambda_1 - (k_{tc} + k_{td})\lambda_0\lambda_1 - (k_{tc}^{tert-sec} + k_{td}^{tert-sec})\delta_0\lambda_1 \quad 3.65.$$

$$\frac{d\lambda_2}{dt} = 2fk_d[I] + k_p([R_2^*] + \lambda_0 + 2\lambda_1)[M] + k_p^{tert}\delta_2[M] - \left(k_{bb} + k_{fm}[M] + k_{fS}[S]\right)\lambda_2 - (k_{tc} + k_{td})\lambda_0\lambda_2 - (k_{tc}^{tert-sec} + k_{td}^{tert-sec})\delta_0\lambda_2 \quad 3.66.$$

$$\frac{d\delta_0}{dt} = k_{bb}\lambda_0 - \left(k_p^{tert}[M] + k_\beta\right)\delta_0 - (k_{tc}^{tert-tert} + k_{td}^{tert-tert}){\delta_0}^2 - (k_{tc}^{tert-sec} + k_{td}^{tert-sec})\lambda_0\delta_0 \quad 3.67.$$

$$\frac{d\delta_1}{dt} = k_{bb}\lambda_1 - \left(k_p^{tert}[M] + k_\beta\right)\delta_1 - (k_{tc}^{tert-tert} + k_{td}^{tert-tert})\delta_0\delta_1 - (k_{tc}^{tert-sec} + k_{td}^{tert-sec})\lambda_0\delta_1 \quad 3.68.$$

$$\frac{d\delta_2}{dt} = k_{bb}\lambda_2 - \left(k_p^{tert}[M] + k_\beta\right)\delta_2 - (k_{tc}^{tert-tert} + k_{td}^{tert-tert})\delta_0\delta_2 - (k_{tc}^{tert-sec} + k_{td}^{tert-sec})\lambda_0\delta_2 \quad 3.69.$$

$$\frac{d\mu_0}{dt} = \left(k_{fm}[M] + k_{fS}[S]\right)\lambda_0 + k_\beta\delta_0 + (k_{td} + 0.5k_{tc}){\lambda_0}^2 + 2(k_{td}^{tert-sec} + 0.5k_{tc}^{tert-sec})\lambda_0\delta_0 + (k_{td}^{tert-tert} + 0.5k_{tc}^{tert-tert}){\delta_0}^2 \quad 3.70.$$

$$\frac{d\mu_1}{dt} = \left(k_{fm}[M] + k_{fS}[S]\right)\lambda_1 + k_\beta\delta_1 + (k_{td} + k_{tc})\lambda_0\lambda_1 + (k_{td}^{tert-sec} + k_{tc}^{tert-sec})(\lambda_0\delta_1 + \lambda_1\delta_0) + (k_{td}^{tert-tert} + k_{tc}^{tert-tert})\delta_0\delta_1 \quad 3.71.$$

$$\frac{d\mu_2}{dt} = \left(k_{fm}[M] + k_{fS}[S]\right)\lambda_2 + k_\beta\delta_2 + k_{tc}\left(\lambda_0\lambda_2 + {\lambda_1}^2\right) + k_{td}\lambda_0\lambda_2 + k_{tc}^{tert-sec}(\lambda_0\delta_2 + 2\lambda_1\delta_1 + \lambda_2\delta_0) + k_{td}^{tert-sec}(\lambda_0\delta_2 + \lambda_2\delta_0) + k_{tc}^{tert-tert}\left(\delta_0\delta_2 + {\delta_1}^2\right) + k_{td}^{tert-tert}\delta_0\delta_2 \quad 3.72.$$

Using the moment equations and monomer and radical balances, the number of (short) chain branches per chain, CBC, and the number of terminal double bonds per chain, TDBC, can be calculated:

$$CBC = \frac{[SCB]}{\mu_1} \quad 3.73.$$

$$TDBC = \frac{[TDB]}{\mu_1} \quad 3.74.$$

Molecular weight, conversion and other reaction outputs are calculated in the standard fashion (see section 3.3, Reaction Outputs). The kinetic parameters for butyl acrylate (backbiting and beta-scission included) can be found in the monomer database within the appendices. Several case studies of butyl acrylate at elevated temperatures discussed later demonstrate the accuracy of the model's ability to simulate the backbiting and beta-fragmentation phenomena.

3.3. Reaction Outputs

Virtually anything can be set as an output and produced either as a final result, in tabulated values for the course of the reaction, or displayed pictorially usually against time or conversion. Of the obvious choices, conversion, polymer composition, molecular weight, sequence length and dyad/triad fractions are determined, however, monomer flowrates, volume, parameter values, polymerization rates, radical and monomer concentrations and monomer feed ratios as well as others can also be presented with ease.

3.3.1. Conversion

One of the most commonly desired simulation outputs is conversion. It is computed quite easily as the amount of monomer reacted divided by the total amount entered (being the initial amount entered in batch cases):

$$X = \frac{[M]_0 - [M]}{[M]_0} = \frac{\sum_{i=1}^{6} P_i}{\sum_{i=1}^{6}(N_i + P_i)} \qquad 3.75.$$

where P_i is the number of moles of monomer species i bound as polymer. Partial conversion is calculated in a similar fashion:

$$X_i = \frac{P_i}{N_i + P_i} \qquad 3.76.$$

3.3.2. Polymer Composition

An instantaneous polymer composition equation for hexa-polymerization cases has been developed after the Mayo-Lewis (co-polymer), Alfrey-Goldfinger (ter-polymer) and Wallings-Briggs (ter- and higher) equations by Jung (2008):

$$F_i = \frac{dN_i}{\sum_{i=1}^{6}(dN_i)} = \frac{R_{pi}}{R_p} = \frac{\sum_{j=1}^{6} R_{ji}}{\sum_{i=1}^{6}\sum_{j=1}^{6} R_{ji}} = \frac{\sum_{j=1}^{6}(k_{pji}\phi_j^*)f_i}{\sum_{j=1}^{6}\sum_{i=1}^{6}(k_{pji}\phi_j^*)f_i} \qquad 3.77.$$

Polymer composition is highly dependent on the monomer reactivity ratios. A large difference in ratios will induce a phenomenon known as 'compositional drift', whereby the more reactive monomer will be consumed early on in the reaction leaving only the less reactive monomer present in the final stages of the reaction. Realistically, a large enough difference would create almost two (successive) homo-polymerizations instead of a co-polymerization. Reactivity ratios, under the terminal model, are defined as the ratio of the homo-propagation rate constant to the cross-propagation rate constant:

$$r_{ij} = \frac{k_{pii}}{k_{pij}} \tag{3.78.}$$

where i refers to the radical species and j to the monomer species; $i \neq j$.

The accurate determination of these ratios is quite crucial in modeling polymer composition. In order to avoid compositional drift, the experiments undertaken to estimate the reactivity ratios are stopped at conversion levels less than 5%. The initial co-polymer compositions are determined through NMR and the ratios are estimated by nonlinear least-squares or Error-in-Variables-Model (EVM) techniques.

The accumulated polymer composition is measured over the course of the reaction to show how the amount of monomer reacted changes:

$$\bar{F}_i = \frac{P_i}{\sum_{i=1}^{6} P_i} \tag{3.79.}$$

3.3.3. Molecular Weight and Branching

The method of moments is used to determine the cumulative number- and weight-average molecular weights as well as the tri- and tetra-functional branches per molecule. A basic explanation of the *ith* moment of polymer distribution, μ_i, and radical distribution, λ_i is shown following:

$$\mu_i = \sum_{r=1}^{\infty} r^i \, [P_r] \tag{3.80.}$$

$$\lambda_i = \sum_{r=1}^{\infty} r^i \, [R_r^*] \tag{3.81.}$$

The zeroth, first and second order moments of each of the distributions are then determined. The complete derivation can be found in Jung (2008) or a simplified derivation (with backbiting present) can be found in section 3.2.7. The cumulative number- and weight-average molecular weights are then determined as:

$$\bar{M}_n = Mw_{eff} \frac{\mu_1}{\mu_0} \tag{3.82.}$$

$$\bar{M}_w = Mw_{eff} \frac{\mu_2}{\mu_1} \tag{3.83.}$$

$$Mw_{eff} = \sum_{i=1}^{6}\left[Mw_i\left(\frac{R_{pi}}{R_p}\right)\right] = \sum_{i=1}^{6} Mw_i F_i \qquad 3.84.$$

The average number of tri- and tetra-functional branches per molecule is found by using these equations from Dubé *et al.* (1991).

$$\frac{d(V\mu_0\overline{B_{N3}})}{dt} = \left(k_{fp}\mu_1 + k_p^*\mu_0\right)\lambda_0 V \qquad 3.85.$$

$$\frac{d(V\mu_0\overline{B_{N4}})}{dt} = k_p^{**}\mu_2\lambda_0 V \qquad 3.86.$$

3.3.4. Sequence Length

Not only the polymer composition but also the average sequence length of each monomer type also portrays valuable information about the final polymer's properties. For example, a block co-polymer (A-A$_n$-A-B-B$_n$-B-A-A$_n$-A…) and an alternating co-polymer (A-B-A-B-A-B-…) can have identical polymer compositions but will have widely differing sequence length distributions (and properties affected by sequence length). The information gathered from both will be essential in determining the finer steps of the polymerization as well as what properties can be expected from the initial monomers added.

A statistical approach from Koenig (1980) is implemented in the model with the full derivation found in Jung (2008).

3.3.5. Dyad/Triad Fractions

The probability of forming a dyad (also from Koenig, 1980), is explained as the probability of a monomer species *j* reacting with a polymer chain ending with unit *i*, and is given by

$$p_{ij} = \frac{k_{pij}[R_i^*][M_j]}{\sum_{i=1}^{6} k_{pij}[R_i^*][M_j]} = \frac{k_{pij}[M_j]}{\sum_{i=1}^{6} k_{pij}[M_j]} = \frac{k_{pij}f_j}{\sum_{i=1}^{6} k_{pij}f_j} \qquad 3.87.$$

The probability of forming a triad fraction is simply the likelihood of forming two specific dyad fractions in a row:

$$A_{iii} = p_{ii}^2 = \left(\frac{r_{ij}f_i}{f_j + r_{ij}f_i}\right)^2 \qquad 3.88.$$

$$A_{jij} = p_{ij}^2 = \left(\frac{f_j}{f_j + r_{ij}f_i}\right)^2 \neq p_{ji}p_{ij} \quad 3.89.$$

$$A_{iij} = A_{jii} = p_{ii}p_{ij} = p_{ii}(1 - p_{ii}) = \frac{r_{ij}f_i f_j}{\left(f_j + r_{ij}f_i\right)^2} \quad 3.90.$$

In the hexa-polymer case, there are 216 possible triads where only 126 can be distinguished separately. For example, centered on monomer 1, the triad fraction 314 (monomer 3, 1 and 4 added in that order) cannot be distinguished from the triad fraction 413. Performance of our triad fraction simulations can be found in sections 4.5 and 4.6. A complete breakdown of the triad fraction calculation and various simulation results can also be found in Jung (2008).

3.3.6. Extension to Pentad Fractions

An extension to pentad fractions was considered but the amount of coding required was unreasonable and therefore not implemented as of yet. The massive undertaking will be completed once there is greater need of pentad fraction capability. In a six monomer system, there are 7776 possible pentad fractions with 3996 distinguishable fractions.

$$A_{iiiii} = p_{ii}^4 \quad 3.91.$$

$$A_{iiiij} = p_{ii}^3 p_{ij} \quad 3.92.$$

$$A_{iiiji} = p_{ii}^2 p_{ij}^2 \quad 3.93.$$

$$A_{iiijj} = p_{ii}^2 p_{ij} p_{jj} \quad 3.94.$$

$$A_{iijk} = p_{ii}^2 p_{ij} p_{jk} \quad 3.95.$$

…

Cumulative sequence distribution is determined by integration of the instantaneous values. As it cannot be solved analytically, two different approaches (with differing assumptions) have been added into the model. The main difference between the two, one method by Ray (1977) and the other by Hamielec *et al.* (1987a), is that the latter method is normalized potentially leading to more accurate results.

In general, sequence length is affected by the monomer reactivity ratios as well as by the initial monomer feed ratio. Figure 3.8 is the simulation of styrene's number-average

sequence length versus conversion against data from Garcia-Rubio *et al.* (1985). The reactivity ratios for the system come from the same paper: $r_{Sty\text{-}AN} = 0.36$, $r_{AN\text{-}Sty} = 0.078$. With an equal monomer feed ratio ($f_{Sty0} = 0.5$), the polymer chains resemble an alternating co-polymer (-ABABAB-), but when styrene is fed at 90% by weight, block co-polymers (-AAAABBAAA-) are produced instead.

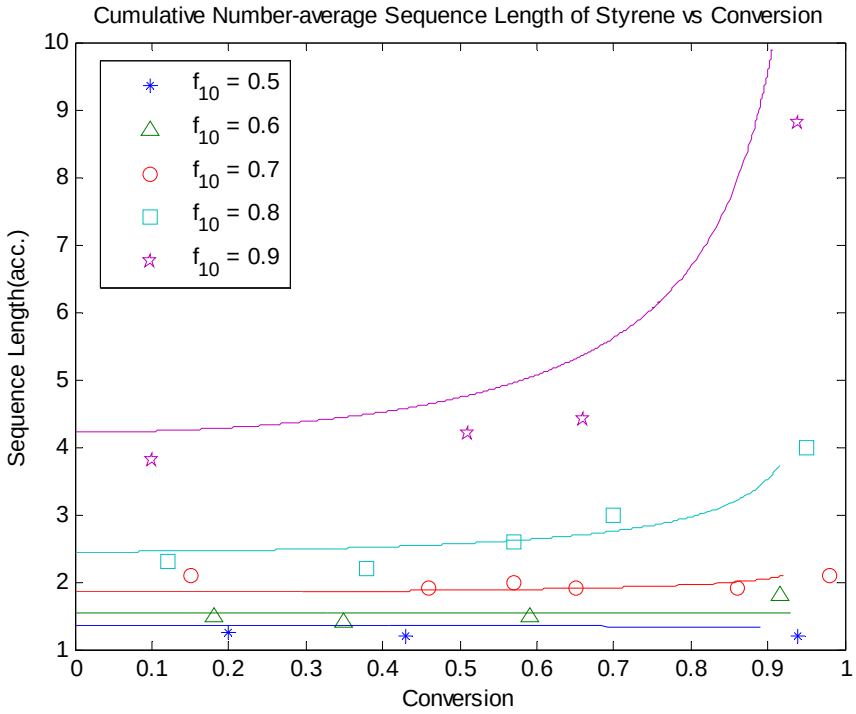

Figure 3.8: Simulation of the co-polymerization of Sty/AN at 60°C $[AIBN]_0 = 0.05$ M

3.4. Model Features/Options

Although mentioned in passing through the earlier sections, the complete model features and options as well as a more thorough list of available outputs is summarized within this section. The model can handle the following configurations/conditions:

1. Homo- up to a hexa-polymerization system
2. Bulk and solution
3. Batch and semi-batch
4. Isothermal and non-isothermal scenarios (where a temperature profile is present)
5. Ideal and diffusion-controlled kinetics
6. Self/thermal initiation of styrenics
7. Branching and cross-linking reactions
8. Depropagation
9. Composition control
10. Multiple initiators
11. Backbiting of butyl acrylate

The following outputs can be generated instantaneously, tabulated over the entire reaction or generated as a figure:

1. Overall and partial conversion
2. Overall and individual rate of polymerization
3. Total reaction volume
4. Monomer and radical species concentrations
5. All other species concentrations (initiator(s), solvent, CTA, inhibitor, etc.)
6. Residual monomer fraction and radical fraction
7. Instantaneous/accumulated polymer composition
8. Instantaneous/accumulated polymer composition distribution
9. Instantaneous/accumulated number- and weight-average molecular weights
10. Instantaneous/accumulated polydispersity index (PDI)
11. Instantaneous/accumulated molecular weight distribution (linear chains only)
12. Instantaneous/accumulated number- and weight-average sequence lengths
13. Sequence length distribution
14. Instantaneous/accumulated triad fractions
15. Number-average tri/tetra-functional branches per molecule
16. Polymer glass-transition temperature and free volume characteristics

17. Pseudo termination/propagation/transfer reaction rate constants and initiator efficiency

3.5. Database Characteristics

Within the database, there are thousands of different combinations of ingredients available. This is due to the large number of monomers accessible within the database. Most of the monomers were archived many years ago and have been significantly refined; as such, they produce excellent results time and time again without changing the ingredient database characteristics. One relatively new monomer to the database is glycidyl methacrylate. These are the monomers available for simulation:

1. Acrylic acid (AA)
2. Acrylontrile (AN)
3. Alpha-methyl styrene (AMS)
4. n-Butyl acrylate (BA)
5. n-Butyl methacrylate (BMA)
6. Ethyl acrylate (EA)
7. Glycidyl methacrylate (GMA)
8. Hydroxyethyl acrylate (HEA)
9. Hydroxyethyl methacrylate (HEMA)
10. Methacrylic acid (MAA)
11. Methyl methacrylate (MMA)
12. Styrene
13. Vinyl acetate (VAc)

The initiators available to our disposal are as follows:

1. Azobisisobutyronitrile (AIBN)
2. Butyl peroxide (BPO)
3. Di-tert-butyl peroxide (dTBPO or Trigonox B)
4. Tert-butyl peroxybenzoate (TBPB or Trigonox C)
5. Tert-butyl peroxyacetate (TBPA or Lupersol 70)

Possible chain transfer agents:

1. Carbon tetrachloride
2. Octanethiol

3. Dodecanethiol

There are four solvents currently available in the modeling package:

1. Toluene
2. Xylene
3. Benzene
4. Ethyl acetate

Finally, the inhibitors present, if required, in the simulations are as follows:

1. Oxygen
2. Benzoquinone

Several more initiators, solvents, chain transfer agents and inhibitors are currently accessible and easily adaptable from the original polymerization modeling software WATPOLY (Gao and Penlidis, 2000). A comprehensive database for monomers, solvents, initiators and chain transfer agents has been prepared and included in the appendices.

4. Model Testing/Troubleshooting

Several examples used to test and perhaps refine the model are shown in the following sections. As this thesis is a continuation of the work completed by Jung (2008), several more polymerizations (see Table 4-1) have been simulated previously in his thesis. With performance under so many different conditions, the model can definitely be considered diverse and effective:

Table 4-1: Previous Model Simulations from Jung (2008)

Homo-polymerization:	AN
	BA
	BMA
	EA
	HEA
	MMA
	Sty
	VAc
Co-polymerization:	BA/MMA
	BA/VAc
	MMA/VAc
	Sty/AN
	Sty/BA
	Sty/EA
	Sty/HEA
Ter-polymerization:	BA/MMA/VAc
	EA/HEA/MAA
	EA/HEA/Sty
	EA/MAA/Sty
Tetra-polymerization:	EA/HEA/MAA/Sty

4.1. Homo-polymerization of Ethyl Acrylate

Van Herk (2009) presents a paper on the history and development of the kinetics of acrylates in free radical polymerization. Two of the acrylates that are discussed, ethyl acrylate and butyl acrylate, are of interest to this modeling software. Table 4-2 gives the parameters found by Van Herk (2009) for these two monomers and Table 4-3 presents the parameters used in the model. There are two interesting observations that one can make while comparing the two tables: one, Van Herk has found parameters that are very similar for the two acrylates, and two, the values between Van Herk and the current database are very close for BA. The propagation rate constants for BA in the database work very well with backbiting and beta-scission phenomena as they represent a much faster propagation rate both at low and high temperatures.

Table 4-2: Propagation Rate Constants of Acrylates from Van Herk (2009)

Monomer	LogA		E_a (kJ/mol)		k_p (mol/L/s)
Ethyl acrylate	7.43		18.59		3300
n-Butyl acrylate	7.44		18.55		3400

Table 4-3: Propagation Rate Constants of Acrylates from Database

Monomer	LogA		E_a (kJ/mol)		k_p (mol/L/s)
Ethyl acrylate (Gao and Penlidis, 1997)	8.70		33.48		45
n-Butyl acrylate (Nikitin *et al.*, 2007)	7.34		17.90		3770

The parameters obtained from Gao and Penlidis (1997) produces a much slower rate of propagation required for polymerizations where backbiting and beta-scission are not hindering the reaction (see section 5.2). Figure 4.1 and Figure 4.2 are simulations of a batch homo-polymerization of EA using the Gao and Penlidis rate constant and Van Herk rate constant, respectively. The experimental data are from Gao *et al.* (1997).

Quite plainly, the propagation rate data from Van Herk in Figure 4.2 is much too fast to model EA at lower temperatures. Ethyl acrylate is much better modeled without backbiting under these conditions.

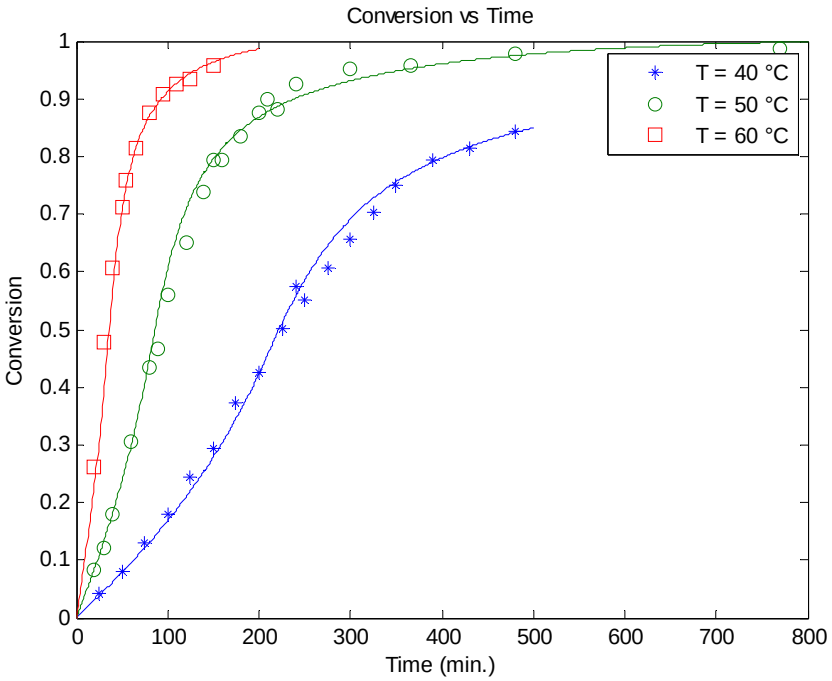

Figure 4.1: Simulation of the batch homo-polymerization of EA $[AIBN]_0$ = 0.0008 M using Gao and Penlidis rate constant

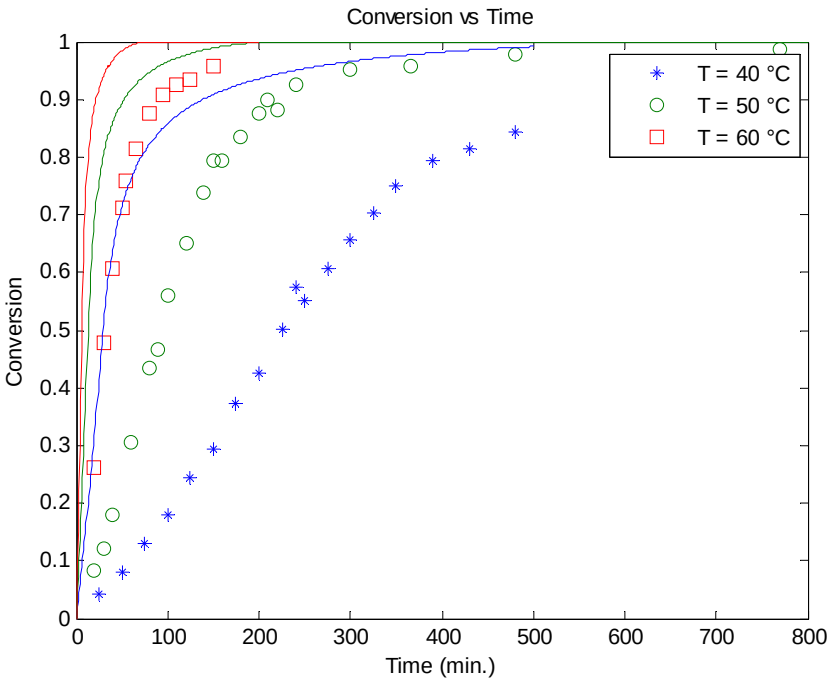

Figure 4.2: Simulation of the batch homo-polymerization of EA $[AIBN]_0$ = 0.0008 M using Van Herk rate constant

4.2. Homo-polymerization of Butyl Methacrylate

Sensitivity is an important issue in modeling. The following example of the homo-polymerization of BMA by Nair and Muthana (1961) explains just that. Upon initiating this project, there were several differences noted with the results produced previously in Jung (2008). The underlying problem was that the model was reaching drastic limiting conversions where no such limitation should be found. Figure 4.3 is a conversion vs. time plot for five different initiator amounts simulated by the software in Jung (2008).

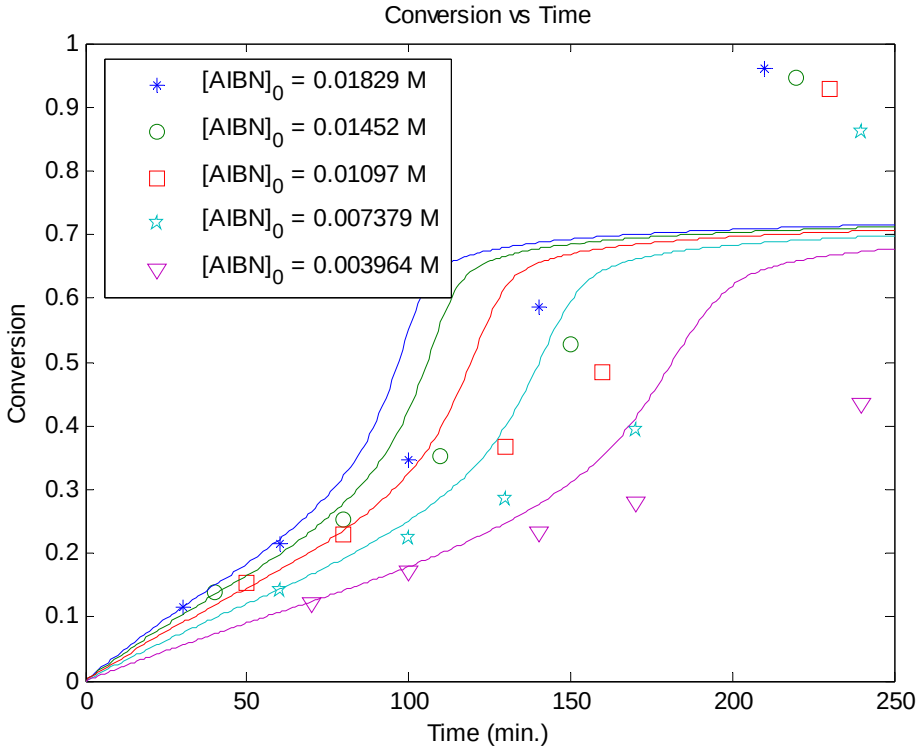

Figure 4.3: Simulation of the homo-polymerization of BMA T = 60°C pre-correction

As one can see, the simulations fail to accurately follow the data past 20% conversion. After analyzing the different calculations that effect diffusion-control kinetics, the typing error in the code became evident. An excerpt of the weight fraction calculation is shown as follows:

```
w1 = P0_1*mw_1/(P0_1*mw_1 + P0_2*mw_2 + P0_3*mw_3 + P0_4*mw_4 + …
w2 = P0_2*mw_1/(P0_1*mw_1 + P0_2*mw_2 + P0_3*mw_3 + P0_4*mw_4 + …
w3 = P0_3*mw_1/(P0_1*mw_1 + P0_2*mw_2 + P0_3*mw_3 + P0_4*mw_4 + …
w4 = P0_4*mw_1/(P0_1*mw_1 + P0_2*mw_2 + P0_3*mw_3 + P0_4*mw_4 + …
w5 = P0_5*mw_1/(P0_1*mw_1 + P0_2*mw_2 + P0_3*mw_3 + P0_4*mw_4 + …
w6 = 1 - w1 - w2 - w3 - w4 - w5;
```

For an unknown reason, the weight fractions of the polymer were calculated erroneously. The difference between the molecular weight of styrene (commonly monomer 1) and BMA had a significant effect. This is logical as the weight fraction of BMA would approach unity (signaling a complete conversion) at approximately 60% conversion. By correcting the obvious mistake, a considerably better simulation is found. This is true not only for Figure 4.4 but also for all premature limiting conversions found before the correction.

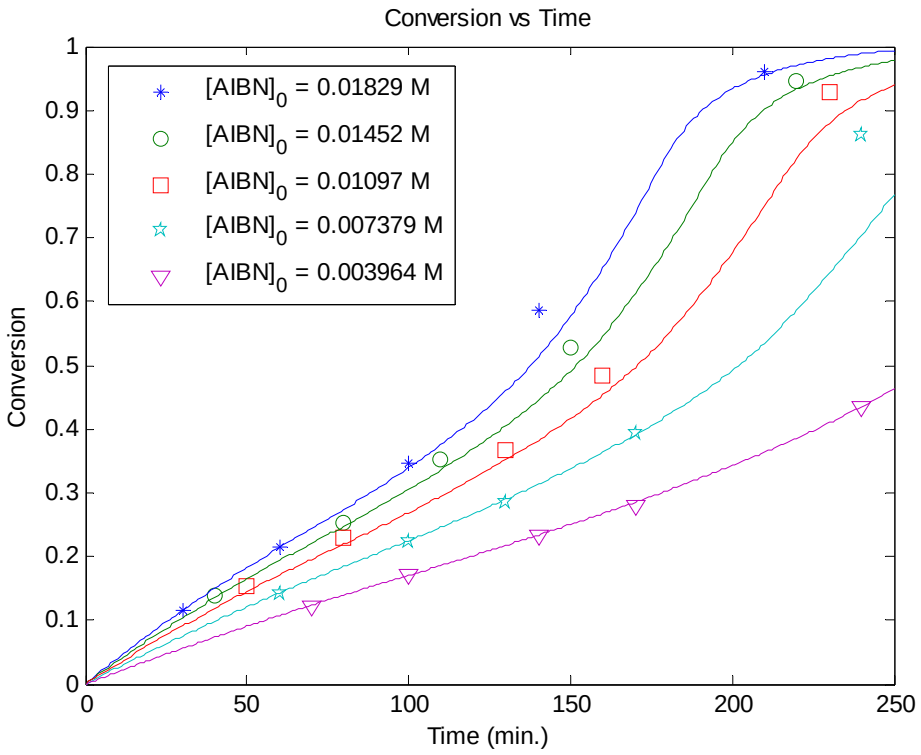

Figure 4.4: Simulation of the homo-polymerization of BMA T = 60°C post-correction

This example of model troubleshooting demonstrates that certain parameters or calculations can be very significant to the overall simulation. A single typing error of a parameter value within a calculation within another calculation all within tens of thousands of lines of code can have a large effect on the model predictions.

4.3. Co-Polymerization of Styrene and Ethyl Acrylate

Abdollahi *et al.* (2007) conducted experiments of the co-polymerization of styrene (Sty) and ethyl acrylate at 70°C in benzene-d_6 solution. Conversion and polymer composition were recorded for five different initial monomer mole fractions, f_{Sty0} = 0.1668, 0.271, 0.548, 0.715, and 0.894, as well as partial conversion for the f_{sty0} = 0.1668 and 0.548 experiments. The reactivity ratios used, $r_{Sty\text{-}EA}$ = 0.717 and $r_{EA\text{-}Sty}$ = 0.128, were previously tested against data reported by McManus and Penlidis (1996) and Sahloul (2004) by the same software (Jung, 2008). They continued to prove accurate even without large amounts of data on the relatively unused solvent benzene. Figure 4.5 is the conversion versus time plot; Figure 4.6 shows the polymer composition of styrene for each of the runs; and Figure 4.7 and Figure 4.8 show the partial monomer conversions for the first and third experiment. Each prediction follows the partial conversion experimental data very well; all the trends are captured regardless of the initial monomer mole fraction.

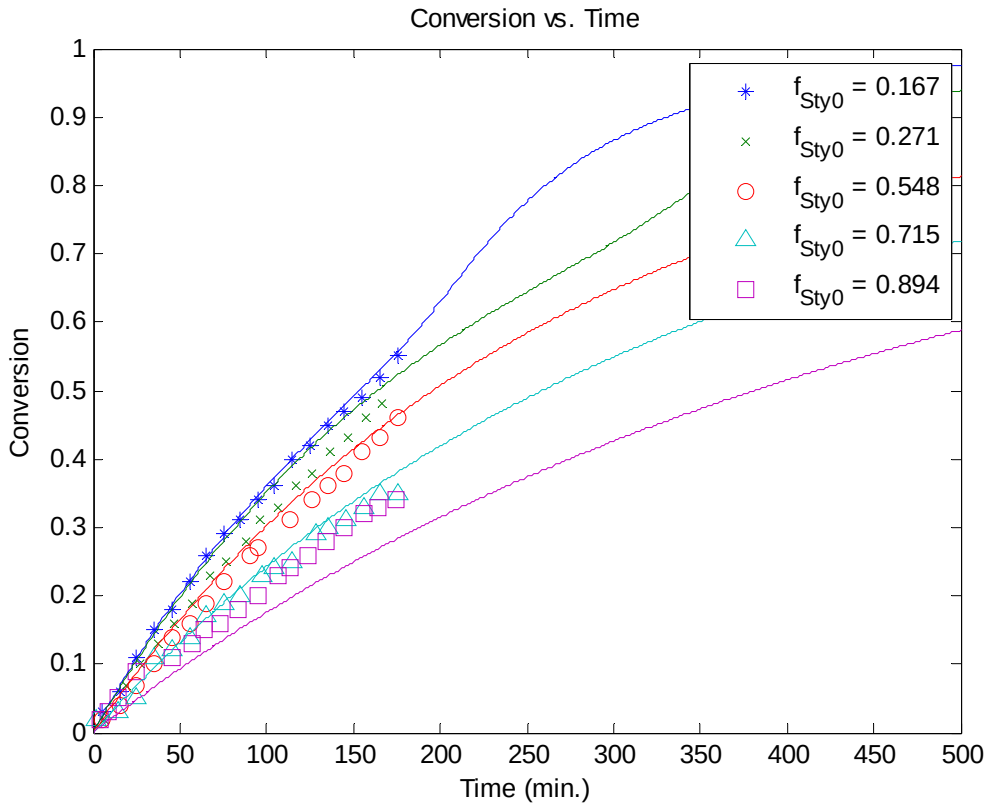

Figure 4.5: Simulation of the co-polymerization of Sty/EA T = 70°C $[BPO]_0$ = 0.045M

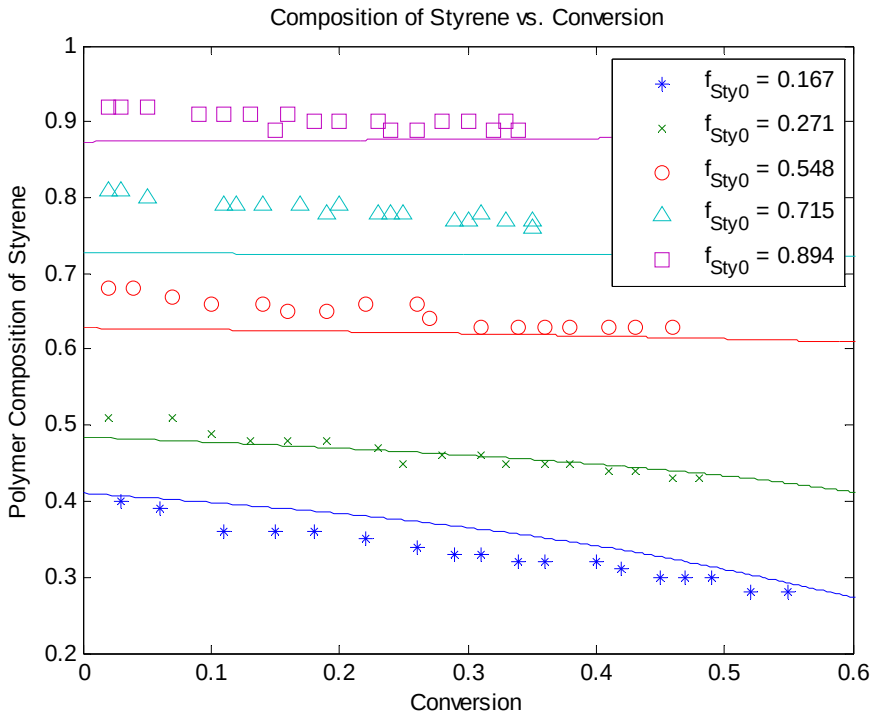

Figure 4.6: Simulation of the co-polymerization of Sty/EA T = 70°C $[BPO]_0$ = 0.045M

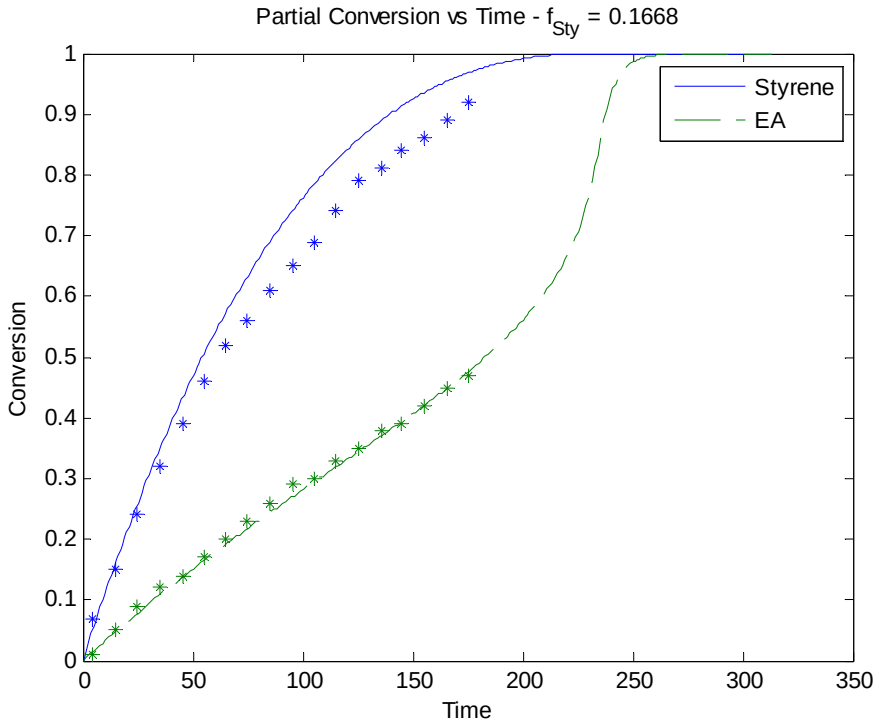

Figure 4.7: Simulation of the co-polymerization of Sty/EA T = 70°C $[BPO]_0$ = 0.045M f_{Sty0} = 0.1668

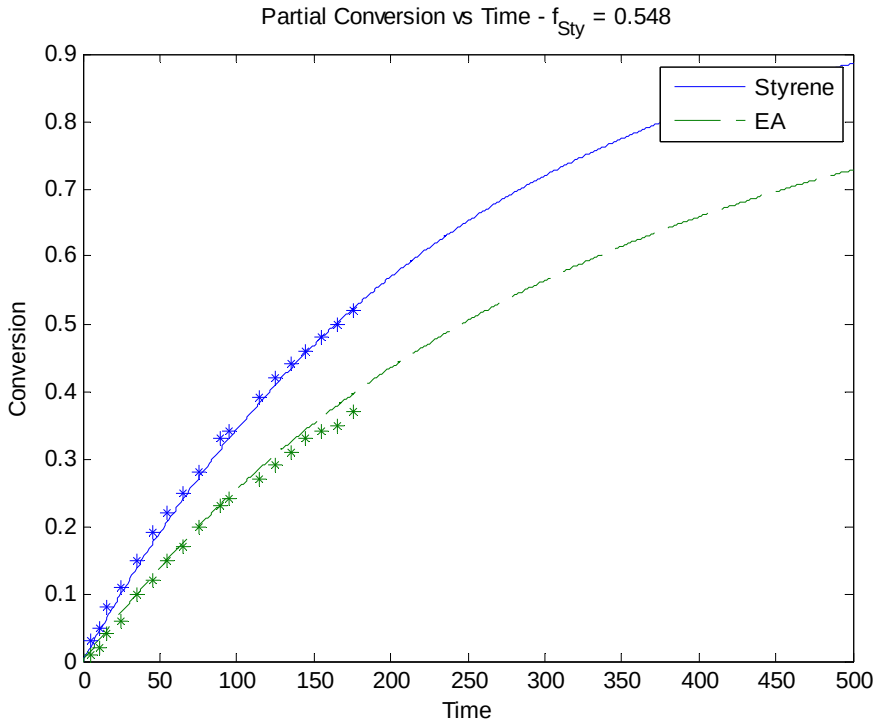

Figure 4.8: Simulation of the co-polymerization of Sty/EA T = 70°C $[BPO]_0$ = 0.047M f_{Sty0} = 0.548

4.4. Co-Polymerization of Methyl Methacrylate and Butyl Acrylate

Methyl methacrylate was co-polymerized with butyl acrylate at 90°C/115°C/140°C using di-tert-butyl peroxide (dTBPO) as an initiator and toluene as a solvent (Dubé *et al.*, 2002). Approximately 0.006M of n-dodecyl mercaptan was used as a chain transfer agent in each of the 18 runs. The reactivity ratios used were taken from an earlier paper by Dubé and Penlidis (1995): $r_{MMA\text{-}BA}$ = 1.78938 and $r_{BA\text{-}MMA}$ = 0.29763. Conversion and polymer composition data were obtained from nearly all of the 18 runs whereas weight-average molecular weight data was only presented for a few of the 90°C runs. Observation of Table 4-4 shows that there are many duplicate reactions: Runs 1/2, 6/7, 10/11, 15/16. As the data was similar and the simulation the same, only one plot of each duplicate is shown in the following analysis.

Table 4-4: Co-polymerization of MMA/BA with dTBPO as initiator and n-dodecyl mercaptan as CTA (Dubé *et al.*, 2002)

Run	Temperature (°C)	f_{MMA0}	Toluene (wt%)	dTBPO (M)
1	90	0.852	30	0.044
2	90	0.852	30	0.045
3	90	0.561	30	0.045
4	90	0.851	23	0.045
5	90	0.561	23	0.045
6	90	0.852	0	0.047
7	90	0.852	0	0.045
8	90	0.745	0	0.046
9	115	0.852	30	0.0062
10	115	0.851	30	0.045
11	115	0.852	30	0.045
12	115	0.852	23	0.0058
13	115	0.561	0	0.0063
14	115	0.852	0	0.0061
15	140	0.852	30	0.00050
16	140	0.852	30	0.00047
17	140	0.852	0	0.00049
18	140	0.745	0	0.00045

Figure 4.9 through Figure 4.20 simply show the conversion versus time prediction against the experimental data for runs 1, 3, 4, 6, 7, 9, 11, 12, 14, 15 and 17. Figure 4.21 through Figure 4.33 are the polymer composition plots for runs 2, 3, 4, 5, 6, 8, 9, 10, 12, 13, 16, 17, and 18. The final three figures, Figure 4.34, Figure 4.35, Figure 4.36, represent the weight-average

molecular weight against conversion for runs 2, 5 and 8. These molecular weight figures show acceptable predictions for the course of the reaction. Each of the conversion and composition simulations proved very accurate under the diverse conditions with the exception of run 17 (see Figure 4.19), where the anticipated reaction proceeded much quicker than shown in the data. One troubleshooting scenario assumed that impurities were present and reacted with a portion of the initiator. Figure 4.20 is the simulation of run 17 with a 76% decrease in initial initiator amount. The final result is quite accurate, however, the difference required to produce such an accurate result is far too large, so there must be another reason at least partially to blame for the discrepancy between the simulation and the data. One possibility is that BA is backbiting, causing the reaction to slow dramatically. This is rarely observed under these conditions as backbiting is much less significant at lower temperatures in a co-polymerization. For a more in-depth explanation of the backbiting phenomenon see section 3.2.7 or the paper by Grady *et al.* (2002).

Depropagation was accounted for in runs 15 through 18 (T = 140°C) as MMA is known to depropagate at elevated temperatures (Leamen, 2005). In terms of depropagation parameters (see section 3.2.5), the data used to model this were given by Leamen (2005): $R_1 = 0$, $R_2 = 0.008$, $R_{11} = 0.085$, $R_{22} = 0$. Basically, R_2 represents the depropagation of MMA from a penultimate unit of BA whereas R_{11} represents the homo-depropagation of MMA. Not only does the reaction proceed much too quickly without depropagation but it reaches complete conversion, a reality that the data do not support.

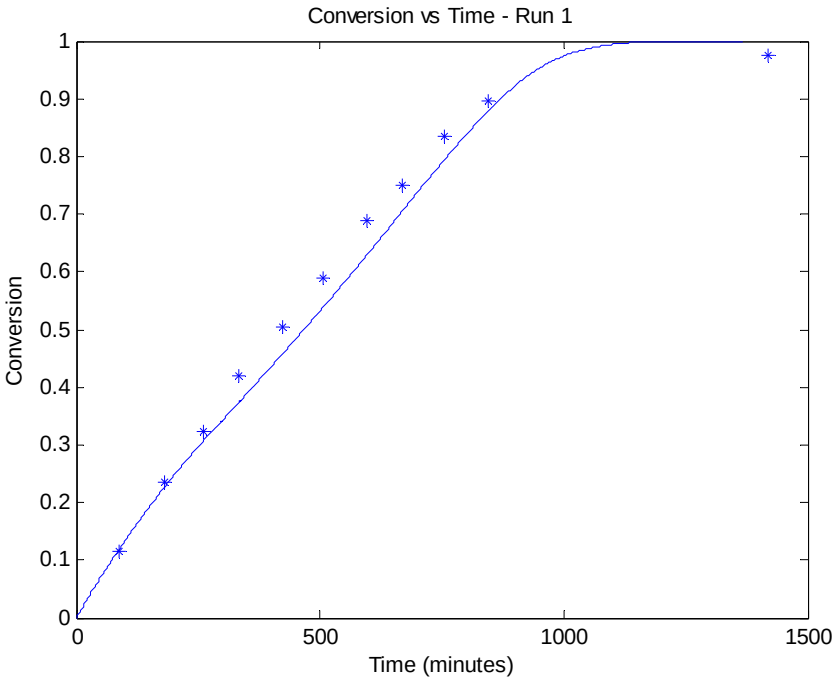

Figure 4.9: Simulation of the co-polymerization of MMA/BA T = 90°C $[dTBPO]_0$ = 0.044M toluene = 30wt% f_{MMA0} = 0.852

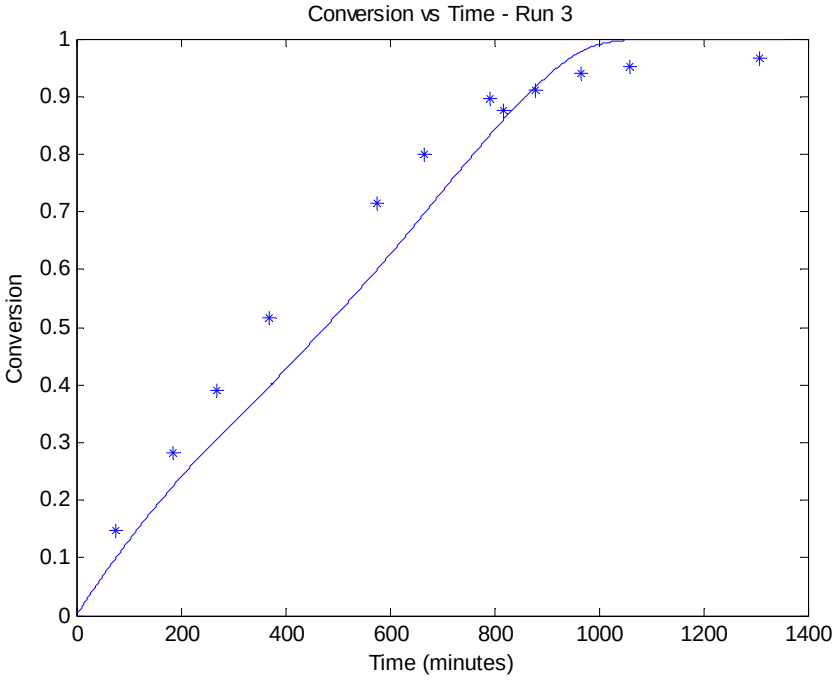

Figure 4.10: Simulation of the co-polymerization of MMA/BA T = 90°C $[dTBPO]_0$ = 0.045M toluene = 30wt% f_{MMA0} = 0.561

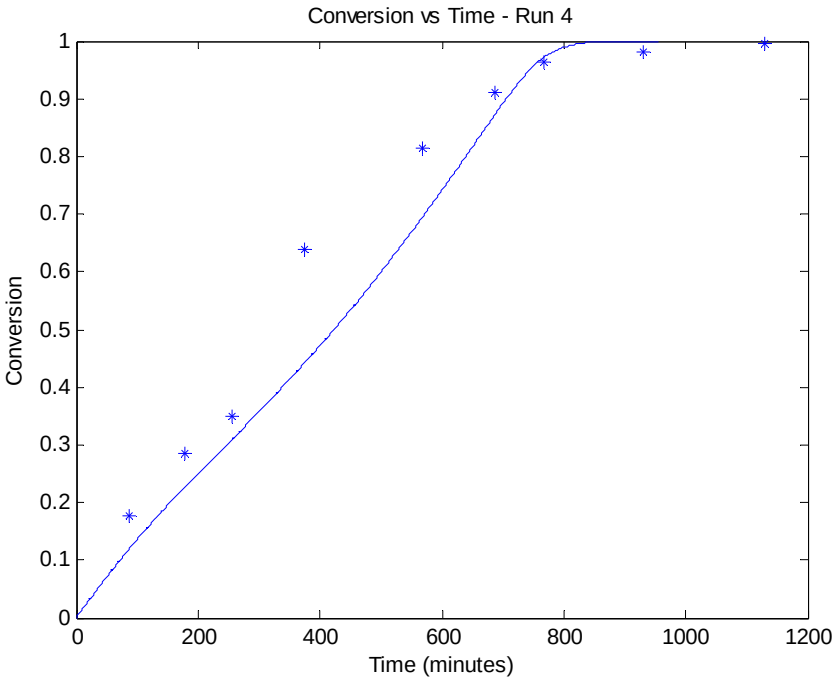

Figure 4.11: Simulation of the co-polymerization of MMA/BA T = 90°C $[dTBPO]_0$ = 0.045M toluene = 23wt% f_{MMA0} = 0.851

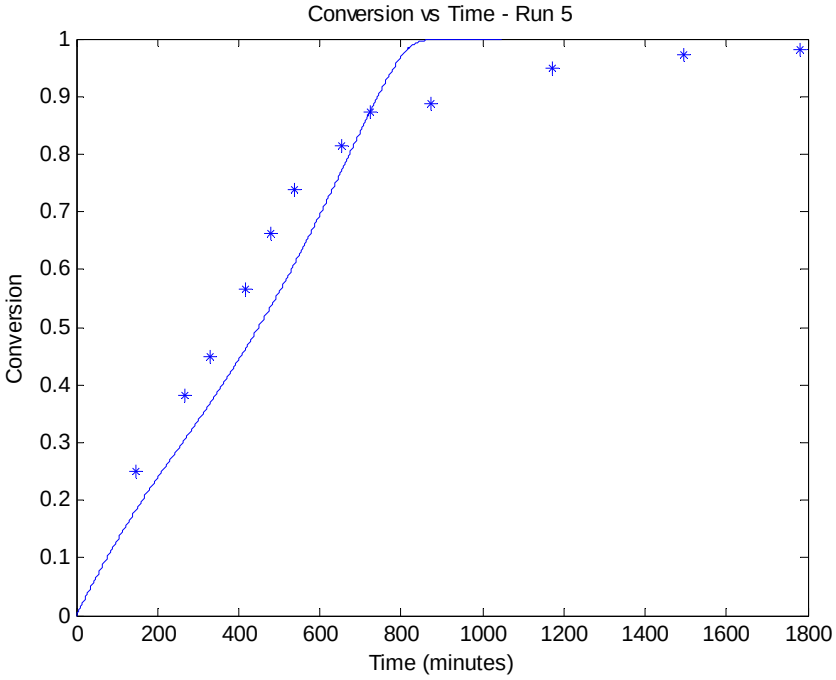

Figure 4.12: Simulation of the co-polymerization of MMA/BA T = 90°C $[dTBPO]_0$ = 0.045M toluene = 23wt% f_{MMA0} = 0.561

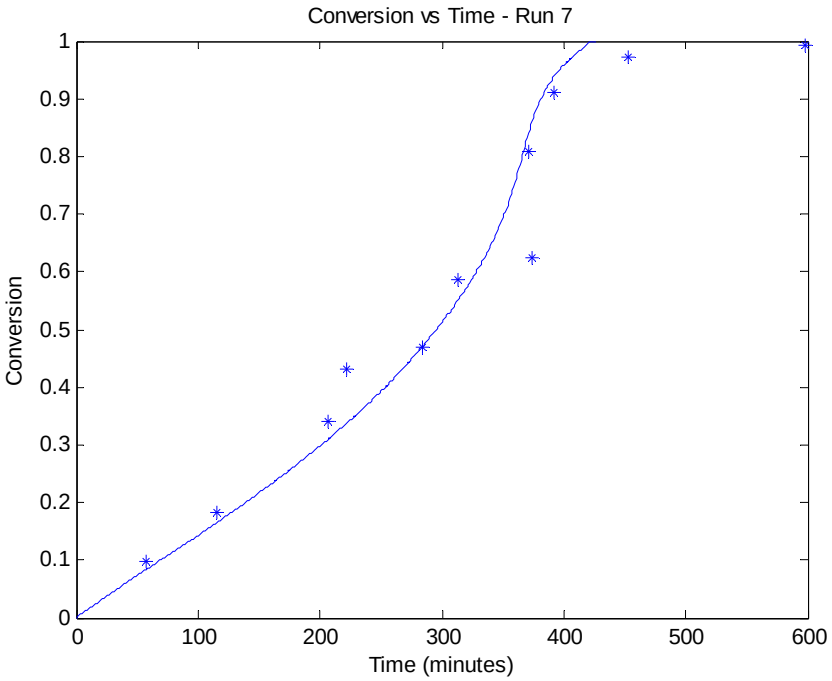

Figure 4.13: Simulation of the co-polymerization of MMA/BA T = 90°C $[dTBPO]_0$ = 0.045M toluene = 0wt% f_{MMA0} = 0.852

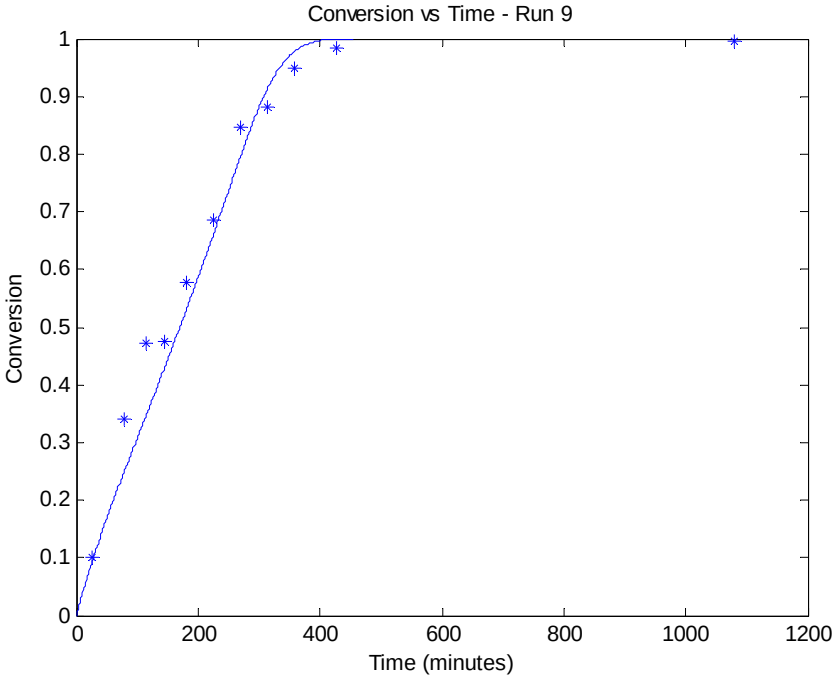

Figure 4.14: Simulation of the co-polymerization of MMA/BA T = 115°C $[dTBPO]_0$ = 0.0062M toluene = 30wt% f_{MMA0} = 0.852

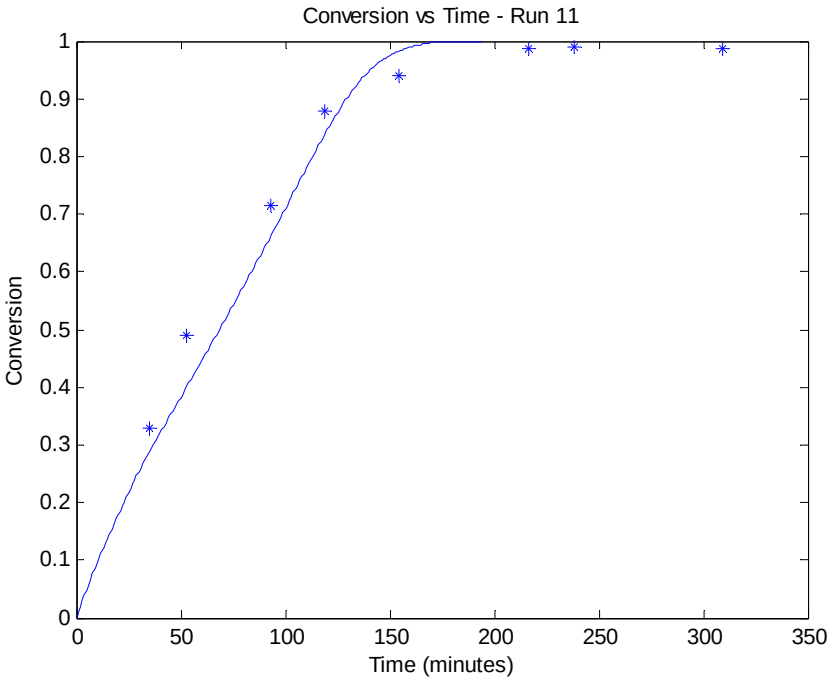

Figure 4.15: Simulation of the co-polymerization of MMA/BA T = 115°C $[dTBPO]_0$ = 0.045M toluene = 30wt% f_{MMA0} = 0.852

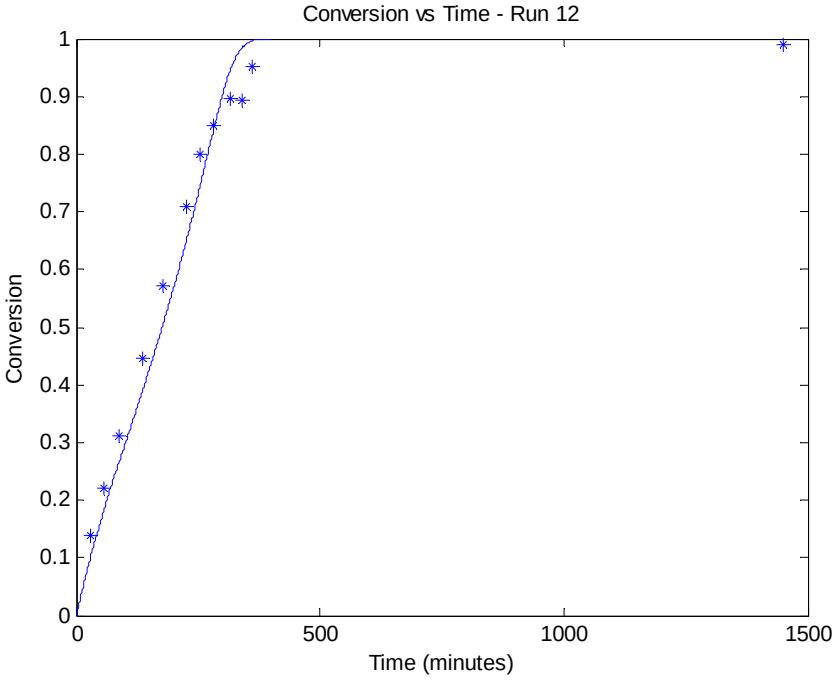

Figure 4.16: Simulation of the co-polymerization of MMA/BA T = 115°C $[dTBPO]_0$ = 0.0058M toluene = 23wt% f_{MMA0} = 0.852

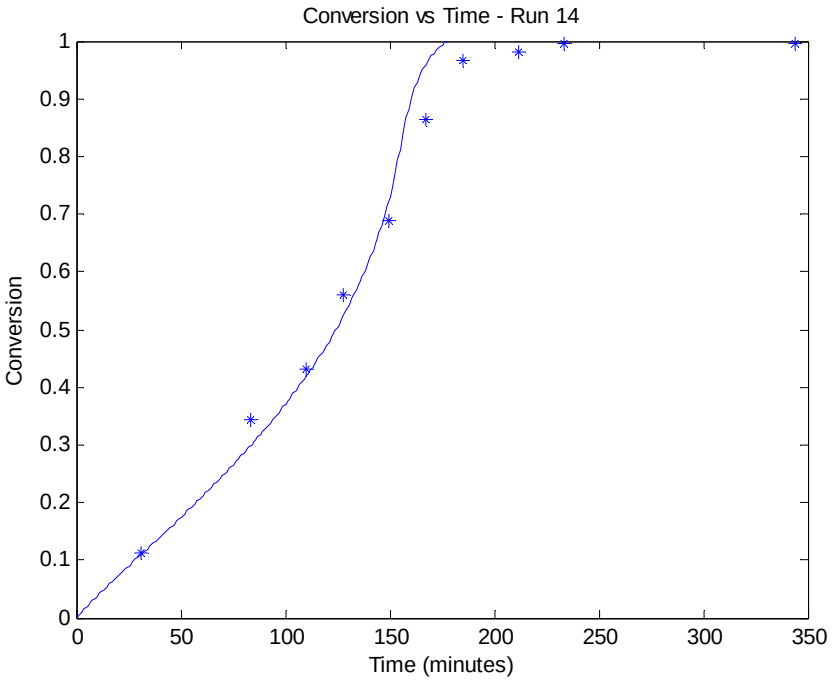

Figure 4.17: Simulation of the co-polymerization of MMA/BA T = 115°C $[dTBPO]_0$ = 0.0063M toluene = 0wt% f_{MMA0} = 0.561

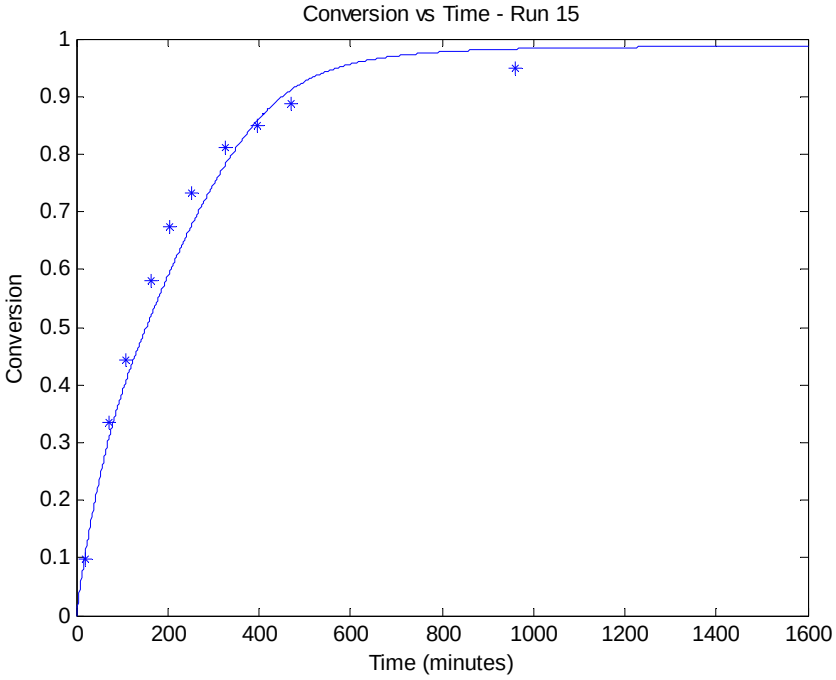

Figure 4.18: Simulation of the co-polymerization of MMA/BA T = 140°C $[dTBPO]_0$ = 0.0005M toluene = 30wt% f_{MMA0} = 0.852

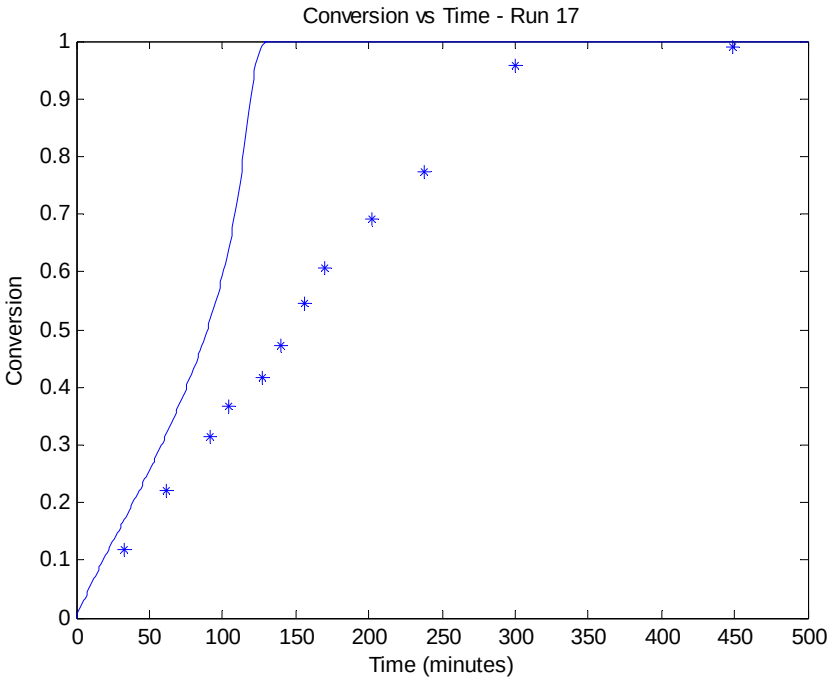

Figure 4.19: Simulation of the co-polymerization of MMA/BA T = 140°C $[dTBPO]_0$ = 0.00049M toluene = 0wt% f_{MMA0} = 0.852

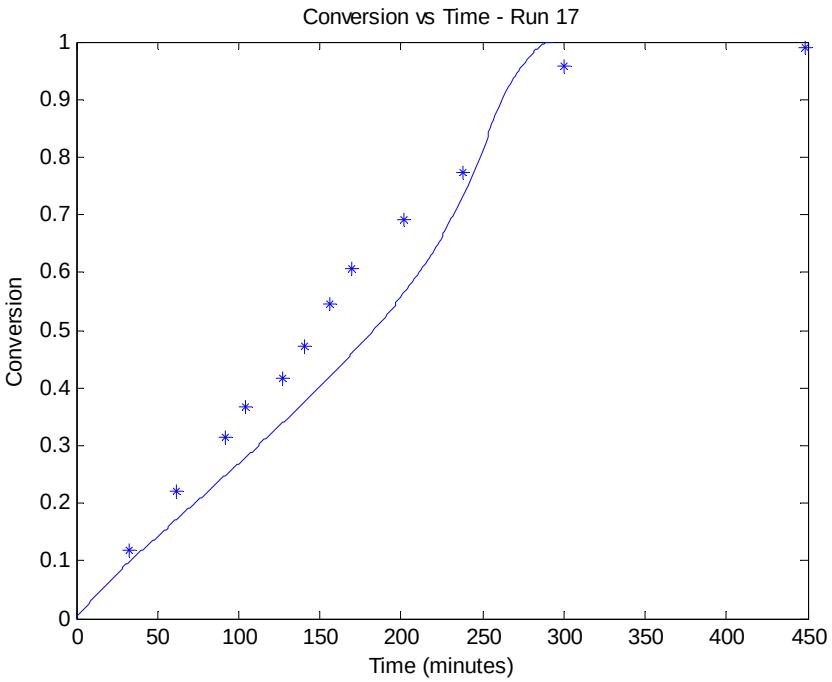

Figure 4.20: Simulation of the co-polymerization of MMA/BA T = 140°C $[dTBPO]_0$ = 0.00012M toluene = 0wt% f_{MMA0} = 0.852

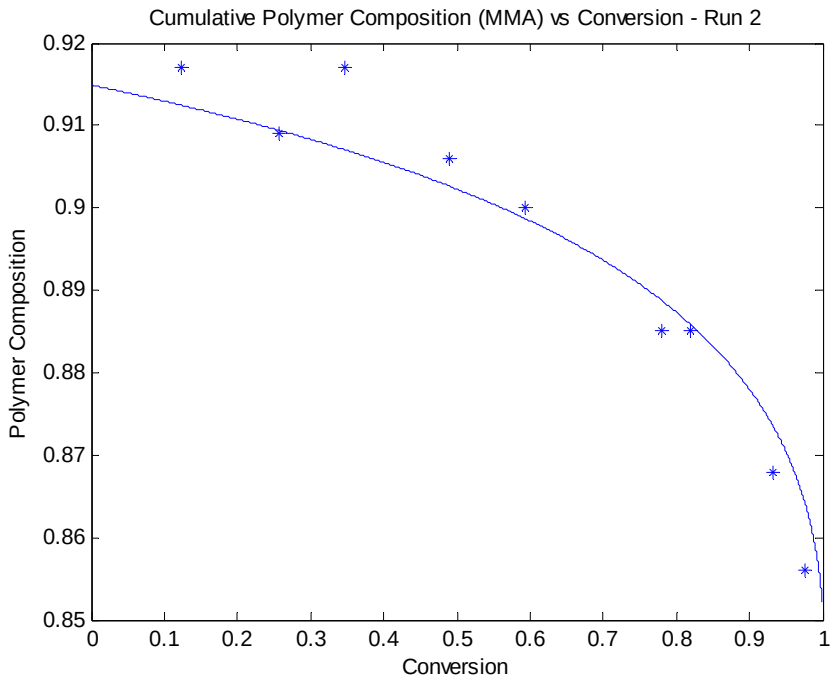

Figure 4.21: Simulation of the co-polymerization of MMA/BA T = 90°C $[dTBPO]_0$ = 0.045M toluene = 30wt% f_{MMA0} = 0.852

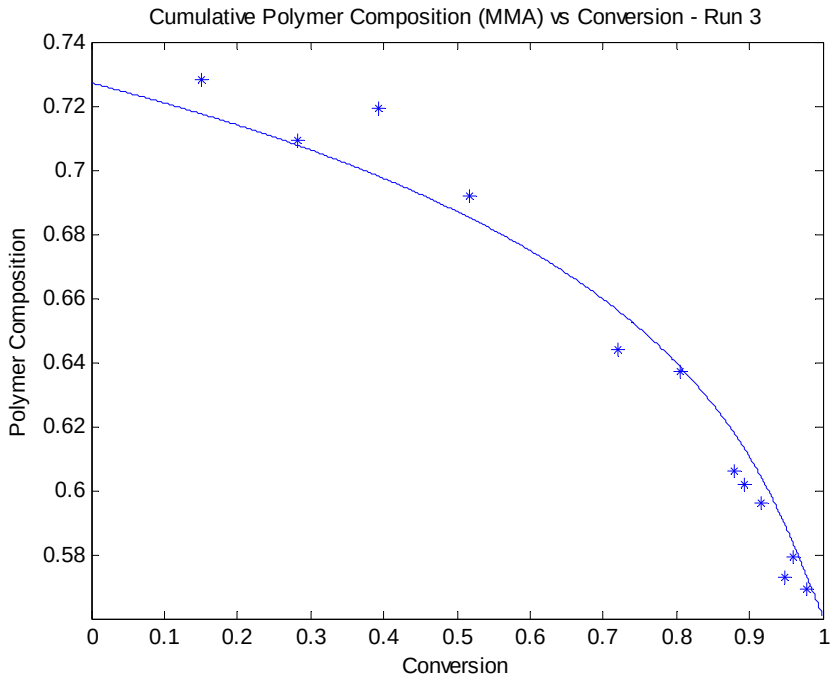

Figure 4.22: Simulation of the co-polymerization of MMA/BA T = 90°C $[dTBPO]_0$ = 0.045M toluene = 30wt% f_{MMA0} = 0.561

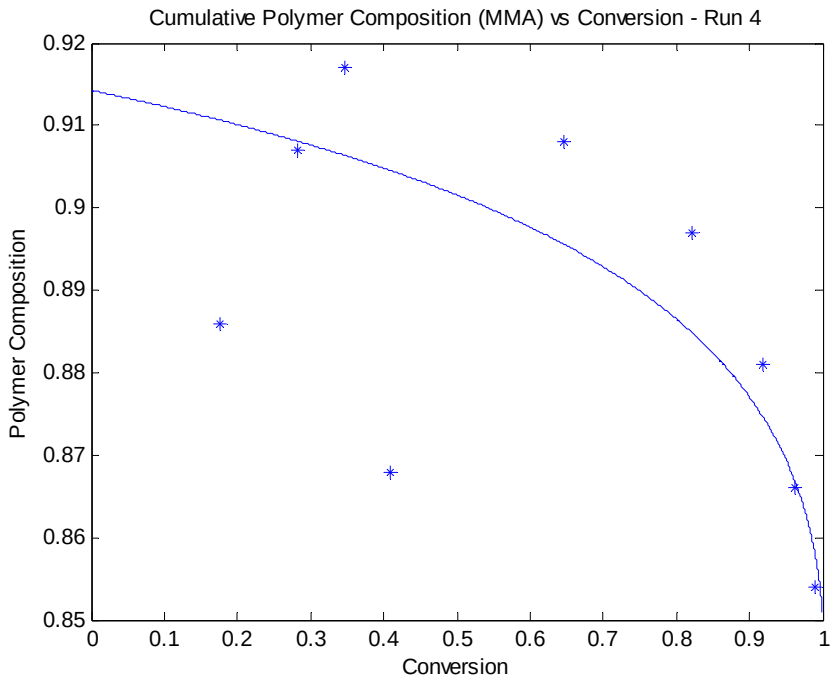

Figure 4.23: Simulation of the co-polymerization of MMA/BA T = 90°C $[dTBPO]_0$ = 0.045M toluene = 23wt% f_{MMA0} = 0.851

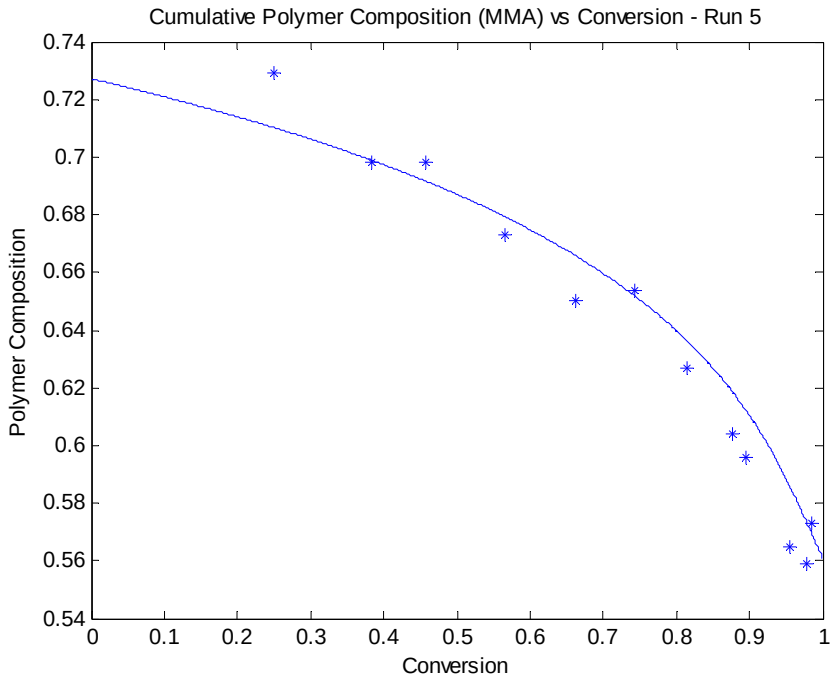

Figure 4.24: Simulation of the co-polymerization of MMA/BA T = 90°C $[dTBPO]_0$ = 0.045M toluene = 23wt% f_{MMA0} = 0.561

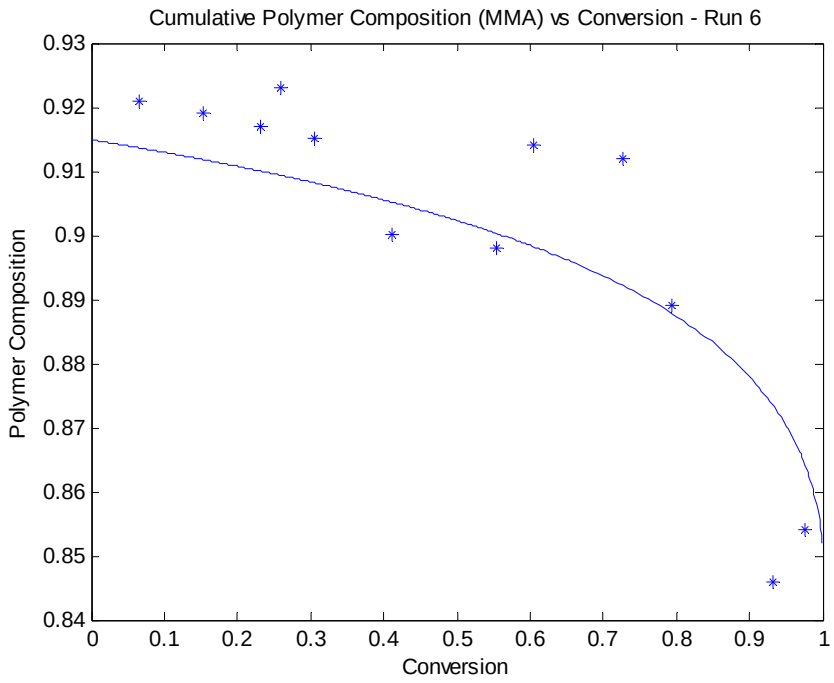

Figure 4.25: Simulation of the co-polymerization of MMA/BA T = 90°C $[dTBPO]_0$ = 0.047M toluene = 0wt% f_{MMA0} = 0.852

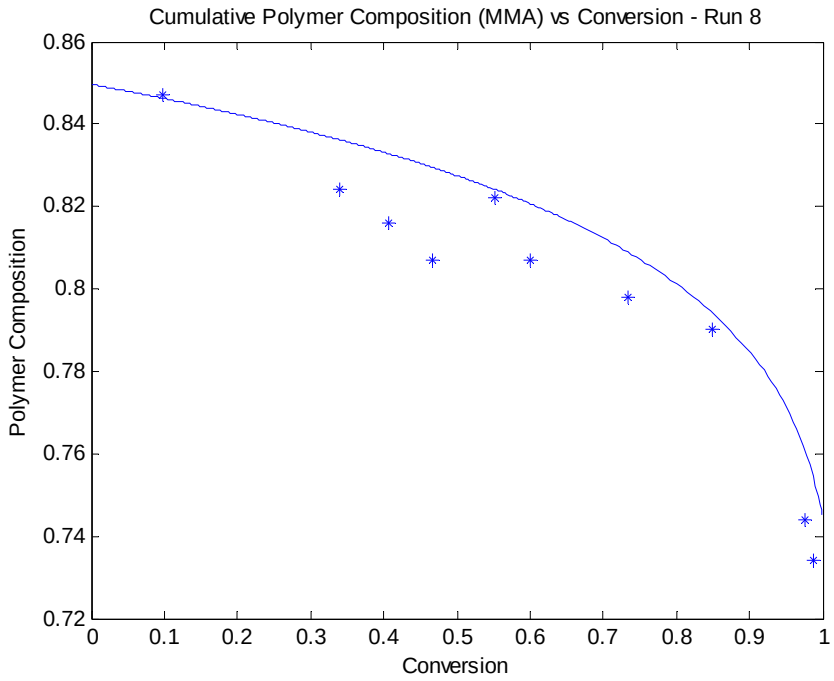

Figure 4.26: Simulation of the co-polymerization of MMA/BA T = 90°C $[dTBPO]_0$ = 0.046M toluene = 0wt% f_{MMA0} = 0.745

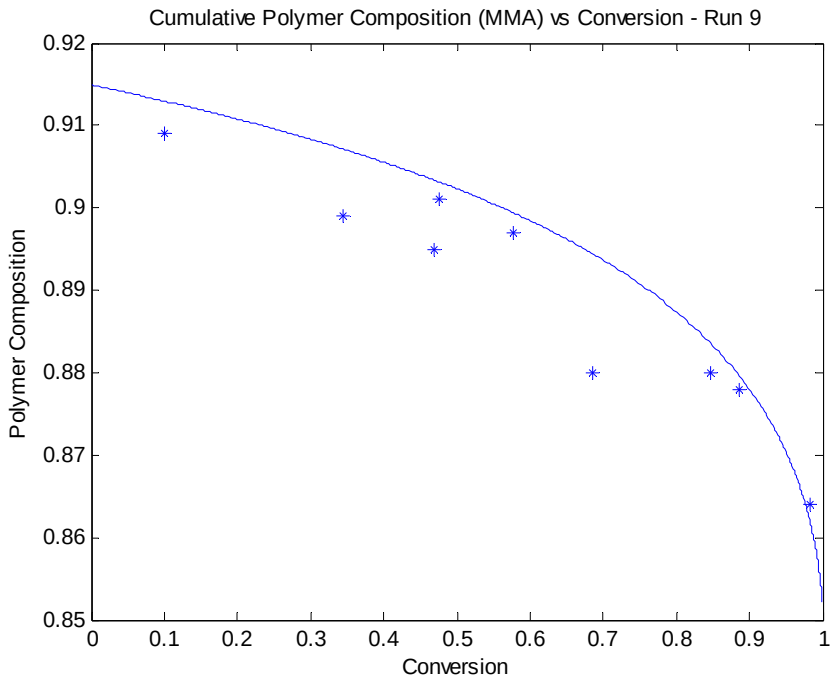

Figure 4.27: Simulation of the co-polymerization of MMA/BA T = 115°C $[dTBPO]_0$ = 0.0062M toluene = 30wt% f_{MMA0} = 0.852

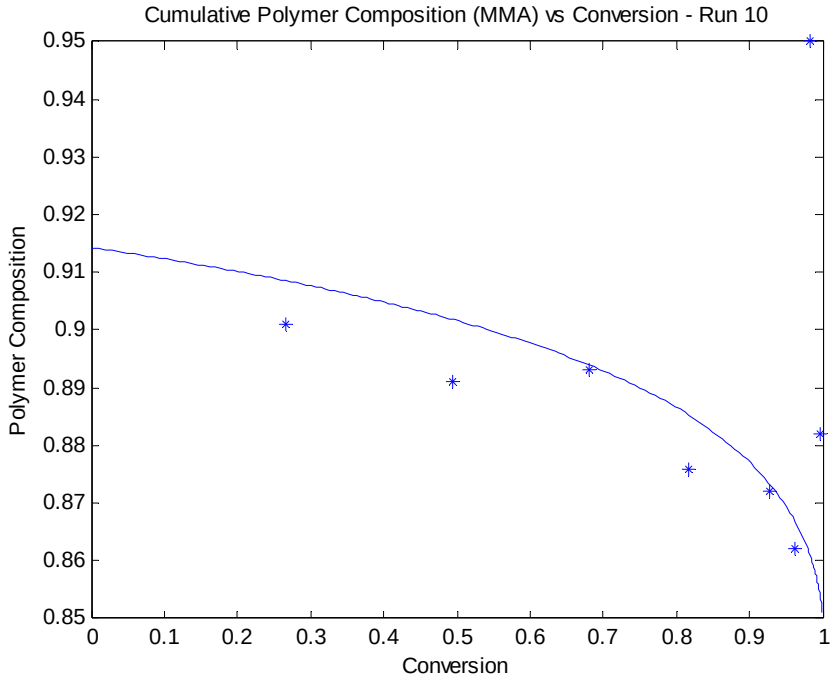

Figure 4.28: Simulation of the co-polymerization of MMA/BA T = 115°C $[dTBPO]_0$ = 0.045M toluene = 30wt% f_{MMA0} = 0.851

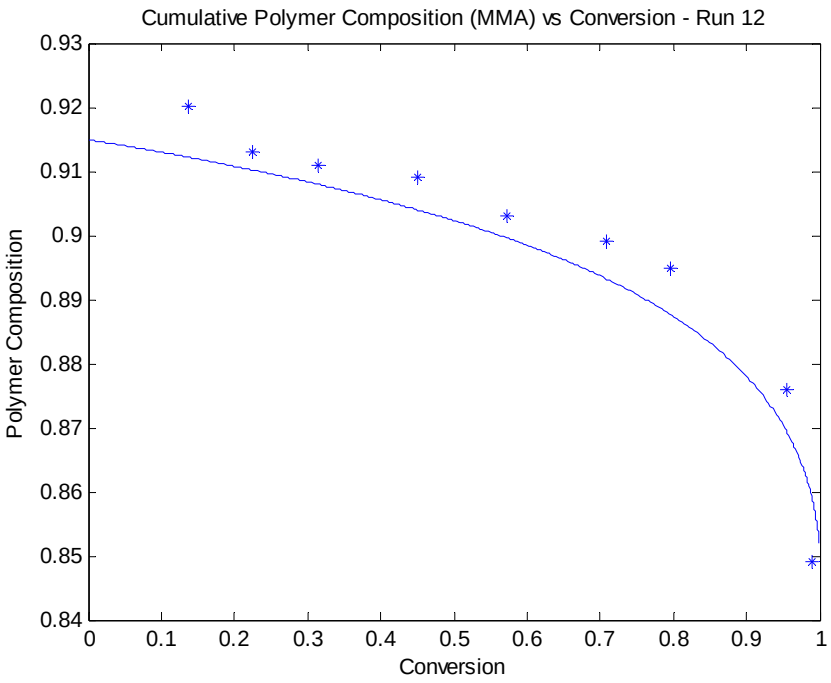

Figure 4.29: Simulation of the co-polymerization of MMA/BA T = 115°C $[dTBPO]_0$ = 0.0058M toluene = 23wt% f_{MMA0} = 0.852

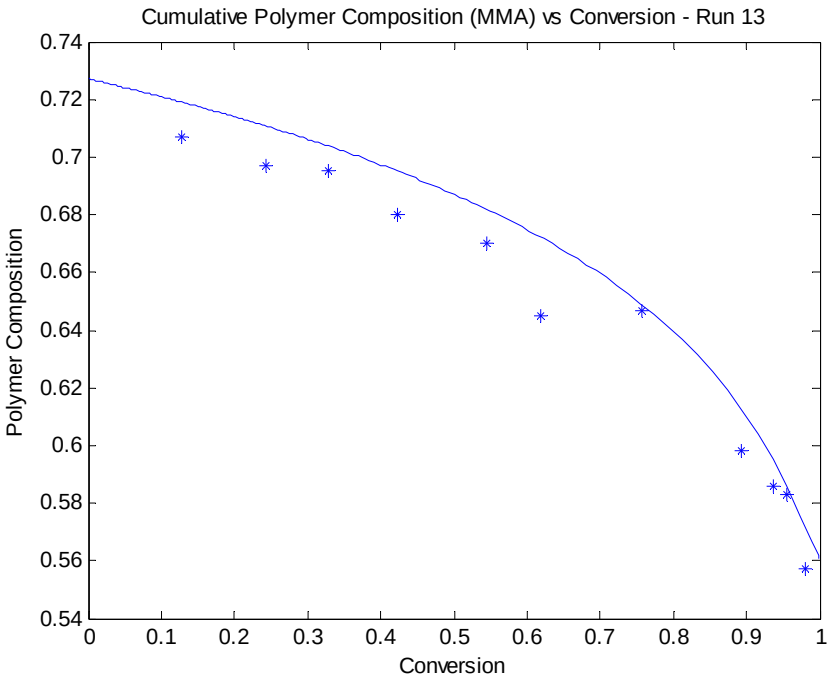

Figure 4.30: Simulation of the co-polymerization of MMA/BA T = 115°C $[dTBPO]_0$ = 0.0063M toluene = 0wt% f_{MMA0} = 0.561

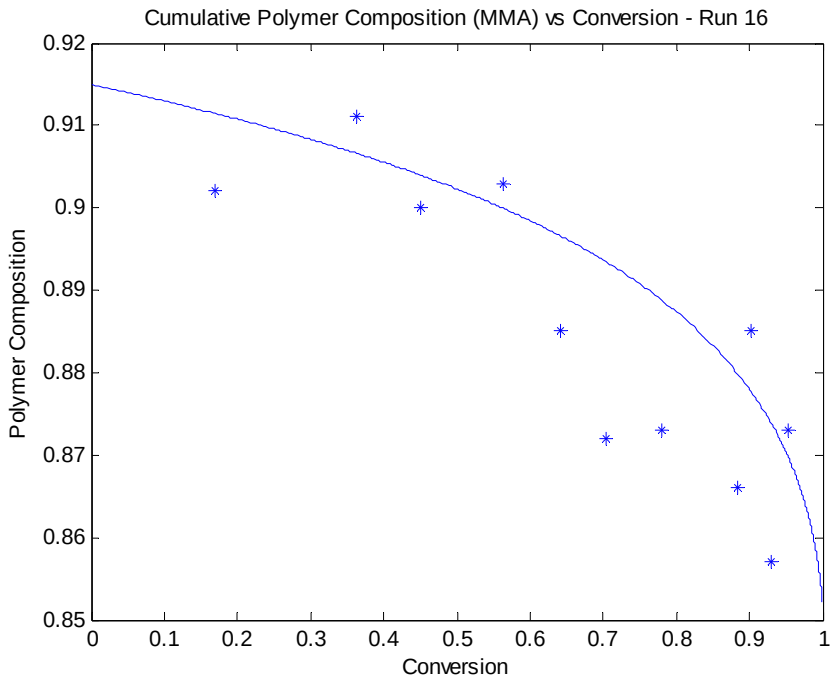

Figure 4.31: Simulation of the co-polymerization of MMA/BA T = 140°C $[dTBPO]_0$ = 0.00047M toluene = 30wt% f_{MMA0} = 0.852

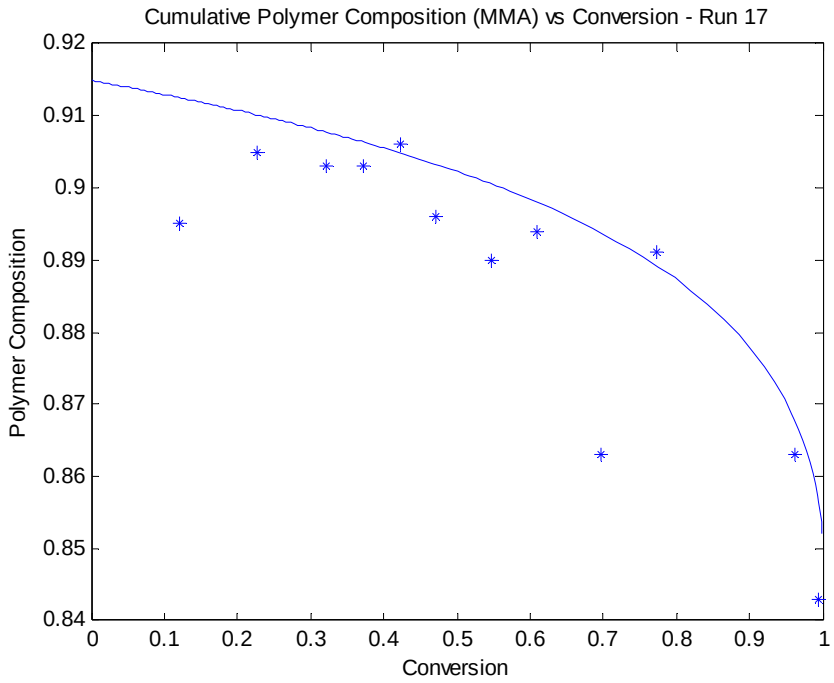

Figure 4.32: Simulation of the co-polymerization of MMA/BA T = 140°C $[dTBPO]_0$ = 0.00049M toluene = 0wt% f_{MMA0} = 0.852

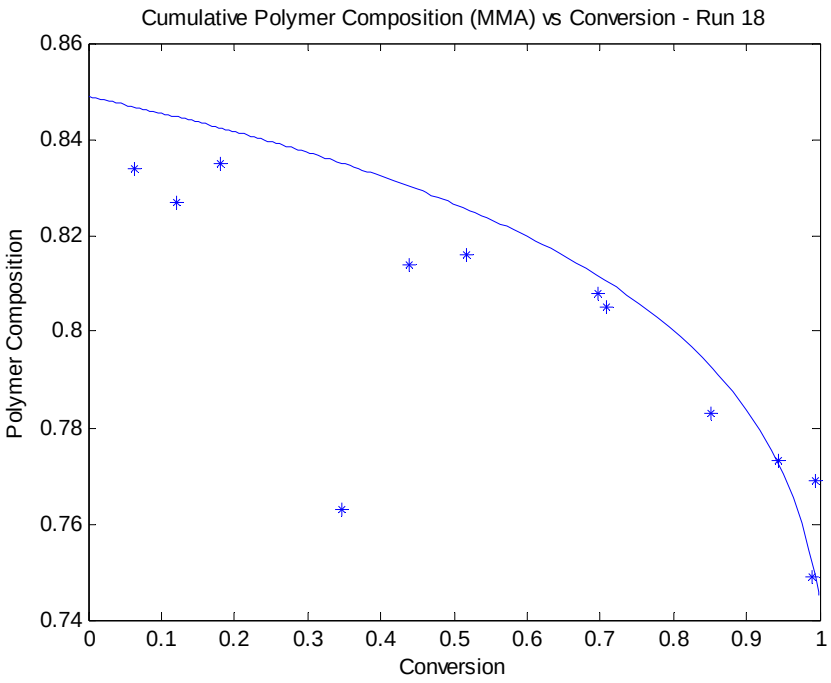

Figure 4.33: Simulation of the co-polymerization of MMA/BA T = 140°C $[dTBPO]_0$ = 0.00045M toluene = 0wt% f_{MMA0} = 0.745

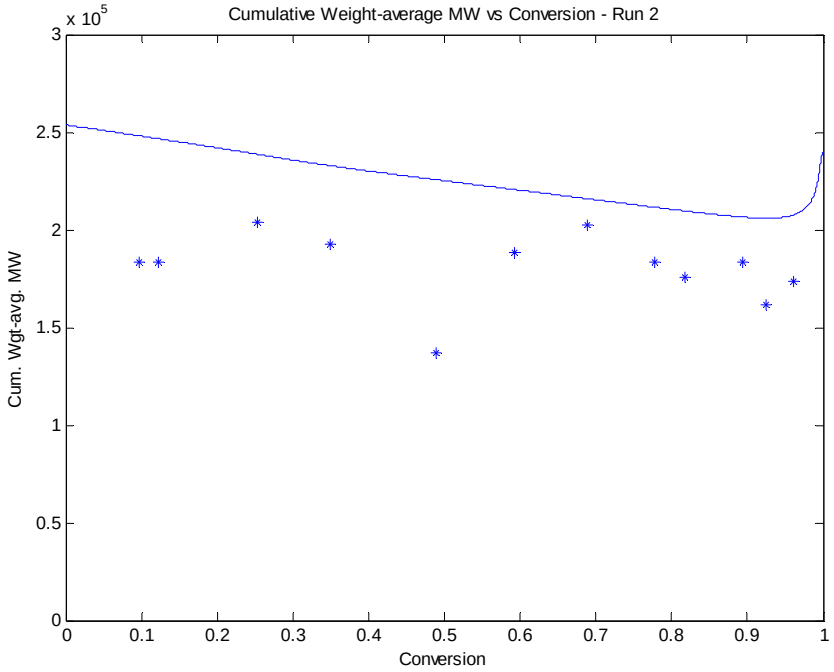

Figure 4.34: Simulation of the co-polymerization of MMA/BA T = 90°C $[dTBPO]_0$ = 0.045M toluene = 30wt% f_{MMA0} = 0.852

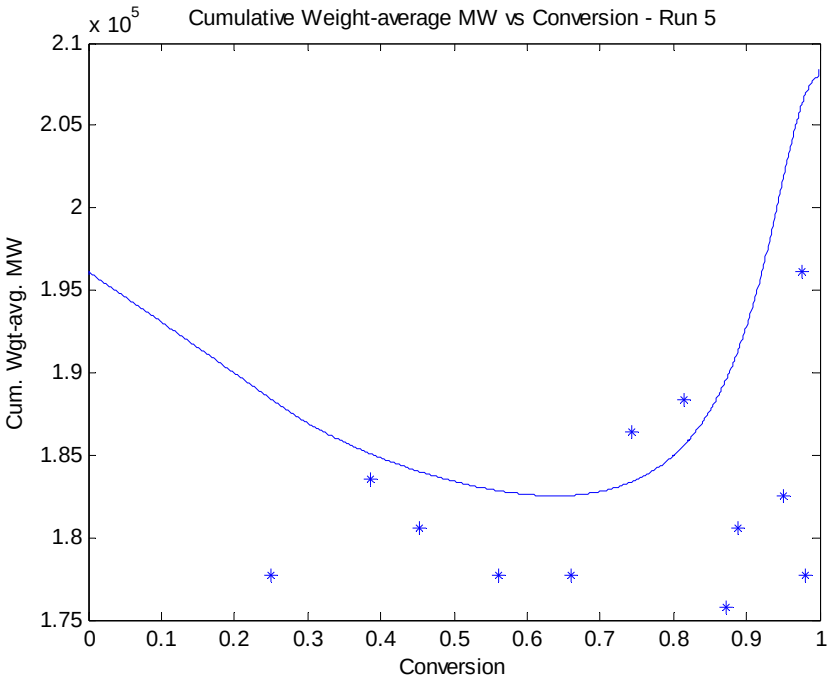

Figure 4.35: Simulation of the co-polymerization of MMA/BA T = 90°C $[dTBPO]_0$ = 0.045M toluene = 23wt% f_{MMA0} = 0.561

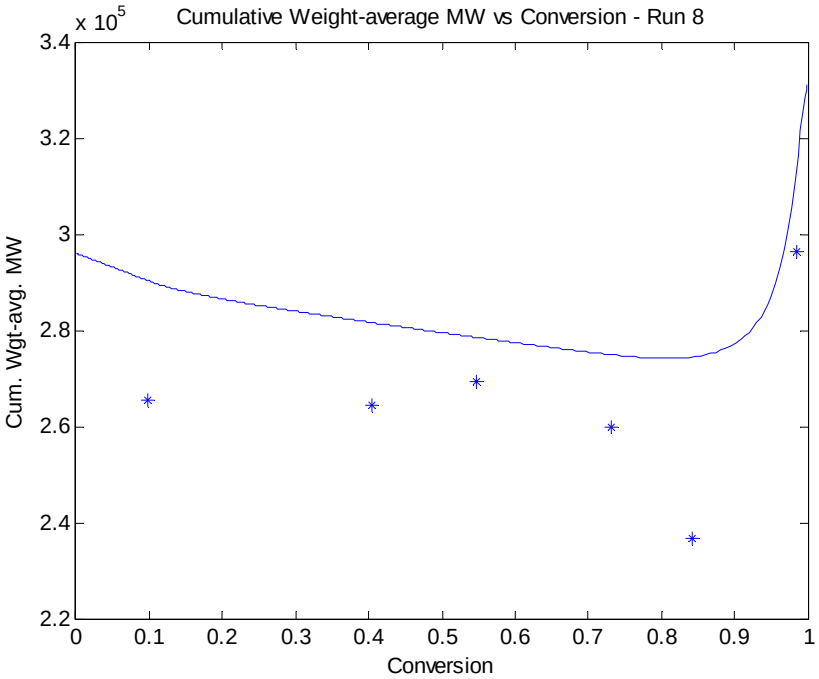

Figure 4.36: Simulation of the co-polymerization of MMA/BA T = 90°C $[dTBPO]_0$ = 0.046M toluene = 0wt% f_{MMA0} = 0.745

4.5. Co-polymerization of Styrene and Acrylonitrile

The co-polymerization of styrene and acrylonitrile was simulated ten times at 60°C, each time with a different starting monomer mole fraction. The conversion was kept very low and the triad fraction data against the mole fraction of styrene were plotted. Hill *et al.* (1982) conducted the same runs and their experimental data are shown in the figures below. The reactivity ratios, $r_{Sty\text{-}AN} = 0.36$ and $r_{AN\text{-}Sty} = 0.078$, were taken from Garcia-Rubio *et al.* (1985). Figure 4.37 shows the styrene-centered triad fractions and Figure 4.38 shows the AN-centered triad fraction (212 represents the triad fraction of AN-Sty-AN). As expected, both the simulations and the experimental data show that styrene is more reactive than AN. The simulations prove to be very accurate and follow the trends very well.

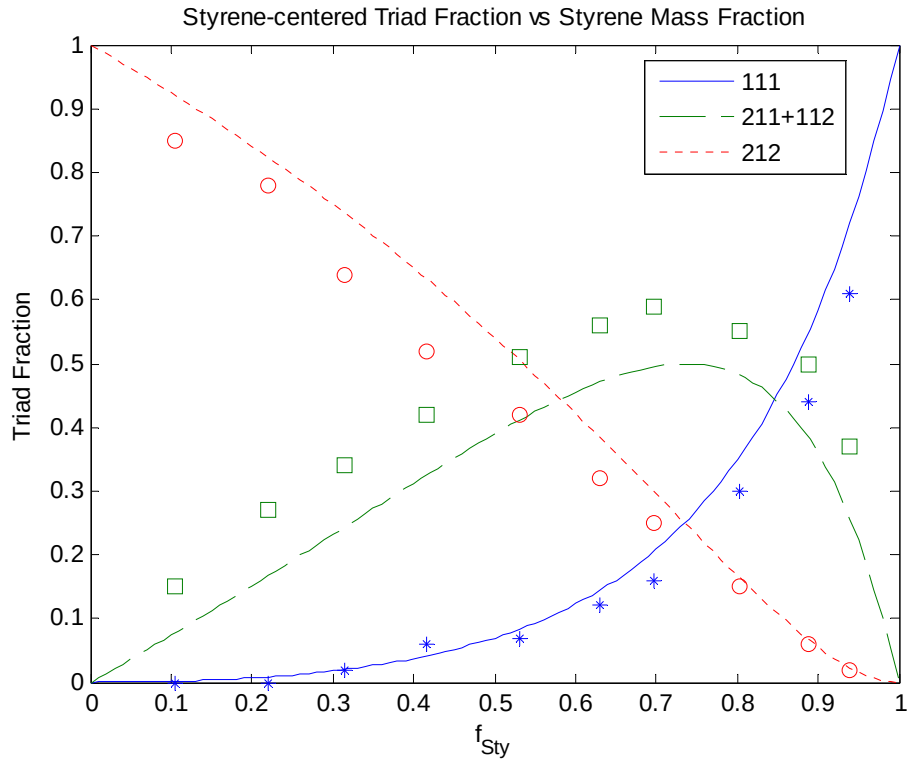

Figure 4.37: Simulation of the batch co-polymerization of Sty/AN T = 60°C

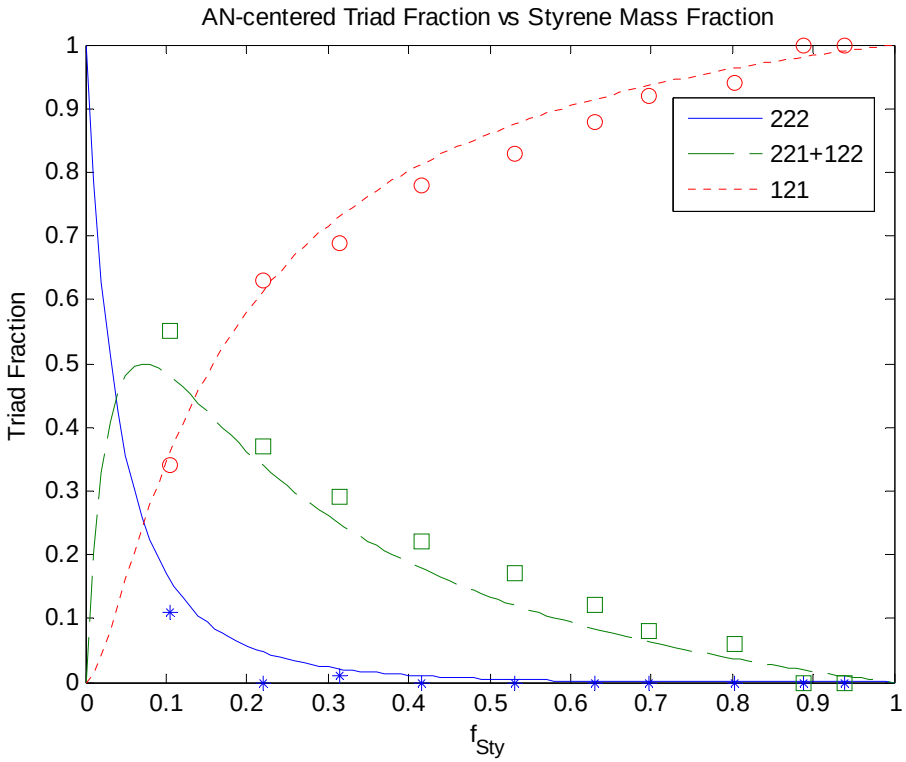

Figure 4.38: Simulation of the batch co-polymerization of Sty/AN T = 60°C

4.6. Co-polymerization of Methyl Methacrylate and Methyl Acrylate

Methyl methacrylate and methyl acrylate were co-polymerized at 50°C by Kim and Harwood (2002) at six different monomer mole fractions. The triad fraction data against the MMA mole fraction at the initial stages of each of the reactions are shown in Figure 4.39 (MMA-centered) and Figure 4.40 (MA-centered). The reactivity ratios used come from the same paper as the experimental data being tested (Kim and Harwood, 2002): $r_{MMA\text{-}MA} = 2.60$ and $r_{MA\text{-}MMA} = 0.27$. This means that the results of this section primarily prove the functionality of our triad fraction calculations.

The modeling software shows a very good fit with the experimental data in both simulations. Note, 212 in this case represents the triad fraction MA-MMA-MA.

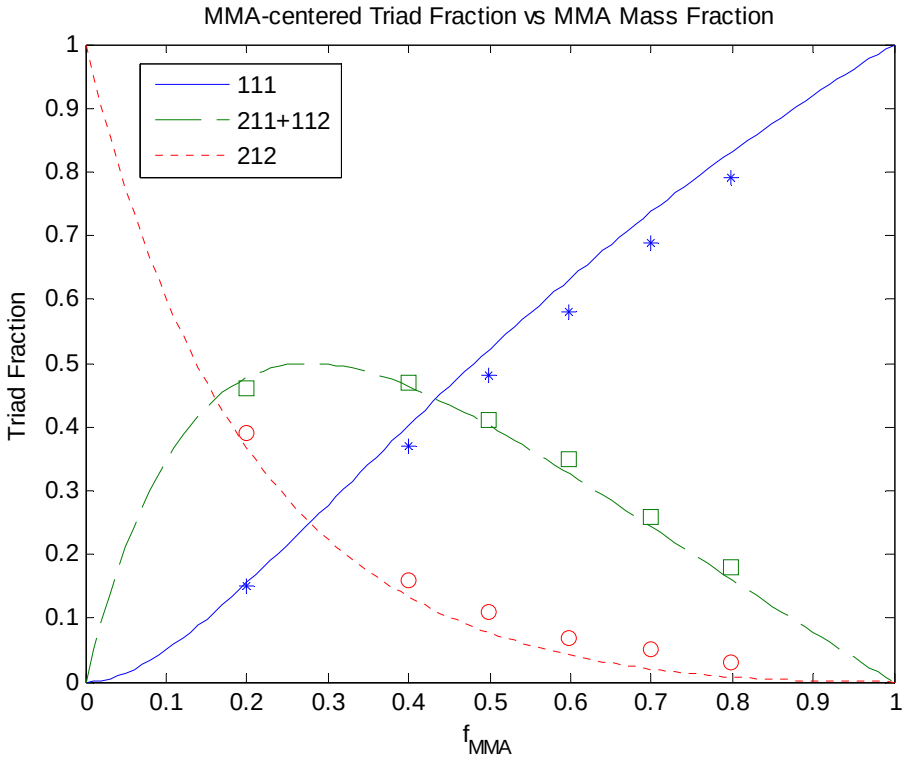

Figure 4.39: Simulation of the co-polymerization of MMA/MA T = 50°C

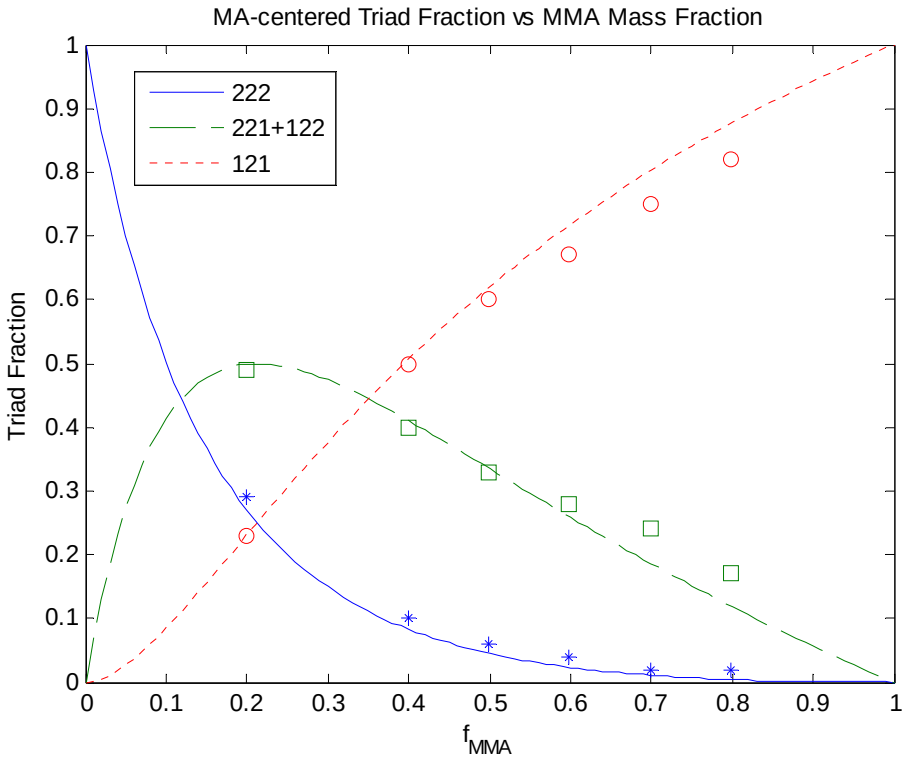

Figure 4.40: Simulation of the co-polymerization of MMA/MA T = 50°C

4.7. Co-polymerization of Alpha Methyl Styrene and Methyl Methacrylate

A co-polymerization of AMS and MMA was performed at lower temperatures by Martinet and Guillot (1999). Composition drift data were taken at 50°C, 60°C and 80°C. As AMS is known to depropagate at lower than average temperatures, simulations were carried out with and without depropagation to show the large effect that the reverse reaction has. The reactivity ratios as well as the cross- and homo-depropagation ratios were taken from Palmer *et al.* (2001):

$r_{AMS\text{-}MMA} = 0.734$ $r_{MMA\text{-}AMS} = 0.548$

$R_1 = \exp(-6222/T + 18.34)$ $R_2 = 0$

$R_{11} = 253469.8*\exp(-3489.1/T)*r_{AMS\text{-}MMA}$ $R_{22} = 0$

Figure 4.41 shows the instantaneous composition drift at 60°C whereas Figure 4.42 shows the same effect at 80°C. The polymerizations were done at five different monomer mole fractions for each temperature. The accuracy of Krüger's model shows the presence of depropagation and is very important for accurate multi-component modeling.

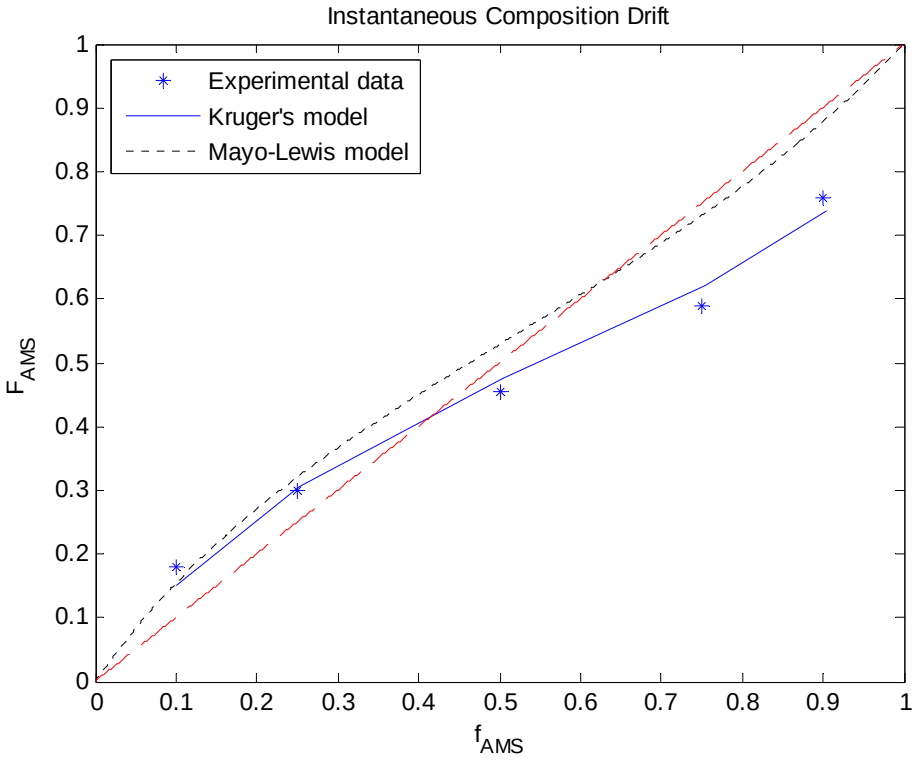

Figure 4.41: Simulation of the co-polymerization of AMS/MMA at 60°C

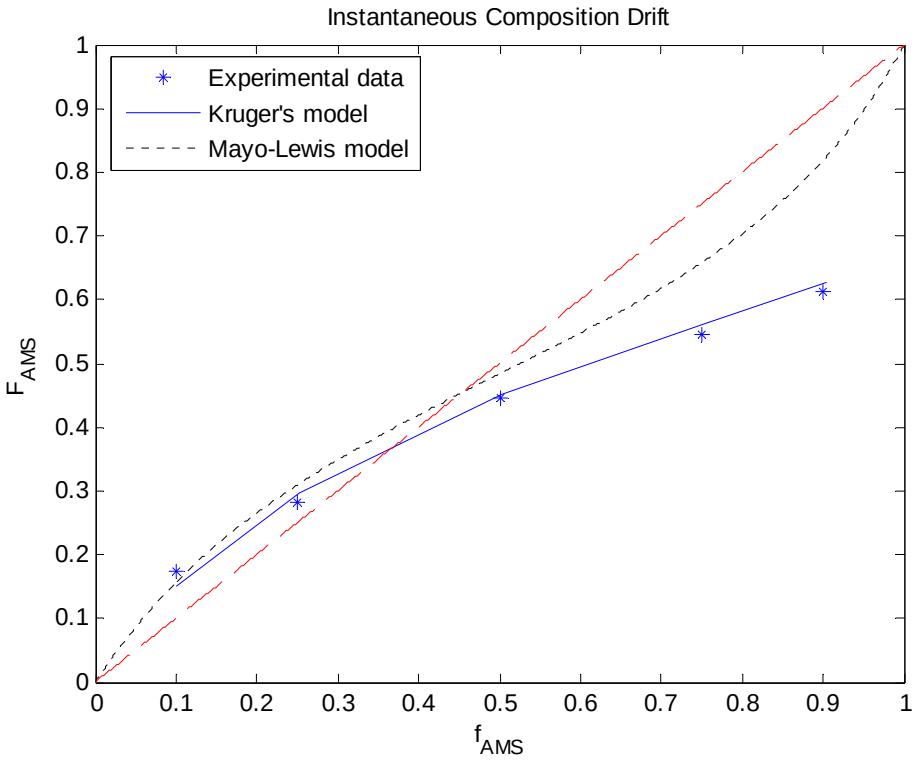

Figure 4.42: Simulation of the co-polymerization of AMS/MMA at 80°C

5. Model Extensions/Refinements and Case Studies

5.1. Depropagation

The importance of depropagation can be seen in a conversion versus time simulation of the co-polymerization of MMA and BA at 140°C with 30% by weight toluene (Dubé *et al.*, 2002). Quite simply, Figure 5.1 displays the simulation against literature data with the standard termination reaction constant between MMA and BA and the simulation with a severely increased termination reaction constant. The drastic increase had minimal effect on conversion. The next plot, Figure 5.2, uses the standard termination constant but accounts for depropagation of MMA at this elevated temperature.

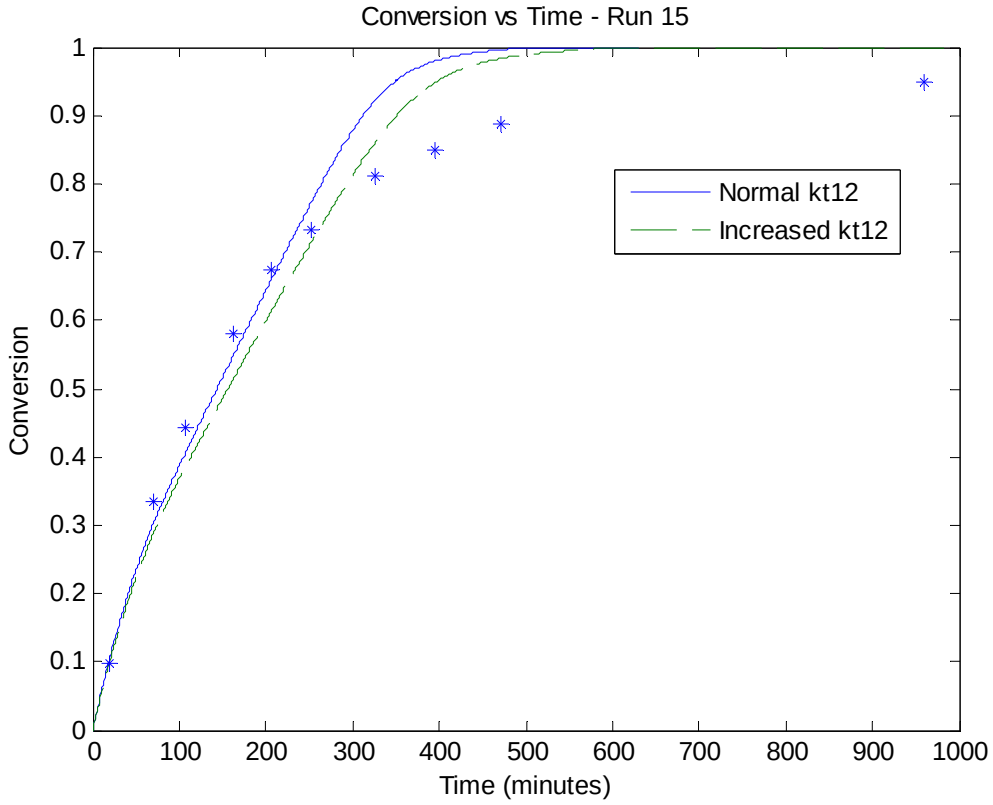

Figure 5.1: Simulation of the co-polymerization of MMA/BA T = 140°C $[dTBPO]_0$ = 0.0005M toluene = 30 wt% f_{BA0} = 0.148

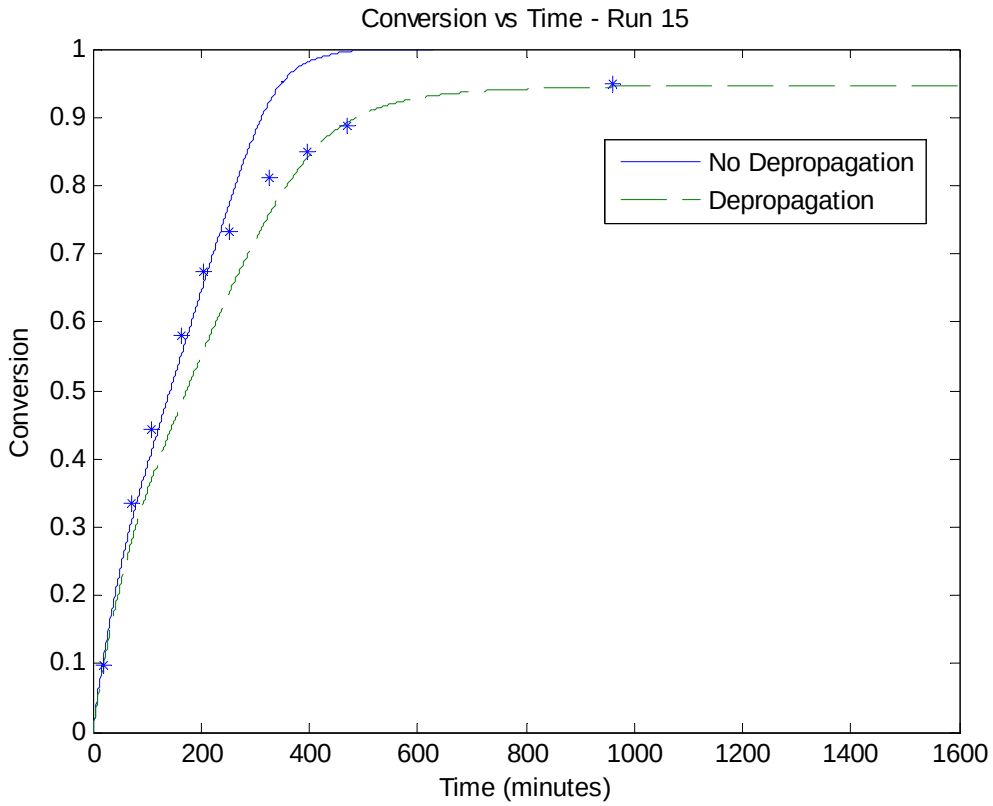

Figure 5.2: Simulation of the co-polymerization of MMA/BA T = 140°C $[dTBPO]_0$ = 0.0005M toluene = 30 wt% f_{BA0} = 0.148

This shows that at elevated temperatures depropagation is a fundamental modeling extension and requires adequate explanation. This alters the original propagation reactions and consequently, all of the monomer and radical balances. As such, the effects of depropagation are observed not only in conversion but also in polymer composition, molecular weight, and sequence length distribution. The additional complexity arising to account for depropagation was explained in section 3.2.5.

5.1.1. Case Study 1: Homo-polymerization of Butyl Methacrylate

Butyl methacrylate was polymerized in solution at two different temperatures and three different monomer concentrations: 17 wt% at 110°C and 9/17/34 wt% at 132°C (Wang *et al.*, 2009a). The initiator, di-tert-butyl peroxide, was used at 1 wt% of monomer. Xylene was used as the solvent and no chain transfer agents or inhibitors were present. Monomer concentration and molecular weight data versus time were extracted from Wang *et al.* (2009a).

This example has been included here to illustrate the sensitivity of monomer concentration and related variables when accounting for depropagation. An earlier paper by Li *et al.* (2005) had a depropagation rate constant slightly higher than the results found in Wang *et al.* (2009a); the difference being in the exponential term:

k_{dp}	$k_p*(1.76-1.37*w_p)*10^6*\exp(-\mathbf{6145}/T)$	Li *et al.*, 2005
k_{dp}	$k_p*(1.76-1.37*w_p)*10^6*\exp(-\mathbf{6240}/T)$	Wang *et al.*, 2009a

As one can see, Figure 5.3, representing the depropagation rate constant from Li *et al.* (2005), shows quite unfavorable results arising from the higher depropagation rate constant. Figure 5.4, however, produces a simulation much more true to the data obtained.

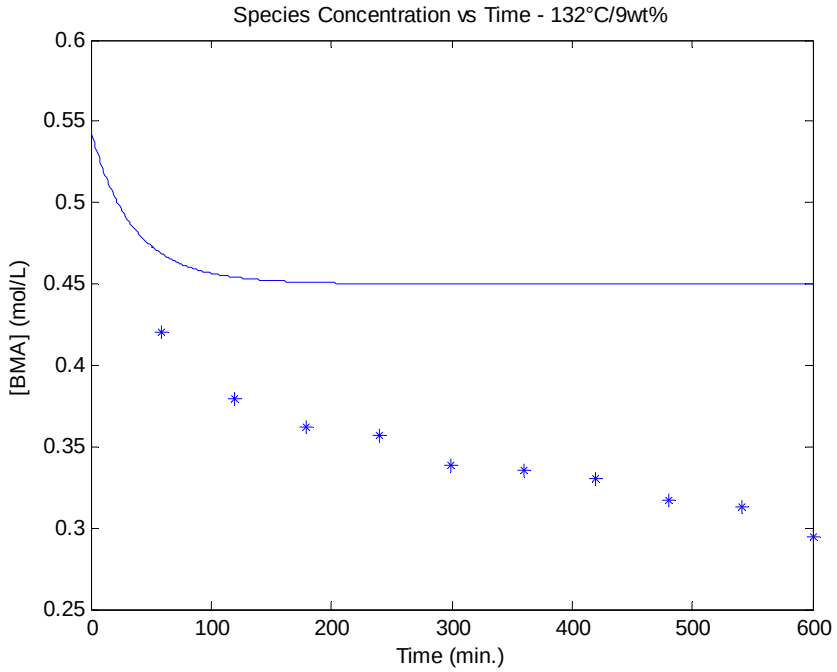

Figure 5.3: Simulation of the homo-polymerization of BMA T = 132°C $[dTBPO]_0$ = 0.09 wt% xylene = 91 wt% k_{dp} from Li *et al.* (2005)

With only the depropagation rate constant exponential term changing slightly (Li *et al.* being only 1.26 times larger than Wang *et al.* [at 132°C]), the difference in final conversion achieved, or more specifically to the plots at hand, the difference in the total amount of monomer consumed, is quite significant. This shows how precise the depropagation rate constant must be in order to accurately model depropagation.

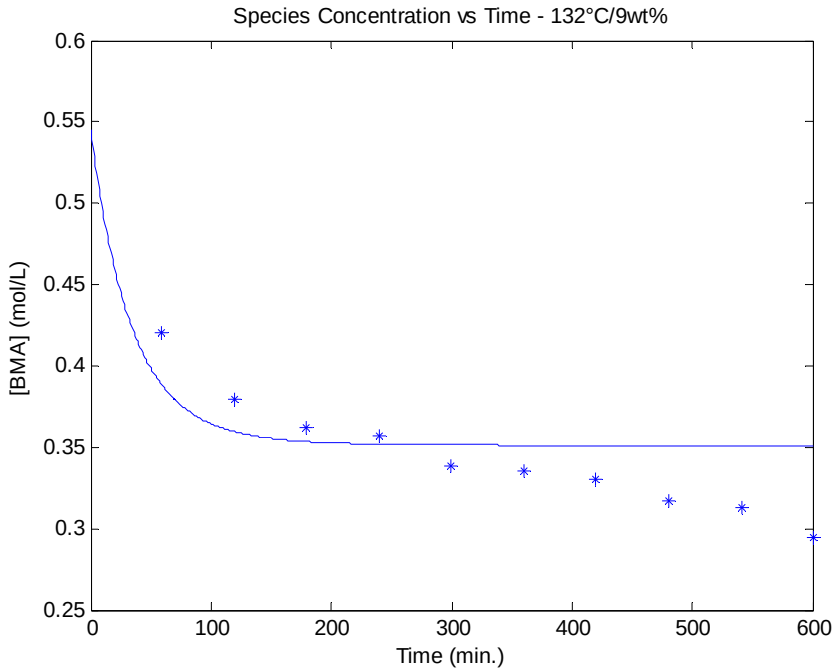

Figure 5.4: Simulation of the homo-polymerization of BMA T = 132°C $[dTBPO]_0$ = 0.09 wt% xylene = 91 wt% k_{dp} from Wang *et al.* (2009a)

The remainder of the simulations use the more accurate depropagation rate constant. Figure 5.5 through Figure 5.7 show the three other monomer concentration versus time plots, all showing good results. Figure 5.8 through Figure 5.10 are the molecular weight versus time plots at 132°C; all three simulating both the number- and weight-average molecular weight against the corresponding data.

Each simulation follows the data trends quite well with some room for improvement. The example in the appendices on initiator sensitivity (section Appendix I) shows the same homo-polymerization with further improvement in monomer concentration against time. The problem with implementing such a solution is that the molecular weight data become further skewed, making depropagation a difficult add-on to refine and perfect.

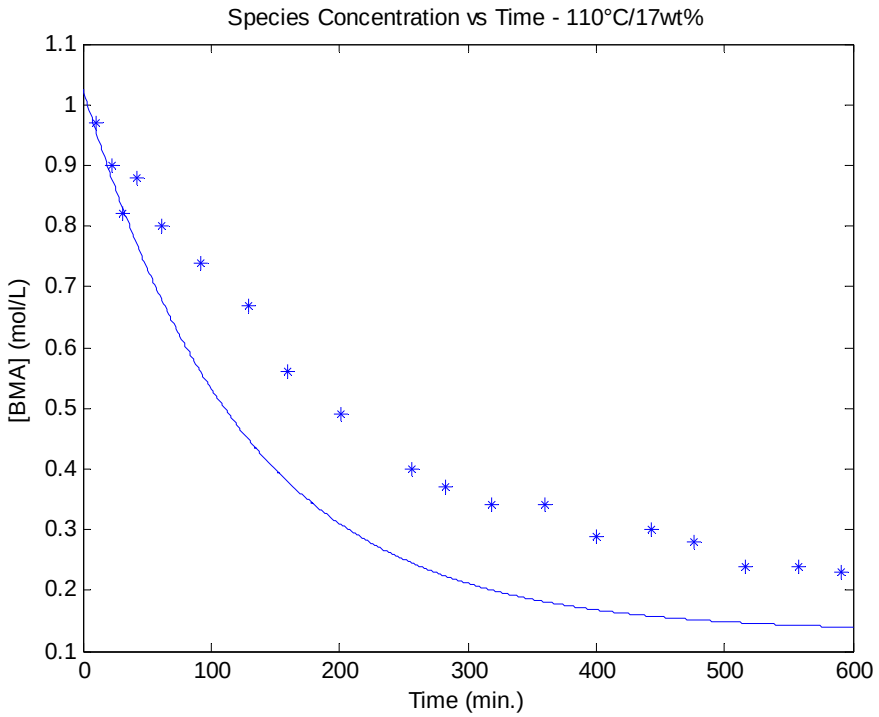

Figure 5.5: Simulation of the homo-polymerization of BMA T = 110°C $[dTBPO]_0$ = 0.17 wt% xylene = 83 wt%

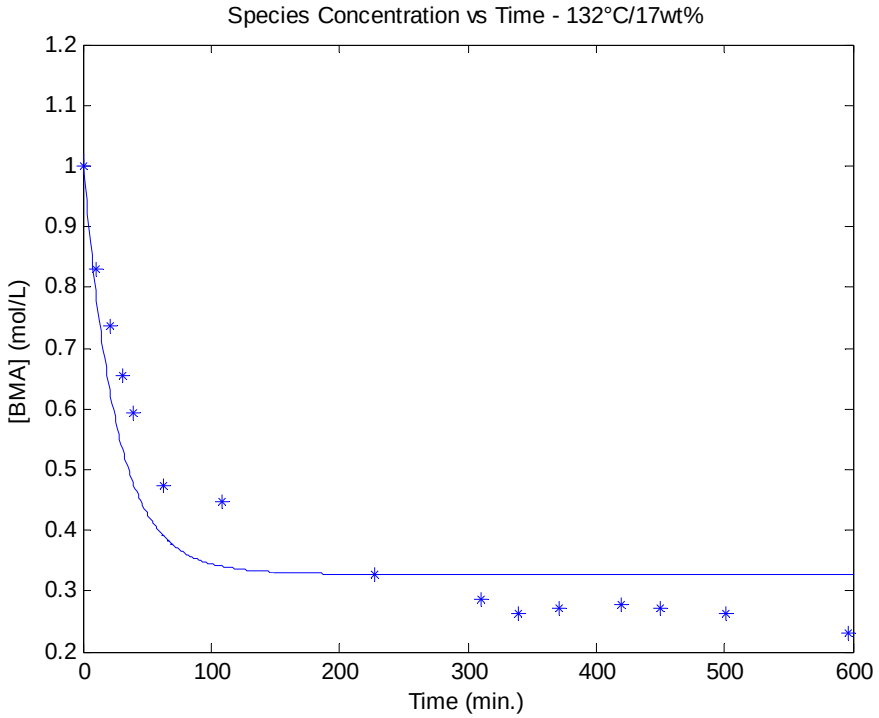

Figure 5.6: Simulation of the homo-polymerization of BMA T = 132°C $[dTBPO]_0$ = 0.17 wt% xylene = 83 wt%

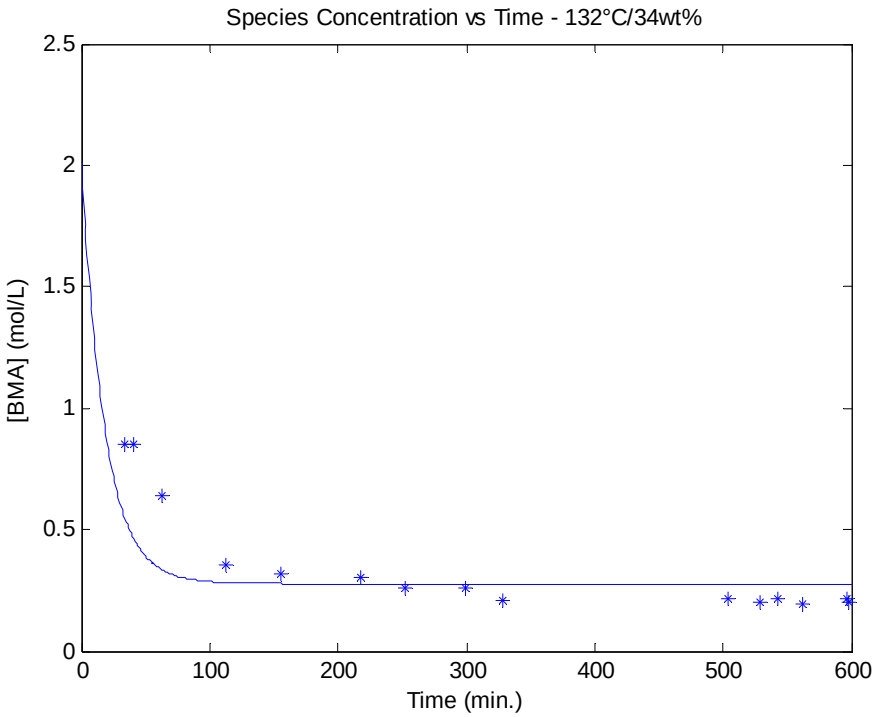

Figure 5.7: Simulation of the homo-polymerization of BMA T = 132°C $[dTBPO]_0$ = 0.34 wt% xylene = 66 wt%

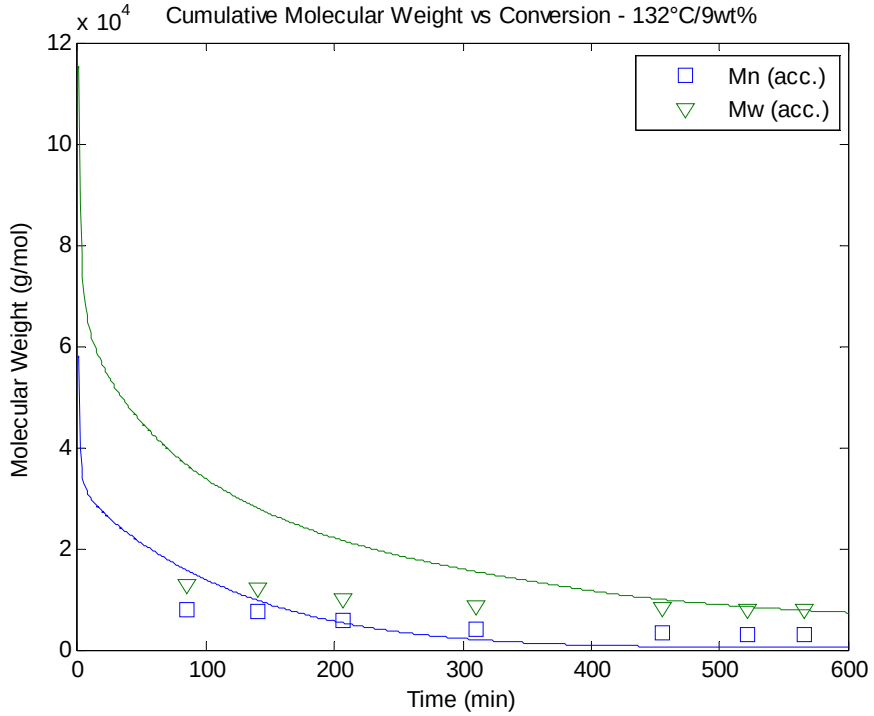

Figure 5.8: Simulation of the homo-polymerization of BMA T = 132°C $[dTBPO]_0$ = 0.09 wt% xylene = 91 wt%

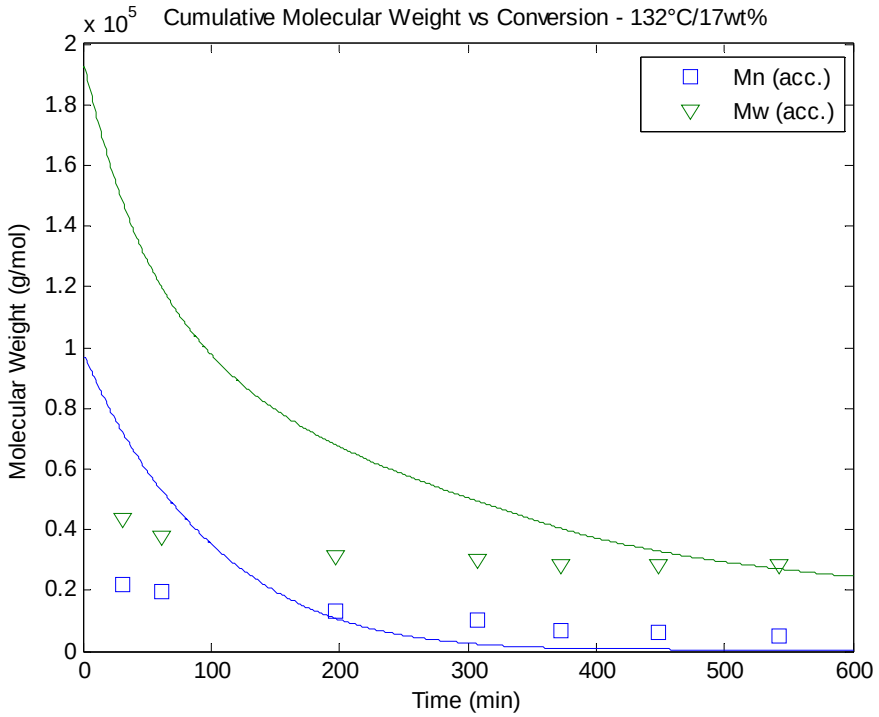

Figure 5.9: Simulation of the homo-polymerization of BMA T = 132°C $[dTBPO]_0$ = 0.17 wt% xylene = 83 wt%

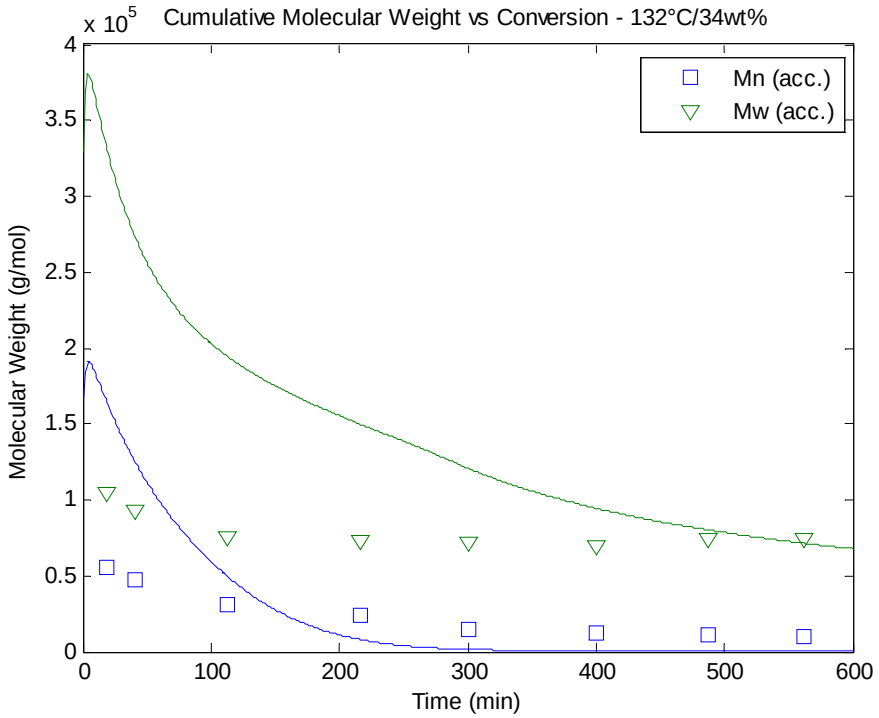

Figure 5.10: Simulation of the homo-polymerization of BMA T = 132°C $[dTBPO]_0$ = 0.34 wt% xylene = 66 wt%

5.1.2. Case Study 2: Co-polymerization of Alpha Methyl Styrene and Styrene

This case study is another prime example demonstrating the importance of depropagation. Fischer (1972) ran four co-polymerizations of AMS and styrene at different temperatures recording the composition drift throughout. The reactivity ratios and depropagation data were taken from Fischer (1972):

Table 5-1: Kinetic Data for the Co-polymerizations of AMS and Styrene

T (°C)	$r_{AMS-Sty}$	$r_{Sty-AMS}$	K_{eq} (mol/L)*	R_2
60	0.15	1.00	7.1	0
90	0.30	1.09	17.2	0
110	0.40	1.13	28.5	0
150	0.80	1.20	67.0	0.8

*From section 3.2.5, $k_{dp,AMS} = K_{eq} * k_{p,AMS}$

As seen in section 4.7, AMS is known to homo-depropagate at low temperatures. The same phenomenon is observed here as well. Figure 5.11 is the co-polymerization of AMS and styrene at 60°C. The small effect that the depropagation of AMS has is shown as the slight departure from the Mayo-Lewis curve. As expected, with each increase in temperature follows a greater difference between our model and the Mayo-Lewis prediction. By the time the co-polymerization reaches 150°C in Figure 5.14 (90°C and 110°C can be seen in Figure 5.12 and Figure 5.13, respectively), the difference has become quite large. At that point, AMS has begun to depropagate from penultimate units of styrene as simulated by the cross-depropagation ratio, $R_2 = 0.8$. Another trend with increasing temperature is that the Mayo-Lewis curve nears the 45° line. This is a result of the change in reactivity ratios; $r_{AMS-Sty}$ and $r_{Sty-AMS}$ become closer and closer to unity as the steric hindrances of AMS become less predominant at high temperatures.

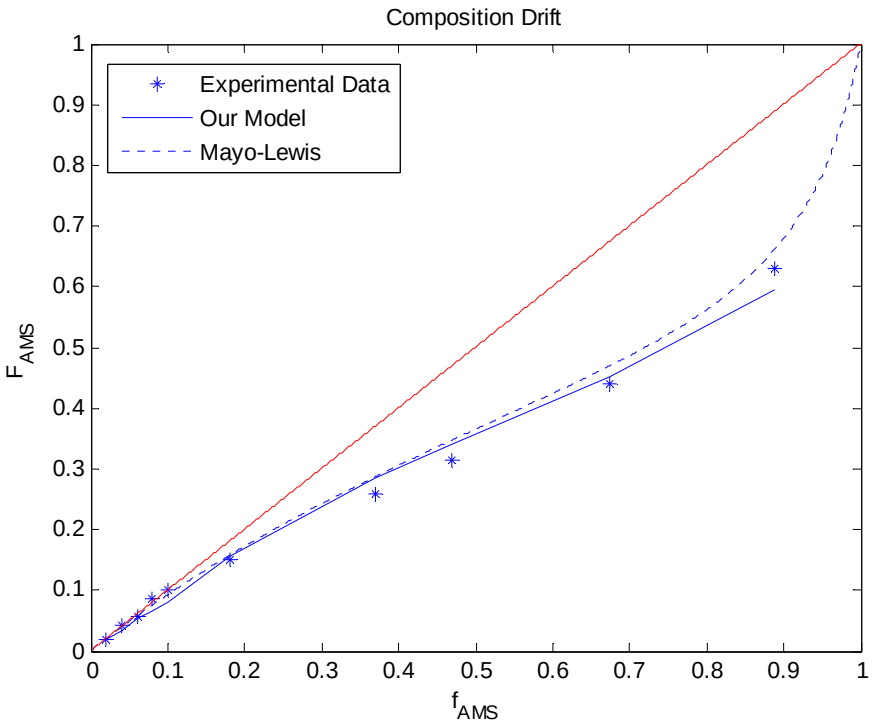

Figure 5.11: Simulation of the co-polymerization of AMS/Sty T = 60°C

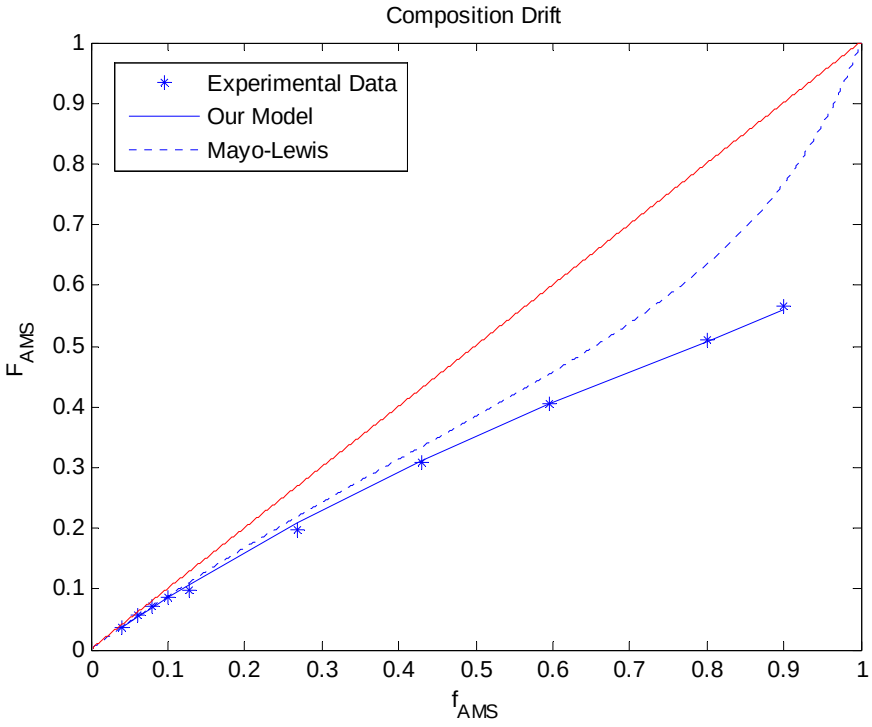

Figure 5.12: Simulation of the co-polymerization of AMS/Sty T = 90°C

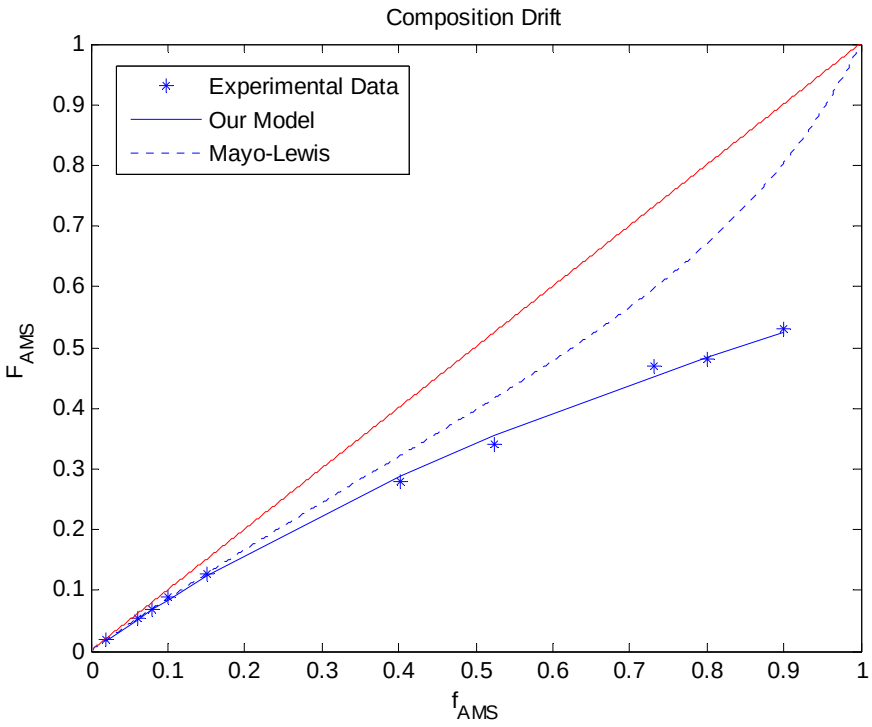

Figure 5.13: Simulation of the co-polymerization of AMS/Sty T = 110°C

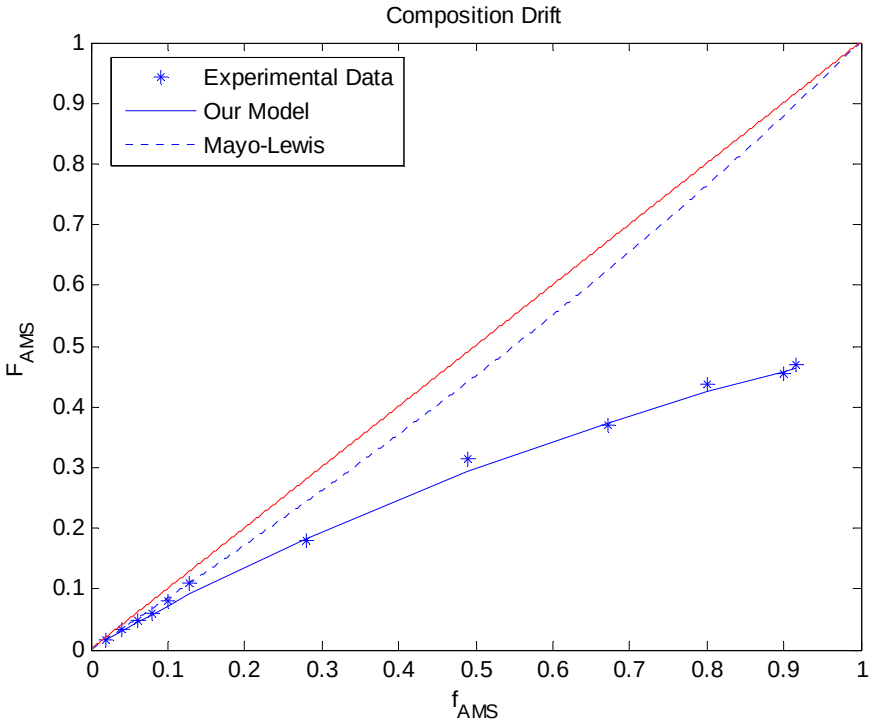

Figure 5.14: Simulation of the co-polymerization of AMS/Sty T = 150°C

5.1.3. Case Study 3: Co-polymerization of AMS and MMA

Palmer *et al.* (2000) conducted several bulk co-polymerizations of AMS and MMA at 115°C and 140°C using di-*tert*-butyl peroxide (dTBPO) as initiator. The reactivity and depropagation ratios for 140°C are $r_{AMS\text{-}MMA} = 0.003$, $r_{MMA\text{-}AMS} = 0.42$, $R_1 = 1.388$, $R_2 = 24.96$, $R_{11} = 0.163$ and $R_{22} = 0.192$; the kinetic data for 115°C have much less depropagation present: $r_{AMS\text{-}MMA} = 0.009$, $r_{MMA\text{-}AMS} = 0.404$, $R_1 = 0$, $R_2 = 11.28$, $R_{11} = 0.285$ and $R_{22} = 0.083$ (Palmer *et al.*, 2000). A summary of each experiment is presented below in Table 5-2 with the corresponding figure numbers shown in the rightmost column:

Table 5-2: Reaction Conditions for the Co-polymerizations of AMS and MMA

Run	Temperature (°C)	Monomer Composition (AMS/MMA wt%)	Initiator Amount (wt%)	Figure Number
1	140	45/55	2	Figure 5.15
				Figure 5.16
				Figure 5.17
2	140	45/55	0.5	Figure 5.18
				Figure 5.19
				Figure 5.20
3	140	29/71	1	Figure 5.21
				Figure 5.22
				Figure 5.23
4	115	45/55	8	Figure 5.24
				Figure 5.25
				Figure 5.26
5	115	45/55	2	Figure 5.27
				Figure 5.28
				Figure 5.29

For each of the simulations, the polymer composition and molecular weight predictions were very accurate. Overall monomer conversion data were also represented quite well by the modeling software except when the initiator was at exceedingly high or low levels.

The simulation in Figure 5.18 shows a cut-off point for the reaction at 49%. Comparing with the same conditions and four times the amount of initiator in Figure 5.15, this is logical. The data and prediction in Experiment 1 have a final conversion of about 58% and if a large amount of the initiator was removed, as is the difference between the two runs, fewer chains would be present resulting in higher molecular weights. The data, however, do not agree with this hypothesis; by superimposing the two runs on top of each other, the experimental

data would virtually overlap, showing only a difference in the rate of polymerization. This could be the result of flawed data. Figure 5.18 still shows an acceptable prediction and the remainder of the simulations at 140°C agree well with the data.

At 115°C, Figure 5.24 shows that the simulation slightly over-anticipates the final conversion. This is surprising as the data taken from Palmer *et al.* (2000) shown in Figure 5.27 reach the same final conversion of approximately 79%. Why would more initiator create a lower cut-off? In this case, it should only increase the rate of reaction and nothing more. The model agrees with this logic so the data might potentially be skewed by an unknown factor. Palmer *et al.* (2000) actually conducted a replicate of the first experiment which showed a large difference in the initial rate of reaction; it does not look as though the run was completed, however, as the data points do not continue past 200 minutes. The remaining figures at 115°C, including the conversion figure at 2 wt% dTBPO, all represent the data with reasonable accuracy. Another run was completed by Palmer *et al.* (2000) at 115°C but was not shown here; it also produced accurate results.

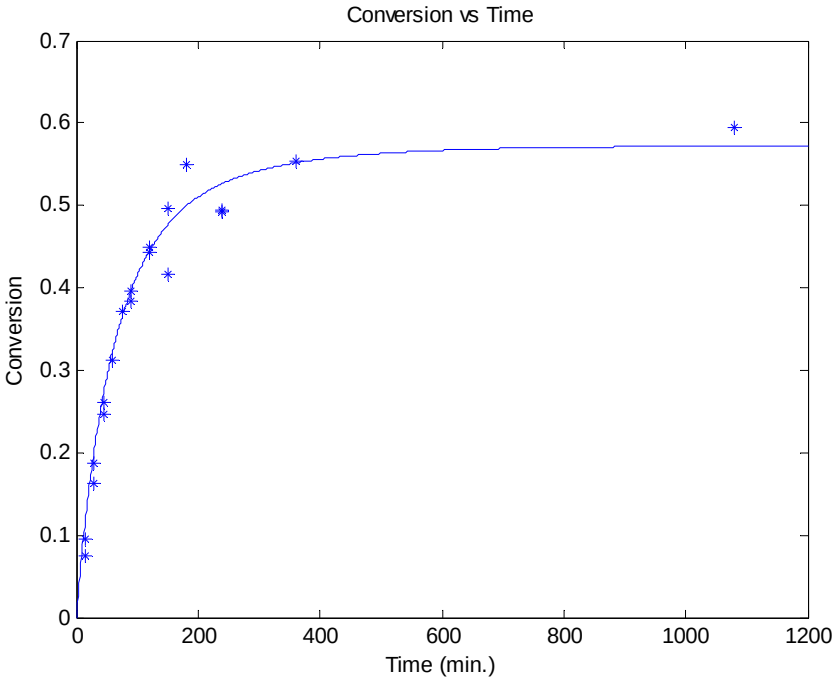

Figure 5.15: Simulation of the bulk co-polymerization of AMS/MMA T = 140°C $[dTBPO]_0$ = 2 wt% f_{AMS0} = 45 wt%

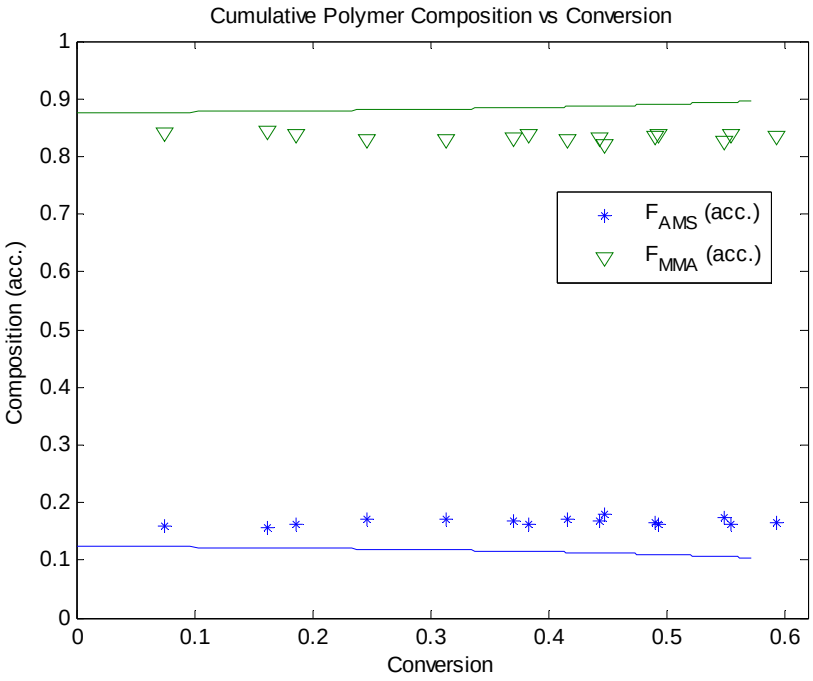

Figure 5.16: Simulation of the bulk co-polymerization of AMS/MMA T = 140°C $[dTBPO]_0$ = 2 wt% f_{AMS0} = 45 wt%

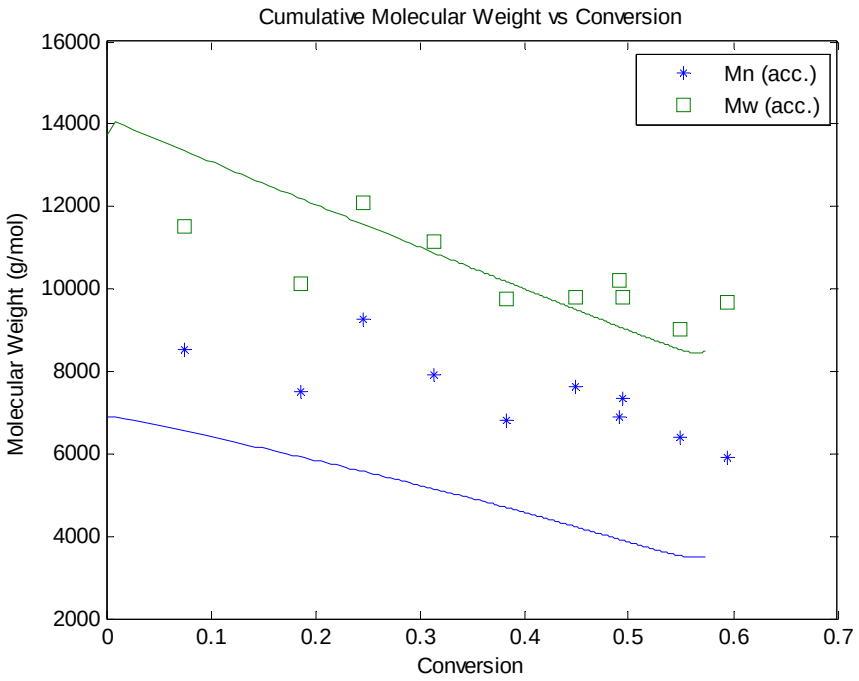

Figure 5.17: Simulation of the bulk co-polymerization of AMS/MMA T = 140°C $[dTBPO]_0$ = 2 wt% f_{AMS0} = 45 wt%

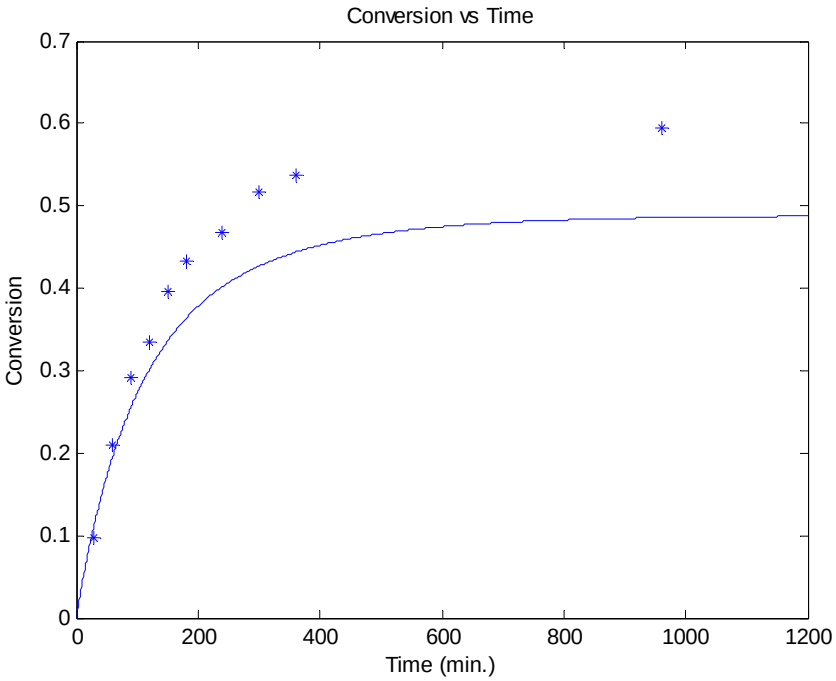

Figure 5.18: Simulation of the bulk co-polymerization of AMS/MMA T = 140°C $[dTBPO]_0$ = 0.5 wt% f_{AMS0} = 45 wt%

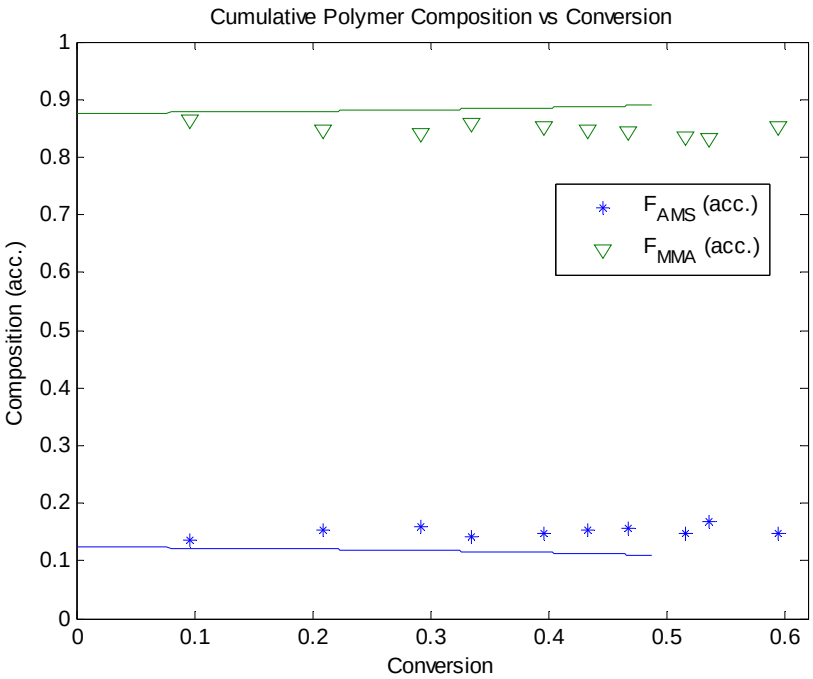

Figure 5.19: Simulation of the bulk co-polymerization of AMS/MMA T = 140°C $[dTBPO]_0$ = 0.5 wt% f_{AMS0} = 45 wt%

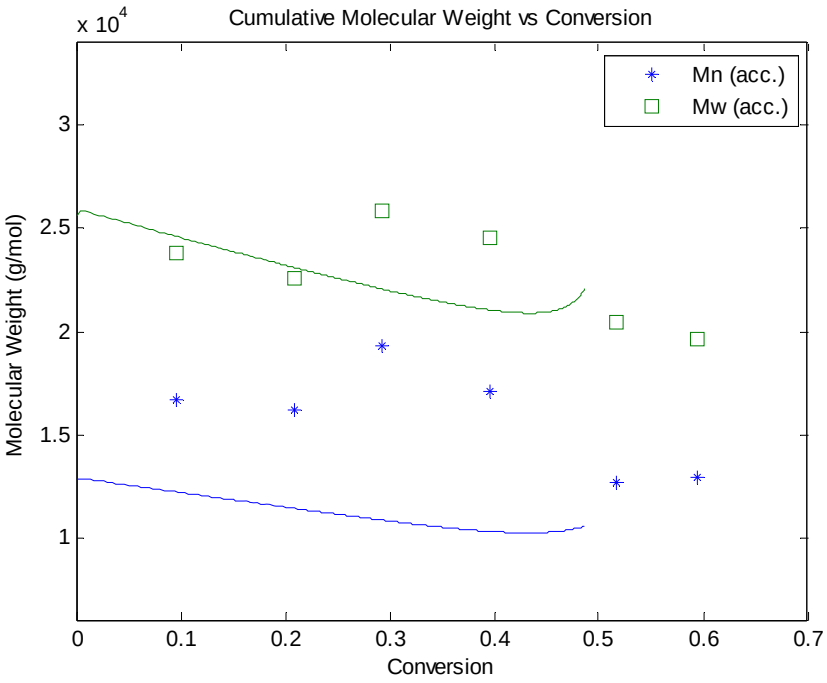

Figure 5.20: Simulation of the bulk co-polymerization of AMS/MMA T = 140°C $[dTBPO]_0$ = 0.5 wt% f_{AMS0} = 45 wt%

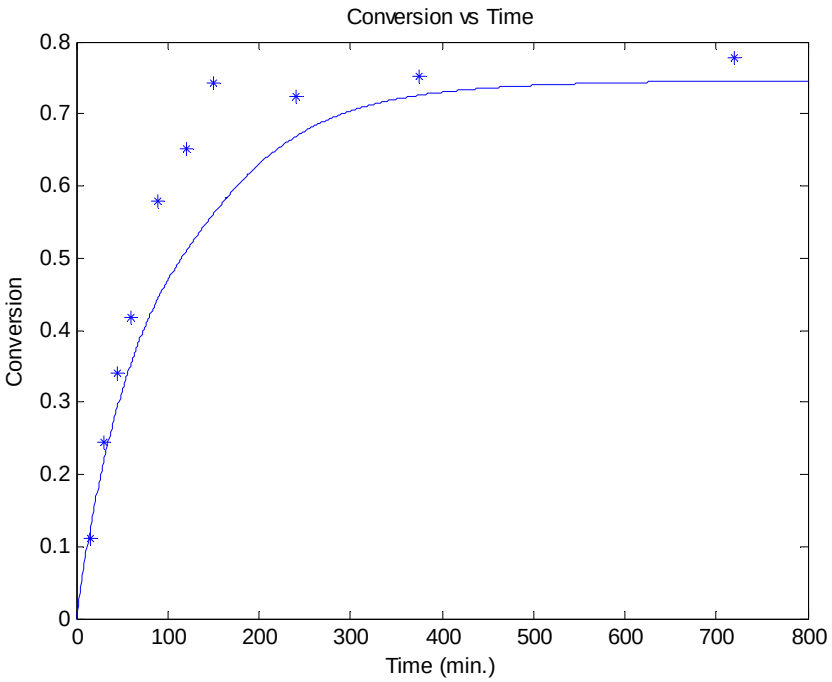

Figure 5.21: Simulation of the bulk co-polymerization of AMS/MMA T = 140°C $[dTBPO]_0$ = 1 wt% f_{AMS0} = 29 wt%

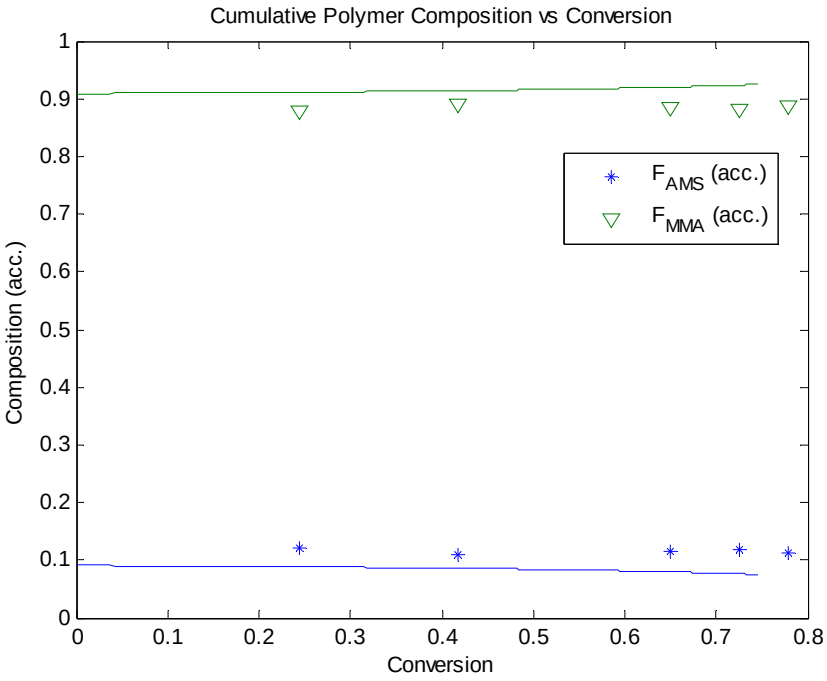

Figure 5.22: Simulation of the bulk co-polymerization of AMS/MMA T = 140°C $[dTBPO]_0$ = 1 wt% f_{AMS0} = 29 wt%

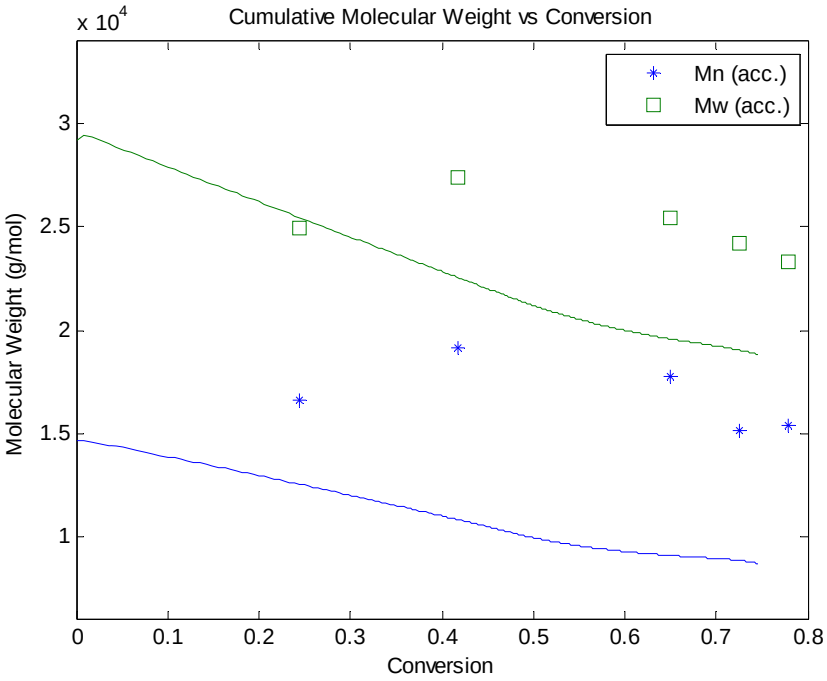

Figure 5.23: Simulation of the bulk co-polymerization of AMS/MMA T = 140°C $[dTBPO]_0$ = 1 wt% f_{AMS0} = 29 wt%

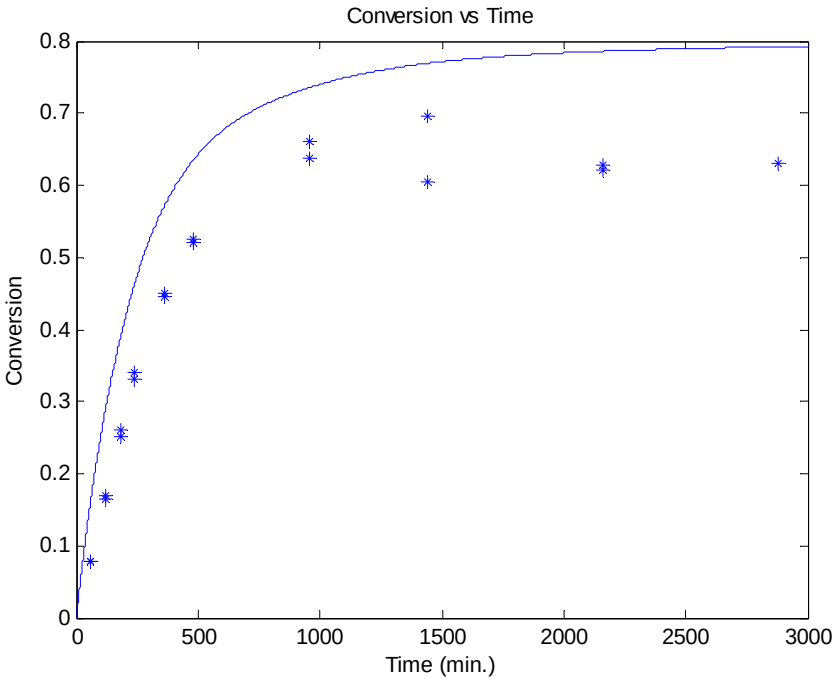

Figure 5.24: Simulation of the bulk co-polymerization of AMS/MMA T = 115°C $[dTBPO]_0$ = 8 wt% f_{AMS0} = 45 wt%

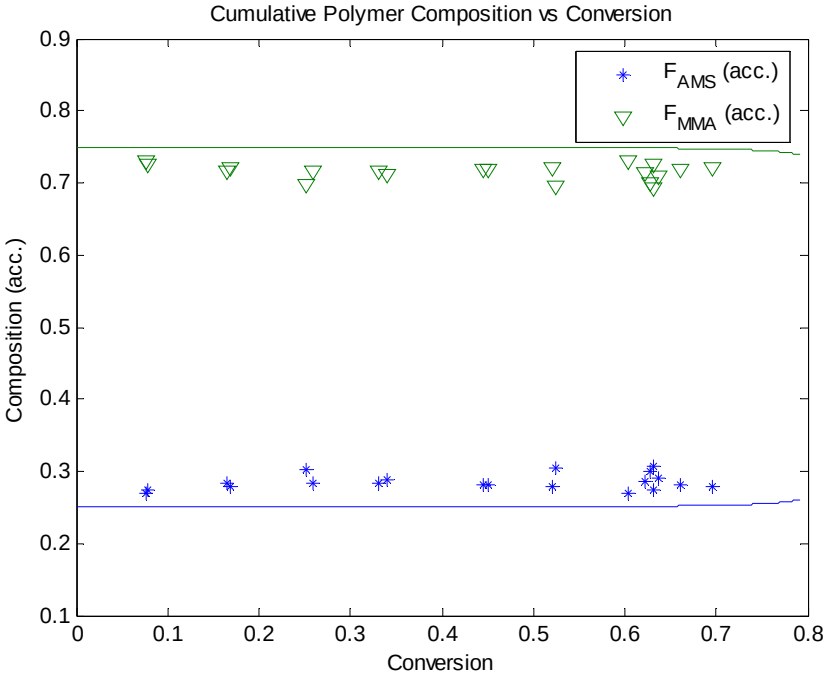

Figure 5.25: Simulation of the bulk co-polymerization of AMS/MMA T = 115°C $[dTBPO]_0$ = 8 wt% f_{AMS0} = 45 wt%

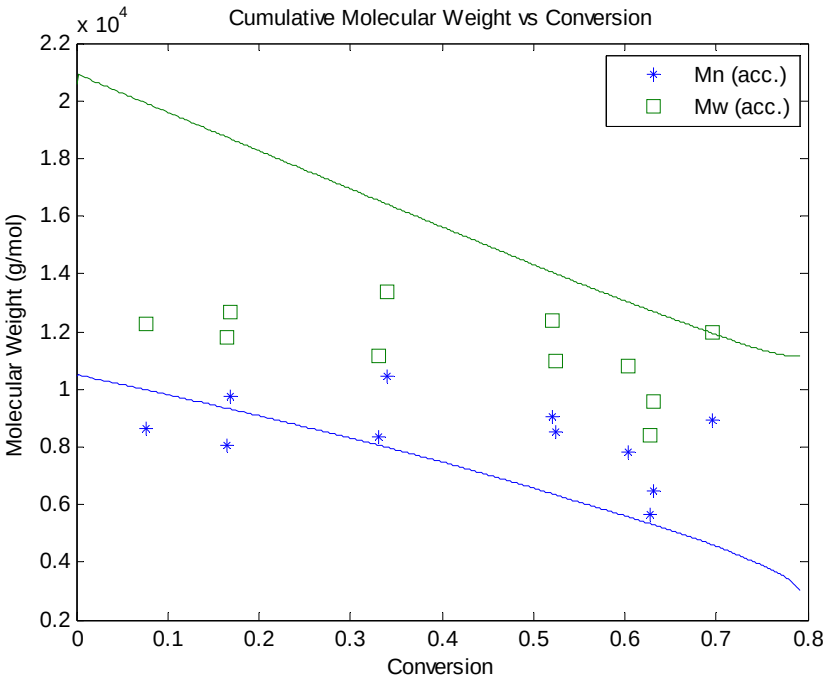

Figure 5.26: Simulation of the bulk co-polymerization of AMS/MMA T = 115°C $[dTBPO]_0$ = 8 wt% f_{AMS0} = 45 wt%

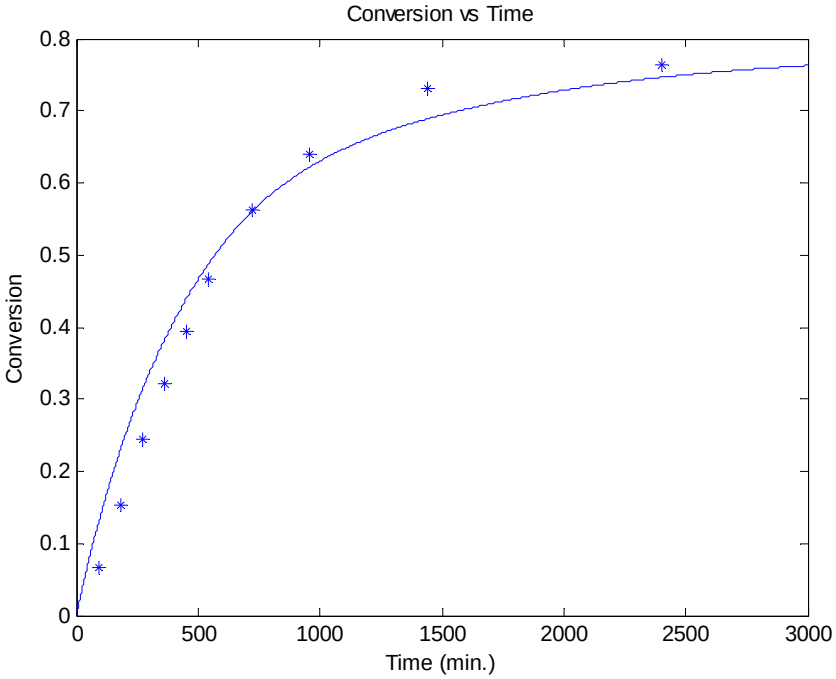

Figure 5.27: Simulation of the bulk co-polymerization of AMS/MMA T = 115°C $[dTBPO]_0$ = 2 wt% f_{AMS0} = 45 wt%

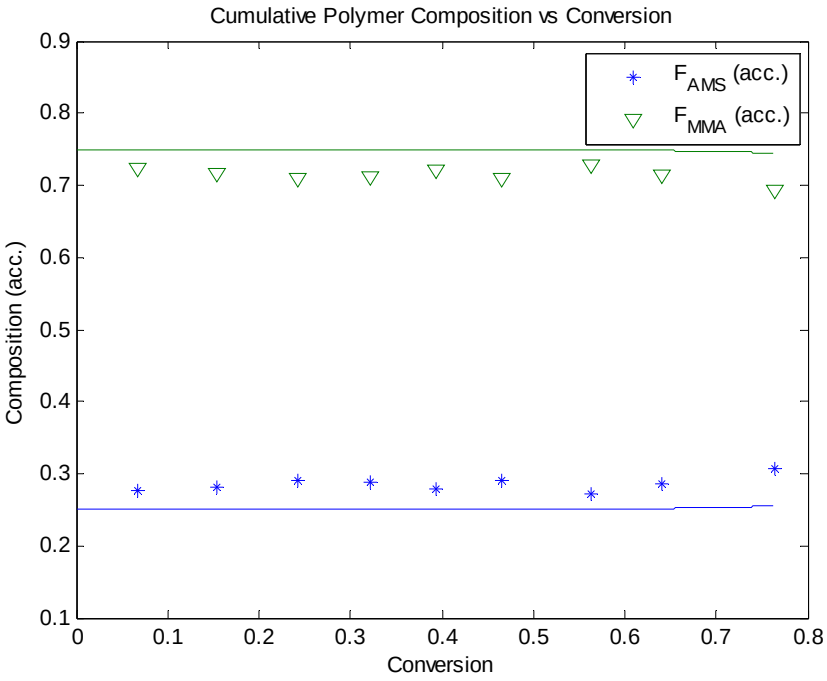

Figure 5.28: Simulation of the bulk co-polymerization of AMS/MMA T = 115°C $[dTBPO]_0$ = 2 wt% f_{AMS0} = 45 wt%

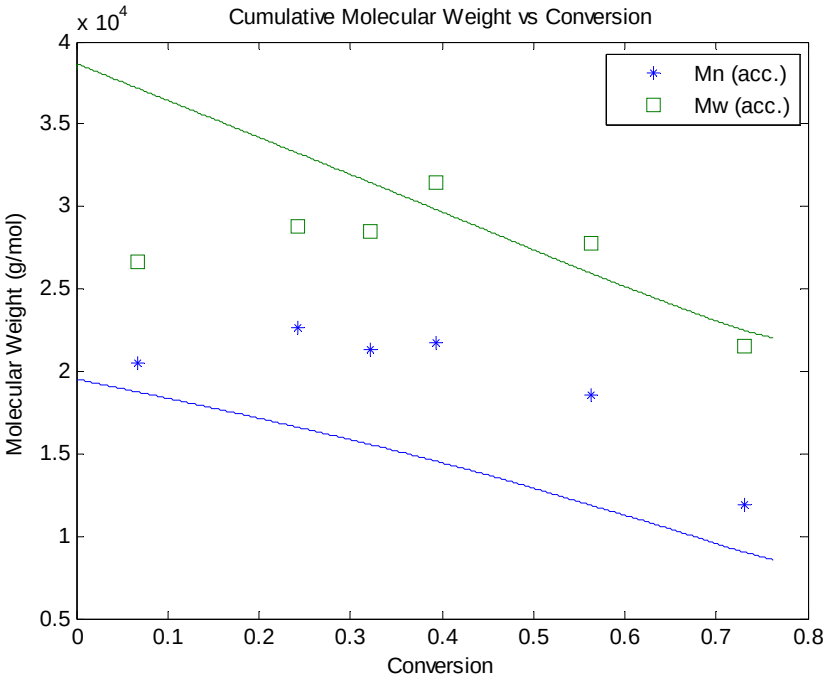

Figure 5.29: Simulation of the bulk co-polymerization of AMS/MMA T = 115°C $[dTBPO]_0$ = 2 wt% f_{AMS0} = 45 wt%

5.1.4. Case Study 4: Co-polymerization of Styrene and Glycidyl Methacrylate

Eight co-polymerizations of styrene and GMA were carried out at 170°C, 190°C and 230°C by Wolf *et al.* (2002). Polymer composition data against monomer conversion was recorded. No initiator was present as styrene is known to self-initiate at elevated temperatures. Three of the experiments were carried out with 30wt% xylene. Due to the effect that solvent has on monomer concentration, homo-depropagation of GMA was assumed to occur when solvent was present. GMA has been cited to homo-depropagate following the rate constant

$k_{dp,GMA\text{-}homo}$ = 1.765e14*exp((-1.7065e4)/(R*T)). (Wang and Hutchinson, 2008)

Reactivity ratios were taken from both Brandrup *et al.* (1999) as well as from Wolf *et al.* (2002), presented in Table 5-3. The corresponding figure number for each of the simulations is also shown in the following table:

Table 5-3: Reaction Conditions and Kinetic Data Used for the Co-polymerization of Styrene and GMA

Figure	Temperature (°C)	Solvent	r_{Sty}	r_{GMA}	Source
Figure 5.30	170	No	0.316	0.750	Wolf *et al.* (2002)
Figure 5.31	190	No	0.356	0.785	Wolf *et al.* (2002)
Figure 5.32	190	No	0.356	0.785	Wolf *et al.* (2002)
Figure 5.33	190	No	0.356	0.785	Wolf *et al.* (2002)
Figure 5.34	190	Yes	0.278	0.539	Brandrup *et al.* (1999)
Figure 5.35	190	Yes	0.278	0.539	Brandrup *et al.* (1999)
Figure 5.36	190	Yes	0.278	0.539	Brandrup *et al.* (1999)
Figure 5.37	230	No	0.356	0.785	Wolf *et al.* (2002)

The reason for the discrepancy between the reactivity ratios is because Wolf *et al.* (2002) did not account for depropagation of GMA at elevated temperatures. As this is a co-polymerization, a reduction in the amount of depropagation, $\frac{k_{dp,GMA,homo}}{100}$, was used to account for the presence of styrene. Cross-depropagation of GMA from styrene was assumed negligible.

For each of the simulations, the results were quite accurate. This proves the above methods were valid in their approach.

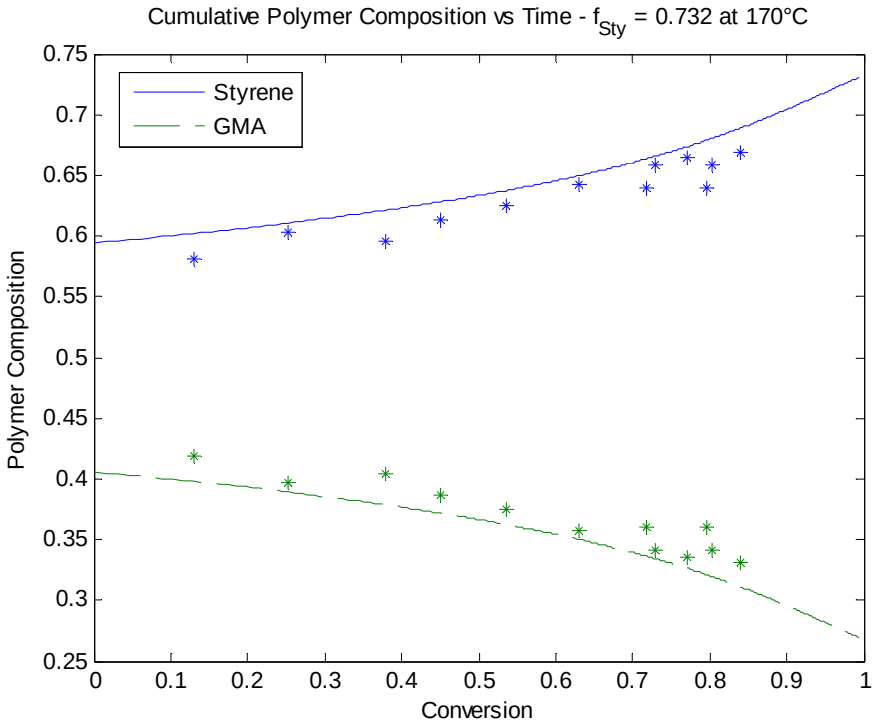

Figure 5.30: Simulation of the co-polymerization of Sty/GMA T = 170°C f_{Sty0} = 0.732

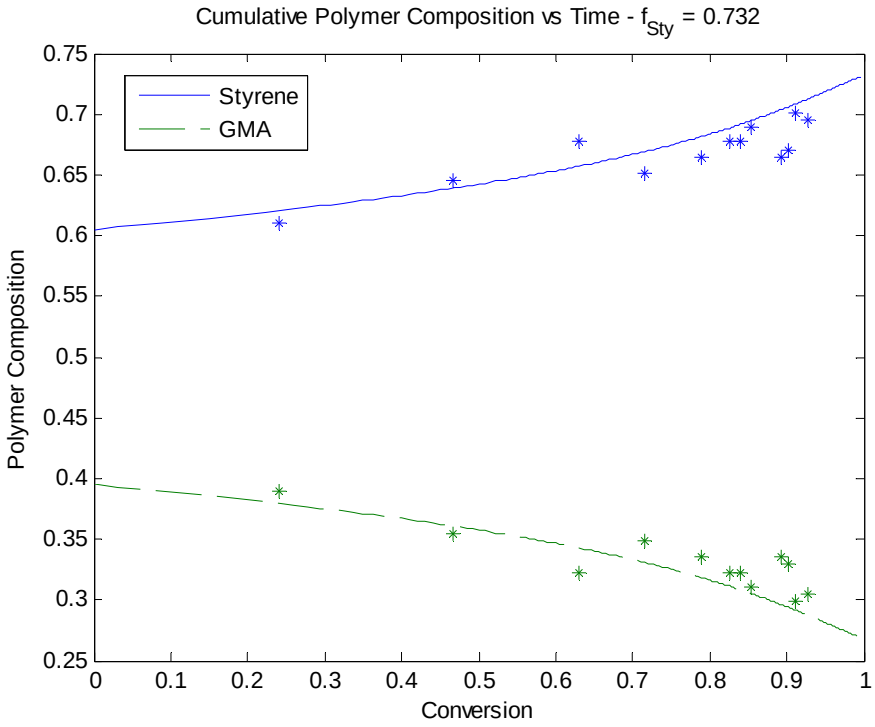

Figure 5.31: Simulation of the co-polymerization of Sty/GMA T = 190°C f_{Sty0} = 0.732

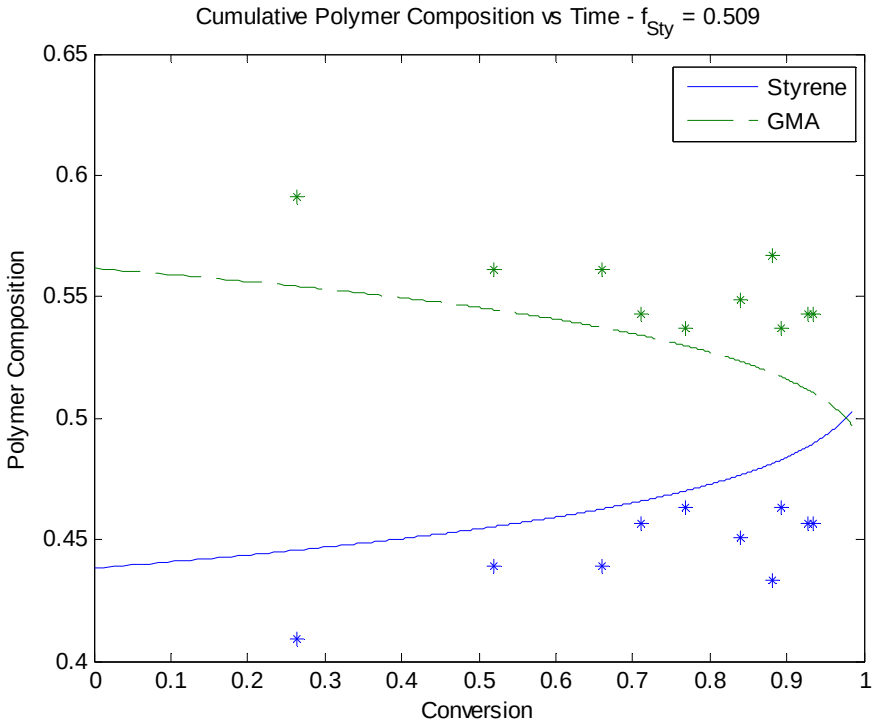

Figure 5.32: Simulation of the co-polymerization of Sty/GMA T = 190°C f_{Sty0} = 0.509

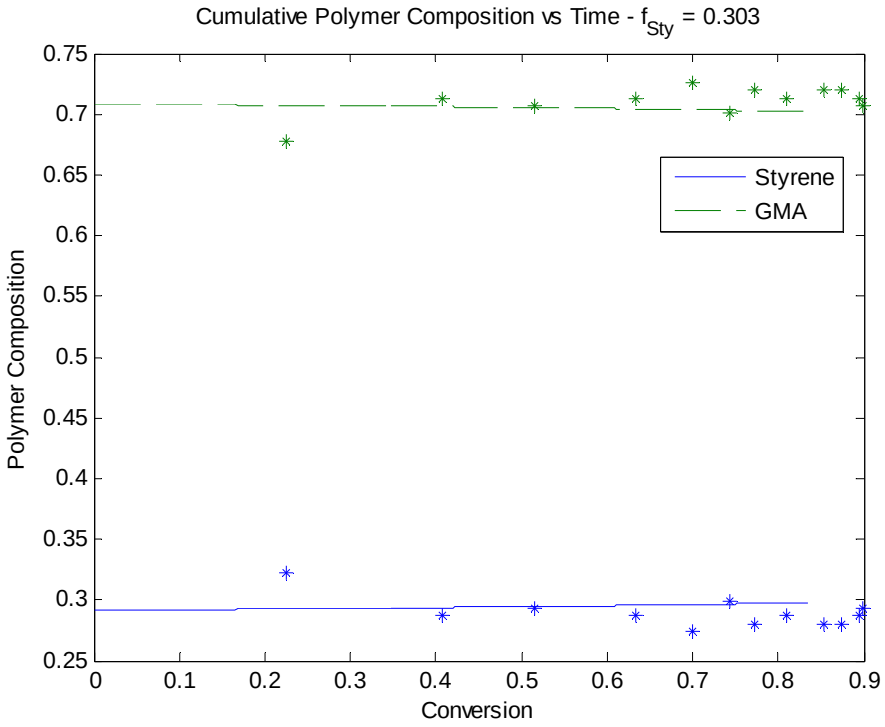

Figure 5.33: Simulation of the co-polymerization of Sty/GMA T = 190°C f_{Sty0} = 0.303

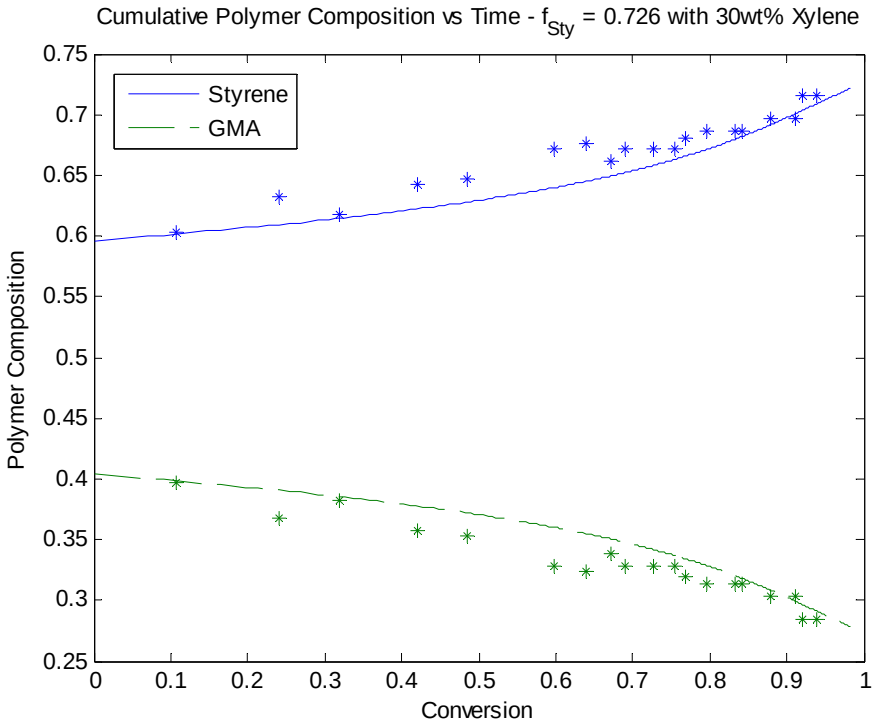

Figure 5.34: Simulation of the co-polymerization of Sty/GMA T = 190°C xylene = 30wt% f_{Sty0} = 0.726

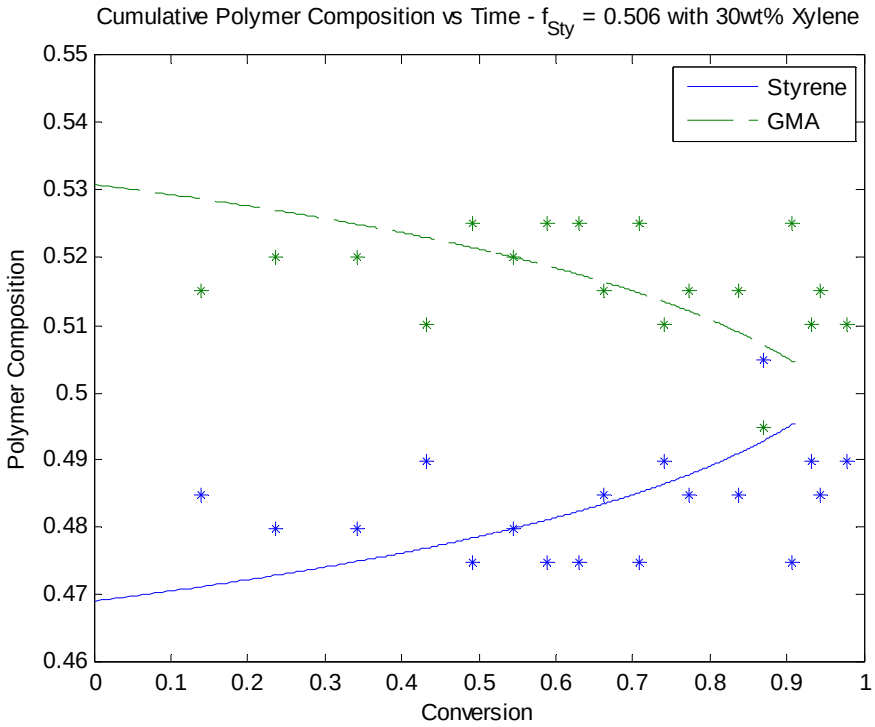

Figure 5.35: Simulation of the co-polymerization of Sty/GMA T = 190°C xylene = 30wt% f_{Sty0} = 0.506

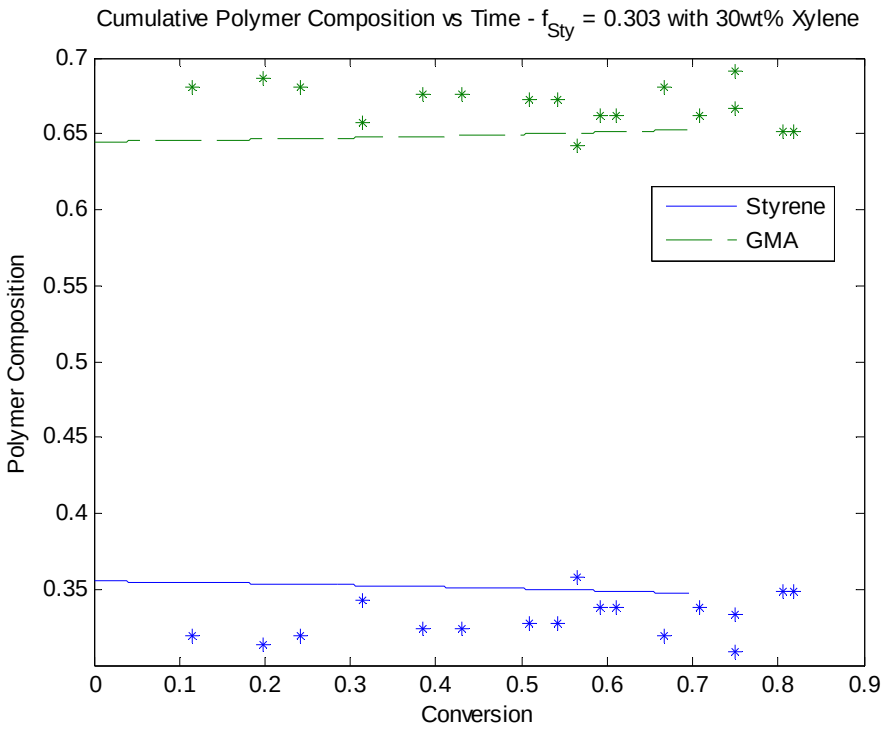

Figure 5.36: Simulation of the co-polymerization of Sty/GMA T = 190°C xylene = 30wt% f_{Sty0} = 0.303

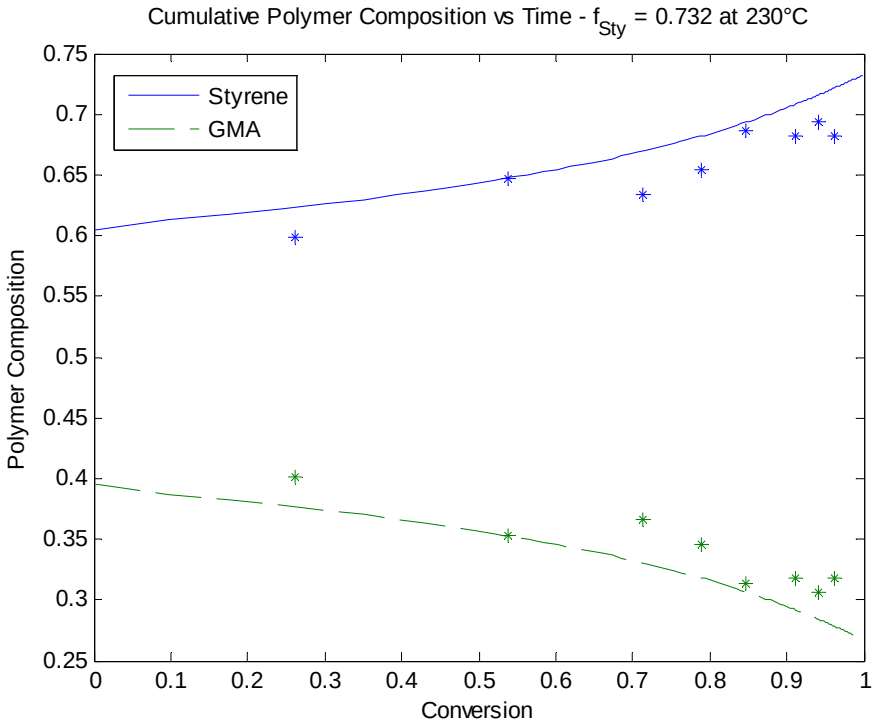

Figure 5.37: Simulation of the co-polymerization of Sty/GMA T = 230°C f_{Sty0} = 0.732

Another co-polymerization of styrene and GMA at elevated temperatures was conducted by Wang (2010). Five semi-batch co-polymerizations were completed in total at 138°C using 2 wt% of tert-butyl peroxyacetate relative to monomer and 30 wt% xylene. The reactor was initially charged with the solvent; the monomers were fed evenly over 360 minutes and the initiator was fed evenly over 375 minutes. The reactivity ratios used are $r_{Sty\text{-}GMA} = 0.306$ and $r_{GMA\text{-}Sty} = 0.508$ from Wang (2010). Only homo-depropagation of GMA was assumed with the same experimental rate used in the previous co-polymerization to account for the presence of a second monomer.

Figure 5.38 and Figure 5.39 show the concentration of each monomer in the system throughout the reaction with the simulations represented by the solid lines. In the previous section, styrene and GMA were tested against polymer composition and performed quite well. Here, the same two monomers are tested against concentration data with again, exceptional results. Even with some kinetic data borrowed from BMA and HEMA, the newly added monomer has done exceedingly well and given us a solid base on which to work from. Kinetic data from GMA as well as all other monomers in our database can be found in the appendices.

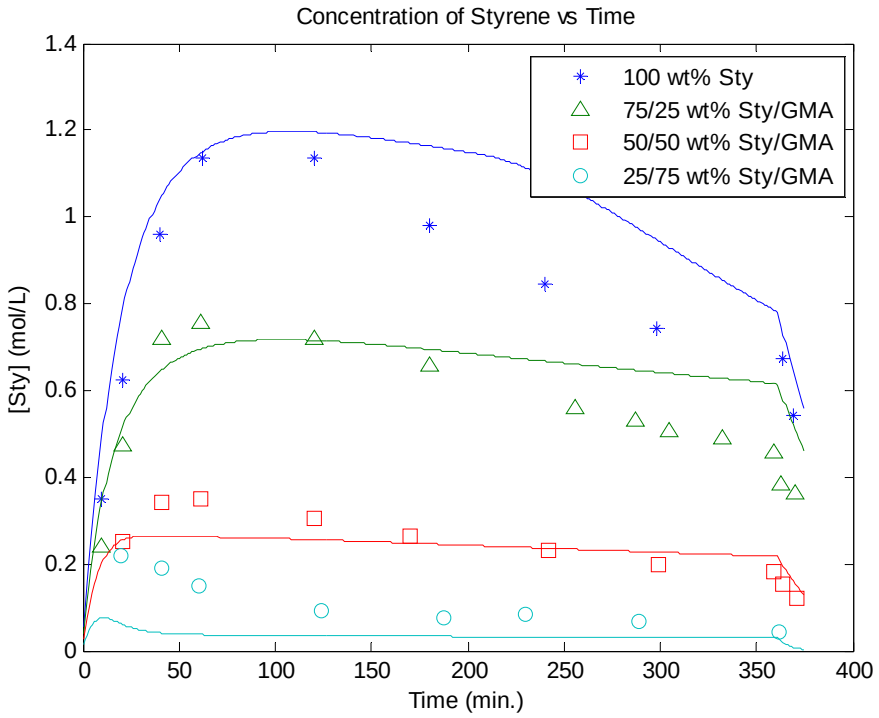

Figure 5.38: Simulation of the co-polymerization of Sty/GMA T = 138°C $[TBPA]_0$ = 2 wt% xylene = 30 wt%

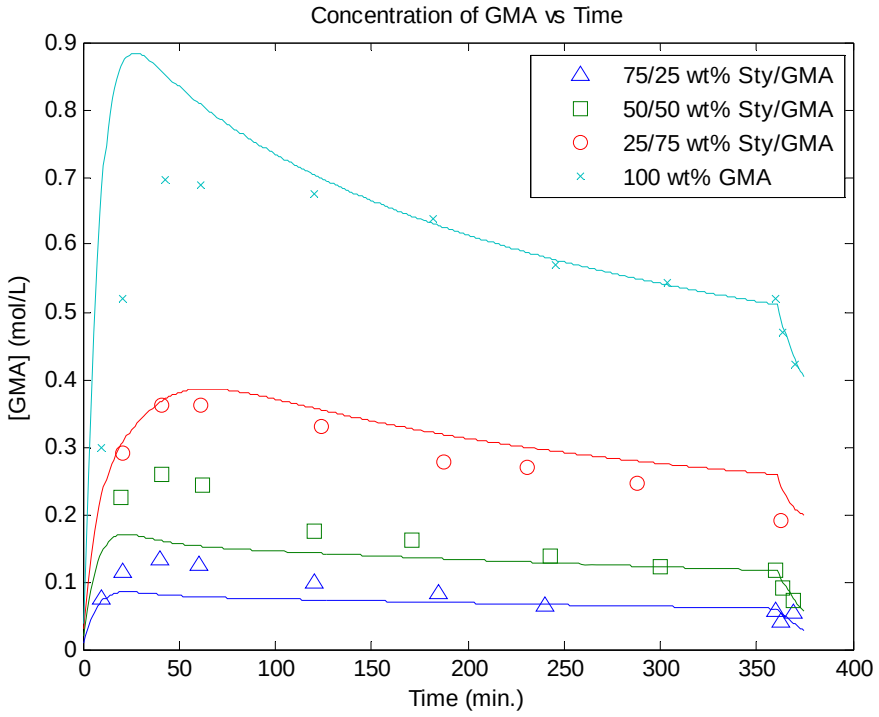

Figure 5.39: Simulation of the co-polymerization of Sty/GMA T = 138°C $[TBPA]_0$ = 2 wt% xylene = 30 wt%

5.1.5. Case Study 5: Ter-polymerization of AMS, MMA and BA

The next case study presented is a ter-polymerization of AMS, MMA and BA. The four experiments were conducted by McManus *et al.* (2004) involving different monomer feed ratios at 140°C. Polymer composition data were taken for three of the experiments and molecular weight data, both number-average and weight-average, were recorded for only one of the runs. Again, dTBPO was used as the initiator at 0.5 wt%. The reactivity and depropagation ratios are shown in Table 5-4.

Table 5-4: Reactivity and Depropagation Ratios for the Ter-polymerization of AMS, MMA and BA at 140°C

Reactivity Ratio		Source
$r_{AMS-MMA}$	0.003	Palmer *et al.* (2000)
r_{AMS-BA}	0.5575	Leamen *et al.* (2006)
$r_{MMA-AMS}$	0.42	Palmer *et al.* (2000)
r_{MMA-BA}	1.905	Leamen *et al.* (2006)
r_{BA-AMS}	0.143	Leamen *et al.* (2006)
r_{BA-MMA}	0.348	Leamen *et al.* (2006)
R_1	1.388	Palmer *et al.* (2000)
*R_2	11.28	Palmer *et al.* (2000)
R_{11}	0.1634	Palmer *et al.* (2000)

*Value used for 120°C

When determining the ideal kinetic data for this scenario, several considerations were taken into account. In terms of reactivity ratios, we know from the previous case study that the values given by Palmer *et al.* (2000) haven proven quite accurate when dealing with AMS and MMA at 140°C. In all other cases, the only values we have for a ter-polymerization of AMS, MMA and BA are given by Leamen *et al.* (2006) and were used accordingly. As this is a ter-polymerization with a non-depropagating monomer, less depropagation is expected. As such, the homo-depropagation of MMA, R_{22}, was set to zero. Also, the cross-depropagation ratio of AMS from MMA, R_2, was set to the 120°C value from Palmer *et al.* (2000). With these settings, the following plots were generated.

Figure 5.40 is the simulation of conversion versus time for each of the monomer feed ratios. Three of the four predictions follow the data very well. The final simulation, $f_{AMS0} = f_{BA0} = 30$ wt%, shows a final monomer conversion of 80%, about 15 points lower than the experimental data. The major difference between this run and the others is the amount of butyl acrylate. With more BA present, should it not be expected that the reaction would run

slower, not faster? At 140°C, backbiting and beta-scission of BA is known to exist, further inhibiting the reaction (Rantow *et al.*, 2006); see section 5.2. Figure 5.41 shows accurate predictions of polymer composition data against conversion, further testifying that the reactivity ratios are correct. Figure 5.42 depicts an accurate simulation of both number-average and weight-average molecular weights.

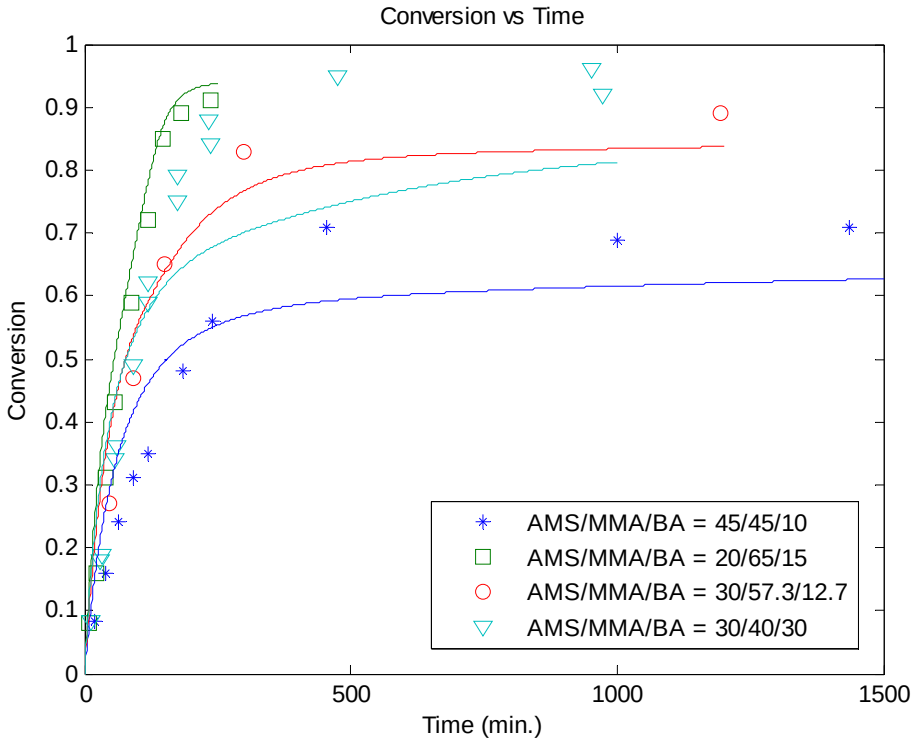

Figure 5.40: Simulation of the bulk ter-polymerization of AMS/MMA/BA T = 140°C $[dTBPO]_0$ = 0.5 wt%

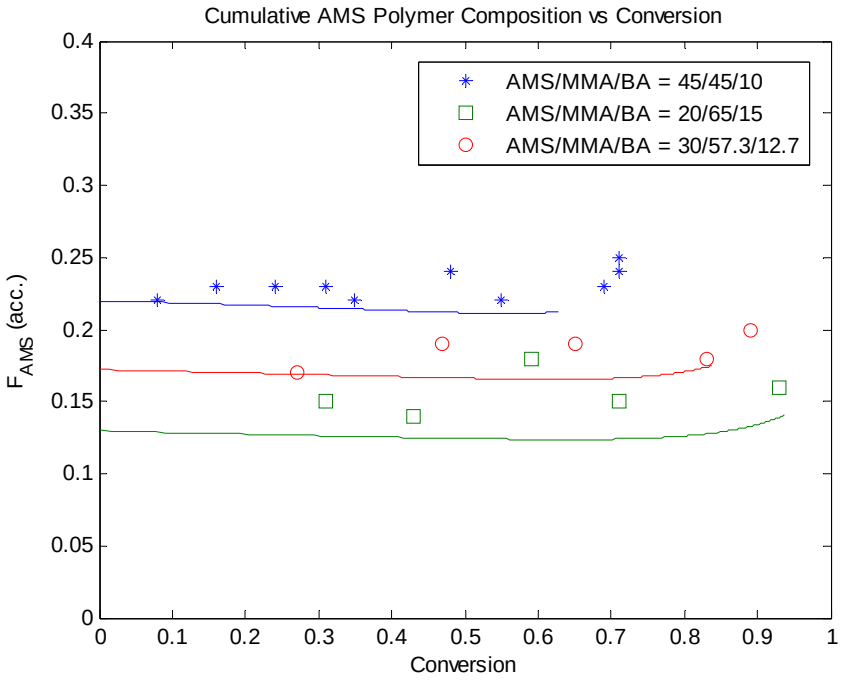

Figure 5.41: Simulation of the bulk ter-polymerization of AMS/MMA/BA T = 140°C $[dTBPO]_0$ = 0.5 wt%

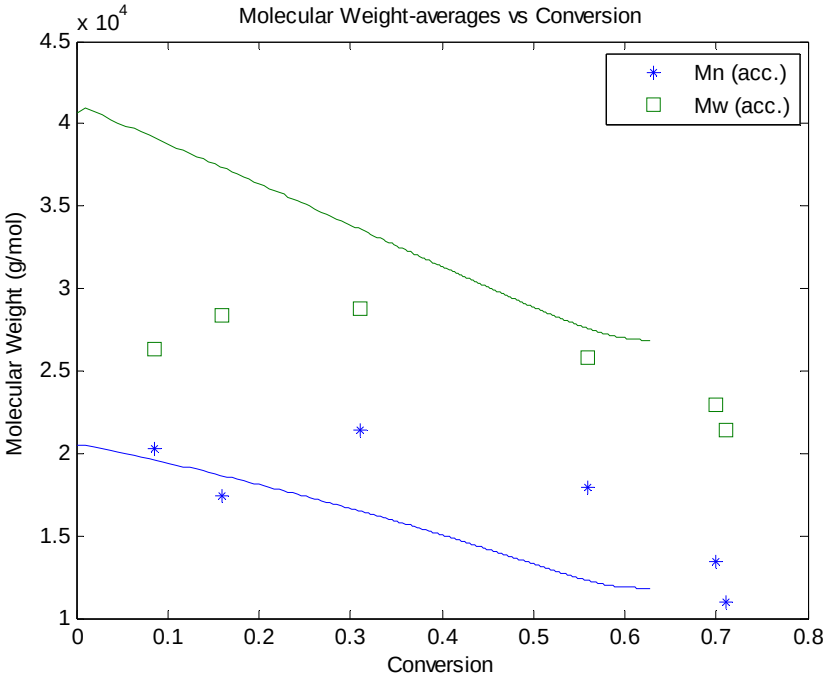

Figure 5.42: Simulation of the bulk ter-polymerization of AMS/MMA/BA T = 140°C $[dTBPO]_0$ = 0.5 wt% f_{AMS0} = f_{MMA0} = 45 wt%

5.1.6. Case Study 6: Hexa-polymerization – Simulation Trends

This report emphasizes, among many things, that the software can model up to six monomers at once. There has been no literature generated on such a large monomer system, primarily because of experimental analysis complexities. This section will show the capabilities of our model by comparing hexa-polymerization with expected trends; the first simulation is at 120°C with no depropagation; the second is at 120°C with depropagation; the third simulation is at 140°C with depropagation; the fourth is with an increased amount of one of the depropagating monomers; and the fifth is with an increased amount of one of the non-depropagating monomers, both at 120°C.

The monomers modeled in this section are alpha methyl styrene, methyl methacrylate, ethyl acrylate, butyl methacrylate, glycidyl methacrylate and acrylonitrile. AMS, MMA, BMA and GMA are expected to depropagate at these temperatures. The reactivity ratios used for these simulations have been included at the end of this section in Table 5-5. The inlet monomer mole fractions for the first three polymerizations (all six monomers) are 16.7 wt% each with 1 wt% of dTBPO to the monomers. The fourth run, MMA dominance, has MMA at 50 wt% and the remaining five monomers at 10 wt%. The initiator remains at 1 wt%. The fifth simulation, EA dominance, is identical except for the role reversal of MMA and EA.

Figure 5.43 shows the conversion versus time plots for all five polymerizations. The simulations with and without depropagation are quite straightforward. Without depropagation, auto-acceleration occurs naturally and the reaction proceeds quite quickly to complete conversion. With depropagation however, the rate of termination may never become diffusion-controlled, leaving the reaction to proceed without the sharp increase. At 120°C, auto-acceleration does occur but it happens several hours later; at 140°C, the rate of termination never reaches zero and the reaction ceases. This is to be anticipated as four of the six monomers depropagate and will eventually reach equilibrium assuming, of course, that auto-acceleration never occurs. With MMA quite dominant in the monomer feed, the reaction proceeds more rapidly. This is simple kinetics, even though MMA depropagates, albeit not very much at 120°C, it is one of the more reactive monomers in the group and has relatively small termination rate constant. These two differences allow the reaction to proceed much faster. EA, although not known to depropagate, has a large termination rate constant and consequently forces the reaction to proceed much slower when present in large amounts. Figure 5.44 shows the overall rate of termination versus conversion. As expected, an increased temperature and increased level of EA have the highest rate of termination curves whereas the MMA dominant simulation has a relatively low overall rate

of termination. One can also see the point at which auto-acceleration begins by observing the rate of termination approaching zero.

Figure 5.45 and Figure 5.46 show the initiator efficiency and glass transition temperature of the polymer versus conversion, respectively. The initiator efficiency is slightly dependent on the monomers involved, hence the differences in the calculations (see Appendix I – Interpolation due to Monomer Effects). The glass transition temperature of the polymer naturally depends on which monomers were incorporated into the polymer; hence a difference in the curves is present.

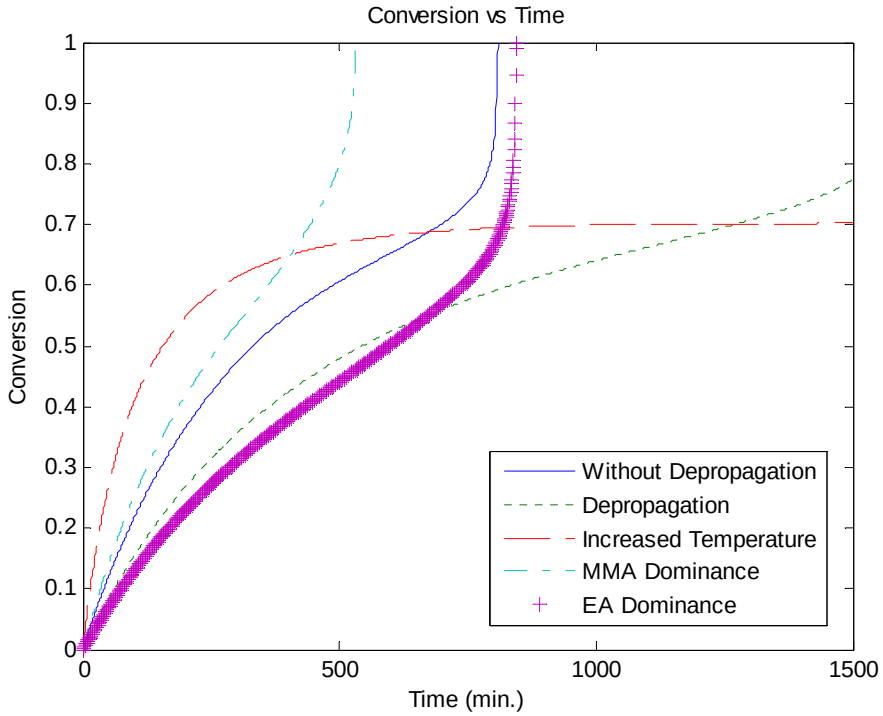

Figure 5.43: Simulation trends of bulk hexa-polymerization with and without depropagation

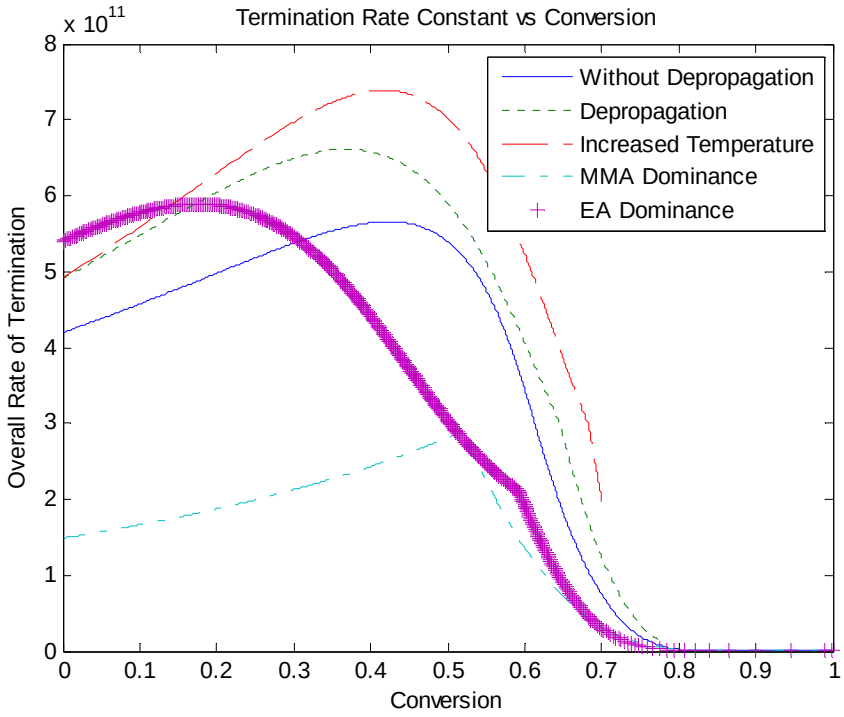

Figure 5.44: Simulation trends of bulk hexa-polymerization with and without depropagation

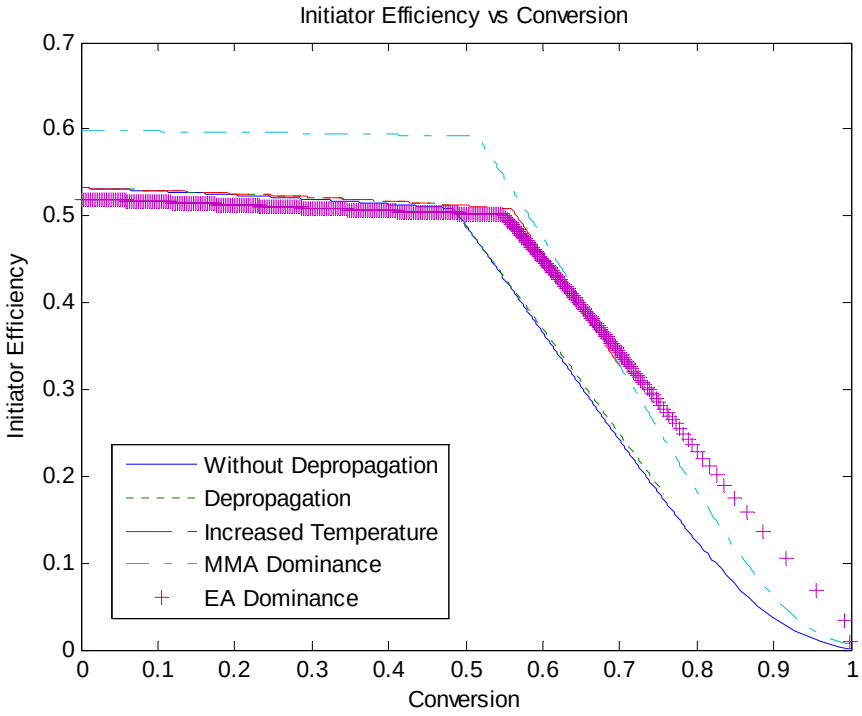

Figure 5.45: Simulation trends of bulk hexa-polymerization with and without depropagation

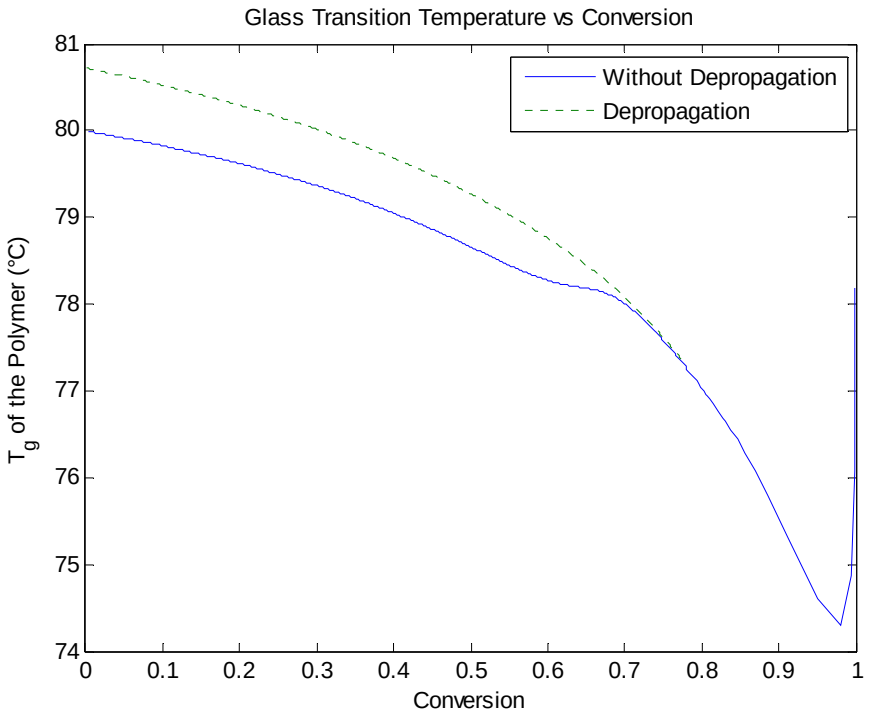

Figure 5.46: Simulation trends of bulk hexa-polymerization with and without depropagation

Sequence length is a very complex process and modeling with six monomers makes it even more difficult. Figure 5.47 to Figure 5.51 show the number-average sequence length versus conversion with and without depropagation for EA, MMA, BMA, GMA and AN, respectively. AMS remains at a sequence length of one regardless because its ceiling temperature is 61°C and at any temperature above this, homo-depropagation becomes greater than propagation (Palmer *et al.*, 2000). MMA with its smaller depropagation rate constant and relative high reactivity, shown in Figure 5.48, increases in sequence length when depropagation is constant. With the other monomers depropagating at a higher rate, this is a feasible result. Ethyl acrylate has a lower number-averaged sequence length when depropagation is present probably due to quite the opposite reasons of MMA; EA is less reactive in general and as such, when the more reactive monomers are depropagating (AMS, BMA, GMA), AN and MMA are more likely to react in place of EA. BMA and GMA both show a decrease in sequence length and AN shows a relatively large increase in sequence length when depropagation is accounted for.

This model also has the capacity to compute weight-average sequence length. Figure 5.52 and Figure 5.53 are the simulations of the weight-average sequence length without and with

depropagation, respectively. They are for demonstrative purposes only as they will be very difficult to analyze in print.

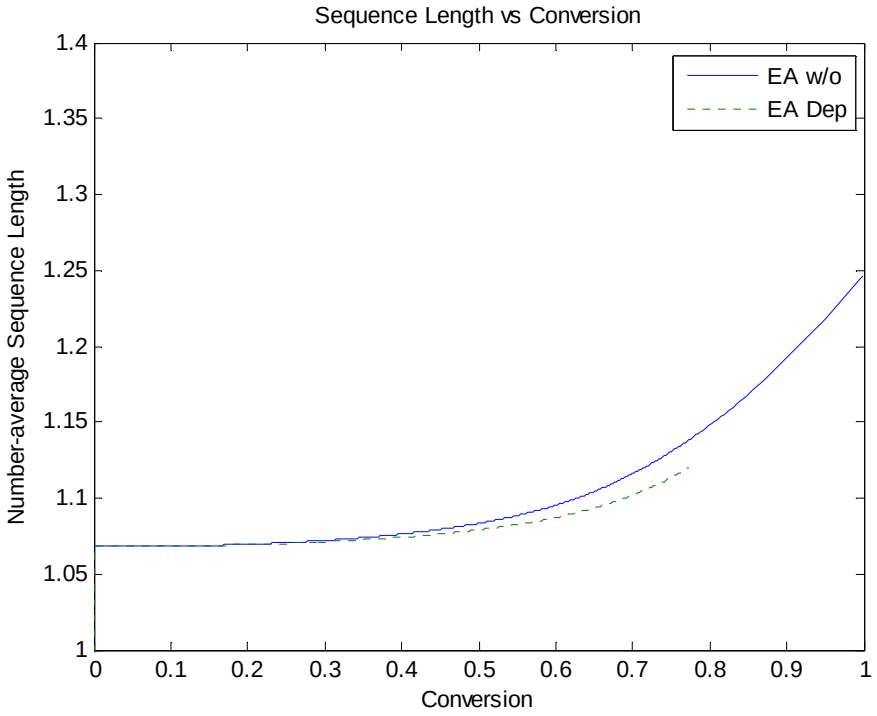

Figure 5.47: Simulation trends of bulk hexa-polymerization with and without depropagation

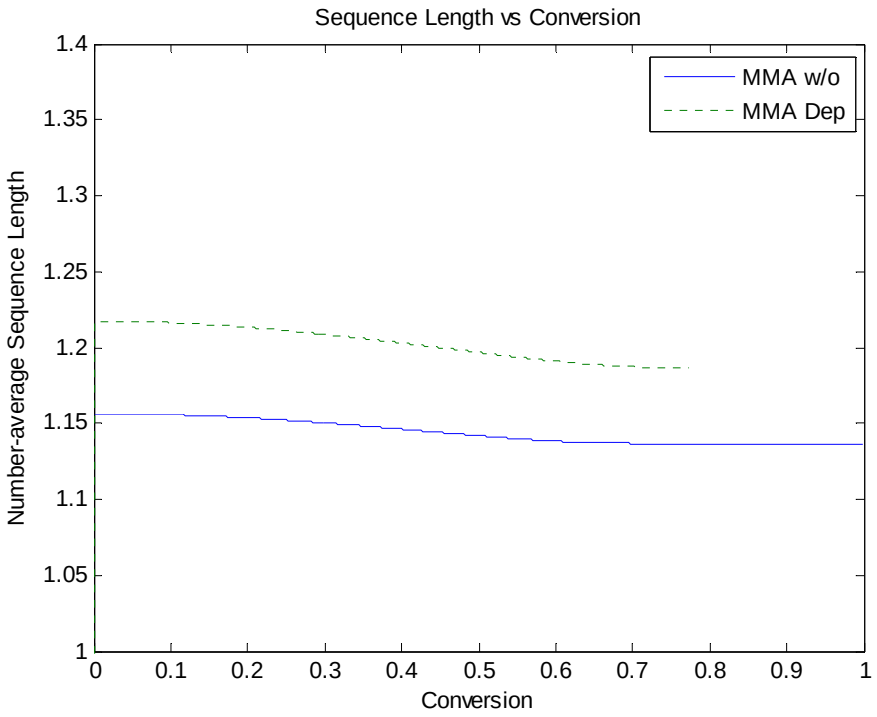

Figure 5.48: Simulation trends of bulk hexa-polymerization with and without depropagation

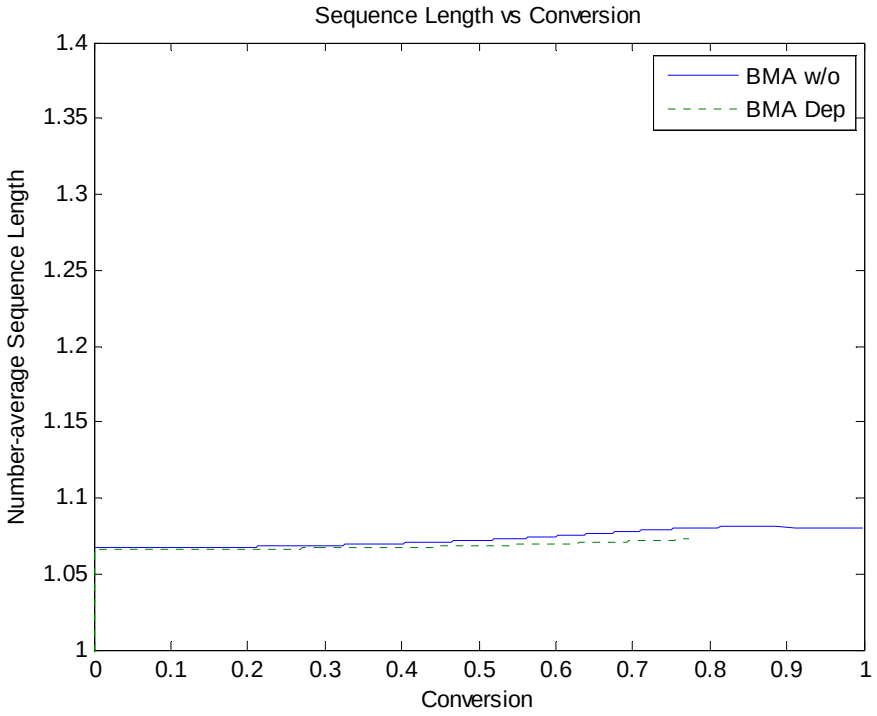

Figure 5.49: Simulation trends of bulk hexa-polymerization with and without depropagation

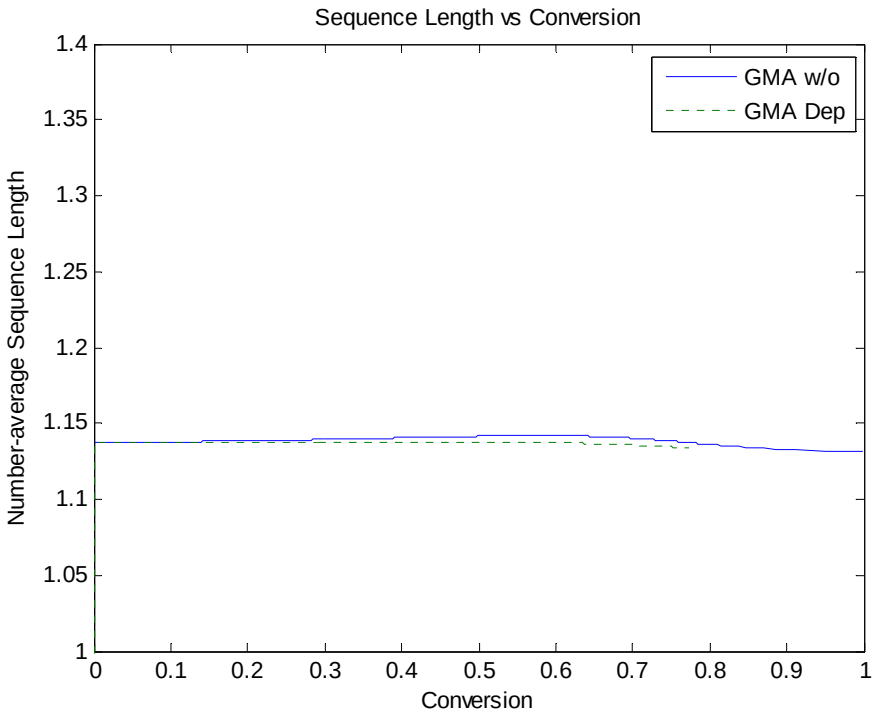

Figure 5.50: Simulation trends of bulk hexa-polymerization with and without depropagation

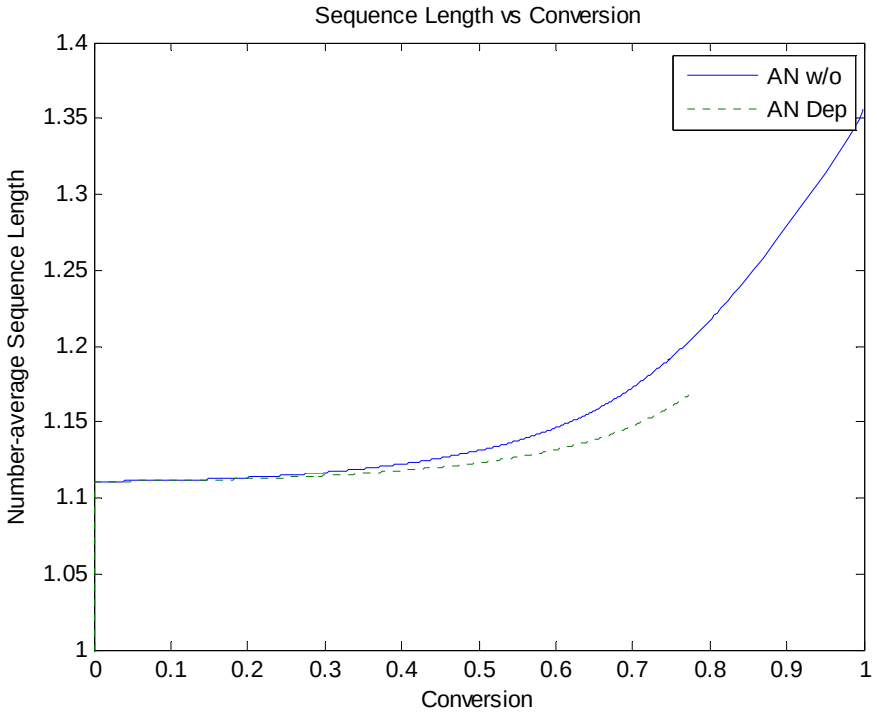

Figure 5.51: Simulation trends of bulk hexa-polymerization with and without depropagation

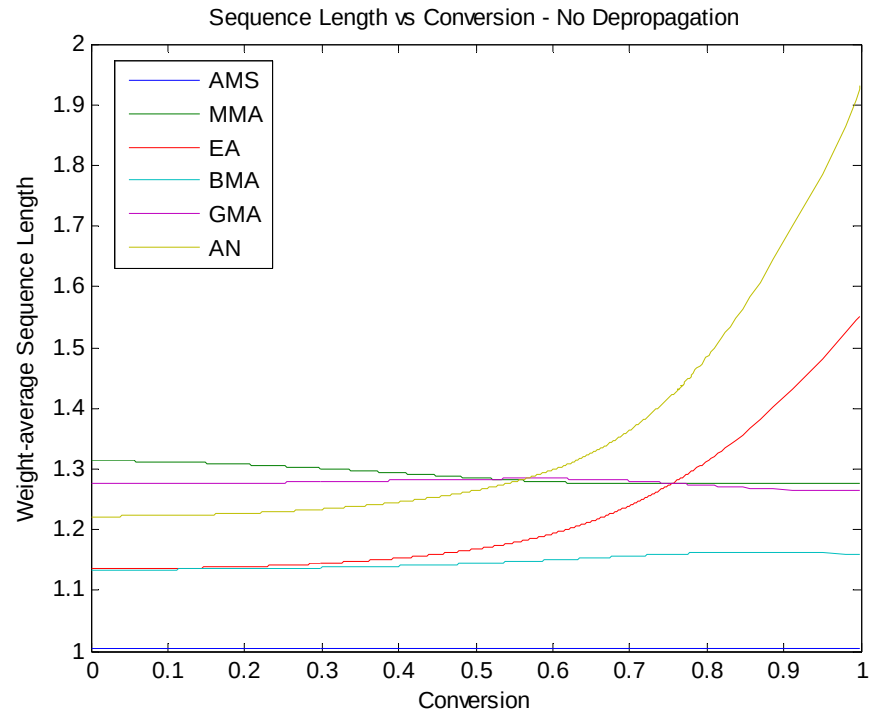

Figure 5.52: Simulation trends of bulk hexa-polymerization without depropagation

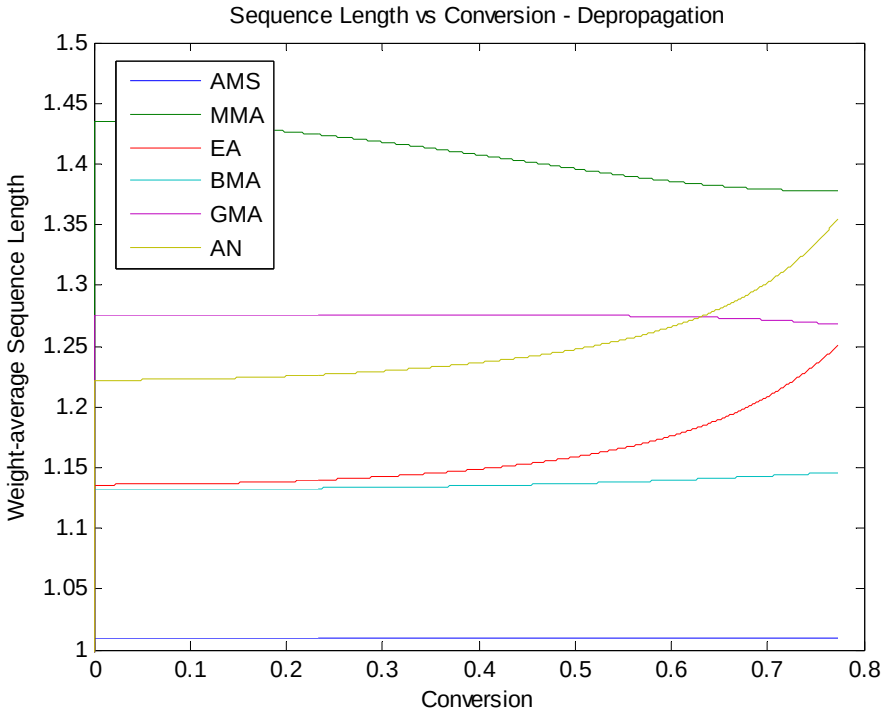

Figure 5.53: Simulation trends of bulk hexa-polymerization with depropagation

Figure 5.54 shows the amount of monomers left throughout the reaction. The more reactive monomers are consumed first (in order of complete consumption, MMA, AMS, GMA and BMA), whereas the less reactive monomers remain until the end of the reaction. AMS is shown here as a reactive monomer which is not entirely true, especially at this temperature; the reason for this is that no reactivity ratio data were available for AMS and several of the other monomers used in this polymerization, therefore styrene data was substituted instead. Although styrene is a highly reactive monomer and would not be substituted in reality, it serves its purpose here as this is simply a simulation used for illustration purposes.

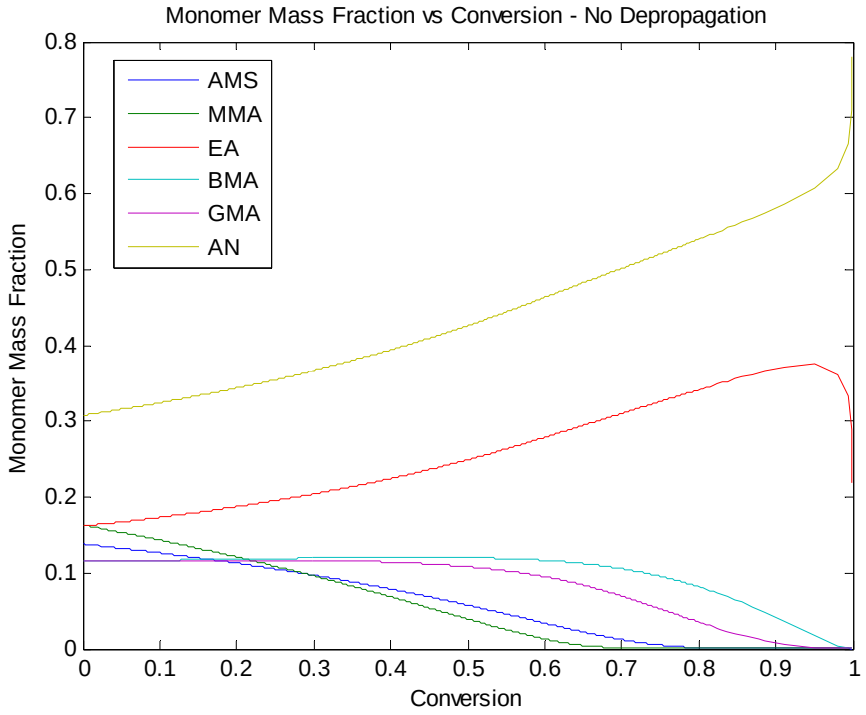

Figure 5.54: Simulation trends of bulk hexa-polymerization with depropagation

Figure 5.55 and Figure 5.56 show the cumulative polymer composition versus conversion without and with depropagation, respectively. During the initial stage of the reaction, AMS and MMA show a decrease in polymer composition, whereas EA, BMA, GMA and AN show an increase when depropagation is present. With the large amounts of AMS and MMA reacting so fast, it follows that they will be the most affected by depropagation. As both simulations have the same amount of each monomer and both reach complete conversion, the final composition of the polymer is identical, as expected.

Figure 5.57 and Figure 5.58 are the instantaneous polymer composition versus conversion with depropagation, and MMA dominance in the monomer feed, respectively. Naturally, the amount of MMA incorporated into the polymer is significantly increased when it is dominant in the monomer feed.

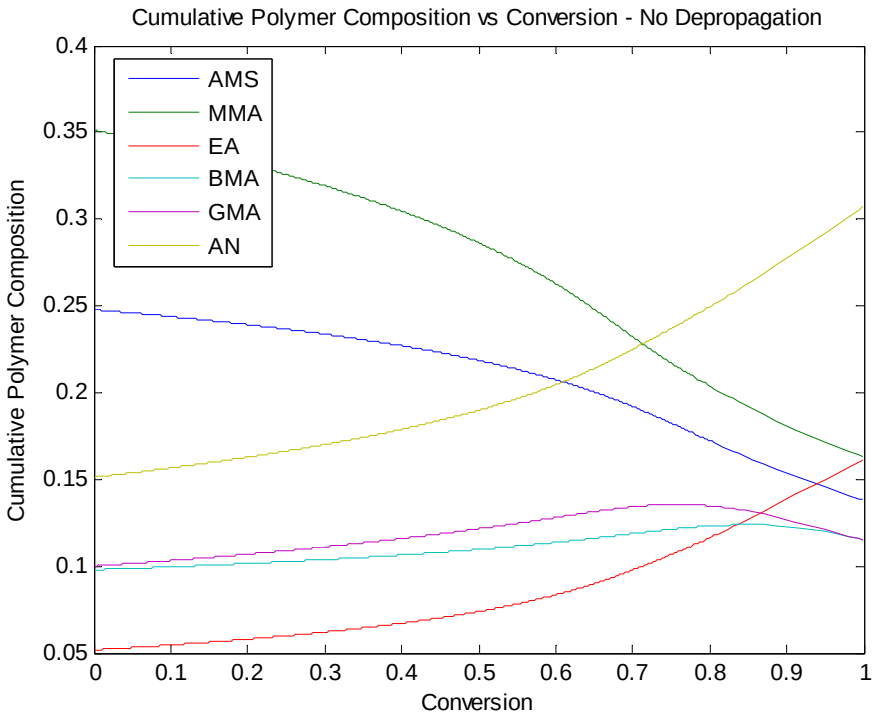

Figure 5.55: Simulation trends of bulk hexa-polymerization without depropagation

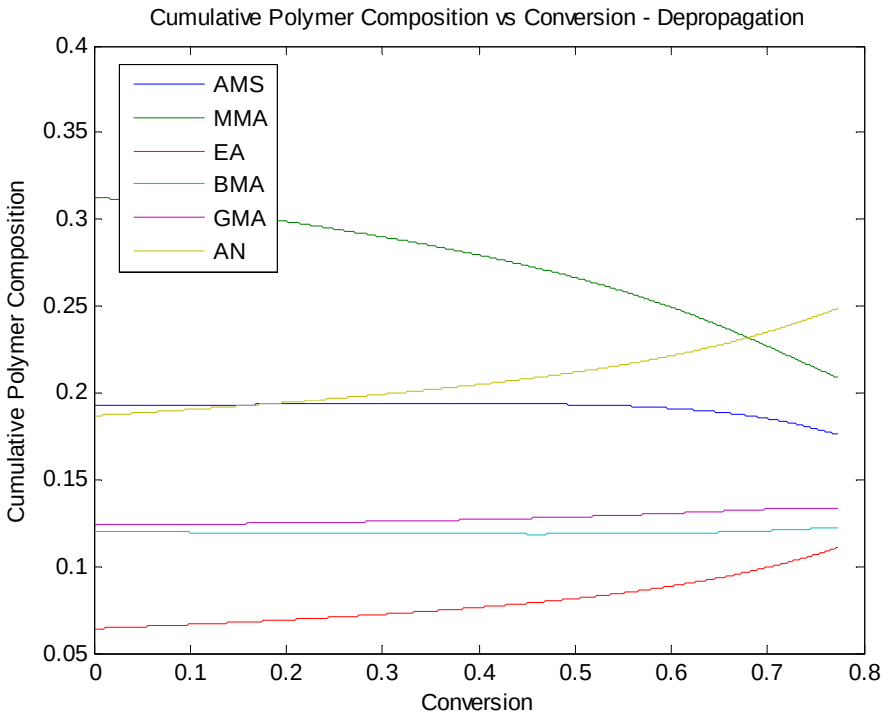

Figure 5.56: Simulation trends of bulk hexa-polymerization with depropagation

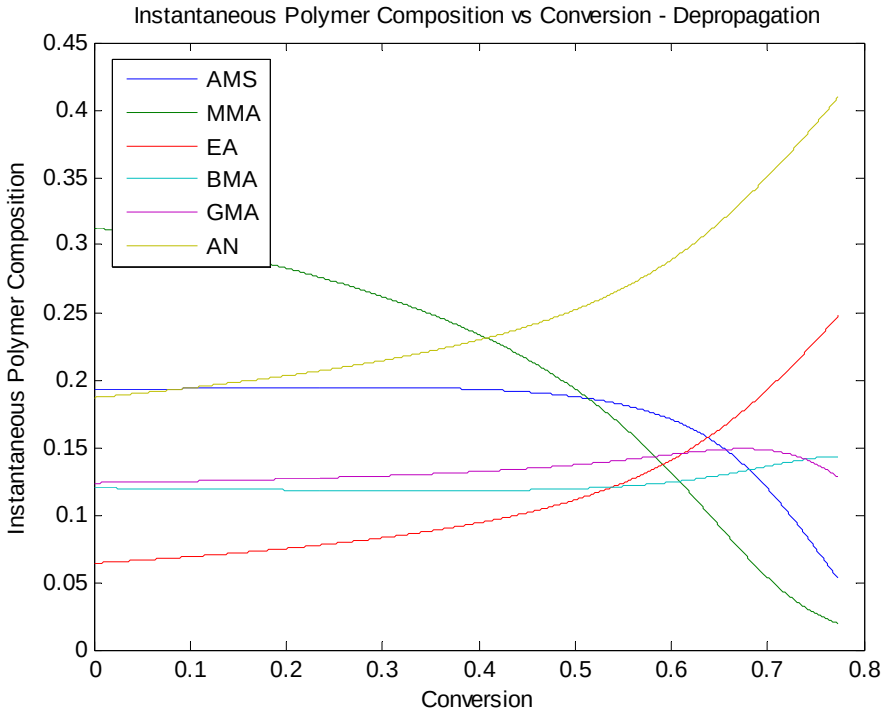

Figure 5.57: Simulation trends of bulk hexa-polymerization with depropagation

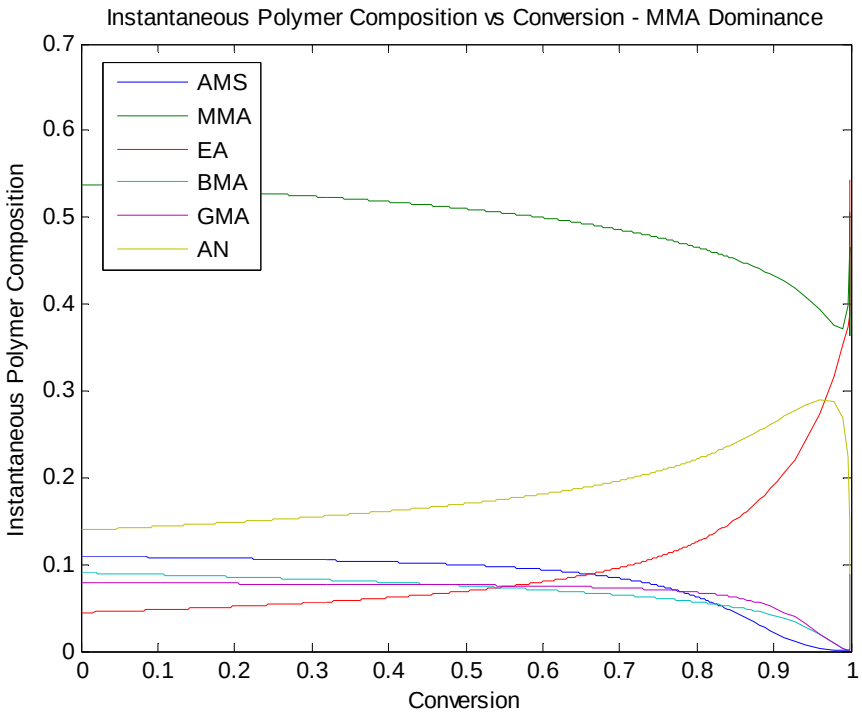

Figure 5.58: Simulation trends of bulk hexa-polymerization with depropagation

Figure 5.59 through Figure 5.62 show the comparisons of number- and weight-average molecular weights: Mn and Mw, respectively. In Figure 5.59, when depropagation is taken into account, the molecular weight averages drop. When the temperature was increased (Figure 5.60), again the molecular weight averages dropped. As the increased temperature simulation never reached complete conversion, the weight-average molecular weight did not spike towards the end of the reaction as in Figure 5.59. With the reaction proceeding much quicker because of the increased amount of MMA (Figure 5.61), fewer chains were initiated and therefore an increase in the molecular weight averages is predicted. Another major factor contributing to molecular weights to keep in mind is the effect each monomer has on chain transfer (chain transfer to monomer rate constants). MMA has a very small chain transfer to monomer rate constant whereas EA has a relatively large one. This can explain the slightly decreased molecular weights seen in Figure 5.62 despite the shorter reaction time.

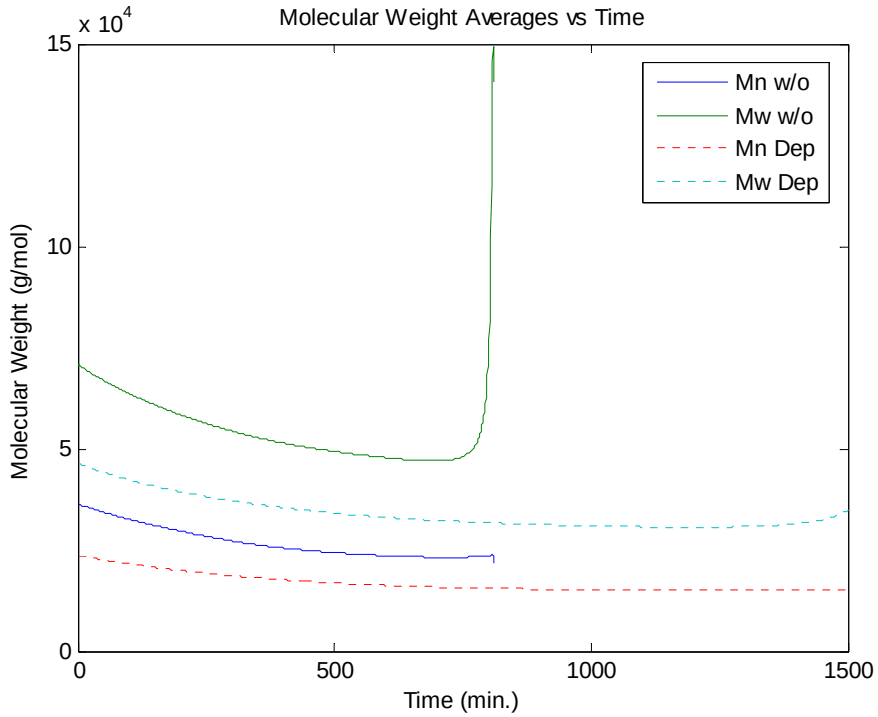

Figure 5.59: Simulation trends of bulk hexa-polymerization with and without depropagation

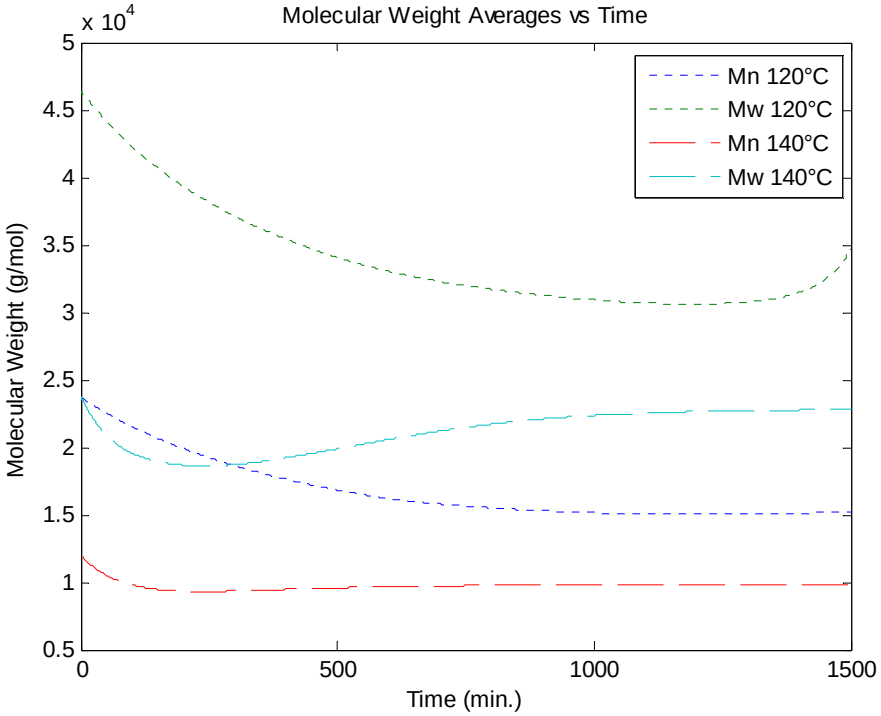

Figure 5.60: Simulation trends of bulk hexa-polymerization with depropagation

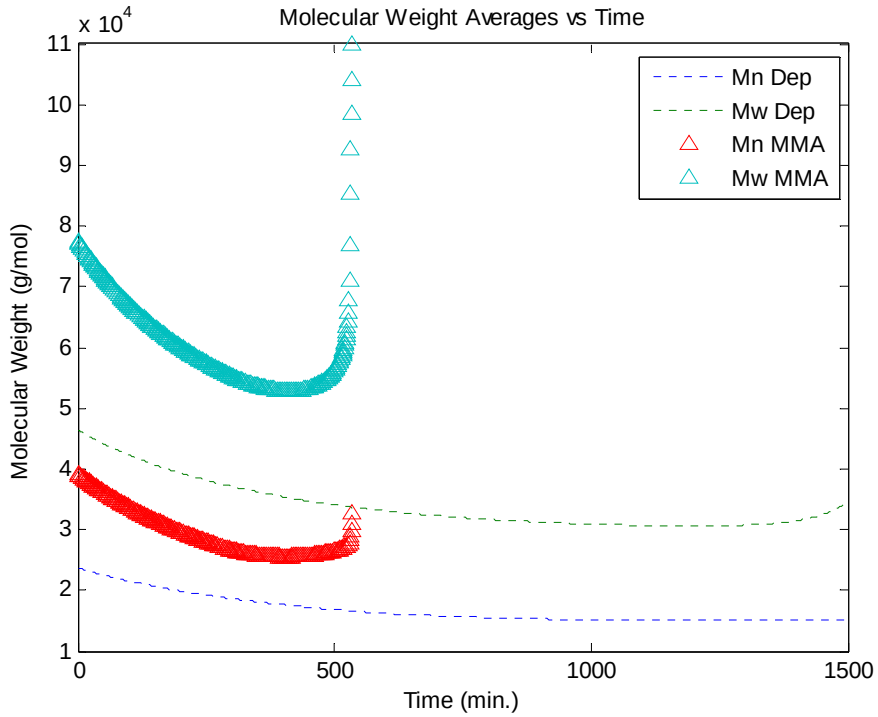

Figure 5.61: Simulation trends of bulk hexa-polymerization with depropagation

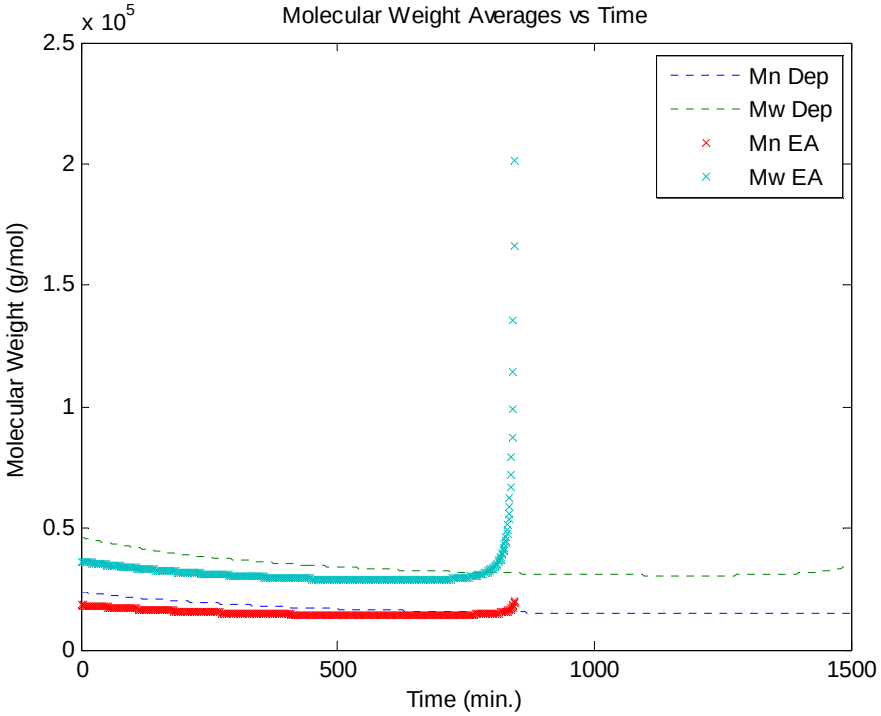

Figure 5.62: Simulation trends of bulk hexa-polymerization with depropagation

The final plot to illustrate some of the various capabilities of this model is the rate of polymerization versus time (see Figure 5.63). The rate of polymerization and conversion are directly related to each other. Revisiting the conversion versus time plot (Figure 5.43), one can observe that the polymerization at an increased temperature was much faster at the start of the reaction. This is depicted in Figure 5.63, whereby the Rp 140°C is much larger than all of the other simulations at low conversion. Auto-acceleration is also represented in Figure 5.63 as the spike around 90% conversion. The larger the increase seen in the rate of polymerization towards the end of the reaction, the further away the reaction was from completion when auto-acceleration occurred. For example, the EA dominance prediction, represented by Rp EA, had the largest increase when termination became diffusion limited.

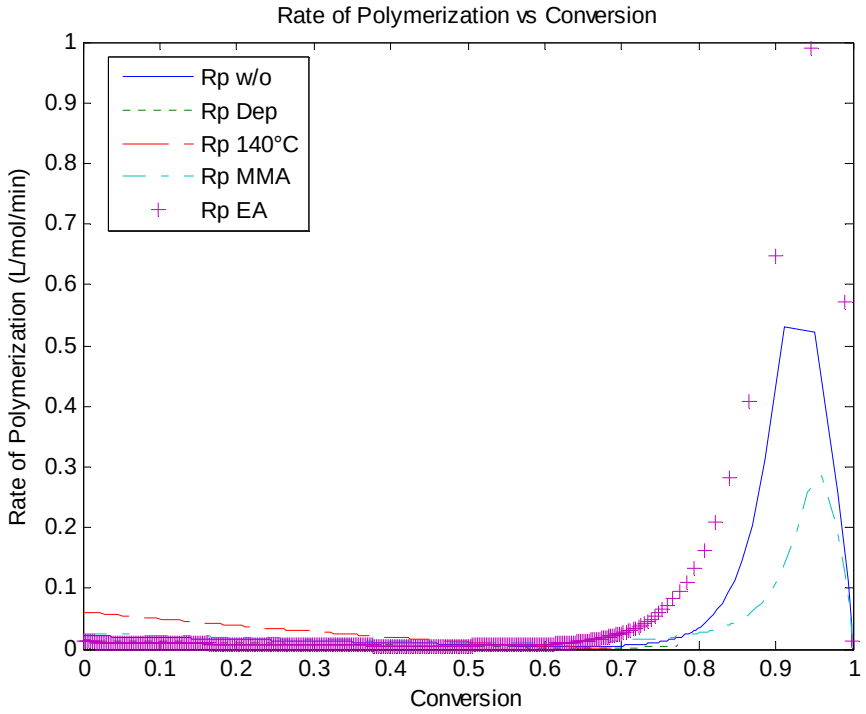

Figure 5.63: Simulation trends of bulk hexa-polymerization with and without depropagation

As with any model, every parameter used to calculate the standard outputs can also be recorded and displayed against any other. This allows for a complete analysis of every part of the reaction kinetics for an improved understanding of the inner workings of free radical polymerization with depropagation. The figures shown in this section only represent a small fraction of the capability of this model and were used to illustrate some of the

versatility and flexibility a simulation model can give the user. Modeling depropagation is a complex undertaking but by doing so with care and accuracy, can we understand more of the finer effects it has on the rest of free radical polymerization.

Table 5-5: Reactivity Ratios for Hexa-polymerization Simulation Trends

Reactivity Ratio	Value	Original Intention of Source	Source
rAMS-MMA	0.003	AMS/MMA 140°C	Palmer *et al.* (2000)
rAMS-EA	0.5575	AMS/BA 140°C	Leamen *et al.* (2006)
rAMS-BMA	0.61	Sty/BMA	Li and Hutchinson (2007)
rAMS-GMA	0.278	Sty/GMA	Brandrup *et al.* (1999)
rAMS-AN	0.36	Sty/AN	Garcia-Rubio *et al.* (1985)
rMMA-AMS	0.42	MMA/AMS 140°C	Palmer *et al.* (2000)
rMMA-EA	1.905	MMA/BA 140°C	Leamen *et al.* (2006)
rMMA-BMA	0.568	MAA/HEA 130°C	Sahloul *et al.* (2005)
rMMA-GMA	0.98	MMA/GMA	Brandrup *et al.* (1999)
rMMA-AN	1	BA/AN	Arbitrary input
rEA-AMS	0.14299	BA/AMS 140°C	Leamen *et al.* (2006)
rEA-MMA	0.34841	BA/MMA 140°C	Leamen *et al.* (2006)
rEA-BMA	0.22	EA/BMA	Gao and Penlidis (1998)
rEA-GMA	exp(0.8124 - 467.1/T)	EA/HEA	Sahloul *et al.* (2005)
rEA-AN	1.2	EA/AN	Gao and Penlidis (1998)
rBMA-AMS	0.42	BMA/Sty	Li and Hutchinson (2007)
rBMA-MMA	exp(-1.4365 + 48.7/T)	HEA/MAA	Sahloul *et al.* (2005)
rBMA-EA	2.43	BMA/EA	Brandrup *et al.* (1999)
rBMA-GMA	0.284	BMA/HEA	Q-e scheme
rBMA-AN	1	BMA/AN	Gao and Penlidis (1998)
rGMA-AMS	0.539	GMA/Sty	Brandrup *et al.* (1999)
rGMA-MMA	1.2	GMA/MAA	Brandrup *et al.* (1999)
rGMA-EA	exp(-1.6962 + 865.3/T)	HEA/EA	Sahloul *et al.* (2005)
rGMA-BMA	0.777	HEA/BMA	Q-e scheme
rGMA-AN	1.56	GMA/AN	Data from Brar and Dutta (1998), reanalyzed by N. Kazemi in house
rAN-AMS	0.078	AN/Sty	Garcia-Rubio *et al.* (1985)
rAN-MMA	1	AN/BA	Arbitrary input
rAN-EA	0.92	AN/EA	Gao and Penlidis (1998)
rAN-BMA	1	AN/BMA	Arbitrary input
rAN-GMA	0.21	GMA/AN	Data from Brar and Dutta (1998), reanalyzed by N. Kazemi in-house

5.2. Backbiting of Butyl Acrylate

Rantow *et al.* (2006) performed two homo-polymerizations of BA at 160°C and 180°C with 60% xylene by weight. No initiator was used as BA can self-initiate at elevated temperatures (Rantow *et al.*, 2006; Zorn *et al.*, 2009). Figure 5.64 through Figure 5.67 each compare the homo-polymerization of BA with and without backbiting. As the data illustrate, modeling without backbiting and beta-scission results in a simulation that follows polymerization behavior very poorly. The reason for such a large difference in the two predictions is that the tertiary radical formed in backbiting is much more stable and results in a slower rate of reaction.

This can be seen directly in Figure 5.64 as the simulation without backbiting reaches complete conversion almost instantly whereas the simulation with backbiting only reaches 81% conversion after 100 minutes. Figure 5.65 is at a higher temperature but still, the reaction is only moderately faster; a conversion of 86% is reached after 100 minutes. This is a result of the increased amount of backbiting at higher temperatures. Plessis *et al.* (2003) supported this theory as they observed that the level of branching measured from ^{13}C NMR spectroscopy was shown to increase as temperature increased.

Figure 5.66 and Figure 5.67 are the molecular weight predictions at 160°C and 180°C, respectively. The backbiting simulation follows the data trend with accuracy whereas the prediction without backbiting (and beta-scission) is much too high. The backbiting simulation is much more accurate due to β-fragmentation. Each time the tertiary radical chain splits, a second chain is created and the molecular weight drops accordingly.

Figure 5.68 and Figure 5.69 represent the average number of short chain branches per chain throughout the reaction (CBC). In spite of the discrepancy between the data and our simulation (given that the measurement has quite a lot of error in it as well), the model still follows the same decreasing trend as the reaction proceeds. As there was no experimental data for the average number of terminal double bonds per chain (TDBC), Figure 5.70 and Figure 5.71 are just the model simulations. As temperature increases from 160°C to 180°C, several trends can be seen. The molecular weight drops, as expected, CBC decreases and TDBC increases. When the temperature is increased, the number of polymer chains increases due to the increased rate of initiator decomposition as well as the increased amount of beta-scission. As CBC is the number average per chain, the reason for the decrease is simply that the number of chains increased more than the average number of short chain branches. When β-scission occurs, the short chain branch is no longer formed as

the midchain radical is converted into a secondary radical and a dead polymer chain with a terminal double bond; thus, the decrease in CBC and the increase in TDBC can both be explained by an increased amount of beta-fragmentation.

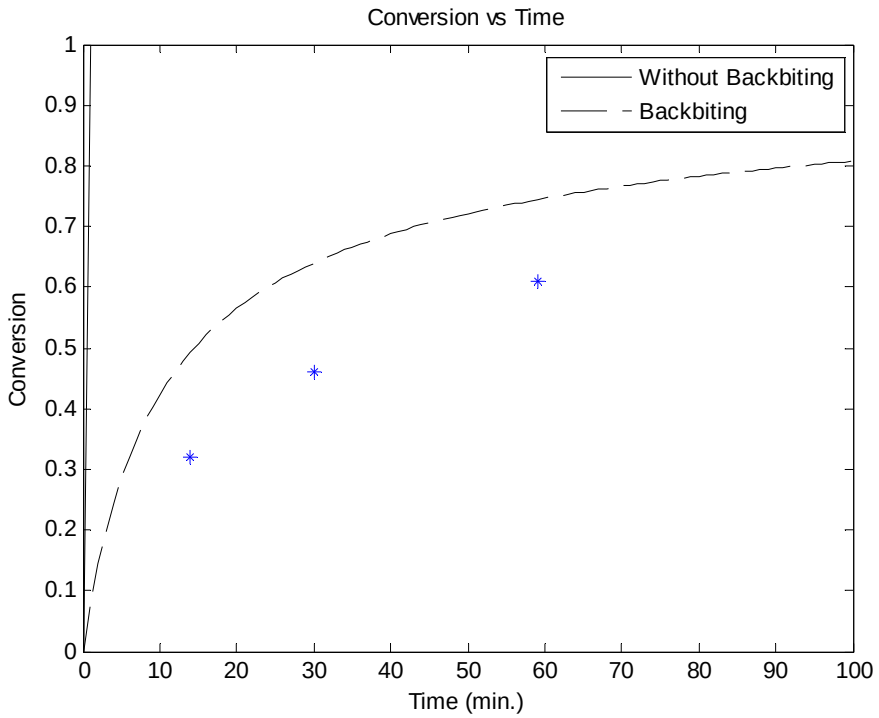

Figure 5.64: Simulation of the homo-polymerization of BA at 160°C with no initiator and 60 wt% xylene

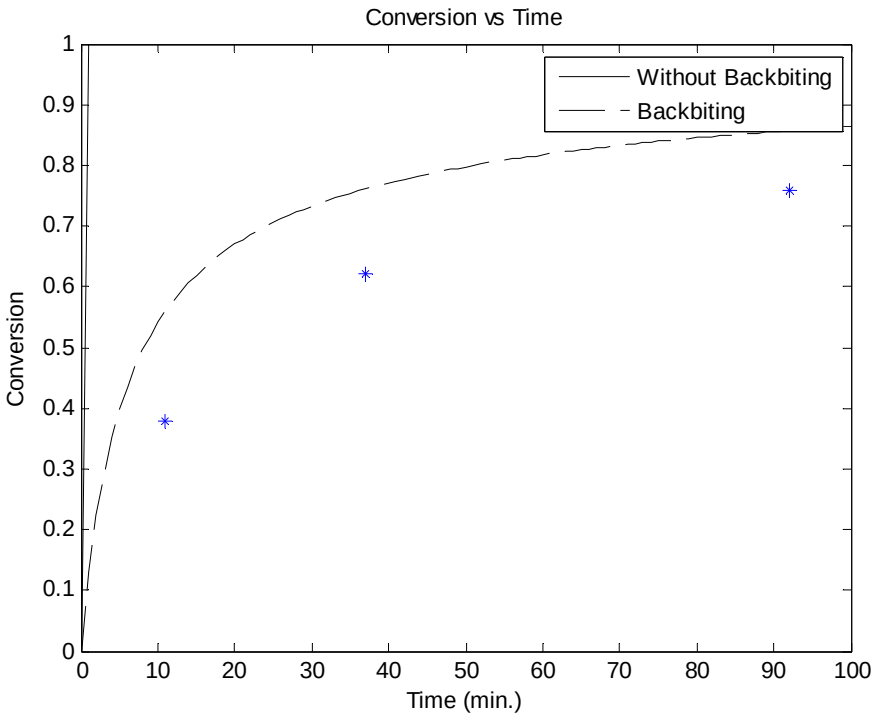

Figure 5.65: Simulation of the homo-polymerization of BA at 180°C with no initiator and 60 wt% xylene

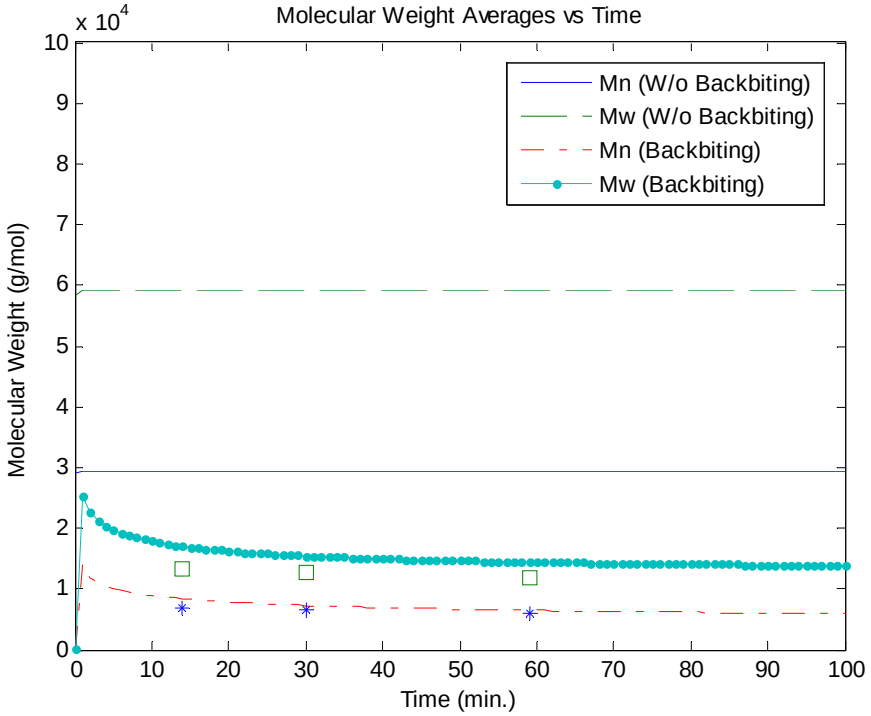

Figure 5.66: Simulation of the homo-polymerization of BA at 160°C with no initiator and 60 wt% xylene

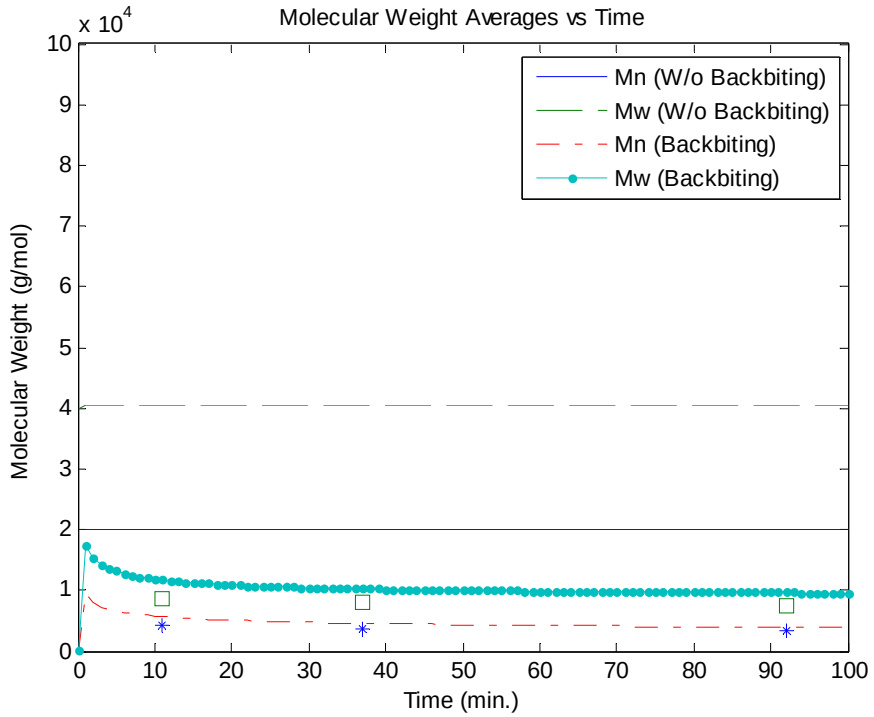

Figure 5.67: Simulation of the homo-polymerization of BA at 180°C with no initiator and 60 wt% xylene

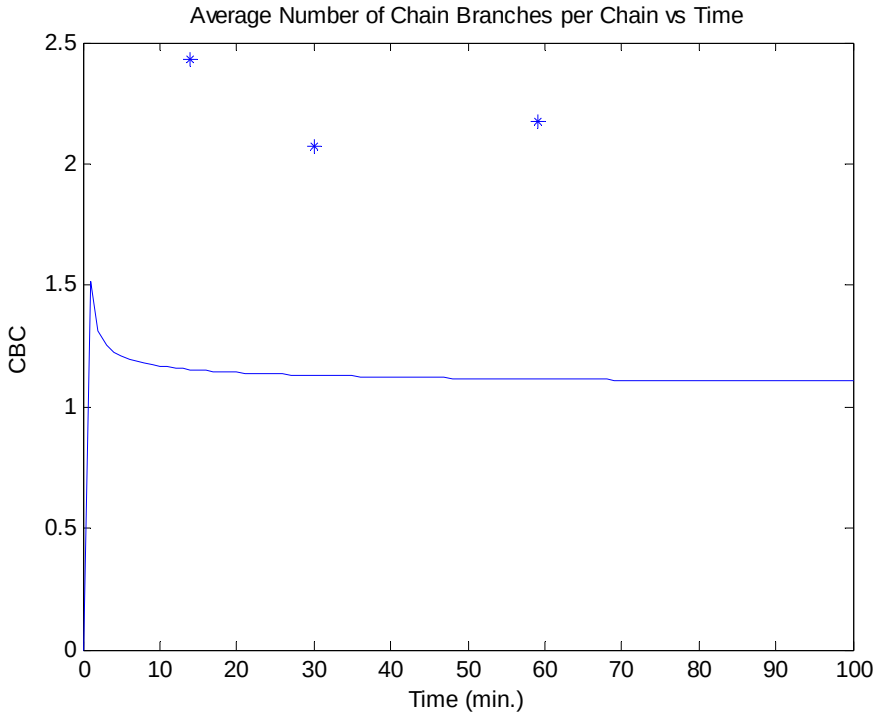

Figure 5.68: Simulation of the homo-polymerization of BA at 160°C with no initiator and 60 wt% xylene

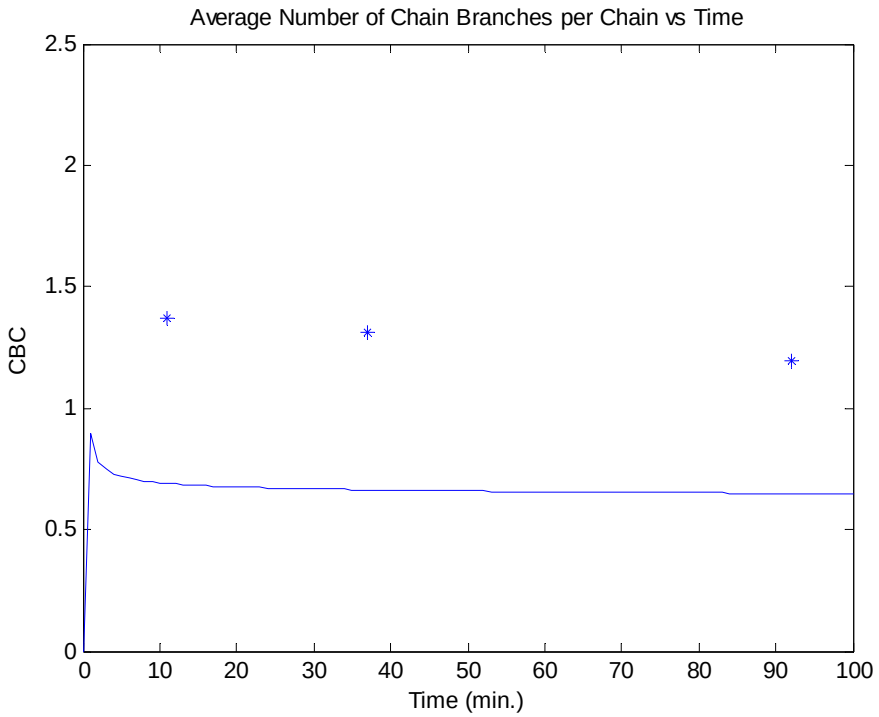

Figure 5.69: Simulation of the homo-polymerization of BA at 180°C with no initiator and 60 wt% xylene

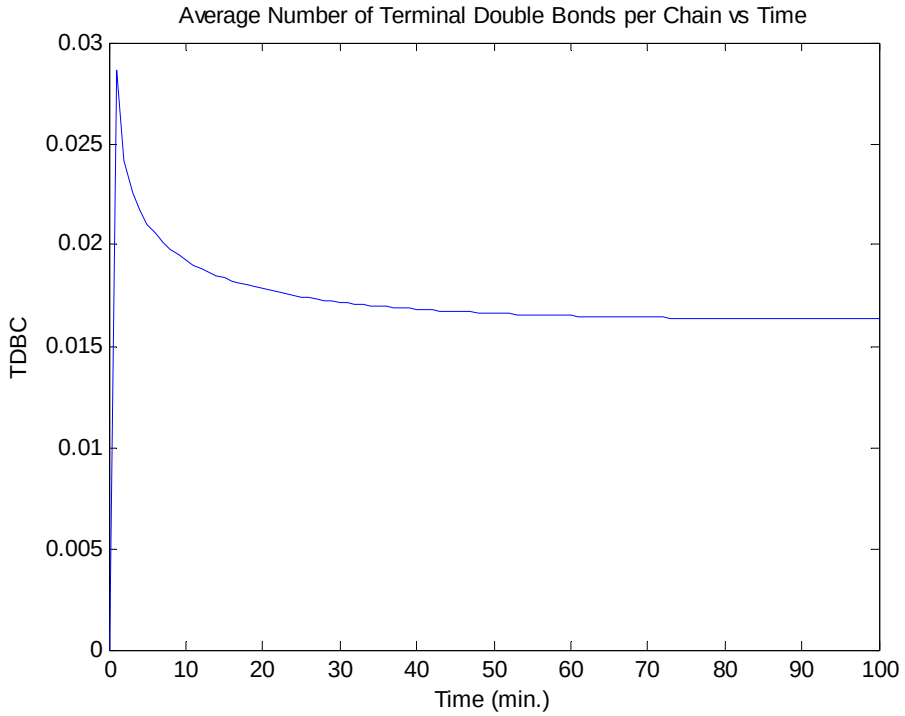

Figure 5.70: Simulation of the homo-polymerization of BA at 160°C with no initiator and 60 wt% xylene

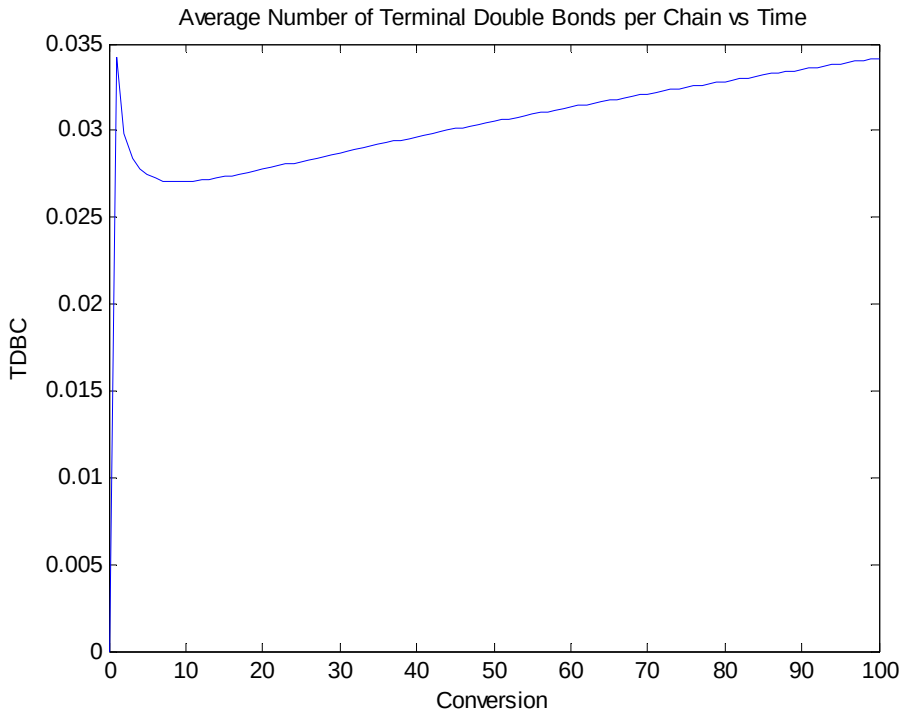

Figure 5.71: Simulation of the homo-polymerization of BA at 180°C with no initiator and 60 wt% xylene

Zorn *et al.* (2009) independently conducted a homo-polymerization of BA at 140°C with no initiator or solvent present. Figure 5.72 shows the conversion versus time plot with decent results. Additional kinetic studies will certainly refine the rate constants and allow for improved simulations in this area.

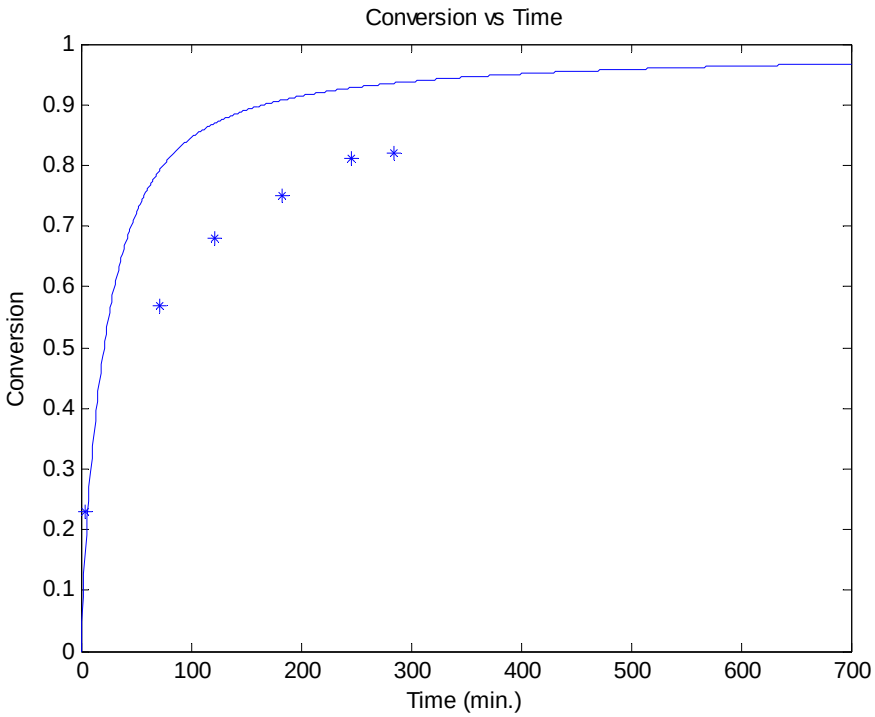

Figure 5.72: Simulation of the homo-polymerization of BA at 140°C

5.2.1 Case Study 7: Homo-polymerization of Butyl Acrylate

A thorough undertaking of the homo-polymerization of BA was completed by Wang *et al.* (2009b). Thirty-five weight-percent of xylene was initially charged into the reactor. The monomer and initiator were then fed constantly over 360 minutes or 180 minutes depending on the experiment. The initiator, dTBPO, was fed at 2 wt% of monomer. Both reactions were maintained at 138°C and data on monomer concentration and weight-average molecular weight were collected.

Figure 5.73 is the original simulation against the monomer concentration data. Quite plainly, the prediction does not align with the data very well. With such a large discrepancy, both the model and the data should be considered as erroneous. One possibility is that the pumps were having difficulty maintaining their set point, especially the small initiator feed in a laboratory setting. Figure 5.74 is the simulation with a constant monomer feed and a ramped initiator feed; starting much lower and constantly increasing until it hits the set point. It is surprising how accurate the model can be with only a slight modification. This does not prove that the initiator feed was ramped but it does show that even small disturbances in the experiment can have large effects on the results. Figure 5.75 is the modified weight-average molecular weight prediction versus time. Again, the model overshot the data but it did, however, reach the same end result. The measurements also have limited accuracy at this range making the simulation an acceptable representation of the data. Figure 5.76 is the modified molar flowrates of the monomer and initiator.

The second reaction produced similar data trends as the first and as such, the ramped initiator feed was used again. Figure 5.77 and Figure 5.78 are the monomer concentration and the weight-average molecular weight versus time, respectively, over a constant feed of 180 minutes. The model follows the data acceptably well in both figures.

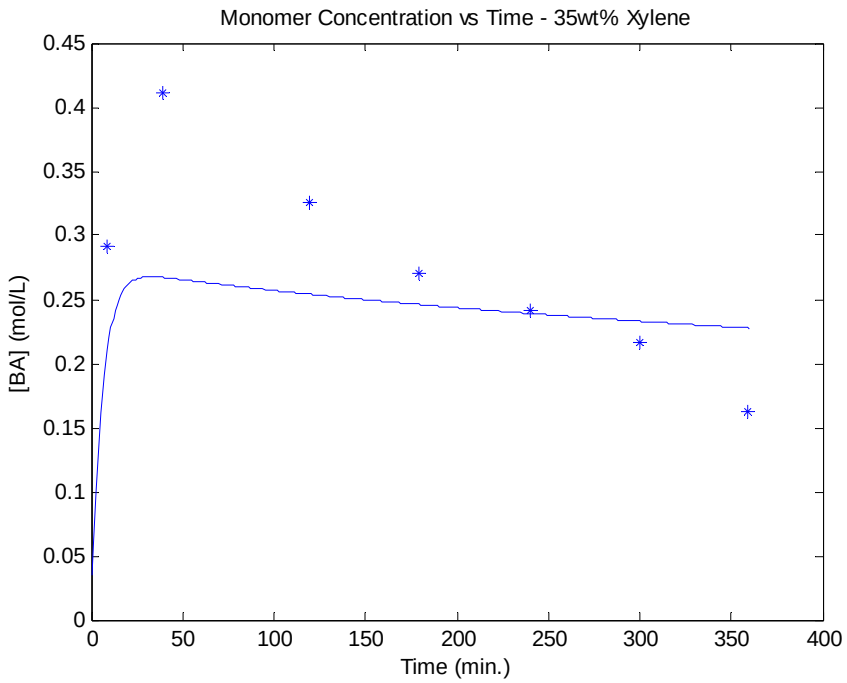

Figure 5.73: Simulation of the homo-polymerization of BA T = 138°C $[dTBPO]_0$ = 2 wt% xylene = 35wt% constant feed time = 360 min

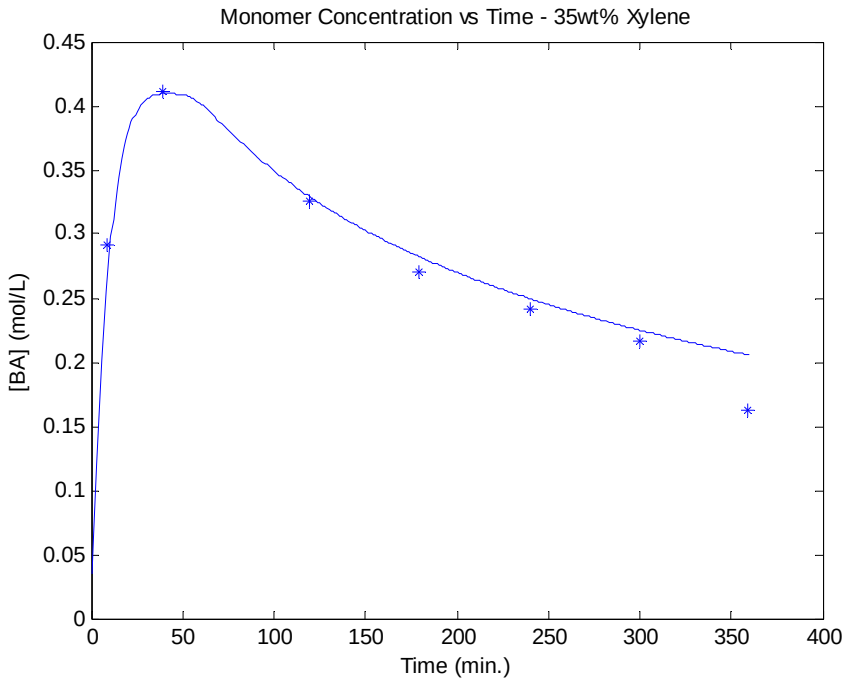

Figure 5.74: Simulation of the homo-polymerization of BA T = 138°C $[dTBPO]_0$ = 2 wt% xylene = 35wt% constant feed time = 360 min

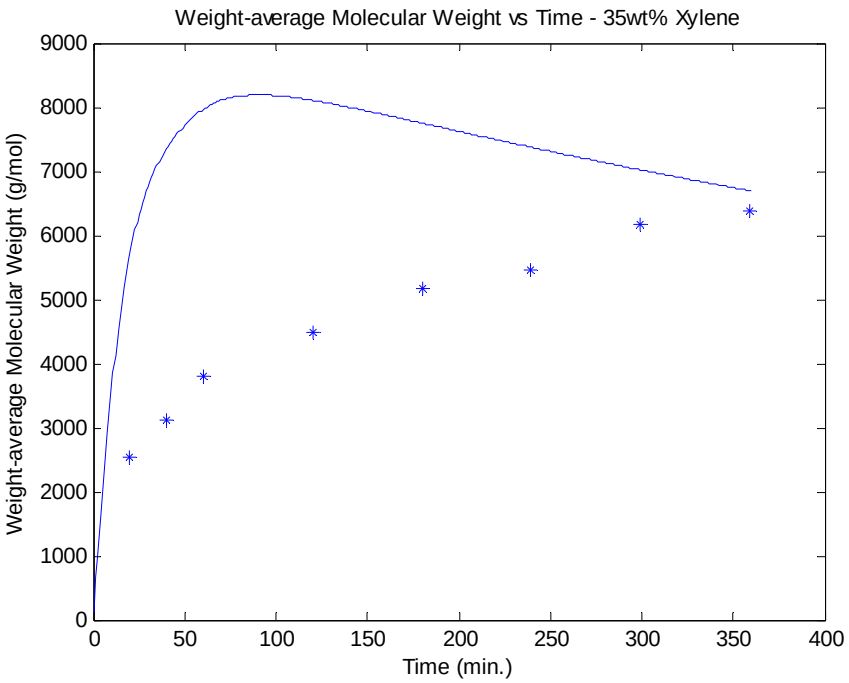

Figure 5.75: Simulation of the homo-polymerization of BA T = 138°C $[dTBPO]_0$ = 2 wt% xylene = 35wt% constant feed time = 360 min

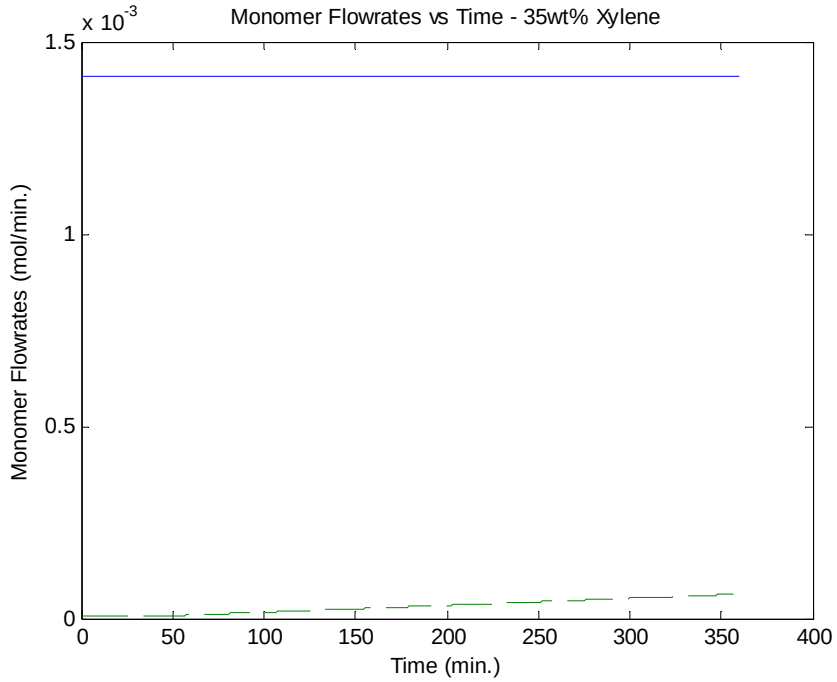

Figure 5.76: Simulation of the homo-polymerization of BA T = 138°C $[dTBPO]_0$ = 2 wt% xylene = 35wt% constant feed time = 360 min

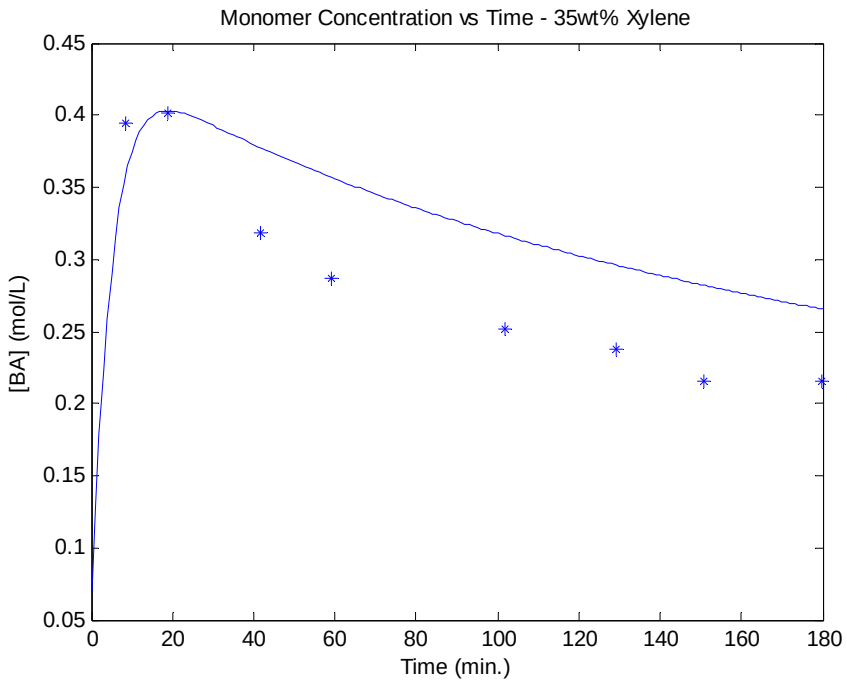

Figure 5.77: Simulation of the homo-polymerization of BA T = 138°C $[dTBPO]_0$ = 2 wt% xylene = 35wt% constant feed time = 180 min

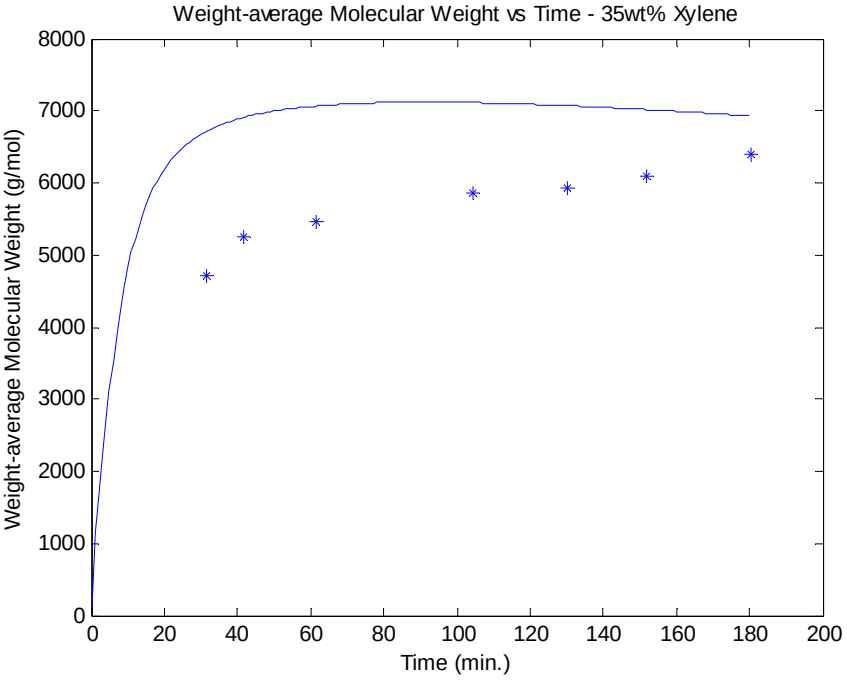

Figure 5.78: Simulation of the homo-polymerization of BA T = 138°C $[dTBPO]_0$ = 2 wt% xylene = 35wt% constant feed time = 180 min

5.2.2 Case Study 8: Co-polymerization of Butyl Acrylate and Butyl Methacrylate

Three co-polymerizations and two homo-polymerizations were conducted by Li *et al.* (2005). The inlet monomer mole fractions of BMA for the five reactions were 100 wt%, 75 wt%, 50 wt%, 25 wt% and 0 wt%. The reactor was initially charged with 30% xylene by weight. The monomer and initiator were then fed constantly over 360 and 375 minutes, respectively. The final amount of monomers and initiator fed were equal to 68.3 wt% and 1.7 wt%, respectively. The reactivity ratios used were $r_{BA\text{-}BMA}$ = 0.8268*exp(282.1/T) and $r_{BMA\text{-}BA}$ = 1.5815*exp(-564.8/T) obtained from Hakim *et al.* (2000). The homo-depropagation rate constant of BMA was equal to k_{pBMA}*(1.76 - 1.37*wp*10^6*exp(-6240/T) taken from Wang *et al.* (2009a); cross-depropagation was assumed negligible.

As these experiments were run at elevated temperatures, backbiting, beta-scission and depropagation all have to be modeled to produce accurate simulations. Backbiting was only assumed to occur when BA was the terminal and pen-penultimate unit of the chain whereas depropagation of BMA only occurred when BMA was the terminal and penultimate unit. With backbiting and β-scission limited, the reaction will proceed much quicker and with higher molecular weights than if it had been a homo-polymerization of butyl acrylate.

Figure 5.79 and Figure 5.80 are the concentration of BMA and BA monomers, respectively. As depropagation kinetics have been researched far more extensively than the relatively new backbiting phenomenon, it is not surprising that the concentration of BMA simulations performed much better than the BA predictions. Some improvement is required but the overall accuracy is on par with the simulations created by Li *et al.* (2005). This just means that BA behaviour is still relatively unexplained and further refinement is required for better model simulations. Li *et al.* (2005) suggested that the $k_{t,co}$ (explained in section 3.2.3) should be set to the homo-termination rate constant of BA only; this produces much better simulations for all co-polymerizations of BA and BMA. Perhaps with some modifications, like altering the cross-termination rate constant, the BA simulations would be more accurate but as it stands now, the predictions are very close in magnitude and produce exceptional results against the remaining data sets.

Figure 5.81 is the weight-average molecular weight versus time for four of the polymerizations. The model is very accurate at each monomer feed ratio. It is also evident that indeed the molecular weights do increase with less butyl acrylate and consequently less beta-scission overall. Figure 5.82 is the cumulative polymer composition of BMA versus time for each of the co-polymerizations. The model performs very well against the data for

all three experiments. Figure 5.83 is the polymer weight fraction versus time for the 50/50 wt% polymerization. Again, the simulation is very precise.

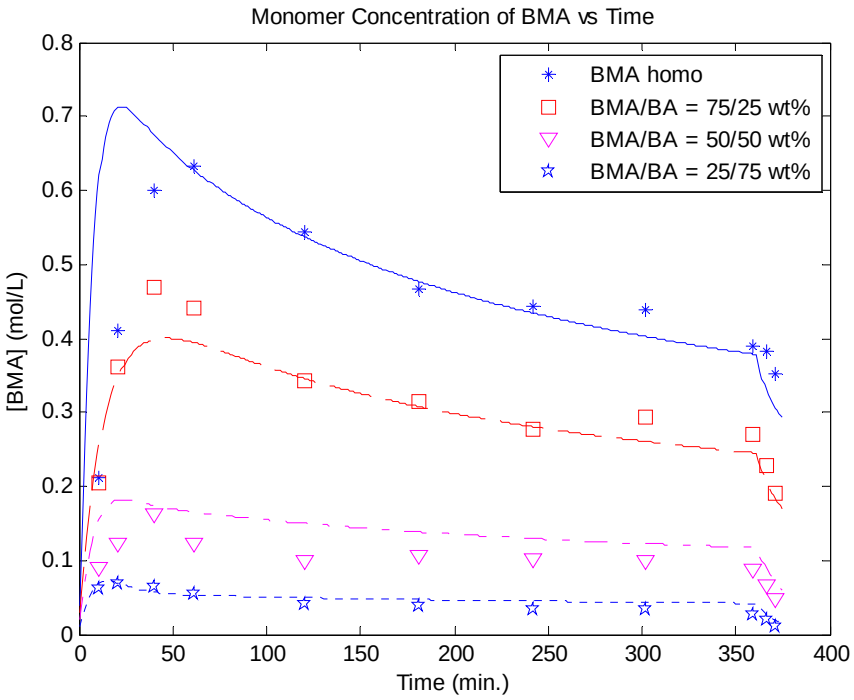

Figure 5.79: Simulation of the co-polymerizations of BMA/BA T = 138°C $[dTBPO]_0$ = 1.7 wt% xylene = 30wt%

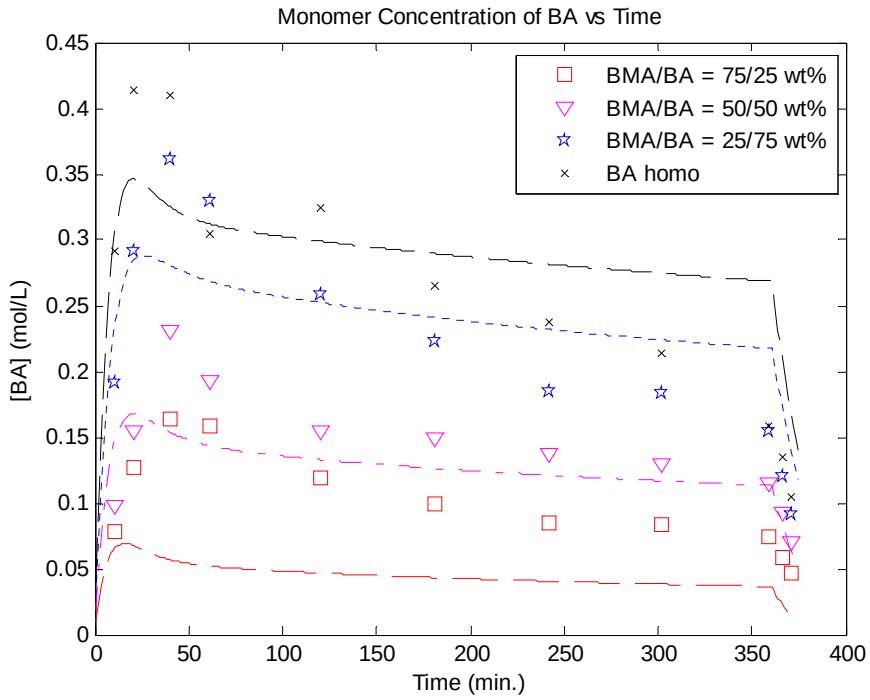

Figure 5.80: Simulation of the co-polymerizations of BMA/BA T = 138°C $[dTBPO]_0$ = 1.7 wt% xylene = 30wt%

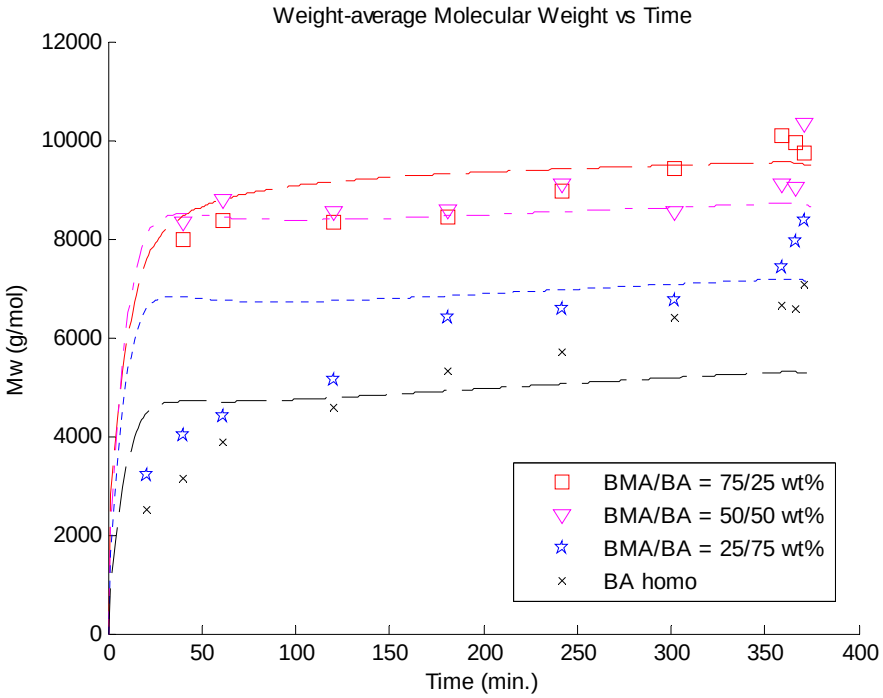

Figure 5.81: Simulation of the co-polymerizations of BMA/BA T = 138°C $[dTBPO]_0$ = 1.7 wt% xylene = 30wt%

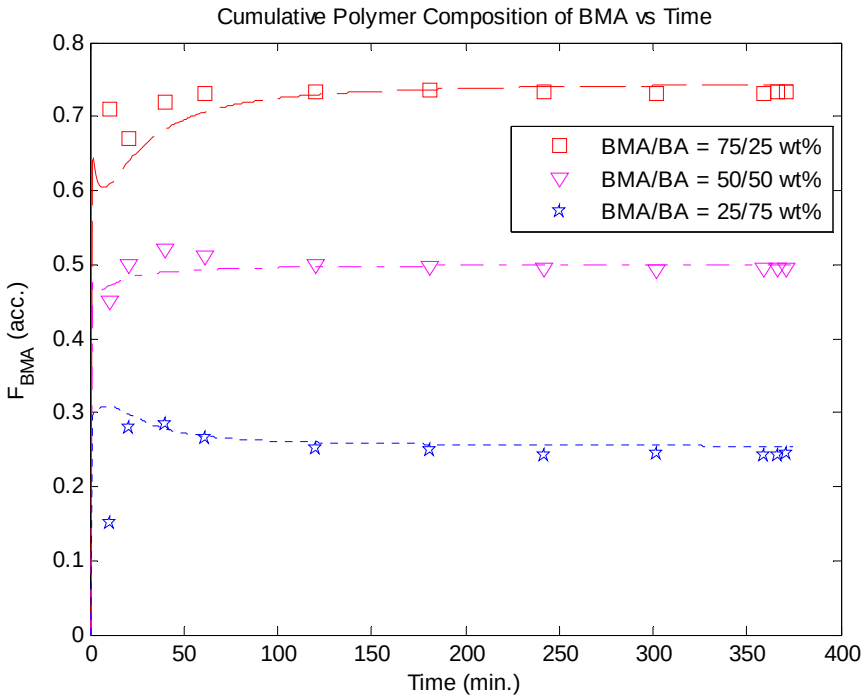

Figure 5.82: Simulation of the co-polymerizations of BMA/BA T = 138°C $[dTBPO]_0$ = 1.7 wt% xylene = 30wt%

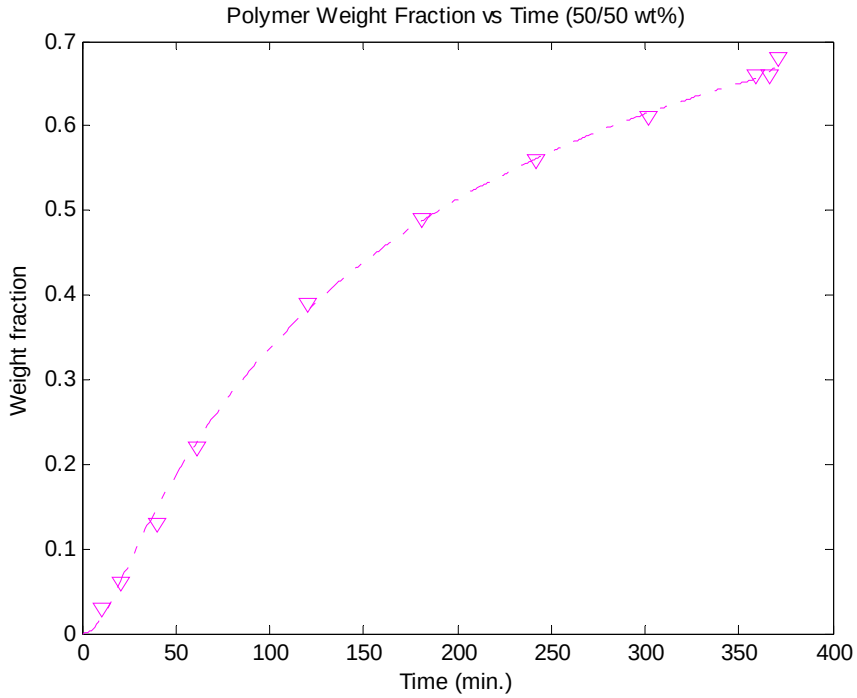

Figure 5.83: Simulation of the co-polymerization of BMA/BA T = 138°C $[dTBPO]_0$ = 1.7 wt% xylene = 30wt% f_{BA0} = 50 wt%

5.2.3 Case Study 9: Co-polymerization of Styrene and Butyl Acrylate

Recently, Wang (2010) published experimental data on the semi-batch co-polymerization of styrene and BA at 138°C. Three different initial monomer mole fractions were examined: 75/25 wt%, 50/50 wt% and 25/75 wt% of styrene and butyl acrylate, respectively. Thirty weight-percent of xylene was charged into the reactor at time zero. The monomers and di-tert butyl peroxyacetate (TBPA) were fed evenly for 360 and 375 minutes, respectively. The reactivity ratios were taken from Gao and Penlidis (1998) as $r_{Sty\text{-}BA} = 0.956$ and $r_{BA\text{-}Sty} = 0.183$.

The simulations of monomer concentration for the monomer mole fraction of 75 wt% styrene in Figure 5.84, Figure 5.85 and Figure 5.86 show very good representation of the data. The molecular weight prediction for this monomer feed overshot the data by about 20%, not that large a margin. The modeling software Wang (2010) used in his thesis also overshot the data, meaning that the data might be slightly under the value of the true molecular weight or improved kinetic data for the butyl acrylate system at elevated temperatures are needed.

Figure 5.87 through Figure 5.89 are the simulations with 50 wt% styrene in the co-polymerization, whereas Figure 5.90 through Figure 5.92 represent the 25 wt% styrene reaction. The predictions in each of these figures mimic the trends found in the data well with relative accuracy throughout. The final weight-average molecular weight estimates were both very precise. Without any modifications to the kinetic parameters, the model performs very well for the styrene/BA system, even at elevated temperatures.

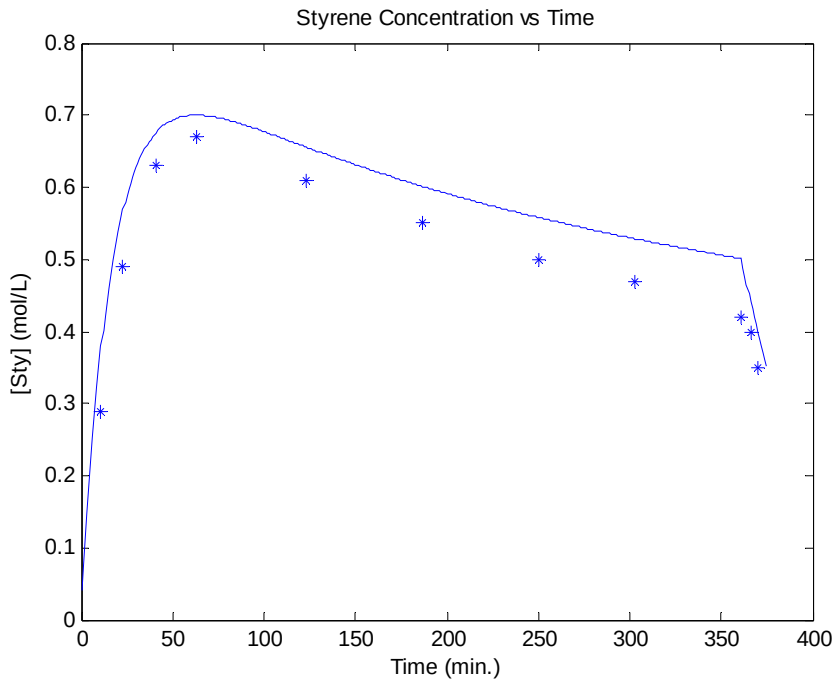

Figure 5.84: Simulation of the semi-batch co-polymerization of Sty/BA T = 138°C $[TBPA]_0$ = 2 wt% xylene = 30wt% f_{Sty0} = 75 wt%

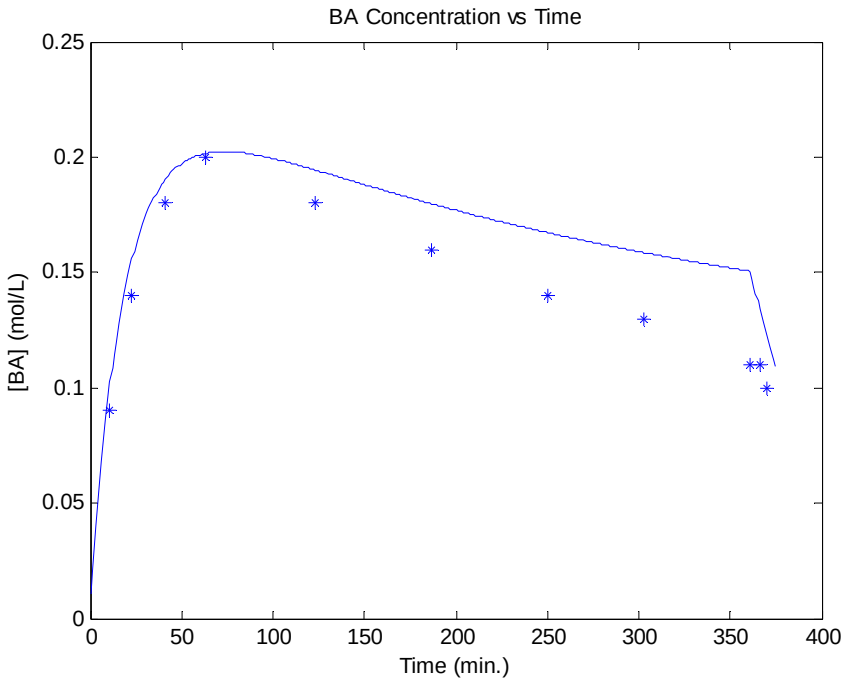

Figure 5.85: Simulation of the semi-batch co-polymerization of Sty/BA T = 138°C $[TBPA]_0$ = 2 wt% xylene = 30wt% f_{Sty0} = 75 wt%

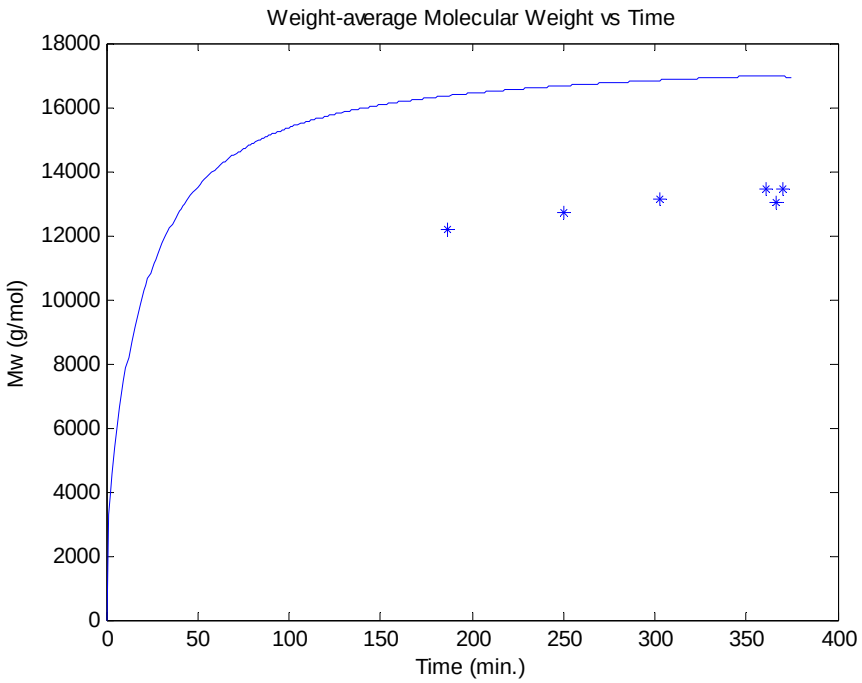

Figure 5.86: Simulation of the semi-batch co-polymerization of Sty/BA T = 138°C $[TBPA]_0$ = 2 wt% xylene = 30wt% f_{Sty0} = 75 wt%

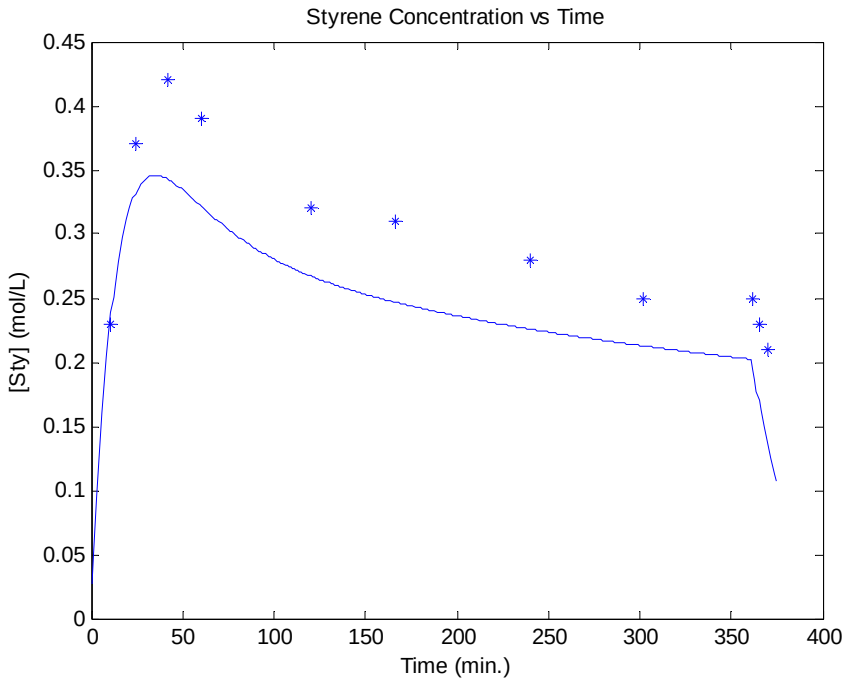

Figure 5.87: Simulation of the semi-batch co-polymerization of Sty/BA T = 138°C $[TBPA]_0$ = 2 wt% xylene = 30wt% f_{Sty0} = 50 wt%

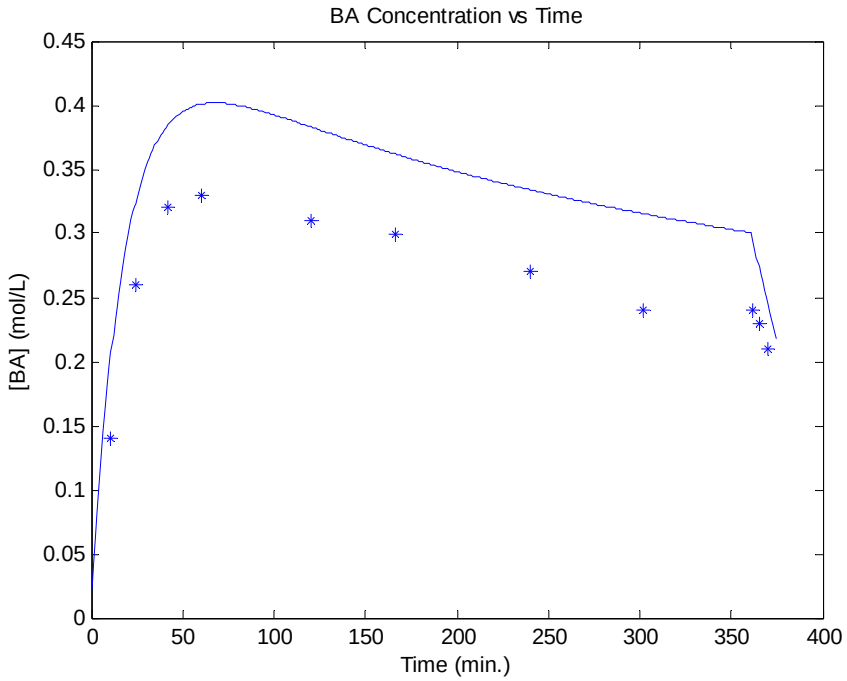

Figure 5.88: Simulation of the semi-batch co-polymerization of Sty/BA T = 138°C $[TBPA]_0$ = 2 wt% xylene = 30wt% f_{Sty0} = 50 wt%

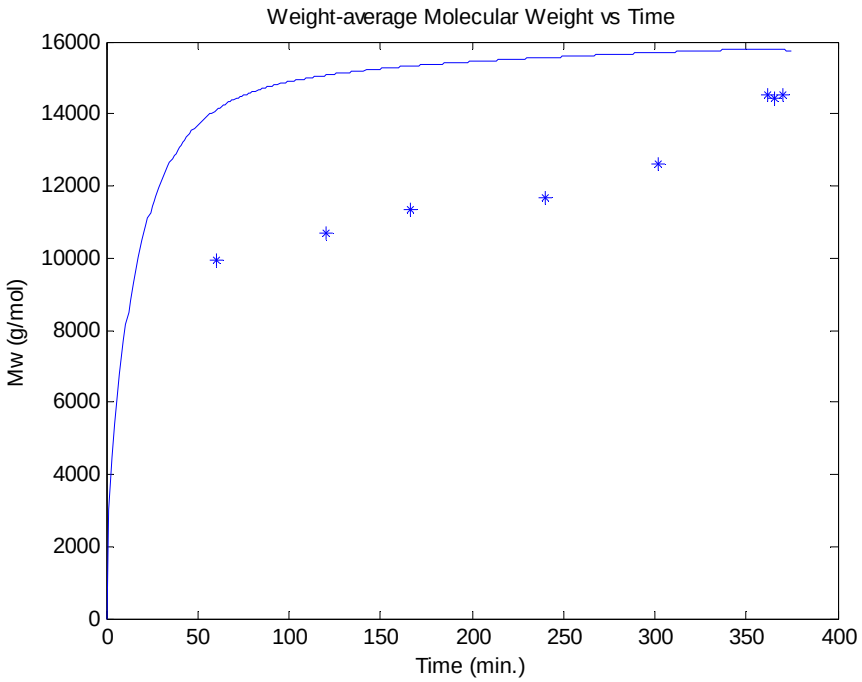

Figure 5.89: Simulation of the semi-batch co-polymerization of Sty/BA T = 138°C $[TBPA]_0$ = 2 wt% xylene = 30wt% f_{Sty0} = 50 wt%

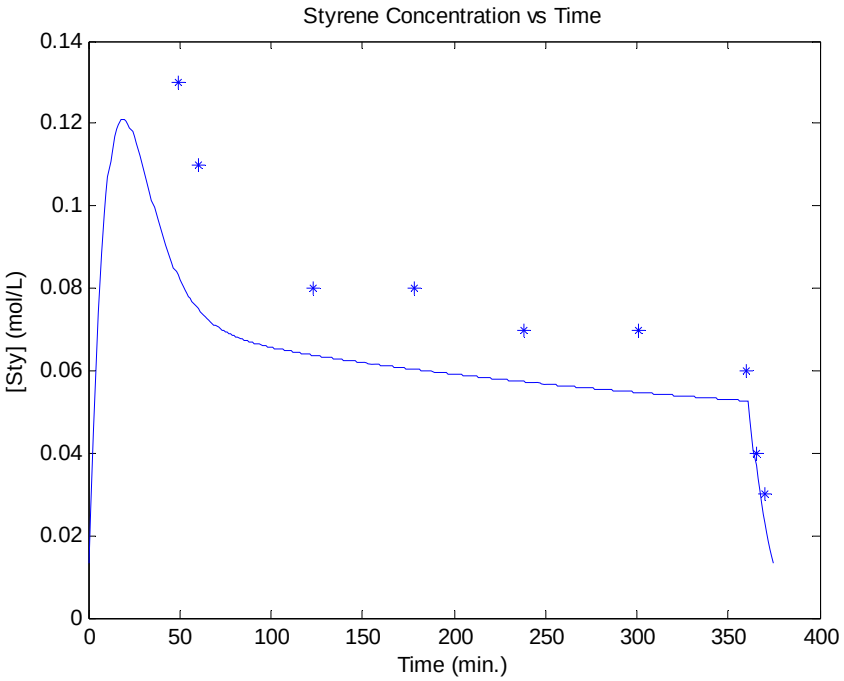

Figure 5.90: Simulation of the semi-batch co-polymerization of Sty/BA T = 138°C $[TBPA]_0$ = 2 wt% xylene = 30wt% f_{Sty0} = 25 wt%

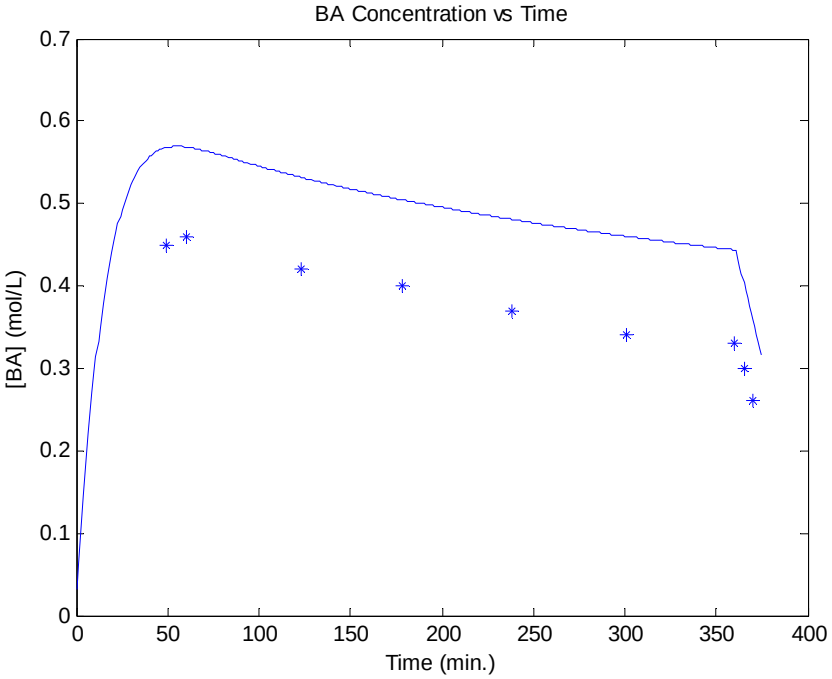

Figure 5.91: Simulation of the semi-batch co-polymerization of Sty/BA T = 138°C $[TBPA]_0$ = 2 wt% xylene = 30wt% f_{Sty0} = 25 wt%

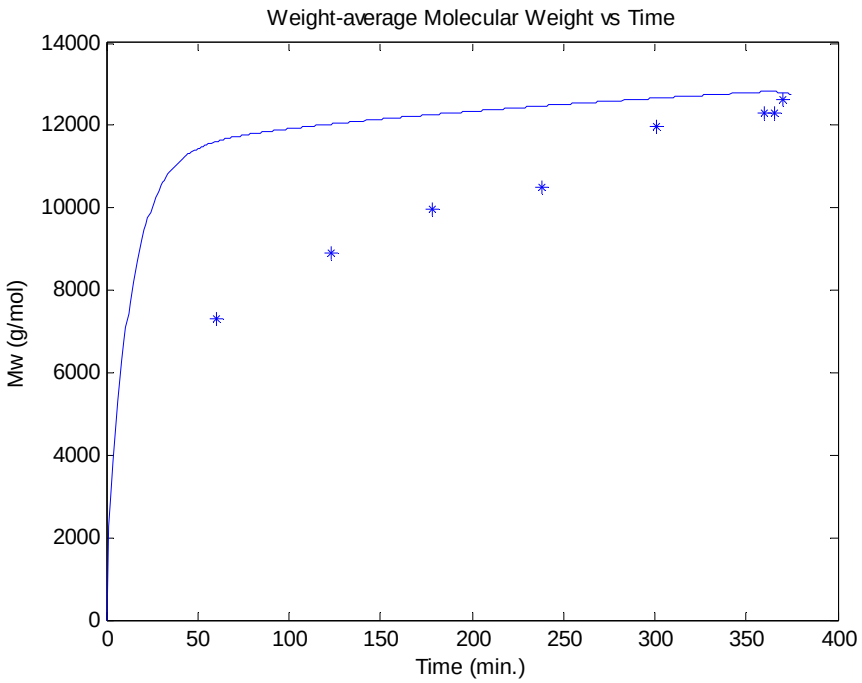

Figure 5.92: Simulation of the semi-batch co-polymerization of Sty/BA T = 138°C $[TBPA]_0$ = 2 wt% xylene = 30wt% f_{Sty0} = 25 wt%

5.2.4 Case Study 10: Ter-polymerization of Styrene, BMA and BA

With this case study, the model was expanded once again to account for backbiting and beta-scission of one monomer, depropagation of another and normal free radical polymerization of the third all at once. The semi-batch ter-polymerization data are from Wang (2010) and cover polymer composition and monomer concentration versus time. The four ter-polymerizations were run using the same method as the previous section; the monomer and initiator were fed evenly over six hours with an extra 15 minutes of feed time for the initiator, TBPA. The starting monomer mole fractions examined were as follows: 33/33/33, 25/50/25, 15/70/15, 15/15/70 wt% of Sty/BMA/BA. The reactivity ratios are in Table 5-6; only homo-depropagation of BMA was assumed to occur as was the case in case study 8, $k_{dpBMA} = k_{pBMA}$*(1.76 - 1.37*wp*10^6*exp(-6240/T) (Wang *et al.*, 2009).

Table 5-6: Reactivity Ratios for the Ter-polymerization of Styrene, Butyl Methacrylate and Butyl Acrylate at 138°C

Reactivity Ratio		Source
r_{Sty-BA}	0.956	Gao and Penlidis (1998)
r_{BA-Sty}	0.183	Gao and Penlidis (1998)
$r_{Sty-BMA}$	0.61	Li *et al.* (2006)
$r_{BMA-Sty}$	0.42	Li *et al.* (2006)
r_{BA-BMA}	1.5815*exp(-564.8/T)	Hakim *et al.* (2000)
r_{BMA-BA}	0.8268*exp(282.1/T)	Hakim *et al.* (2000)

Figure 5.93 through Figure 5.96 are the polymer composition versus time for each of the reactions. Each simulation is extremely accurate, verifying the reactivity ratios used. Figure 5.97, Figure 5.98 and Figure 5.99 are the monomer concentration simulations for styrene, BMA and BA, respectively. The simulations for styrene follow the data well but each slightly overestimates the data with the exception of the fourth run. As styrene is present in the least amount, even a slight deviation from the data appears much larger than it actually is. Both the monomer concentrations of the BMA and BA, however, are quite accurate and follow the pattern established by the data. For such a complex ter-polymerization with depropagation and backbiting, the model performed extremely well and could very well predict an experiment with three monomers at an elevated temperature.

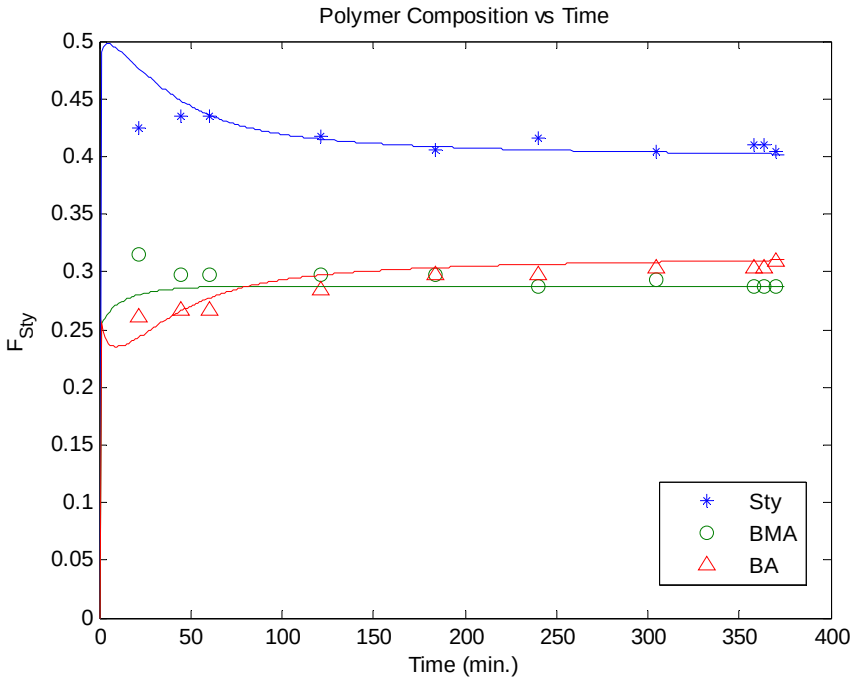

Figure 5.93: Simulation of the semi-batch ter-polymerization of Sty/BMA/BA T = 138°C $[TBPA]_0$ = 2 wt% xylene = 30wt% $f_{Sty0} = f_{BMA0}$ = 33 wt%

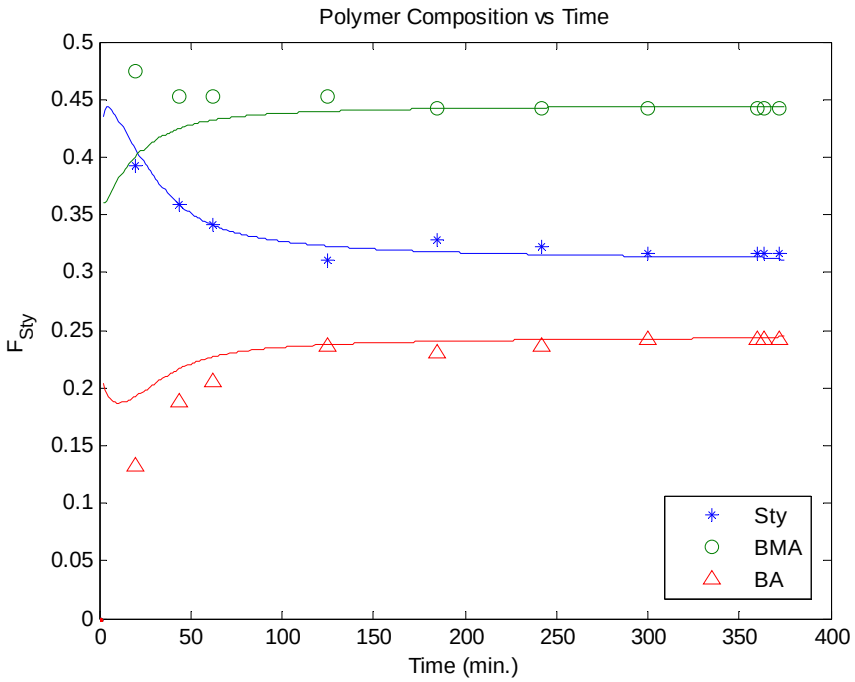

Figure 5.94: Simulation of the semi-batch ter-polymerization of Sty/BMA/BA T = 138°C $[TBPA]_0$ = 2 wt% xylene = 30wt% $f_{Sty0} = f_{BA0}$ = 25 wt%

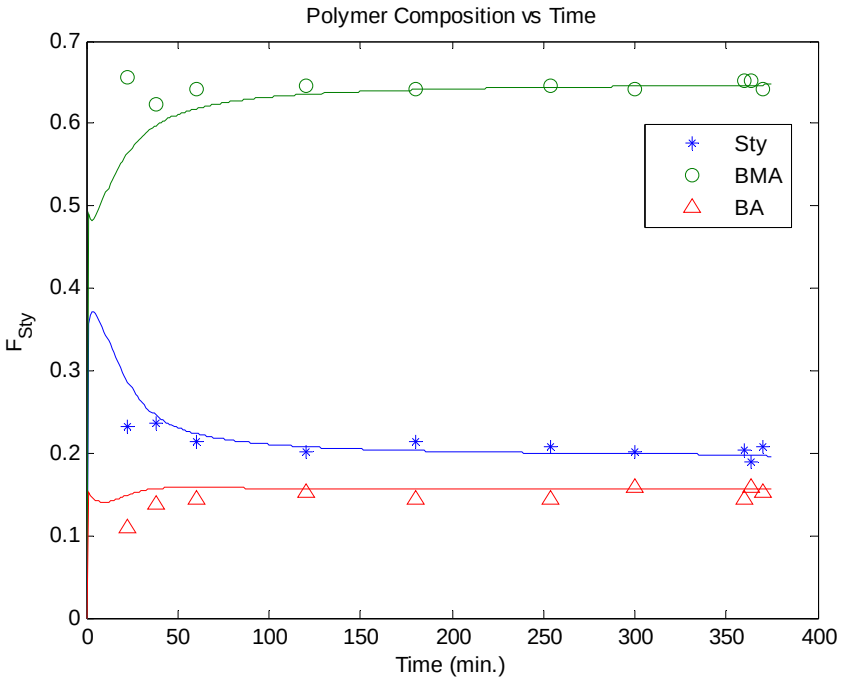

Figure 5.95: Simulation of the semi-batch ter-polymerization of Sty/BMA/BA T = 138°C $[TBPA]_0$ = 2 wt% xylene = 30wt% $f_{Sty0} = f_{BA0}$ = 15 wt%

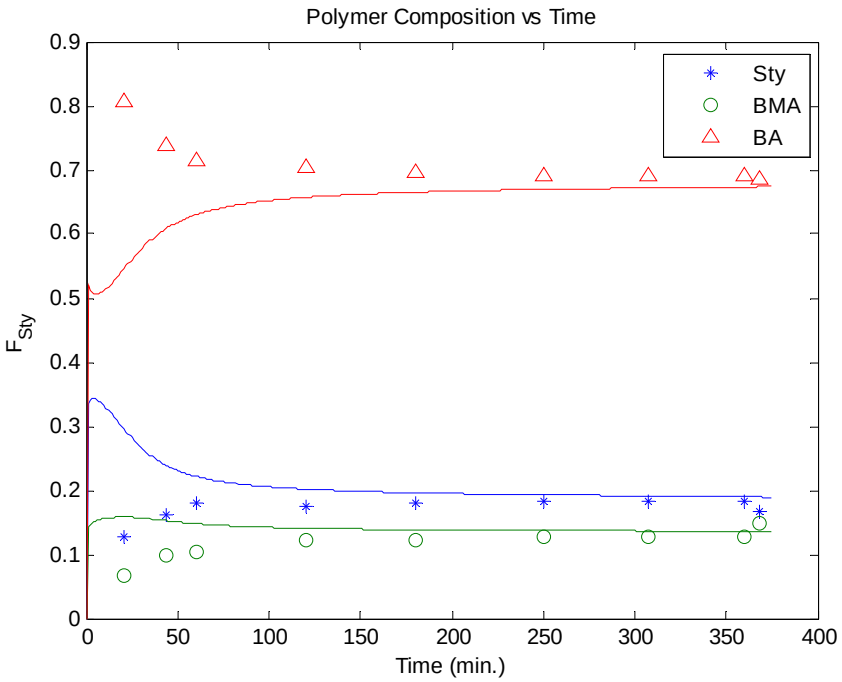

Figure 5.96: Simulation of the semi-batch ter-polymerization of Sty/BMA/BA T = 138°C $[TBPA]_0$ = 2 wt% xylene = 30wt% $f_{Sty0} = f_{BMA0}$ = 15 wt%

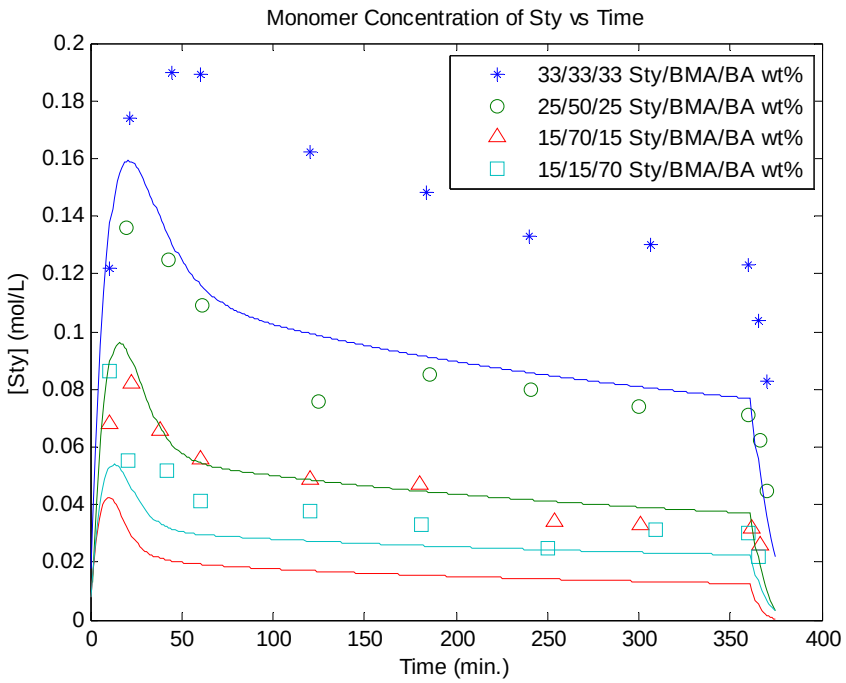

Figure 5.97: Simulation of the semi-batch ter-polymerization of Sty/BMA/BA T = 138°C $[TBPA]_0$ = 2 wt% xylene = 30wt%

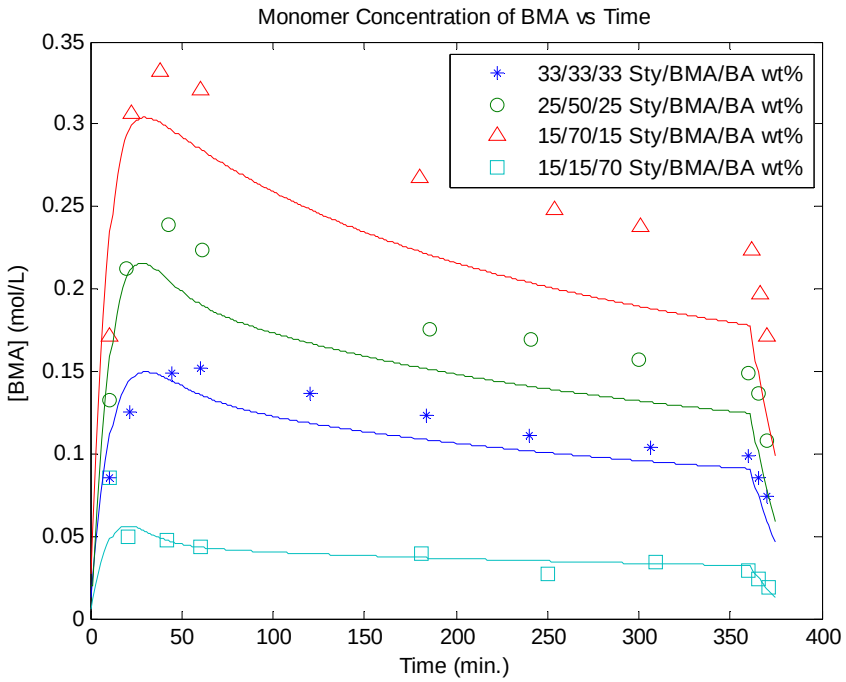

Figure 5.98: Simulation of the semi-batch ter-polymerization of Sty/BMA/BA T = 138°C $[TBPA]_0$ = 2 wt% xylene = 30wt%

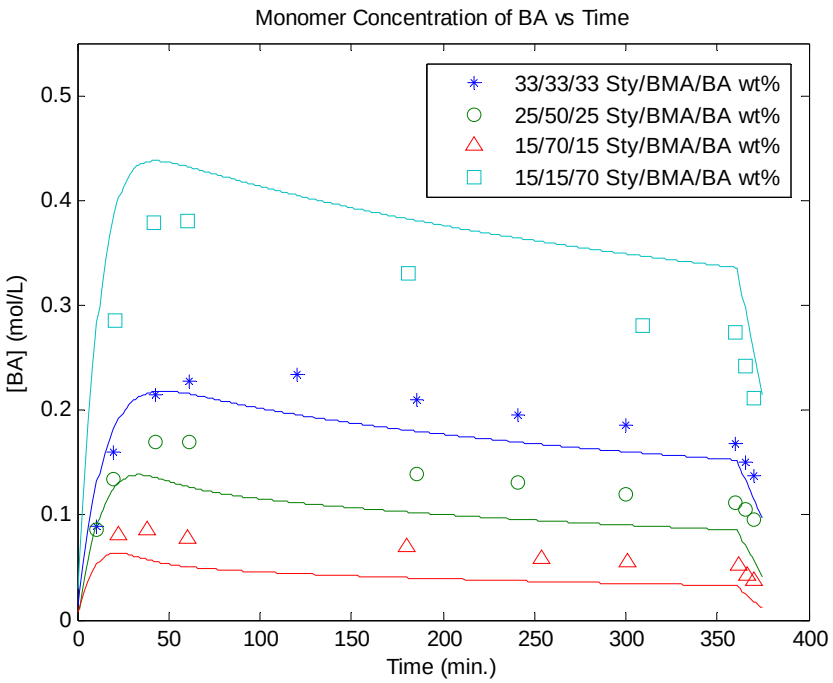

Figure 5.99: Simulation of the semi-batch ter-polymerization of Sty/BMA/BA T = 138°C $[TBPA]_0$ = 2 wt% xylene = 30wt%

5.3.Multiple Initiator Functionality

A new addition to the modeling software is the ability to model up to three initiators in both batch and semi-batch reactor modes. Although it can be easily extended to four or more initiators, this is rarely seen and will probably not be necessary any time soon. The first simulation is a batch co-polymerization of styrene and ethyl acrylate at 80°C using AIBN, BPO and a fictitious initiator at 0.33 wt% each.

The reason for modeling with a fictitious initiator is because the other initiators available in the database (see Database Characteristics, section 3.5) are not as reactive and did not compare favorably with AIBN and BPO. The fictitious initiator used compares to many industrial azo- initiators, having all of its parameter values falling within those of the other initiators mentioned. The characteristics of this initiator can be attained from several of the plots following or from the Initiator Database in the appendices (section Appendix II). Its 10-hour half-life is achieved at 62.6°C.

Observing Figure 5.100, there are many different points in the simulation with an appreciable change in the rate of polymerization. Firstly, the polymerization slows slightly around 40% conversion. This can be explained by the initiator efficiency of BPO becoming diffusion-controlled (see Figure 5.101). The drop in initiator efficiency would decrease the amount of polymer chains being initiated by BPO. Shortly after that, at around 54% conversion, termination becomes diffusion-controlled (see Figure 5.104). As termination is occurring less frequently, there are more polymer chains present, leading to an increase in monomer consumption. In Figure 5.101 again, one can see that the remaining two initiators become diffusion-controlled between 70 and 80% conversion, not only arresting the increase in the rate of polymerization, but eventually decreasing it. Finally, at 90% conversion, the rate of termination approaches zero resulting in a final burst of monomer consumption until complete conversion. The total simulation time is approximately 250 minutes.

Looking at Figure 5.102 and Figure 5.103, the initiator concentration decreases at a rate proportional to the decomposition rate constant. The fictitious initiator having the largest decomposition rate, also has the largest decrease in initiator concentration relative to itself over the course of the reaction.

Figure 5.105 is a plot of both the number- and weight-average molecular weights against conversion showing a large increase in the weight-average molecular weight at around 90% conversion. This can also be explained by Figure 5.104 as the termination rate constant is nearing zero.

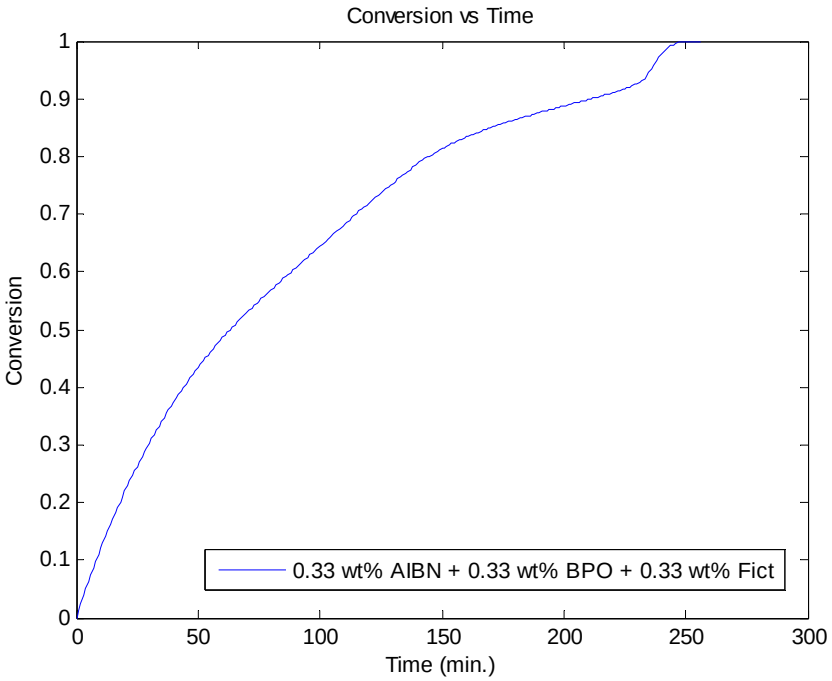

Figure 5.100: Simulation of batch co-polymerization of Sty/BA at 80°C $[AIBN]_0 = [BPO]_0 = [Fict]_0 = 0.33$ wt% $f_{Sty0} = 50$ wt%

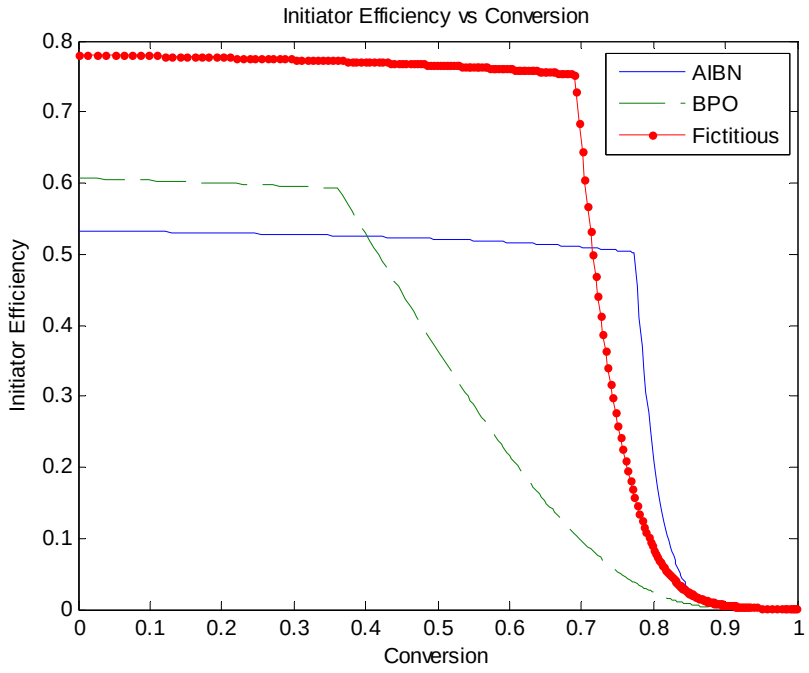

Figure 5.101: Simulation of batch co-polymerization of Sty/BA at 80°C $[AIBN]_0 = [BPO]_0 = [Fict]_0 = 0.33$ wt% $f_{Sty0} = 50$ wt%

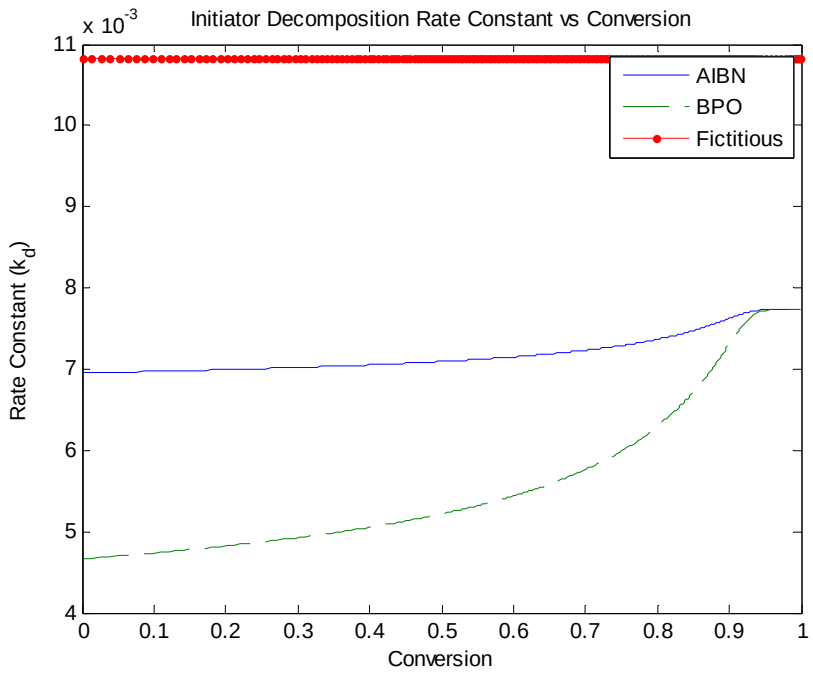

Figure 5.102: Simulation of batch co-polymerization of Sty/BA at 80°C $[AIBN]_0 = [BPO]_0 = [Fict]_0 = 0.33$ wt% $f_{Sty0} = 50$ wt%

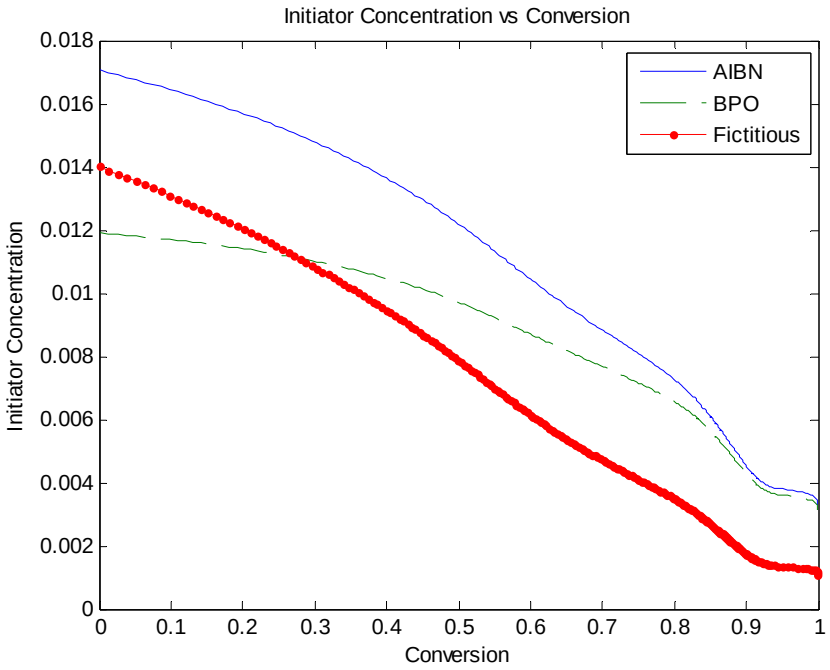

Figure 5.103: Simulation of batch co-polymerization of Sty/BA at 80°C $[AIBN]_0 = [BPO]_0 = [Fict]_0 = 0.33$ wt% $f_{Sty0} = 50$ wt%

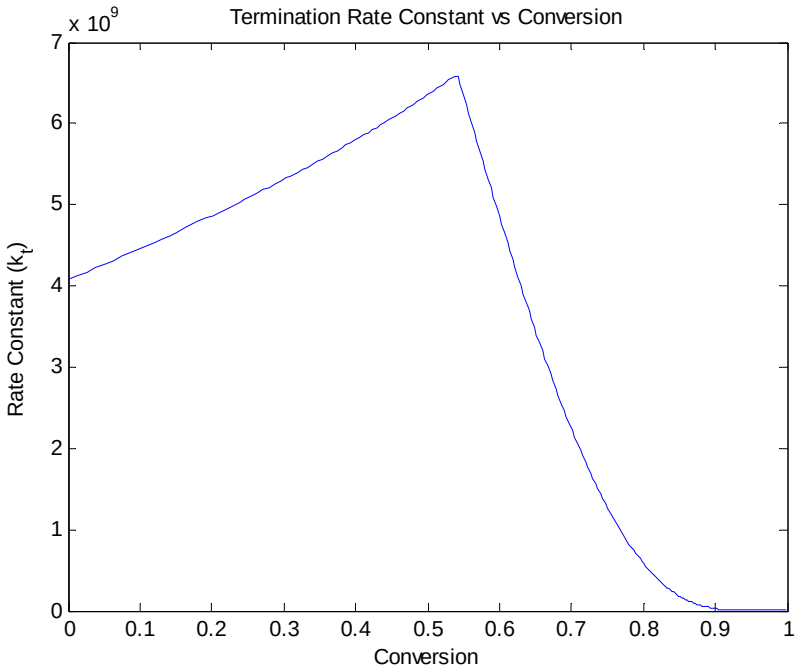

Figure 5.104: Simulation of batch co-polymerization of Sty/BA at 80°C $[AIBN]_0 = [BPO]_0 = [Fict]_0 = 0.33$ wt% $f_{Sty0} = 50$ wt%

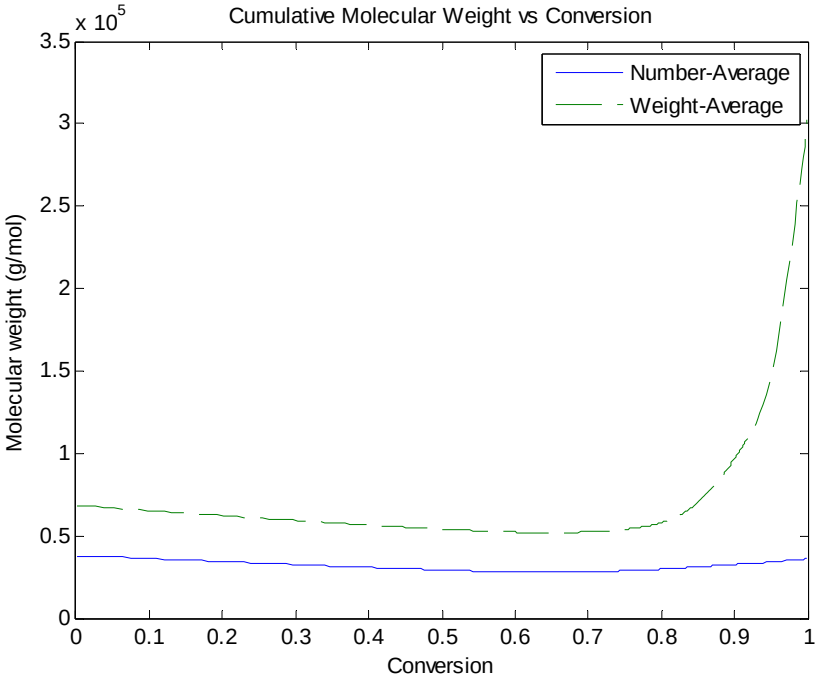

Figure 5.105: Simulation of batch co-polymerization of Sty/BA at 80°C $[AIBN]_0 = [BPO]_0 = [Fict]_0 = 0.33$ wt% $f_{Sty0} = 50$ wt%

The semi-batch case used the same amount of styrene and ethyl acrylate as in the batch case but spread the input out evenly over the first 500 minutes of the reaction. This is represented in Figure 5.106. The initiators added were also eventually equivalent by mass to the batch case; however, they had a variable flowrate and were not completely added until minute 750 of the reaction (see Figure 5.107).

The conversion versus time plot (Figure 5.108) has similar curves as the batch version but with significant differences. Noting the x-axis, the semi-batch simulation occurred over a much longer time period. This is expected as complete conversion is not possible until after all the monomer has been added. Continuing our discussion of Figure 5.108, the first major change in the rate of polymerization occurs at 40% conversion. At this point in the simulation, the initiator feed rate increases substantially. Due to the large increase in initiator concentration (shown in Figure 5.111), the rate of monomer consumption increases. From 40% conversion to 70% conversion, the rate of polymerization remains relatively constant. This is because the decreasing initiator efficiency of BPO counteracts the decreasing rate of termination (shown in Figure 5.112). Once the final monomers are added (occurring at 70% conversion), the reaction is free to reach full conversion. This is shown as an increase in conversion as no more free monomers are being added. Shorty thereafter, both the fictitious initiator and AIBN become diffusion-controlled, resulting in a slower rate of reaction shown in Figure 5.108. The final boost occurs at 90% conversion once the rate of termination approaches zero.

Against conversion, both the initiator efficiency and initiator decomposition rate constant are unchanged from the batch case to the semi-batch case. This can be seen by comparing Figure 5.109 to Figure 5.101 and Figure 5.110 to Figure 5.102.

The termination rate constant seen in Figure 5.112 becomes diffusion-controlled at a slightly lower conversion than in the batch simulation. This is most likely due to the decreased amount of initiator in the system. With less initiator, longer chains are present, thus increasing the viscosity of the reaction mixture. Performing the batch simulation with less initiator would yield a similar result.

Figure 5.113 shows both the number- and weight-average molecular weight plots against conversion. The molecular weights are higher than the batch case due to less initiator present at the beginning of the reaction. The discontinuity point at 40% conversion corresponds to the large increase in the initiator flowrates.

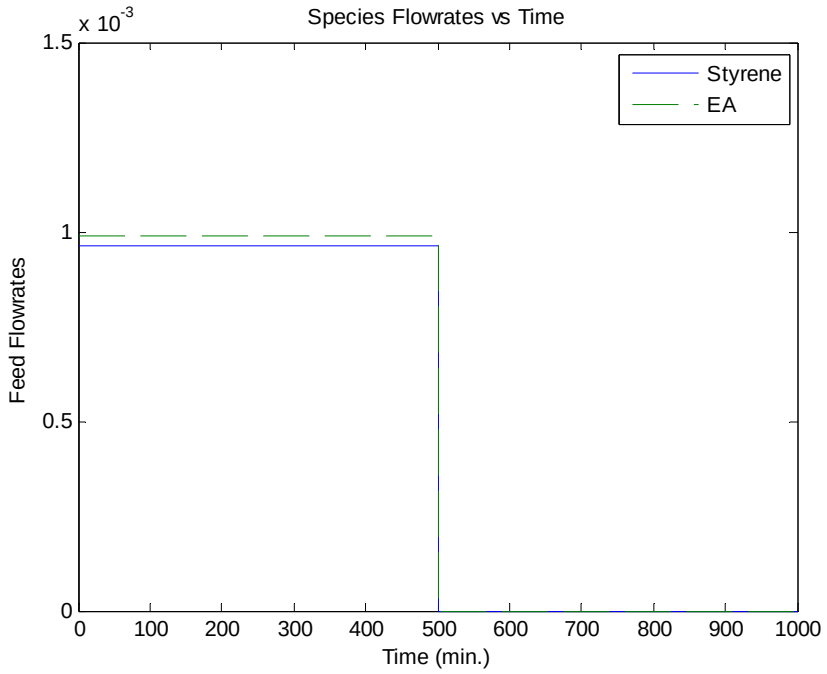

Figure 5.106: Simulation of semi-batch co-polymerization of Sty/BA at 80°C $[AIBN]_0 = [BPO]_0 = [Fict]_0 = 0.33$ wt% $f_{Sty0} = 50$ wt%

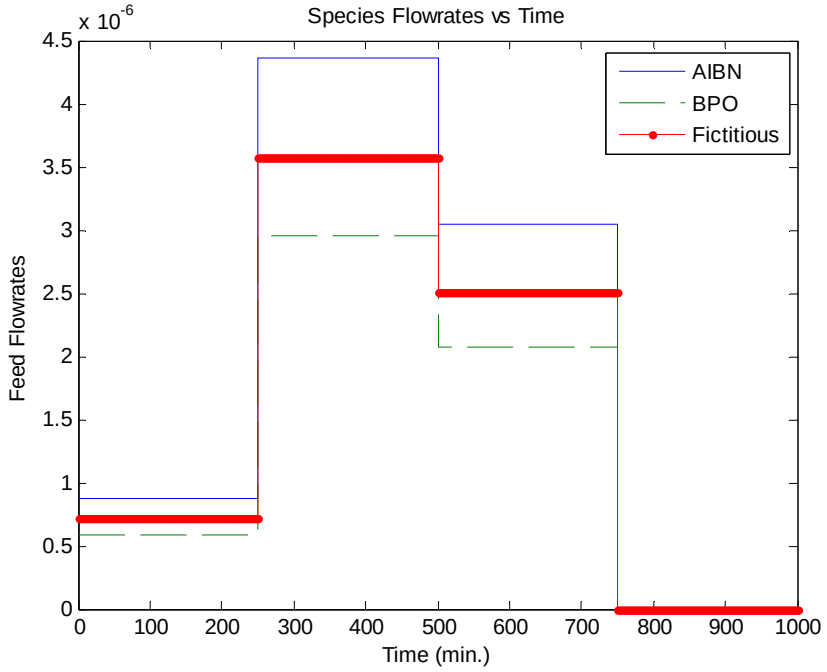

Figure 5.107: Simulation of semi-batch co-polymerization of Sty/BA at 80°C $[AIBN]_0 = [BPO]_0 = [Fict]_0 = 0.33$ wt% $f_{Sty0} = 50$ wt%

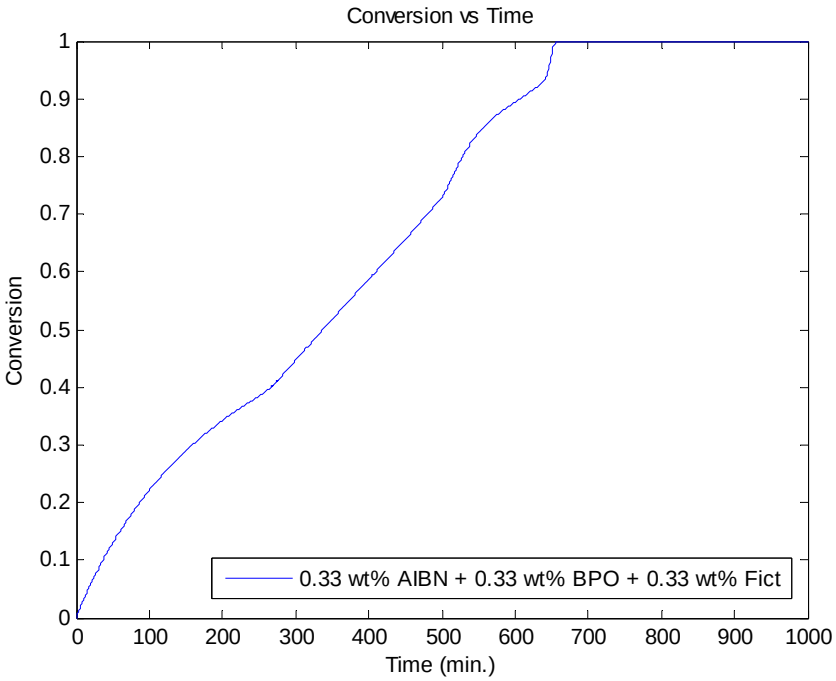

Figure 5.108: Simulation of semi-batch co-polymerization of Sty/BA at 80°C $[AIBN]_0 = [BPO]_0 = [Fict]_0 = 0.33$ wt% $f_{Sty0} = 50$ wt%

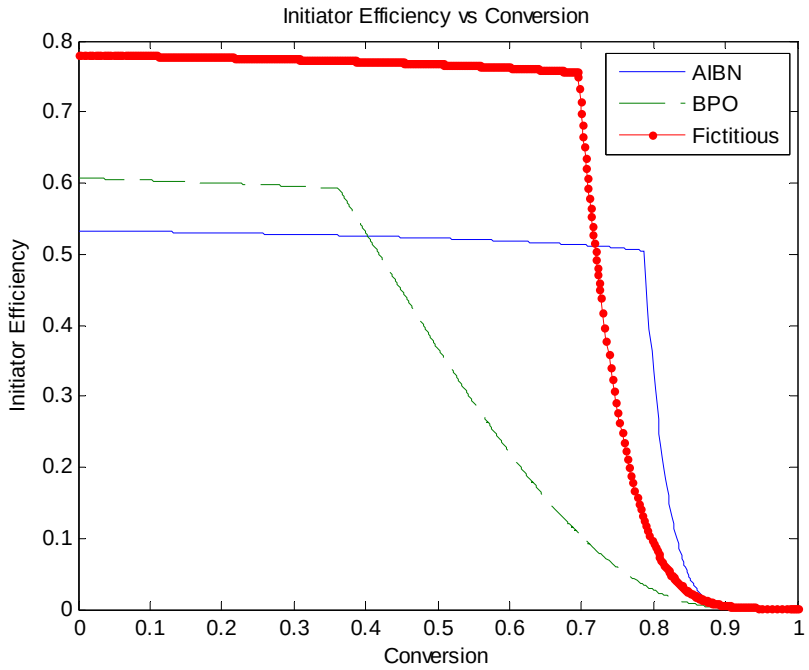

Figure 5.109: Simulation of semi-batch co-polymerization of Sty/BA at 80°C $[AIBN]_0 = [BPO]_0 = [Fict]_0 = 0.33$ wt% $f_{Sty0} = 50$ wt%

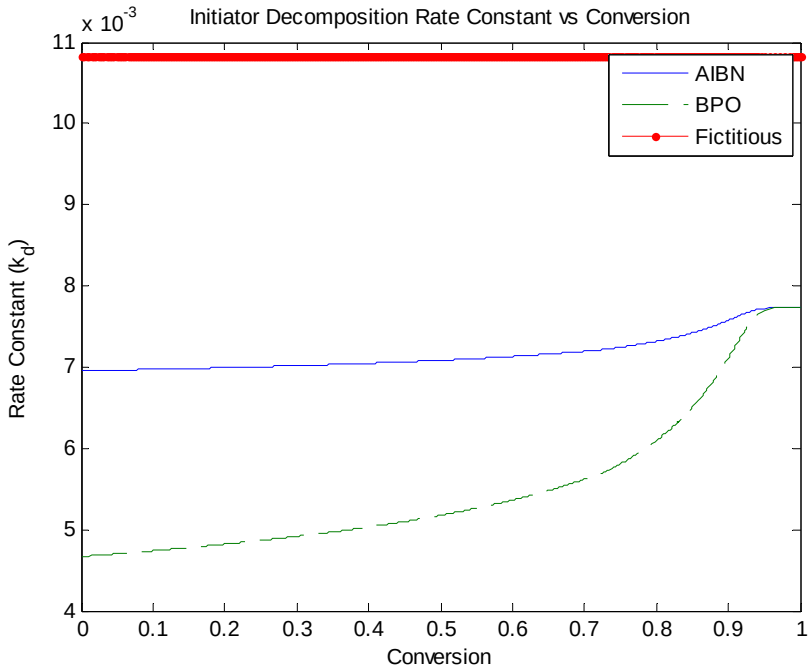

Figure 5.110: Simulation of semi-batch co-polymerization of Sty/BA at 80°C $[AIBN]_0 = [BPO]_0 = [Fict]_0 = 0.33$ wt% $f_{Sty0} = 50$ wt%

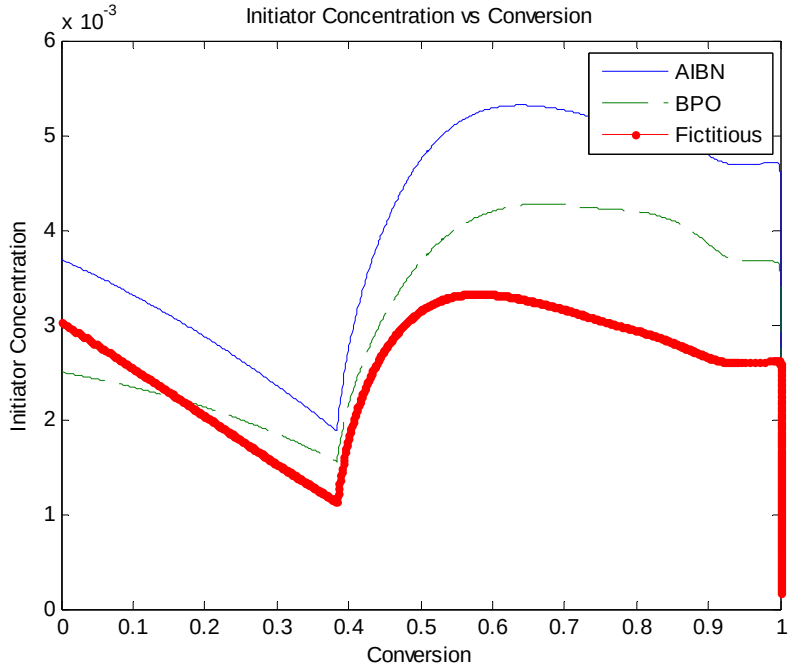

Figure 5.111: Simulation of semi-batch co-polymerization of Sty/BA at 80°C $[AIBN]_0 = [BPO]_0 = [Fict]_0 = 0.33$ wt% $f_{Sty0} = 50$ wt%

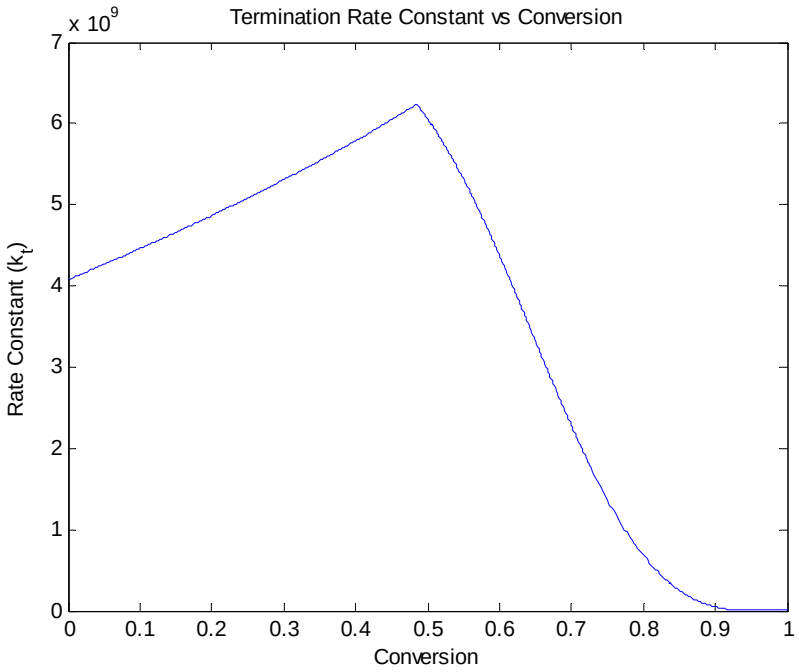

Figure 5.112: Simulation of semi-batch co-polymerization of Sty/BA at 80°C $[AIBN]_0 = [BPO]_0 = [Fict]_0 = 0.33$ wt% $f_{Sty0} = 50$ wt%

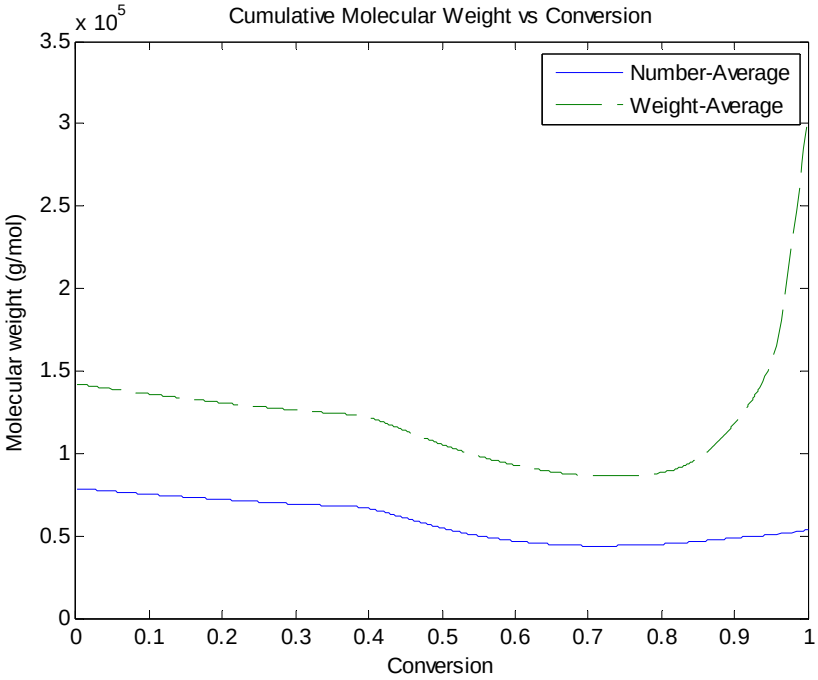

Figure 5.113: Simulation of semi-batch co-polymerization of Sty/BA at 80°C $[AIBN]_0 = [BPO]_0 = [Fict]_0 = 0.33$ wt% $f_{Sty0} = 50$ wt%

Several comparisons between the batch and semi-batch simulations were discussed. Following are four more plots which directly compare the two cases. Figure 5.114 has both the batch and semi-batch conversion versus time plots to show the relative speed of the two reactions. Figure 5.115 shows both the batch and semi-batch simulations of number-average molecular weight against conversion. This illustrates the large difference mentioned earlier, stemming from the decrease in the amount of initiator present in the semi-batch case. Figure 5.116 depicts the weight-average molecular weight versus conversion for both simulations, the semi-batch again having a higher molecular weight. Intriguingly, they overlap towards the end of the reaction. This occurs as the same amount of monomers are present in both cases. Finally, Figure 5.117 shows the reaction volume of both cases. As expected, the reaction volumes of both are equivalent once all the monomers have been added in the semi-batch case (occurring at approximately 70% conversion). This confirms that an equal amount of monomer was added in both simulations.

Some possible next steps for the multiple initiator extension would be to combine it with either the depropagation extension, the composition control extension or perhaps a combination of all three. As mentioned earlier, another possible direction would be to increase the functionality up to four or more initiators, once data from a practical industrial case are found.

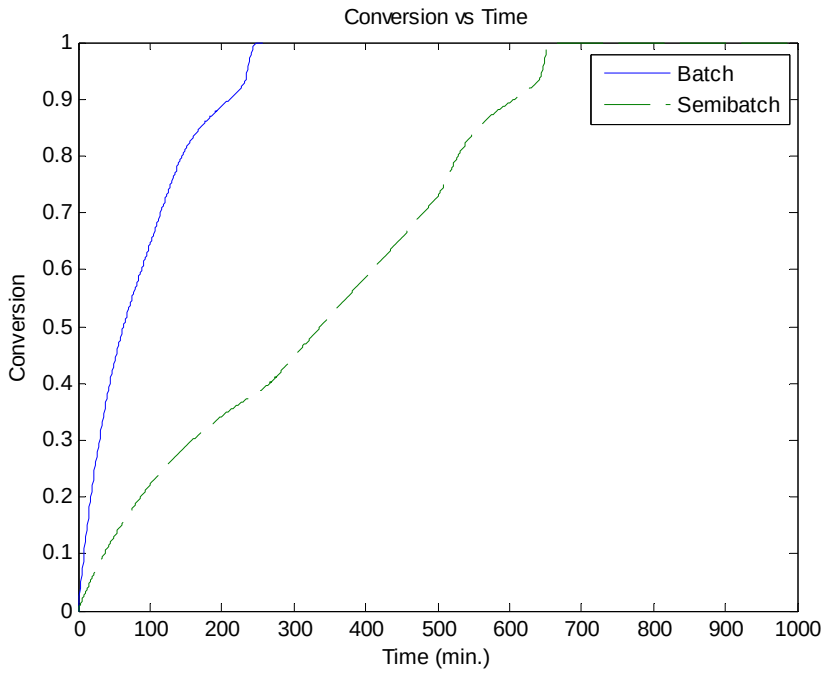

Figure 5.114: Simulation of batch/semi-batch co-polymerization of Sty/BA at 80°C using AIBN, BPO, and Fict f_{Sty0} = 50 wt%

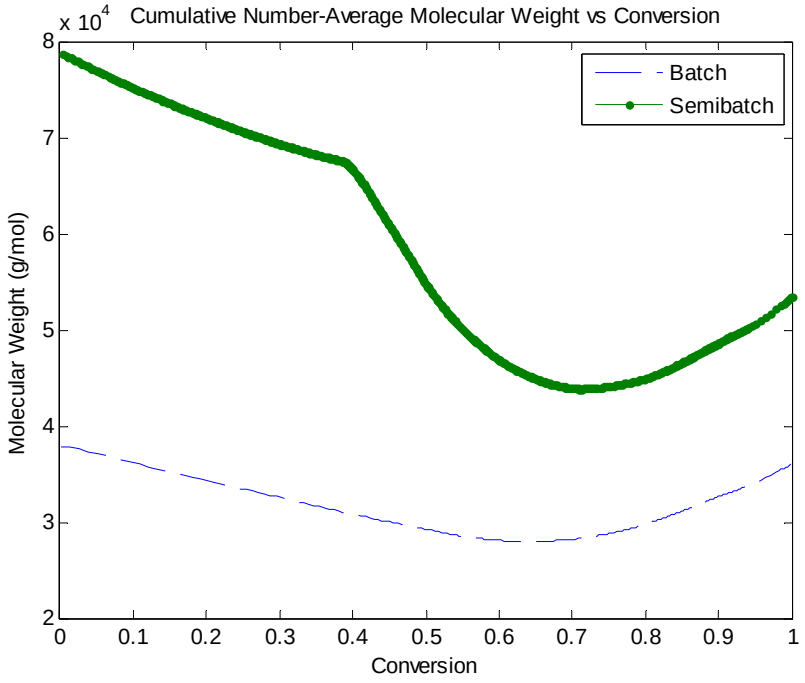

Figure 5.115: Simulation of batch/semi-batch co-polymerization of Sty/BA at 80°C using AIBN, BPO, and Fict f_{Sty0} = 50 wt%

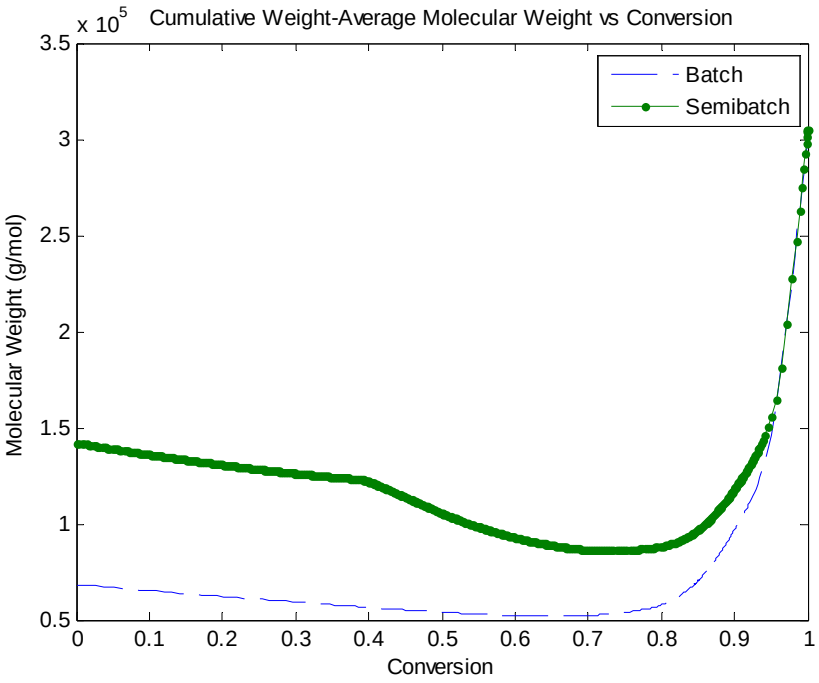

Figure 5.116: Simulation of batch/semi-batch co-polymerization of Sty/BA at 80°C using AIBN, BPO, and Fict f_{Sty0} = 50 wt%

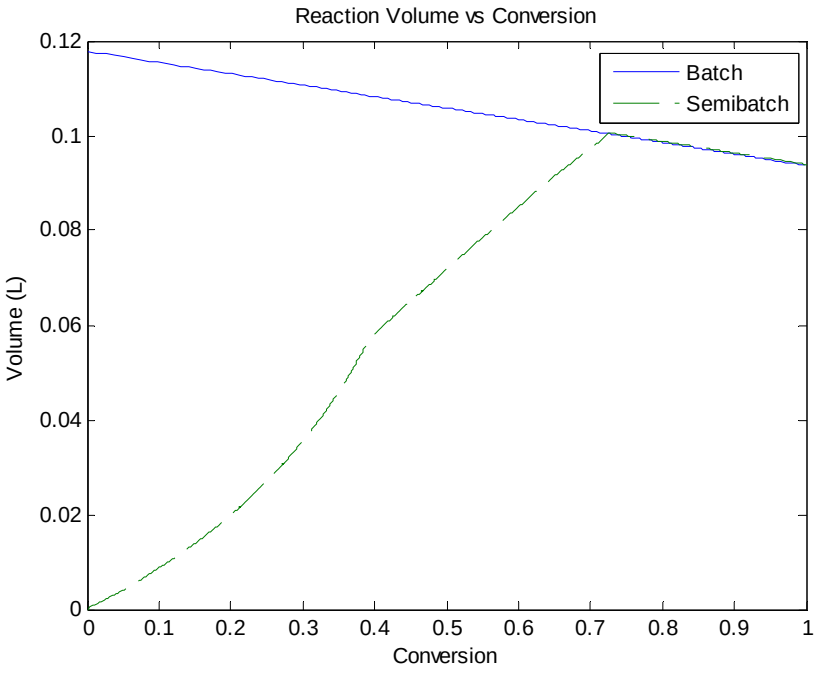

Figure 5.117: Simulation of batch/semi-batch co-polymerization of Sty/BA at 80°C using AIBN, BPO, and Fict f_{Sty0} = 50 wt%

6. Composition Control

Composition control represents a major expansion in the modeling software's capabilities. The basic idea is to maintain a constant polymer composition (co-, ter-, and tetra-polymerizations) throughout the entire reaction. In general, when one monomer is more reactive than another, it will react faster with the appropriate radicals, and hence get incorporated more readily into the polymer. At the same time, as the reaction proceeds, the monomer is consumed at a greater rate, and will become less and less available relative to the other monomer(s). As such, the more reactive monomer becomes ever less present, allowing the other monomer(s) to incorporate at a higher frequency, thus giving rise to a variation in the composition (distribution) of the polymer chain with time, which is commonly referred to as composition drift. By following one of the three composition control policies (to be discussed shortly), a constant amount of each monomer relative to the other(s) will be incorporated into the polymer over the entire course of the reaction. In order to maintain control over the system, the monomer inlet flowrates are manipulated. Thus, the optimal solution for each policy consists of delivering the appropriate monomer flowrate(s).

In policy 1, both monomers are charged into the reactor initially. Only the more reactive monomer is fed during the reaction to maintain a constant N_1/N_2 ratio. By keeping the monomer ratio constant, no composition drift will occur. In policy 2, both monomers are fed into the reactor to maintain constant monomer concentration levels. With constant unreacted monomer concentration in the reactor, the polymer composition will again be unvarying. The third and final policy can be seen as a special case of policy 2. The monomers are fed into the reactor at the same rate they are consumed, thus maintaining the same monomer ratio. This special case occurs when the monomer concentrations in policy 2 approach zero. As one can see, all three policies will achieve the same result but with different approaches. The variations in implementation produce substantially different properties in the final polymer, which will be discussed at length throughout the derivations. Sections 6.1, 6.2 and 6.3 analyze policy 1, 2 and 3, respectively. Extensions to ter- and higher polymerizations will be discussed in section 6.5.

Before the derivation of each policy, the general polymerization rate model equations are cited for quick reference. Additional information on composition control can be found in Fujisawa and Penlidis (2008).

A molar balance for monomer 1 in a semi-batch reactor will give:

$$\frac{dN_1}{dt} = -R_{p1}V + F_{1,in} \tag{6.1.}$$

Similarly, for monomer 2 we obtain:

$$\frac{dN_2}{dt} = -R_{p2}V + F_{2,in} \tag{6.2.}$$

Polymerization rates for monomers 1 and 2, respectively:

$$R_{p1} = R_{11} + R_{21} = k_{p11}[R_1^*][M_1] + k_{p21}[R_2^*][M_1] \tag{6.3.}$$

$$R_{p2} = R_{12} + R_{22} = k_{p12}[R_1^*][M_2] + k_{p22}[R_2^*][M_2] \tag{6.4.}$$

Radical fractions are given by:

$$\phi_1^* = \frac{[R_1^*]}{[R^*]} = \frac{k_{p21}f_1}{k_{p21}f_1 + k_{p12}f_2} \tag{6.5.}$$

$$\phi_2^* = \frac{[R_2^*]}{[R^*]} = \frac{k_{p12}f_2}{k_{p21}f_1 + k_{p12}f_2} \tag{6.6.}$$

Also, by definition, monomer mole fractions:

$$f_1 = \frac{[M_1]}{[M]} \qquad f_2 = \frac{[M_2]}{[M]} \tag{6.7.}$$

$$[R^*] = [R_1^*] + [R_2^*] \qquad [M] = [M_1] + [M_2] \qquad [M] = \frac{N}{V} \tag{6.8.}$$

Substituting equations 6.3 through 6.6 into equations 6.1 and 6.2, we obtain:

$$\frac{dN_1}{dt} = -N_1\left(k_{p11}\phi_1^* + k_{p21}\phi_2^*\right)[R^*] + F_{1,in} \tag{6.9.}$$

$$\frac{dN_2}{dt} = -N_2\left(k_{p12}\phi_1^* + k_{p22}\phi_2^*\right)[R^*] + F_{2,in} \tag{6.10.}$$

In addition, from co-polymerization theory, we know that:

$$R_I = 2fk_d[I] \tag{6.11.}$$

$$[R^*] = \left(\frac{R_I}{k_t}\right)^{1/2} \tag{6.12.}$$

$$\begin{aligned} k_t &= k_{t11}\phi_1^{*2} + 2k_{t12}\phi_1^*\phi_2^* + k_{t22}\phi_2^{*2} \\ &= \frac{k_{t11}k_{p21}{}^2 f_1{}^2 + 2k_{t12}k_{p21}f_1k_{p12}f_2 + k_{t22}k_{p12}{}^2 f_2{}^2}{(k_{p21}f_1 + k_{p12}f_2)^2} \end{aligned} \tag{6.13.}$$

$$\begin{aligned} \frac{dV}{dt} &= inflow\ rate + shrinkage \\ &= \left(\frac{MW_1}{\rho_{m1}}\right)F_{1,in} + \left(\frac{MW_2}{\rho_{m2}}\right)F_{2,in} - V\sum_{i=1}^{2} R_{pi}MW_i\left(\frac{1}{\rho_{mi}} - \frac{1}{\rho_p}\right) \end{aligned} \tag{6.14.}$$

Therefore:

$$\begin{aligned} \frac{dV}{dt} = (inflow\ rate) + {} & MW_1\left(\frac{1}{\rho_{m1}} - \frac{1}{\rho_p}\right)\Phi_1[\mathrm{R}^*]\mathrm{N}_1 \\ & + MW_2\left(\frac{1}{\rho_{m2}} - \frac{1}{\rho_p}\right)\Phi_2[\mathrm{R}^*]\mathrm{N}_2 \end{aligned} \tag{6.15.}$$

$$\Phi_1 = \frac{k_{p11}k_{p21}f_1 + k_{p21}k_{p12}f_2}{k_{p21}f_1 + k_{p12}f_2} \tag{6.16.}$$

$$\Phi_2 = \frac{k_{p12}k_{p21}f_1 + k_{p22}k_{p12}f_2}{k_{p21}f_1 + k_{p12}f_2} \tag{6.17.}$$

In the batch case, the instantaneous polymer composition is given by:

$$F_1 = \frac{dN_1}{dN_1 + dN_2} \tag{6.18.}$$

In general, the instantaneous polymer composition is a function of the rate of propagation (incorporation in the co-polymer chains) of both monomers:

$$F_1 = \frac{R_{p1}}{R_{p1} + R_{p2}} \tag{6.19.}$$

Regardless of the approach, by holding the ratio N_1/N_2 constant, the instantaneous polymer composition given in 6.19 will be constant; and if the instantaneous polymer composition remains unchanged from reaction start to finish, the cumulative (desired) polymer composition will also remain constant.

A co-polymerization is a complex process and there are hundreds of computations occurring at each simulated minute. For a co-polymerization scenario (i.e., two monomers only), it is easy to identify the most reactive comonomer (based on reactivity ratios) and subsequently derive analytical expressions for the appropriate comonomer flowrates in a semi-continuous reactor that will give the desirable constant copolymer composition. These analytical expressions (which can be correct in many cases and/or very reasonable in many other practical situations) are obtained under several simplifying assumptions, hence the resulting flowrates are sub-optimal. In many cases, these sub-optimal comonomer flowrates are very close to the actual optimal ones. However, this is not the case in general (and certainly not the case with three or more monomers (i.e., ter- or higher multi-component polymerization)). No direct analytical solution is generally available to maintain a constant polymer composition without extensive simplifications. Therefore, in order to obtain an optimal solution for the corresponding comonomer flowrates (even in binary co-polymerizations), a numerical solution is required. This will be arrived at in an iterative fashion as the modeling equations involved are non-linear.

Basically, the simulation software will start by running a batch reaction. Depending on the approximately derived analytical solution, certain variables (such as the rate of polymerization and reaction volume) will be recorded for the course of the reaction. These values will then be used to calculate the monomer flowrates for the next iteration, a semi-batch reaction. With each successive iteration, the polymerization simulation approaches a constant polymer composition, resulting in the determination of the ideal monomer flowrate(s). The derivation of the monomer flowrate(s) is shown later in each policy's corresponding section (6.1, 6.2 and 6.3 for policy 1, 2 and 3, respectively), but a summary is shown here merely to present the fields (variables) recorded in each iteration as an overview example.

In policy 1, the reacting volume and the rates of polymerization (propagation) of monomers 1 and 2 are required to calculate the next iteration's flowrate:

$$F_{1,in} = R_{p1}V + \frac{N_1}{N_2}R_{p2}V \qquad 6.20.$$

$$F_{2,in} = 0 \qquad 6.21.$$

With simplification, equation 6.20 is equivalent to equation 6.30 found in section 6.1.

Policy 2, in addition to the rates of polymerization of monomers 1 and 2 and the reacting volume, requires the change of volume per unit time (minutes, in our case) as well as the initial monomer concentrations:

$$F_{1,in} = [M_1]_0 \frac{dV}{dt} + R_{p1}V \quad 6.22.$$

$$F_{2,in} = [M_2]_0 \frac{dV}{dt} + R_{p2}V \quad 6.23.$$

These equations can easily be implemented in a mathematical model but would be very difficult to determine in an industrial setting. Hence, the derivation outlined in section 6.2 uses a practical approach to approximate $\frac{dV}{dt}$ and therefore has a different final solution.

Policy 3, being a limiting case of policy 2 when the monomer concentrations approach zero, is simply:

$$F_{1,in} = R_{p1}V \quad 6.24.$$

$$F_{2,in} = R_{p2}V \quad 6.25.$$

These flowrates are determined based on the previous simulation to improve the polymer composition iteratively. With successive improvement in each iteration, the optimal (ideal) monomer flowrate(s) will eventually be determined and a constant polymer composition achieved.

In step-wise form, the iterative approach is shown as follows:

Step 1: Run the desired monomer recipe as a batch reaction. Record specific fields which vary depending on the policy (examples of some of these fields were given above).

Step 2: Run the polymerization again but as a semi-batch reaction. The inlet flowrates of the monomers will be calculated (and updated) using the appropriate values from step 1. These same values will be recorded again for use in the next iteration.

Step 3: Check whether the final composition of the polymer is equal to the desired composition. If yes, terminate the iteration. Otherwise, repeat step 2.

Although the algorithm is seemingly simple in words, it becomes quite involved in implementation. Several final formulas for the monomer flowrates, shown in bold in

subsequent sections, will be explained for each policy in the corresponding sections upon first use.

After each iteration (completion of step 2 and 3), the approach will use the corresponding variables calculated throughout the simulation to determine the monomer flowrate(s) for the next iteration.

As an example of the iterative scheme described above, the final product of one of the policies (policy 1) is shown in Figure 6.1. There are several different curves on the plot for each monomer; they represent the iterations required (a total of eight, in this case) to determine the correct monomer feed rate that gives a constant polymer composition. The simulation with the greatest drift is the batch reactor case. The final iteration is the constant line from start to finish. In terms of the batch case and the large composition drift, the polymer chains formed at the beginning of the reaction will differ significantly in properties from the chains created at the end. With a constant polymer composition, however, the properties of all the chains will be uniform.

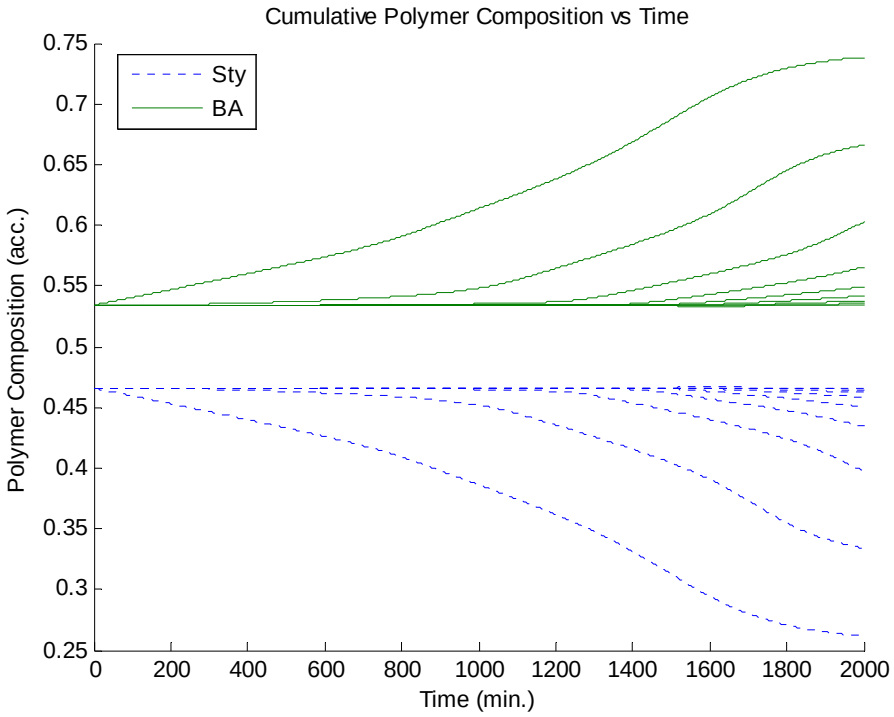

Figure 6.1: Simulation of the co-polymerization of Sty/BA at 50°C with iterations to reach a constant polymer composition

Each of the policies and their approaches to maintaining a constant monomer molar ratio will now be discussed.

6.1. Policy 1

There are several characteristics that make policy 1 distinct. To start, only one monomer is being fed into the system. As N_1/N_2 must be maintained at a constant, pre-fixed value, the concentration of both monomers will drop with respect to time. This will mimic batch operation and result in a higher conversion and lower molecular weights than the other policies (to be described shortly). Each of the following policies, as well as some additional considerations, will be solved for implementation in an industrial setting. With that said, the inlet flowrate of the monomer(s) is bolded for simple comparison between the solutions.

Keeping in mind that N_1/N_2 = const. and $F_{2,in} = 0$:

$$\frac{dN_1}{dt} = -N_1\left(k_{p11}\phi_1^* + k_{p21}\phi_2^*\right)[R^*] + F_{1,in} = -N_1\Phi_1[R^*] + F_{1,in} \tag{6.26.}$$

$$\frac{dN_2}{dt} = -N_2\left(k_{p12}\phi_1^* + k_{p22}\phi_2^*\right)[R^*] = -N_2\Phi_2[R^*] \tag{6.27.}$$

As $\frac{N_1}{N_2} = const.$, then $\frac{d}{dt}\left(\frac{N_1}{N_2}\right) = 0$. Therefore,

$$N_2{}^{-1}\frac{dN_1}{dt} - \frac{N_1}{N_2{}^2}\frac{dN_2}{dt} = 0 \tag{6.28.}$$

$$\frac{dN_1}{dt} = \left(\frac{N_1}{N_2}\right)\frac{dN_2}{dt} = -N_1\Phi_2[R^*] = -N_1\Phi_1[R^*] + F_{1,in} \tag{6.29.}$$

Therefore the inlet flowrate of the more reactive monomer is determined to be,

$$\boldsymbol{F_{1,in} = N_1[R^*](\Phi_1 - \Phi_2)} \tag{6.30.}$$

Also,

$$\frac{dN_1}{dt} = -N_1\Phi_1[R^*] + N_1[R^*](\Phi_1 - \Phi_2) \tag{6.31.}$$

or

$$\frac{dN_1}{dt} = -N_1\Phi_2[R^*] \qquad 6.32.$$

Looking back at equation 6.17, it is obvious that Φ_2 will remain constant as long as $\frac{N_1}{N_2}$ and consequently, f_1 and f_2 are constant. This can be seen in Figure 6.2 where Φ_2 is shown versus time for the final iteration of policy 1. Even with the diffusion control limitations of k_t at minute 606 and initiator efficiency f at minute 1189, Φ_2 remains constant. The reason for the slight increase at the end is that the iterations were terminated once the polymer composition remained unchanged despite the fact that $\frac{N_1}{N_2}$ changed slightly towards the end of the reaction. With a few more iterations, a constant Φ_2 would be seen throughout. Similarly, Φ_1 is also unvarying throughout the reaction.

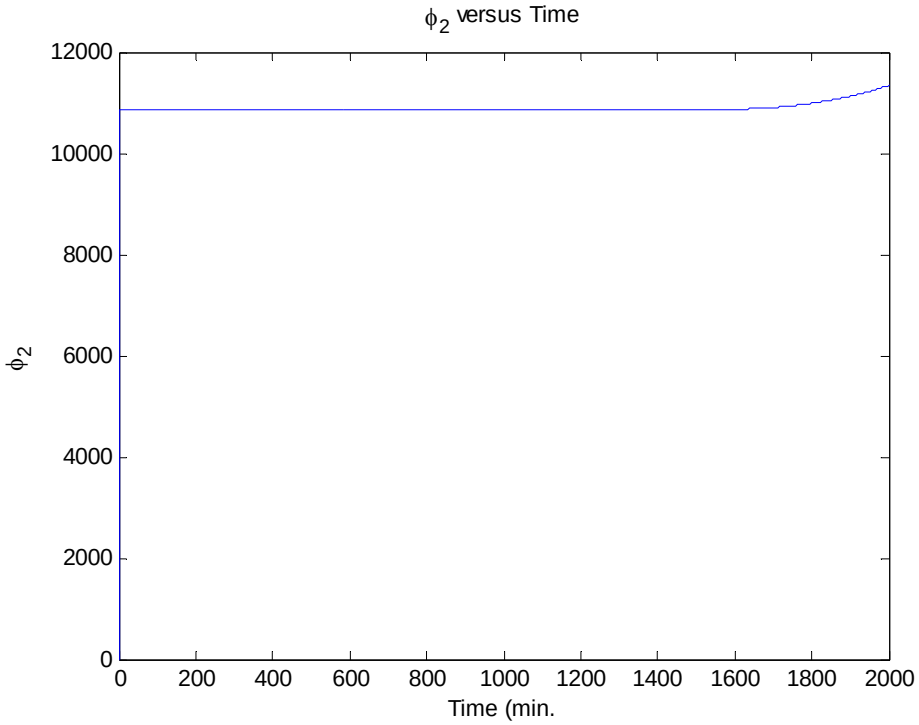

Figure 6.2: Simulation of composition control policy 1, Sty/BA at 50°C $[AIBN]_0$ = 0.05M

For the special case where $[R^*]$ is constant,

$$N_1 = N_{1_0} exp(-\Phi_2[R^*]t) \qquad 6.33.$$

and

$$F_{1,in} = (\Phi_1 - \Phi_2)N_{1_0}[R^*]exp(-\Phi_2[R^*]t) \qquad 6.34.$$

For the special case where $r_1 = r_2 = 1$, $(\Phi_1 - \Phi_2) = 0$. This follows intuitively as neither monomer will require a feed if they both have the same reactivity towards each other. As $[R^*]$ is a function of k_t and $[I]$ (see equation 6.12), and $\frac{dN_I}{dt} = -k_d N_I + F_{I,in}$, we can determine $F_{I,in}$ to maintain $[R^*]$ constant, assuming of course we know how k_t varies with polymer concentration. As the reaction proceeds, the weight of the polymer will continuously increase while the overall rate of termination will decrease causing difficulties in maintaining a constant radical concentration $\bar{F}$

An alternate expression for the volume and the number of moles of monomer polymerized, policy 1 specific, can be found in equations 6.35 and 6.36.

$$\frac{dV}{dt} = \frac{MW_1}{\rho_{m1}} F_{1,in} - R_{p1} V \frac{MW_1}{\rho_{m1}} - R_{p2} V \frac{MW_2}{\rho_{m2}} + \left(R_{p1} MW_1 + R_{p2} MW_2\right) \frac{V}{\rho_p} \qquad 6.35.$$

$$Monomer\ polymerized = N_{1_0} + \int_0^t F_{1,in} t dt - N_1 \qquad 6.36.$$

A co-polymerization of styrene and butyl acrylate at 50°C with 0.05 mol/L of AIBN and $f_{Sty0} = 0.258$ has been successfully simulated with a constant cumulative polymer composition using policy 1. The reactivity ratios used were taken from Gao and Penlidis (1998): $r_{Sty\text{-}BA} = 0.956$ and $r_{BA\text{-}Sty} = 0.183$. This basic recipe will be used for the simulations of compositional control policies 1, 2 and 3. Alternative recipes are discussed in sections 6.5 and 6.6.

The large composition drift present in a batch reactor was completely eliminated in nine iterations (Figure 6.3). In addition to polymer composition, the model has produced simulations of conversion, monomer mole fractions, molar flowrates, and molecular weights versus time (discussed below).

In Figure 6.4, a high monomer conversion is achieved, as expected. This is because both monomers are being consumed throughout the reaction with only enough styrene being added to maintain a constant monomer mole ratio. Figure 6.5 is the monomer mole fraction versus time. As mentioned previously, a constant N_1/N_2 ratio was not required for the final stages of the reaction to reach a constant polymer composition. Granted, the instantaneous polymer composition would begin to drift initially but this would have minimal effect on the cumulative composition. The monomer flowrates in Figure 6.6 show that styrene was the only monomer fed into the reactor. The variable flowrate is a result of diffusion-control. As the rate of polymerization changes, so must the monomer flowrate in order to compensate. Figure 6.7 shows the number-average and weight-average molecular weights.

The values here are relatively low when compared to the other policies, due to the similarities to batch reactor operation.

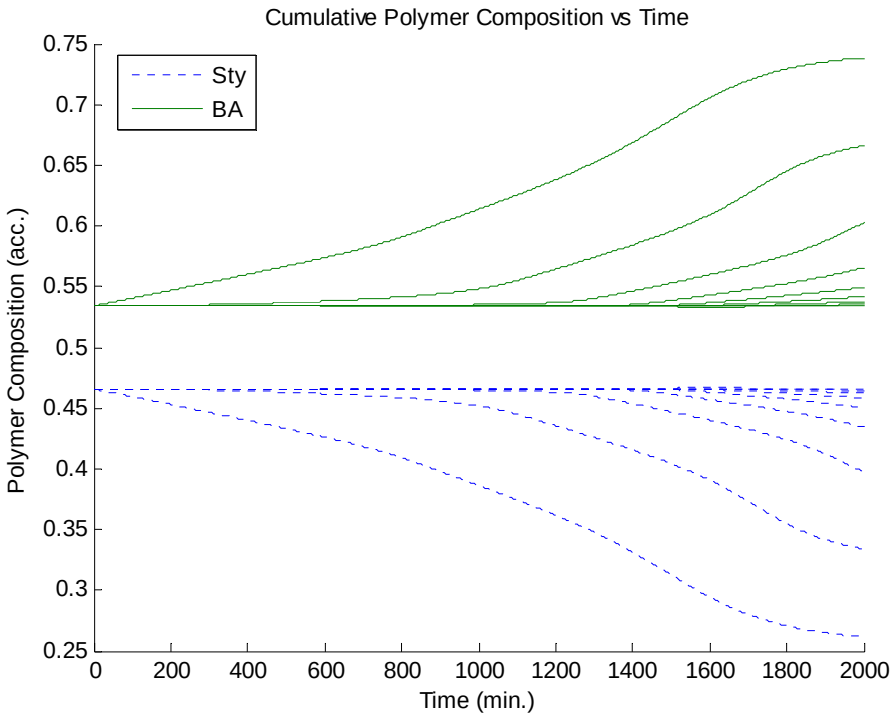

Figure 6.3: Simulation of composition control policy 1, Sty/BA at 50°C $[AIBN]_0$ = 0.05M

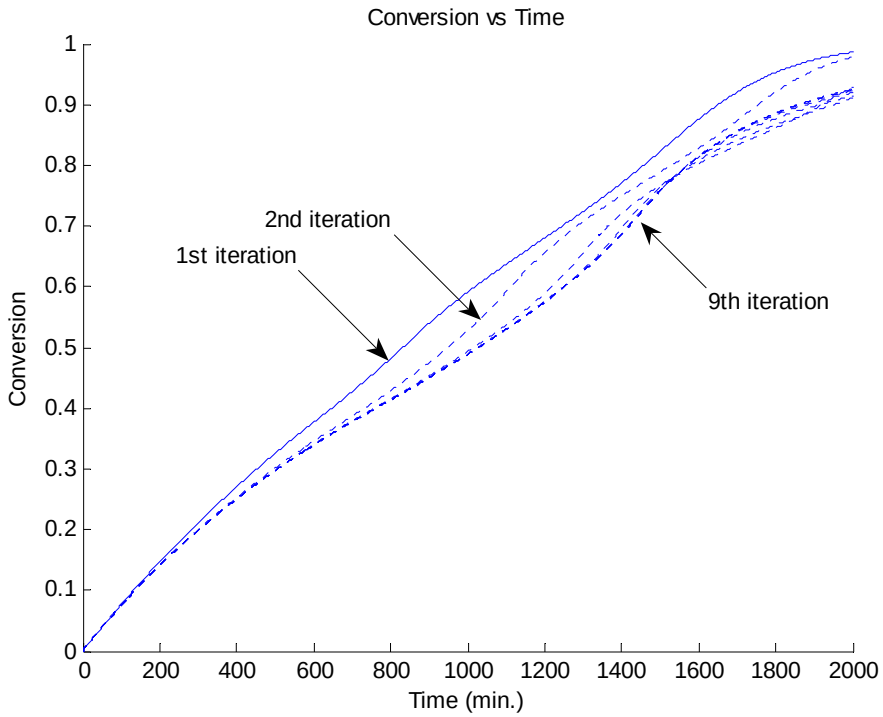

Figure 6.4: Simulation of composition control policy 1, Sty/BA at 50°C $[AIBN]_0 = 0.05M$

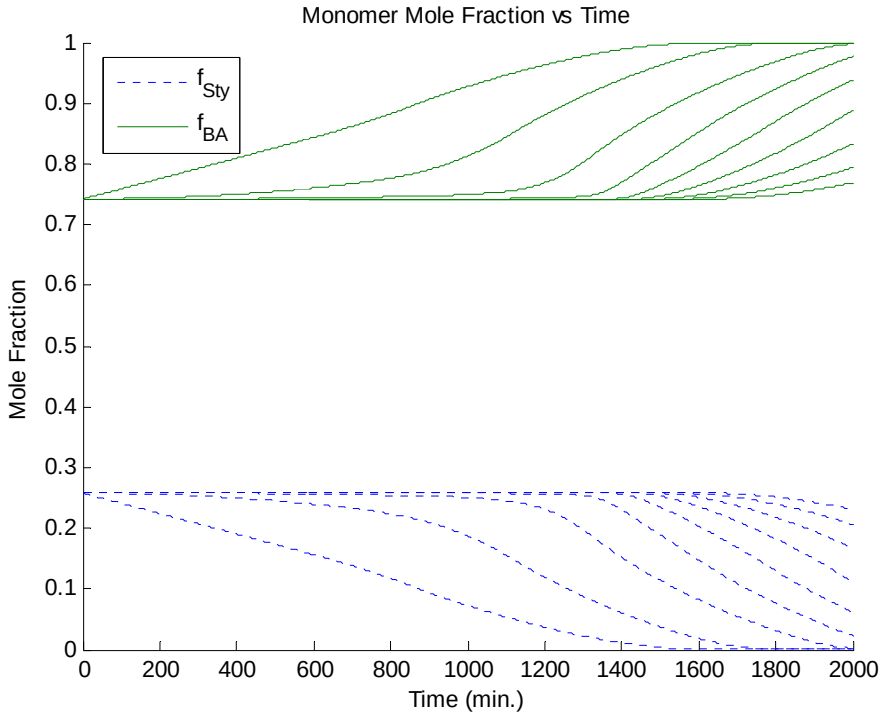

Figure 6.5: Simulation of composition control policy 1, Sty/BA at 50°C $[AIBN]_0 = 0.05M$

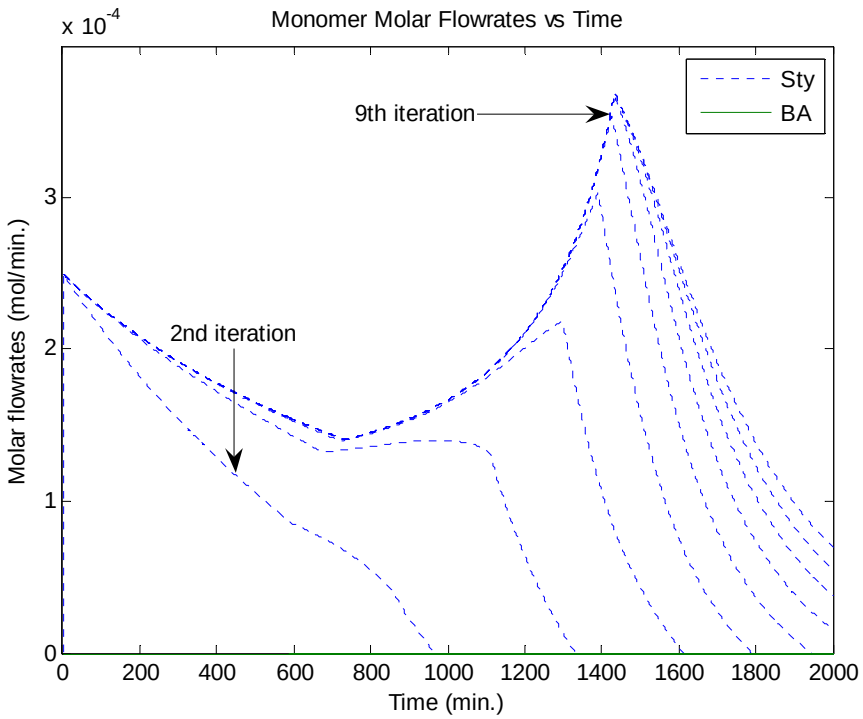

Figure 6.6: Simulation of composition control policy 1, Sty/BA at 50°C $[AIBN]_0 = 0.05M$

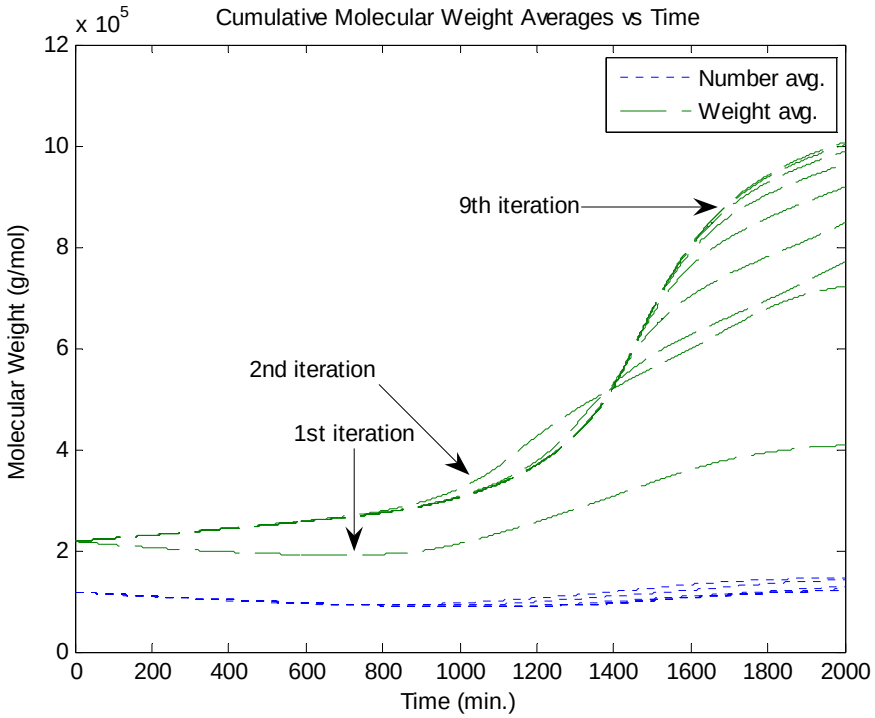

Figure 6.7: Simulation of composition control policy 1, Sty/BA at 50°C $[AIBN]_0 = 0.05M$

6.2. Policy 2

In this policy, the monomer concentrations in the reactor are maintained at a constant level. As the concentration of polymer chains will inevitably increase, so must the amount of monomers in the system. This will limit conversion and naturally produce much higher molecular weights and polymer chain branches than the other policies. We begin the derivation with the same basic equations but with the second monomer flowrate included.

$$\frac{dN_1}{dt} = -N_1\Phi_1[R^*] + F_{1,in} \tag{6.37.}$$

$$\frac{dN_2}{dt} = -N_2\Phi_2[R^*] + F_{2,in} \tag{6.38.}$$

$[M_1] = \frac{N_1}{V}$ and $[M_1] = [M_1]_0 = const$. Therefore,

$$\frac{d}{dt}\left(\frac{N_1}{V}\right) = V^{-1}\frac{dN_1}{dt} - N_1\frac{1}{V^2}\frac{dV}{dt} = 0 \tag{6.39.}$$

$$\frac{dN_1}{dt} = \left(\frac{N_1}{V}\right)\frac{dV}{dt} = [M_1]\frac{dV}{dt} = [M_1]_0\frac{dV}{dt} \tag{6.40.}$$

Similarly,

$$\frac{dN_2}{dt} = [M_2]_0\frac{dV}{dt} \tag{6.41.}$$

The inlet monomer flowrate will be a function of the change in volume, which is a rather complex variable to handle analytically (see equation 6.35). In order to simplify it significantly, an assumption about the densities as well as an assumption removing the shrinkage factor can be made:

$$\rho = \rho_{m1} = \rho_{m2} = \rho_p \tag{6.42.}$$

And therefore,

$$\frac{dV}{dt} = \frac{MW_1}{\rho}F_{1,in} + \frac{MW_2}{\rho}F_{2,in} \tag{6.43.}$$

To check the validity of these assumptions, the co-polymerization of styrene and butyl acrylate was simulated and the change in volume was calculated both with and without the simplifying assumptions in Figure 6.8.

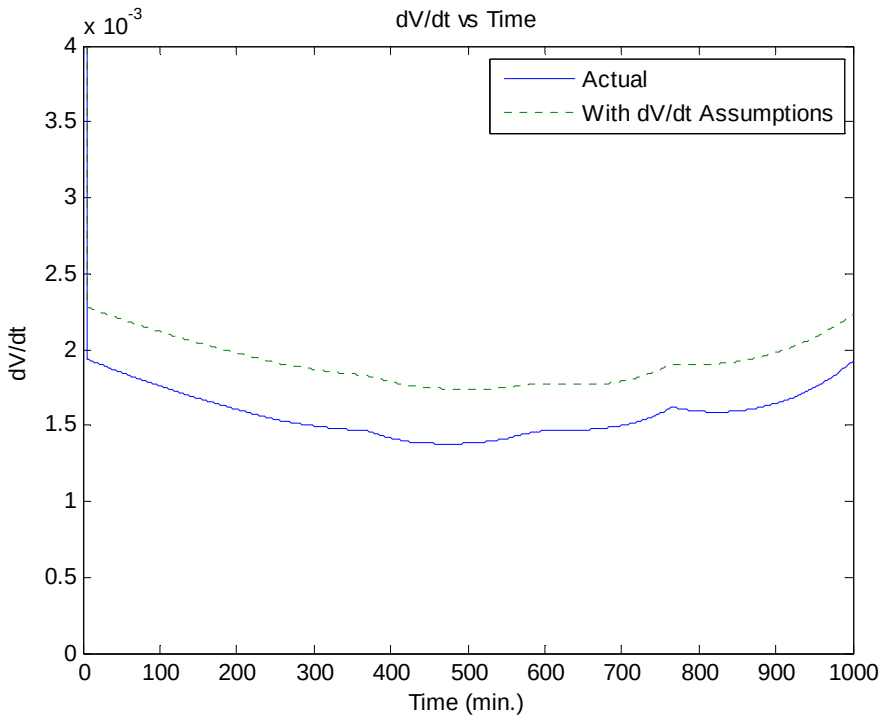

Figure 6.8: Simulation of composition control policy 2, Sty/BA at 60°C $[AIBN]_0$ = 0.05M

The results show that there is very little difference between the two, the largest difference being 2x10^{-4} L/min. This verifies the use of these assumptions for simplifying the following derivations. Something to keep in mind is that the size of the system is approximately three liters, meaning a difference of 0.2mL/min would have little, if any, effect (also see Figure 6.13 later). Again, the flowrates for the two inlet monomers have been bolded to emphasize the practical implementation solution.

Continuing from equations 6.40 and 6.41,

$$-N_1\Phi_1[R^*] + F_{1,in} = [M_1]_0\left(\frac{MW_1}{\rho}F_{1,in} + \frac{MW_2}{\rho}F_{2,in}\right) \qquad 6.44.$$

$$-N_2\Phi_2[R^*] + F_{2,in} = [M_2]_0\left(\frac{MW_1}{\rho}F_{1,in} + \frac{MW_2}{\rho}F_{2,in}\right) \qquad 6.45.$$

These represent a set of two algebraic equations with two unknowns, $F_{1,in}$ and $F_{2,in}$. Solving,

$$\boldsymbol{F_{1,in} = \Theta_1 N_1[R^*]} \text{ and } \boldsymbol{F_{2,in} = \Theta_2 N_2[R^*]} \qquad 6.46.$$

$$\Theta_1 = \rho\left\{\frac{\left(\frac{N_{2_0}}{N_{1_0}}\right)\Phi_2\ell - \Phi_1\varsigma}{\alpha\varsigma - \upsilon\ell}\right\} \tag{6.47.}$$

$$\Theta_2 = \rho\left\{\frac{\left(\frac{N_{1_0}}{N_{2_0}}\right)\Phi_1\upsilon - \Phi_2\alpha}{\alpha\varsigma - \upsilon\ell}\right\} \tag{6.48.}$$

The groups α, ℓ, υ and ς are functions of monomer concentration, molecular weight and density:

$$\alpha = MW_1[M_1]_0 - \rho \tag{6.49.}$$

$$\ell = [M_1]_0 MW_2 \tag{6.50.}$$

$$\upsilon = [M_2]_0 MW_1 \tag{6.51.}$$

$$\varsigma = MW_2[M_2]_0 - \rho \tag{6.52.}$$

Also,

$$\frac{dN_1}{dt} = -N_1\Phi_1[R^*] + \Theta_1 N_1[R^*] = \Psi_1 N_1[R^*] \tag{6.53.}$$

$$\Psi_1 = \Theta_1 - \Phi_1$$

$$\frac{dN_2}{dt} = -N_2\Phi_2[R^*] + \Theta_2 N_2[R^*] = \Psi_2 N_2[R^*] \tag{6.54.}$$

And for the special case where $[R^*]$=const.,

$$N_1 = N_{1_0} exp(\Psi_1[R^*]t) \tag{6.55.}$$

$$N_2 = N_2 exp(\Psi_2[R^*]t) \tag{6.56.}$$

$$F_{1,in} = \Theta_1 N_{1_0}[R^*] exp(\Psi_1[R^*]t) \tag{6.57.}$$

$$F_{2,in} = \Theta_2 N_{2_0}[R^*] exp(\Psi_2[R^*]t) \tag{6.58.}$$

$$\frac{F_{1,in}}{F_{2,in}} = \frac{\Theta_1 N_{1_0}[R^*] exp(\Psi_1[R^*]t)}{\Theta_2 N_{2_0}[R^*] exp(\Psi_2[R^*]t)} \tag{6.59.}$$

As Ψ_1 and Ψ_2 are both constants, when they are approximately equal to each other,

$$\frac{F_{1,in}}{F_{2,in}} = \frac{\Theta_1 N_{1_0}}{\Theta_2 N_{2_0}} = const. \qquad 6.60.$$

With a constant monomer flowrate ratio, premixing of the monomers is possible. A premixed feed requires only one pump which translates into a lower overall cost. A potential alternative solution for policy 2 is presented in the appendices.

The general policy 2 was applied to the same monomer recipe as in policy 1 but at 60°C. Due to the large amount of monomers added, the final conversion reached is low, only about 25%. This can be improved by including a batch finishing step which will be demonstrated in a later section. Increasing the amount of initiator has more effect on the molecular weight levels than on conversion.

Figure 6.9 shows each of the iterations required to attain a constant cumulative polymer composition. In this specific scenario, five iterations were required. Figure 6.10 is the monomer flowrates for the final iteration. In general, they will increase with time but this is hardly observed with this polymerization recipe. Almost 21 moles of monomer are added over the course of the reaction, explaining the low conversion seen in Figure 6.11. The weight-average molecular weight shown in Figure 6.12 reaches 900 000 g/mol when constant composition is achieved; approximately the same values found in policy 1, despite the relevant increase in temperature. Figure 6.13 is the volume of the reaction versus time. The solution, or final iteration of the policy, represents the curve with the largest reaction volume. This is expected as a large amount of monomers were added to maintain the policy requirements.

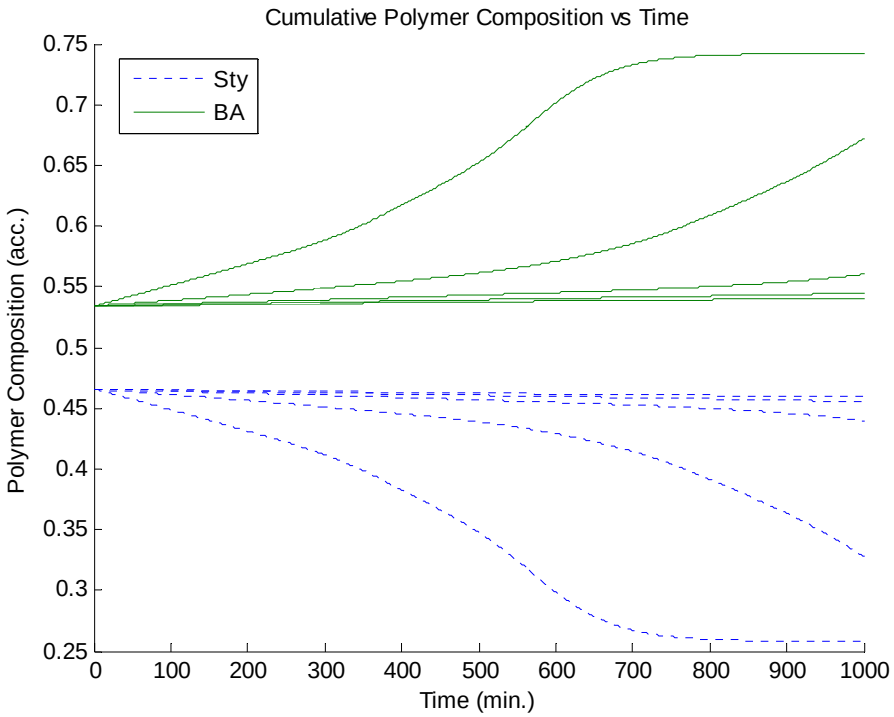

Figure 6.9: Simulation of composition control policy 2, Sty/BA at 60°C $[AIBN]_0 = 0.05M$

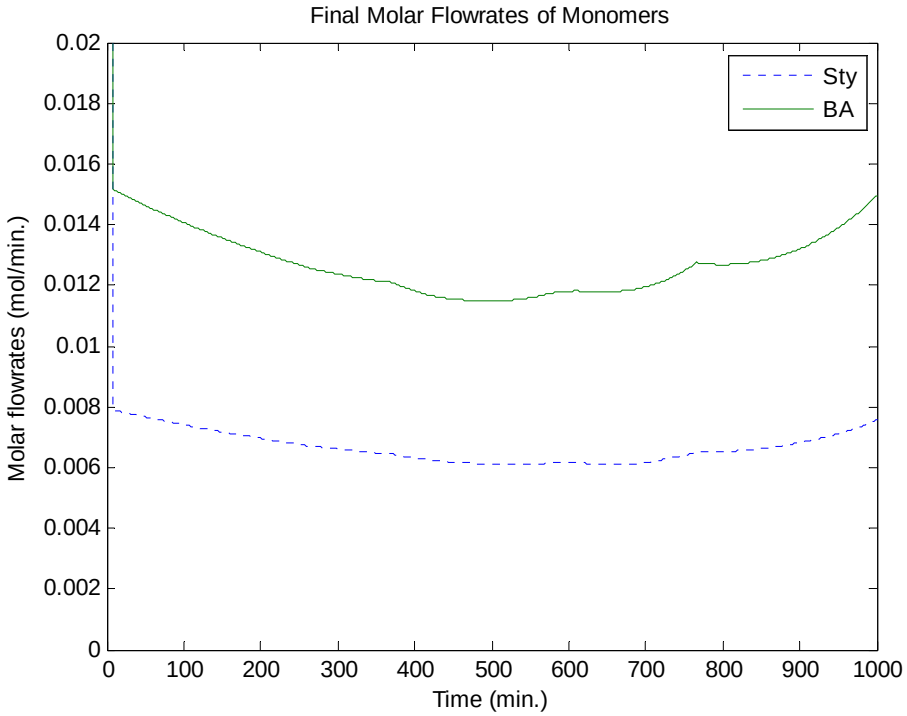

Figure 6.10: Simulation of composition control policy 2, Sty/BA at 60°C $[AIBN]_0 = 0.05M$

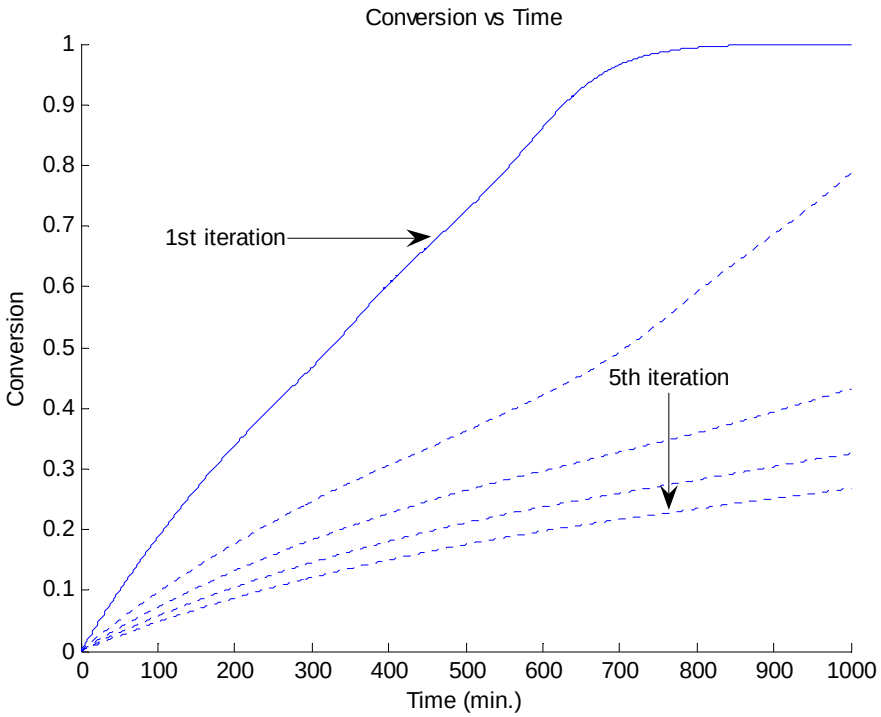

Figure 6.11: Simulation of composition control policy 2, Sty/BA at 60°C $[AIBN]_0 = 0.05M$

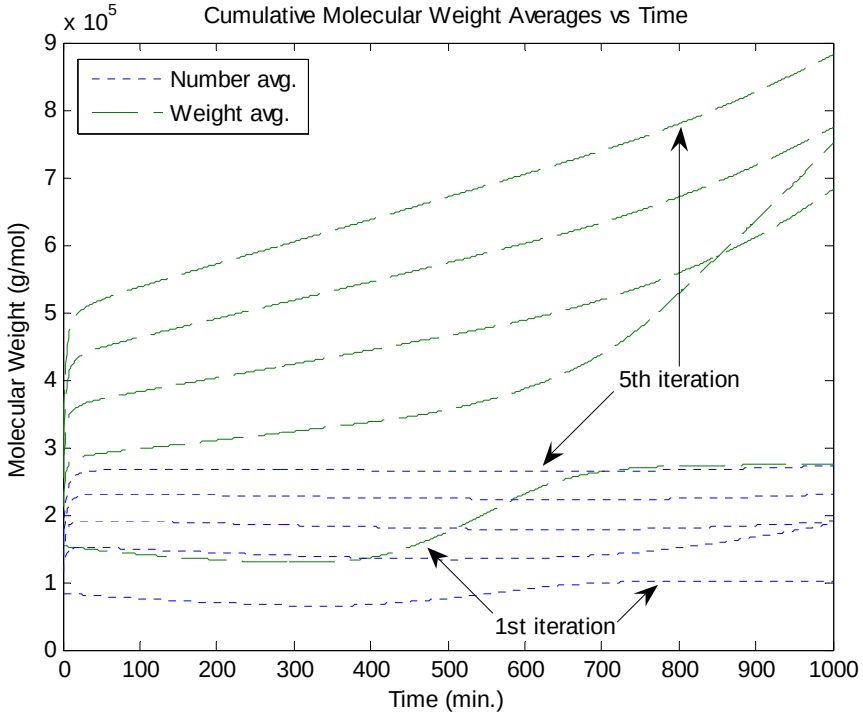

Figure 6.12: Simulation of composition control policy 2, Sty/BA at 60°C $[AIBN]_0 = 0.05M$

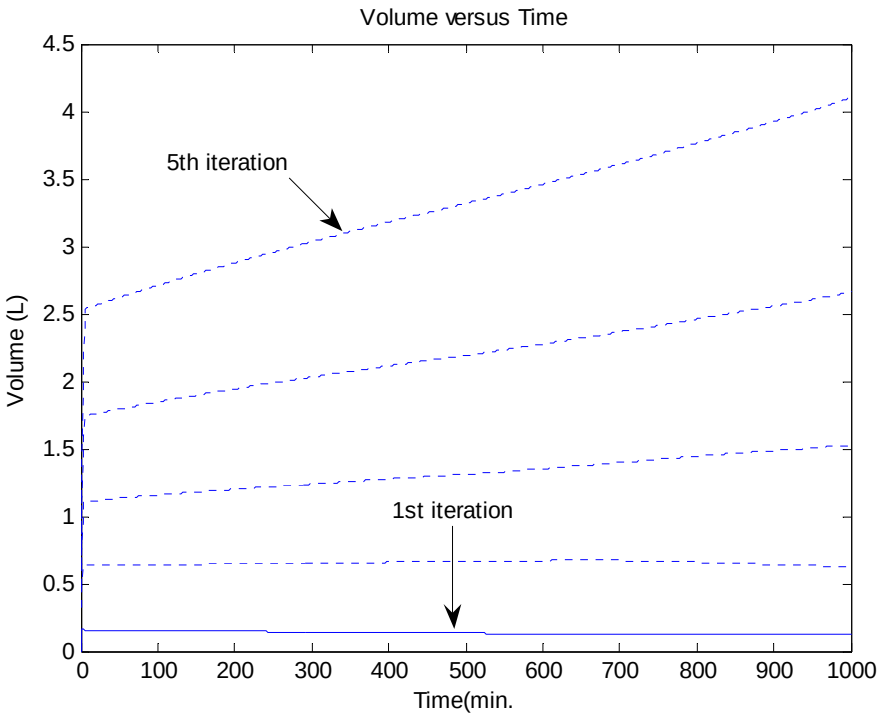

Figure 6.13: Simulation of composition control policy 2, Sty/BA at 60°C $[AIBN]_0 = 0.05M$

6.3. Policy 3

With policy 1 having such high conversion and relative low molecular weights and policy 2 having quite the opposite, it is not surprising that policy 3 falls in between the two on both accounts. As mentioned earlier, policy 3 can be seen as a special case of policy 2. Observe what happens to equations 6.39 and 6.40 when the (free) monomer concentration in the reactor is kept at very low levels (~0):

$$\frac{dN_1}{dt} \cong \frac{dN_2}{dt} \sim 0 \qquad 6.61.$$

A pretty obvious result indeed but it does have a major effect on the monomer flowrates:

$$\boldsymbol{F_{1,in} = R_{p1}V} \qquad 6.62.$$

$$\boldsymbol{F_{2,in} = R_{p2}V} \qquad 6.63.$$

And specific to policy 3, the instantaneous polymer composition if given by:

$$F_1 = \frac{R_{p1}}{R_{p1} + R_{p2}} = \frac{F_{1,in}}{F_{1,in} + F_{2,in}} \qquad 6.64.$$

As this is a starved feed polymerization, the monomers may be premixed, fed with one pump and at a constant rate, if desired. The rate at which the monomers may be fed depends on the reactor conditions. If the system is too "hot", more cooling will be required. As polymerization is exothermic, the temperature of the reactor is directly proportional to the monomer flowrate. The maximum productivity will be obtained by using lowest cooling water temperature available. The reaction temperature could then be controlled by manipulating the monomer feed flowrate. A cold monomer feed would also be quite beneficial. More discussion on practical implementations can be found in section 6.7.

The same recipe was followed for policy 3 as in policy 1 with the cumulative polymer composition seen in Figure 6.14. The final conversion reached was approximately 60%, directly in-between the other two policies (see Figure 6.15). The final molecular weight predictions in Figure 6.16 are comparable to the molecular weights found in policy 1. As always, variations occur from system to system but in general, policy 3 molecular weight predictions will be directly between policy 1 and 2. As evidence to that, the curves in policy 1 reach a plateau whereas the curves in policy 3 increase rather rapidly towards the end of the reaction. The five iterations required to achieve constant composition can be quite

confusing in Figure 6.17, Molar Flowrates of Monomers vs Time; as such, the final monomer flowrates only are presented in Figure 6.18.

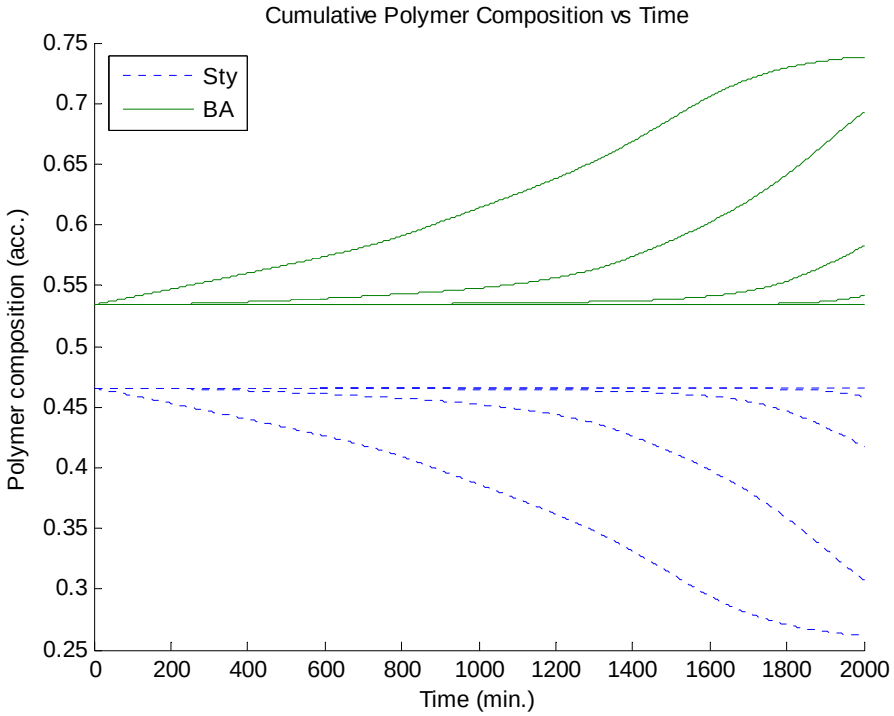

Figure 6.14: Simulation of composition control policy 3, Sty/BA at 50°C $[AIBN]_0$ = 0.05M

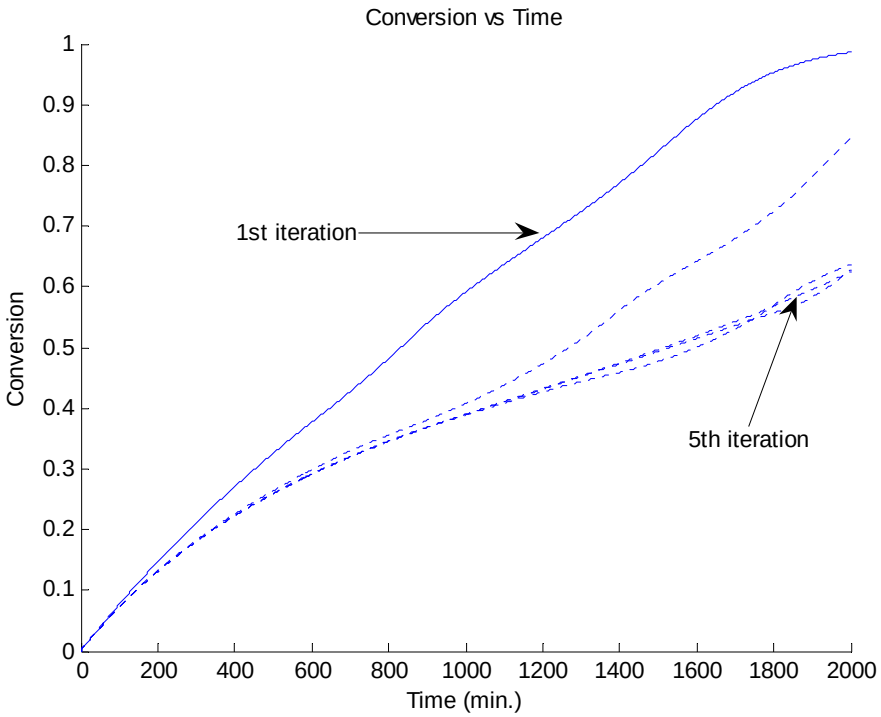

Figure 6.15: Simulation of composition control policy 3, Sty/BA at 50°C $[AIBN]_0 = 0.05M$

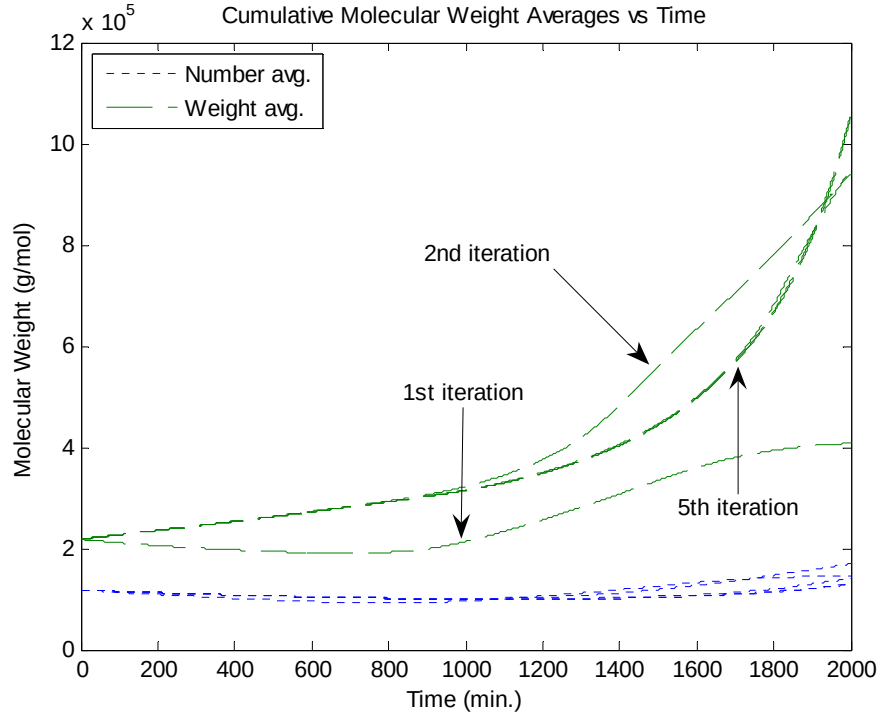

Figure 6.16: Simulation of composition control policy 3, Sty/BA at 50°C $[AIBN]_0 = 0.05M$

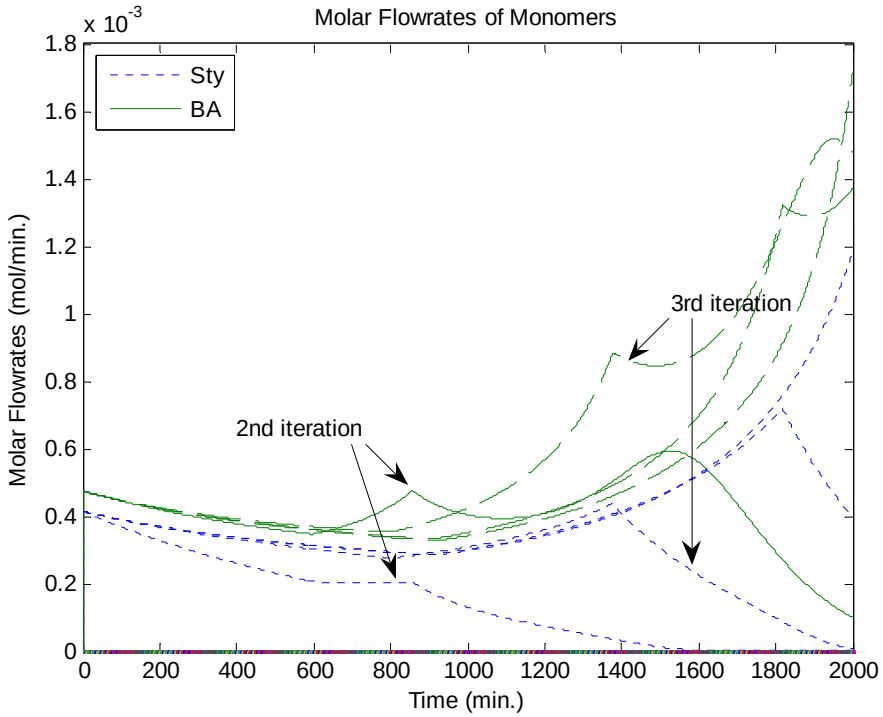

Figure 6.17: Simulation of composition control policy 3, Sty/BA at 50°C $[AIBN]_0 = 0.05M$

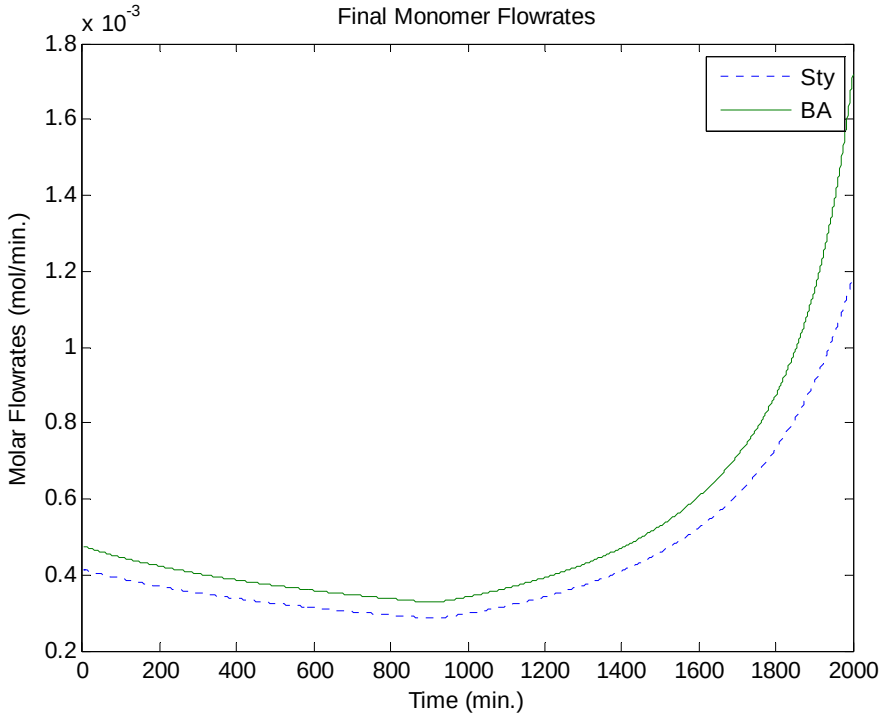

Figure 6.18: Simulation of composition control policy 3, Sty/BA at 50°C $[AIBN]_0 = 0.05M$

6.4. Combinations of Policies

The largest issue with some of the policies is the low final conversion. Specifically, policy 2 and 3 have been as low as 20% and 60%, respectively, which varies depending on the monomer system, recipe and operating conditions. The reaction can be stopped at any point but with such a low conversion, there will be a significant amount of monomers remaining in the reactor. In a co-polymerization, policy 1 is the ideal policy from an overall conversion standpoint. By combining policies, for example, using policy 2 and then finishing with policy 1, a higher final conversion can be reached than in using policy 2 alone. As both combinations of a policy 1 finish produce significant increases in the final conversion, only the combination of policy 2 and policy 1 is presented.

Six iterations were performed in the policy 2 phase in order to reach constant polymer composition. It then took four iterations using policy 1 to reach constant composition over both phases. The combination of the two policies increased the conversion from 20% to 75%; the drastic increase shown in Figure 6.19. With additional time, an even higher conversion can be reached. If time is becoming an issue, a temperature increase would significantly increase the rate of polymerization and speed up the reaction (decreasing time overall). This will be covered in more detail in section 6.6. The composition remains constant after the completion of both policies (Figure 6.20) by the semi-batch input of the monomers shown in Figure 6.21. Another issue with the large amount of monomers added from policy 2 is the high molecular weights of the chains: 4.5×10^6 g/mol. By adding CTA, the molecular weights can be substantially lowered (See Figure 6.22 and Figure 6.23).

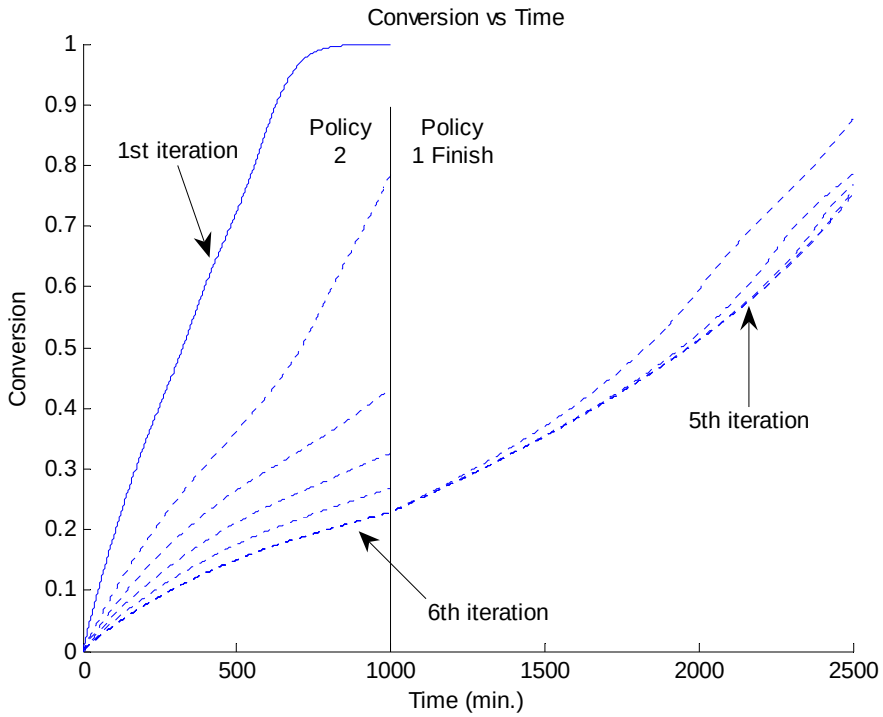

Figure 6.19: Simulation of composition control policy 2 with policy 1 finish, Sty/BA at 60°C $[AIBN]_0 = 0.05M$

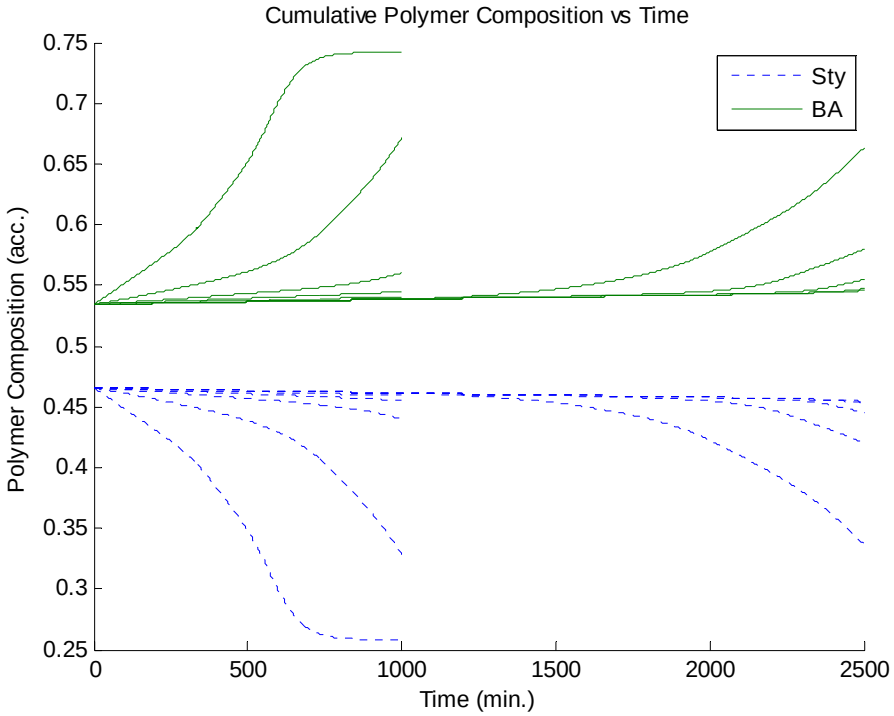

Figure 6.20: Simulation of composition control policy 2 with policy 1 finish, Sty/BA at 60°C $[AIBN]_0 = 0.05M$

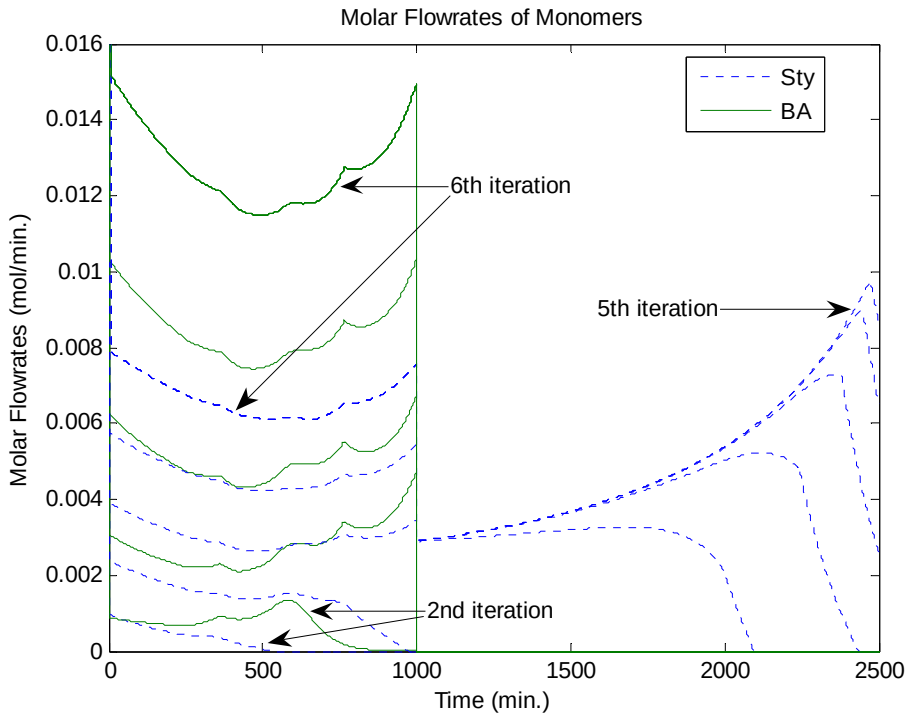

Figure 6.21: Simulation of composition control policy 2 with policy 1 finish, Sty/BA at 60°C $[AIBN]_0 = 0.05M$

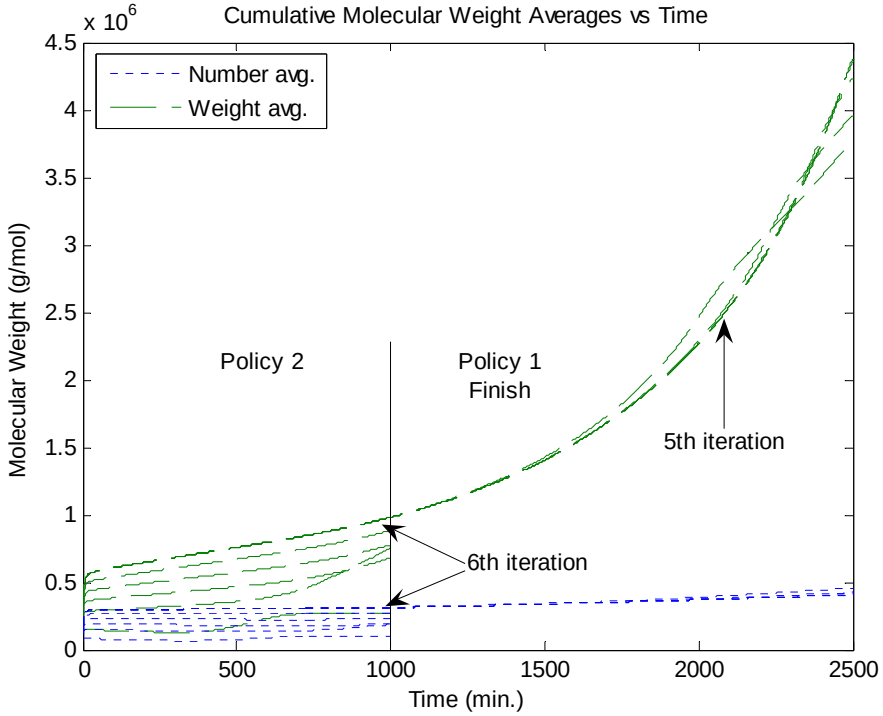

Figure 6.22: Simulation of composition control policy 2 with policy 1 finish, Sty/BA at 60°C $[AIBN]_0 = 0.05M$

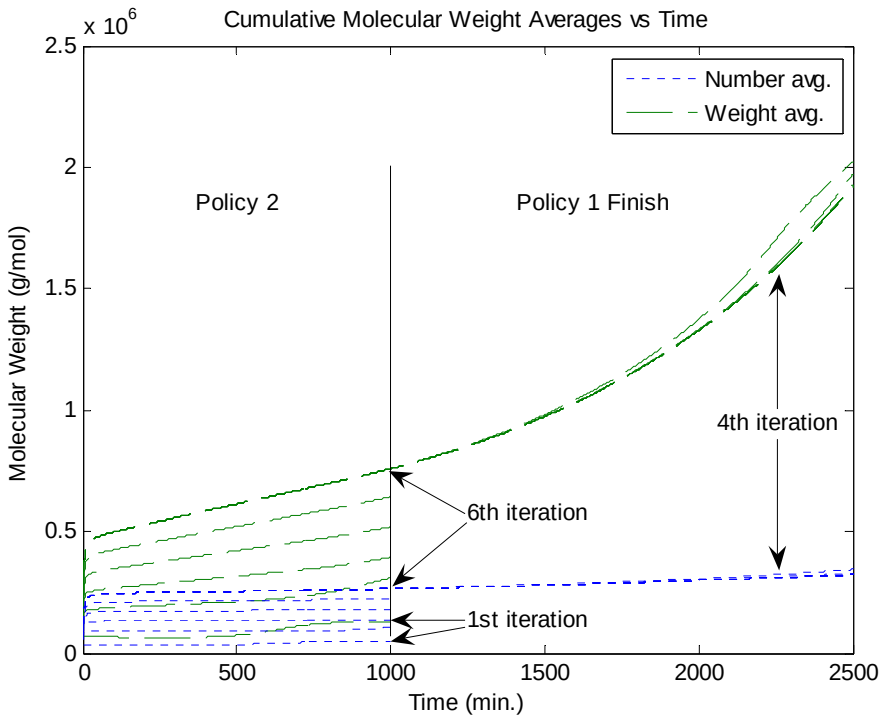

Figure 6.23: Simulation of composition control policy 2 with policy 1 finish, Sty/BA at 60°C $[AIBN]_0$ = 0.05M CTA = 0.3g

Improvement of policies 2 and 3 has been shown by combining them with policy 1 in order to consume the remaining monomers. However, policy 1, itself, does not reach complete conversion, whether in a combination with another policy or on its own. The conversion is at a quite high level though and a simple batch finishing step will not radically affect the polymer composition. A temperature increase at this point in the reaction, although not required, can help speed up the batch phase. Policy 1 with a batch finishing step was produced using a 40°C temperature increase over 120 minutes (see Figure 6.24). This batch portion ended very quickly reaching complete conversion in less than a tenth of the overall reaction time (Figure 6.25). No drastic changes to the cumulative polymer composition were observed, meaning that the finishing step, a strategy to react all the remaining free monomers from the system, was a success (Figure 6.26).

The effects of the batch finishing step can also be seen in the instantaneous monomer mole fractions (Figure 6.27) and the residual monomer concentrations (Figure 6.28); the mole fractions quickly converge to zero and unity whereas the residual monomer concentrations quickly approach zero. The flowrate used during for the entire simulation is shown in Figure 6.29. As explained before, the inlet monomer flowrate of styrene drops to zero once

the finishing step is implemented. Finally, a spike in molecular weight is observed as the reaction is allowed to go to completion; alternatively speaking, no more monomers are being incorporated into the reactor and all of the remaining (free) monomers can react with the radical chains already present (Figure 6.30).

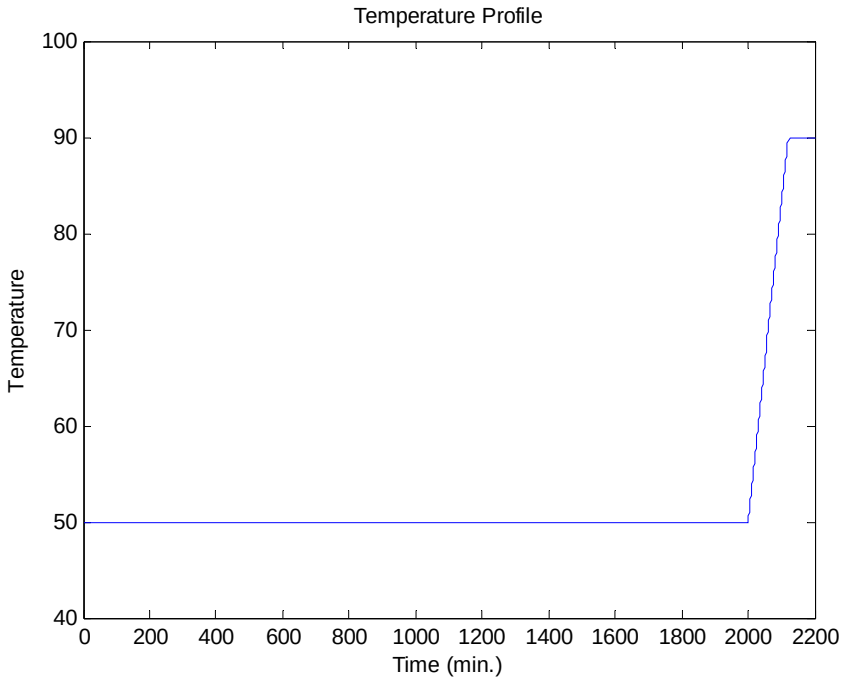

Figure 6.24: Simulation of composition control policy 1 with batch temperature finish, Sty/BA at 50°C $[AIBN]_0 = 0.05M$

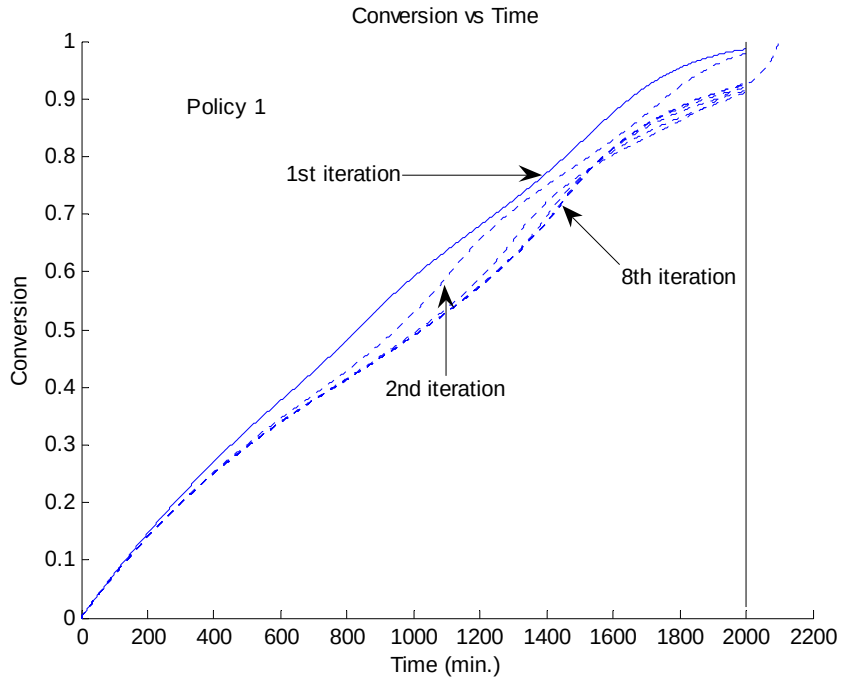

Figure 6.25: Simulation of composition control policy 1 with batch temperature finish, Sty/BA at 50°C $[AIBN]_0 = 0.05M$

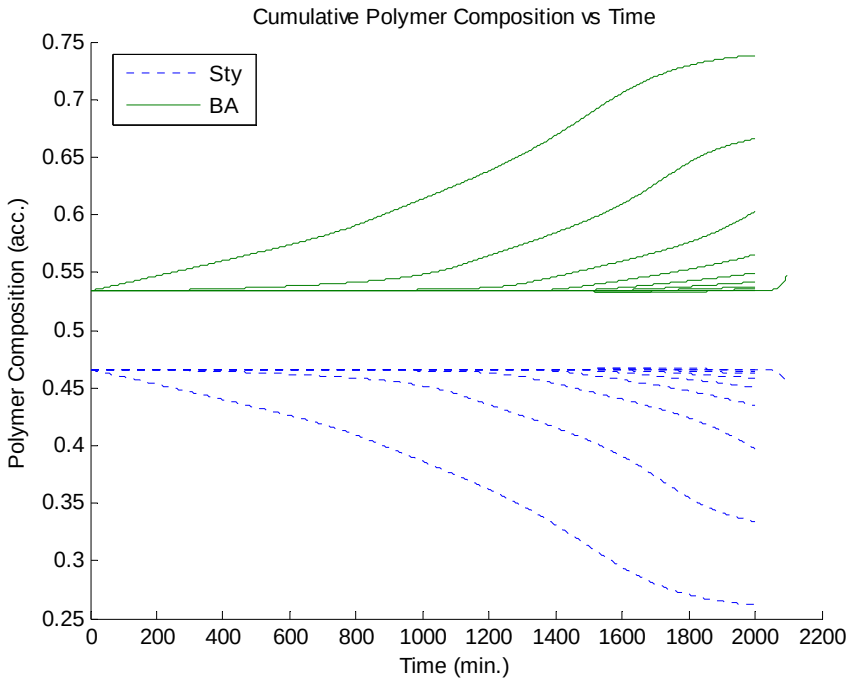

Figure 6.26: Simulation of composition control policy 1 with batch temperature finish, Sty/BA at 50°C $[AIBN]_0 = 0.05M$

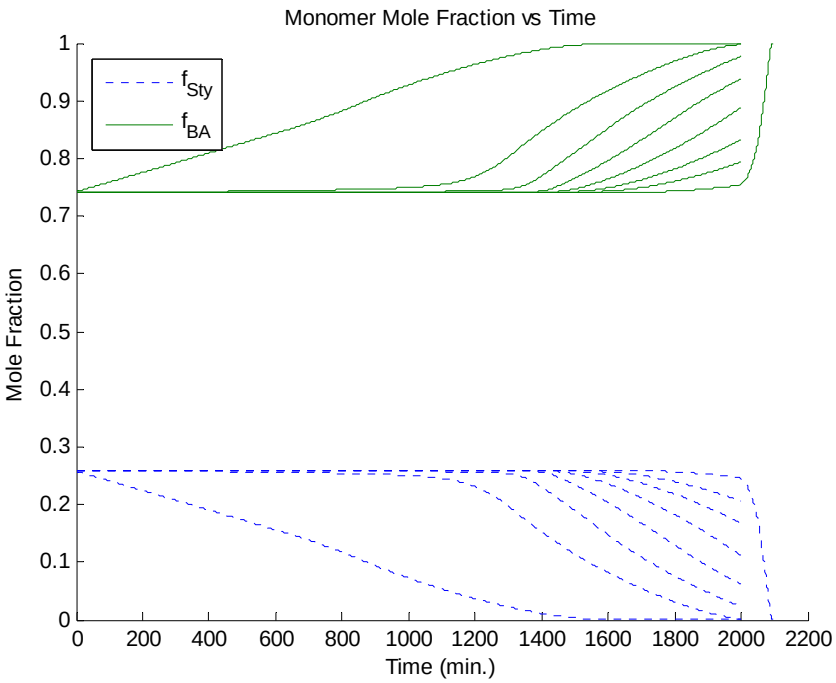

Figure 6.27: Simulation of composition control policy 1 with batch temperature finish, Sty/BA at 50°C $[AIBN]_0 = 0.05M$

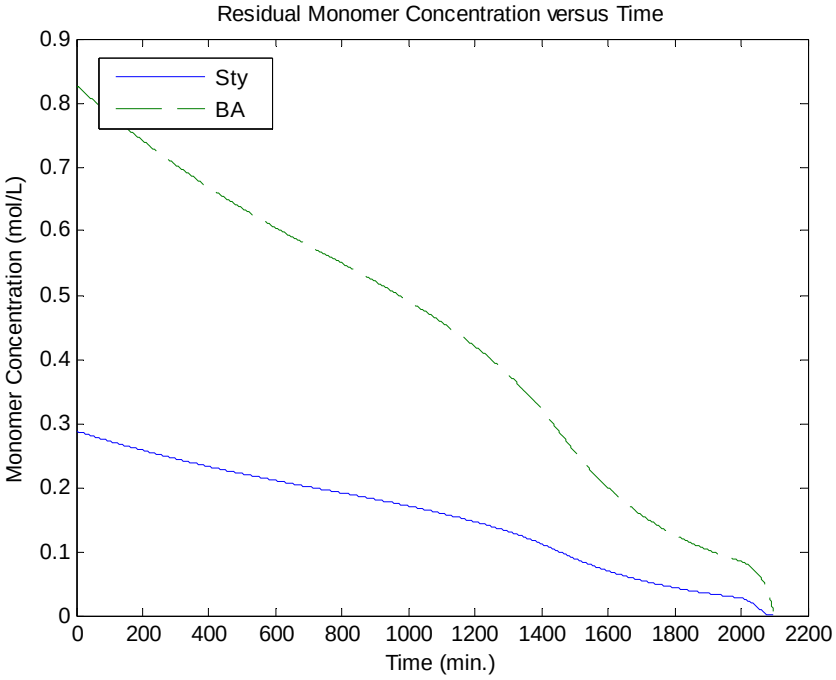

Figure 6.28: Simulation of composition control policy 1 with batch temperature finish, Sty/BA at 50°C $[AIBN]_0 = 0.05M$

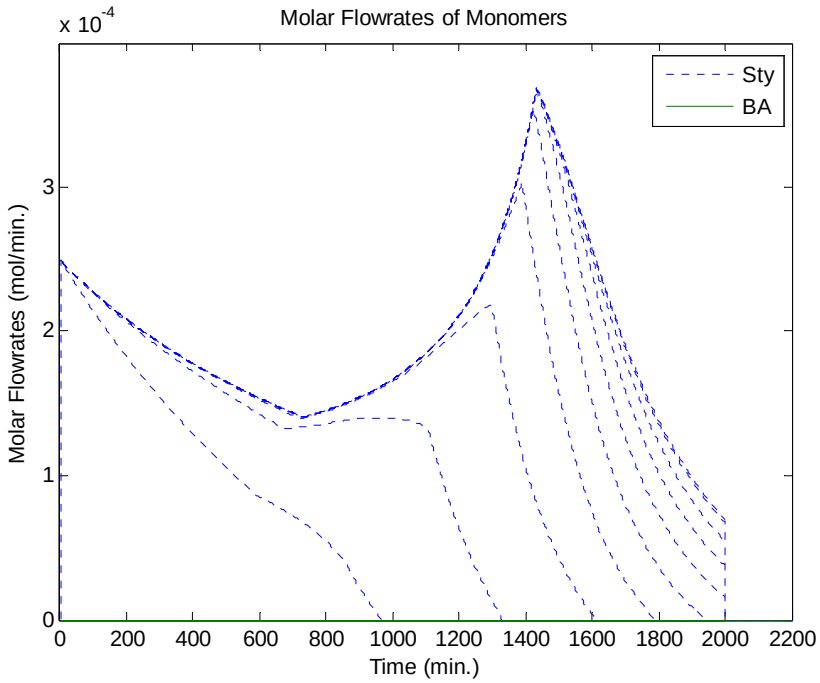

Figure 6.29: Simulation of composition control policy 1 with batch temperature finish, Sty/BA at 50°C $[AIBN]_0 = 0.05M$

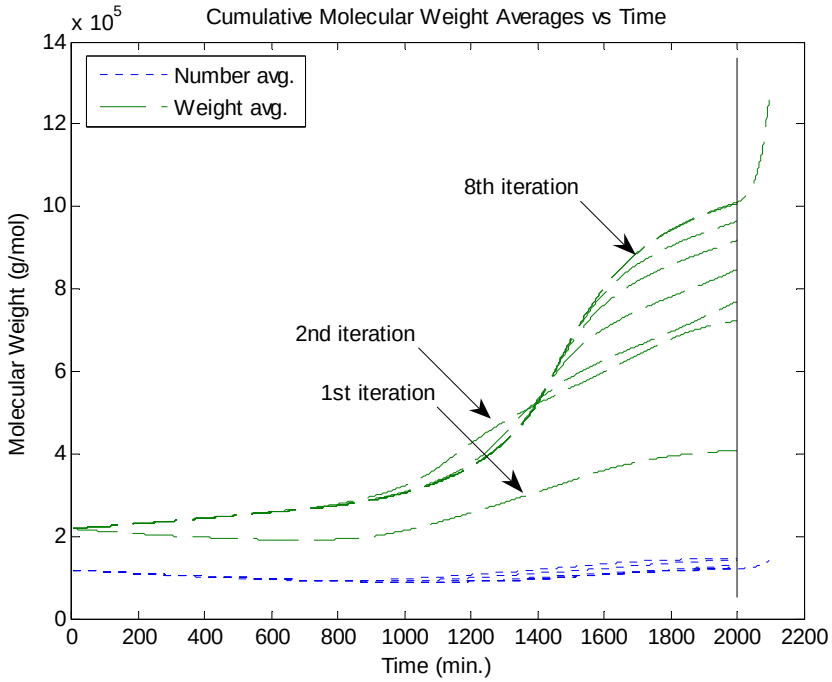

Figure 6.30: Simulation of composition control policy 1 with batch temperature finish, Sty/BA at 50°C $[AIBN]_0 = 0.05M$

6.5. Extensions to Multivariable Cases

Another ability of the model is to control polymer composition in ter- and tetra-polymerizations. The expansion to a five monomer system is straightforward but it is unnecessary at this point. Only two of the three policies could be extended, primarily because policy 1 requires a faster and a slower monomer. When there are more than two monomers present, there is no obvious choice; a grouping of 'slower monomers' and 'faster monomers' was attempted without much success. The basic equations for policy 2 and 3 tetra-polymerization are shown below:

$$\frac{dN_i}{dt} = [M_i]_0 \frac{dV}{dt} \qquad 6.65.$$

$$F_{i,in} = R_{pi} V \qquad 6.66.$$

Only tetra-polymerizations of styrene, BA, EA and BMA are presented here. The initial monomer mole fractions and reactivity ratios of each monomer pair are as follows: f_{Sty0} = 0.173, f_{BA0} = 0.281, f_{EA0} = 0.356, and f_{BMA0} = 0.190. 0.4% by weight of AIBN was initially charged into the reactor at 60°C. The reactivity ratios for these simulations can be found in Table 6-1:

Table 6-1: Reactivity Ratios Used for the Tetra-polymerization of Styrene, BA, EA and BMA

Reactivity Ratio		Source
$r_{Sty\text{-}BA}$	0.956	Gao and Penlidis (1998)
$r_{Sty\text{-}EA}$	0.717	Gao and Penlidis (1998)
$r_{Sty\text{-}BMA}$	0.61	Li *et al.* (2006)
$r_{BA\text{-}Sty}$	0.183	Gao and Penlidis (1998)
$r_{BA\text{-}EA}$	1	Gao and Penlidis (1998)
$r_{BA\text{-}BMA}$	0.29	Li *et al.* (2005)
$r_{EA\text{-}Sty}$	0.128	Gao and Penlidis (1998)
$r_{EA\text{-}BA}$	1	Gao and Penlidis (1998)
$r_{EA\text{-}BMA}$	0.22	Brandrup *et al.* (1999)
$r_{BMA\text{-}Sty}$	0.42	Li *et al.* (2006)
$r_{BMA\text{-}BA}$	1.93	Li *et al.* (2005)
$r_{BMA\text{-}EA}$	2.43	Brandrup *et al.* (1999)

Policy 2 required six iterations to remove the composition drift present in the batch case. As expected, a low conversion and high monomer flowrates occurred. Policy 3 achieved a higher conversion, nearly 80%, after seven iterations. A batch finishing step could be used to

consume the remaining monomers without much adverse effect to the polymer's quality. Observing Figure 6.31 and Figure 6.32, one can see that with two different policies, policy 3 having monomer flowrates one tenth the fraction of policy 2, an identical final result was achieved. Again, similar differences between the policies are found in the tetra-polymerization cases as well. The conversion achieved in policy 2 only reached 25% (Figure 6.33) whereas policy3 reached 75% (Figure 6.34). The monomer flowrates are a whole order of magnitude off of one another with the final flowrates found in policy 2 (Figure 6.35) being ten times as large as those determined in policy 3 (Figure 6.36). Naturally, the volume of each of the systems is also quite different; Figure 6.37 represents the volume of the reacting mixture in policy 2 and Figure 6.38 is the volume for the policy 3 system.

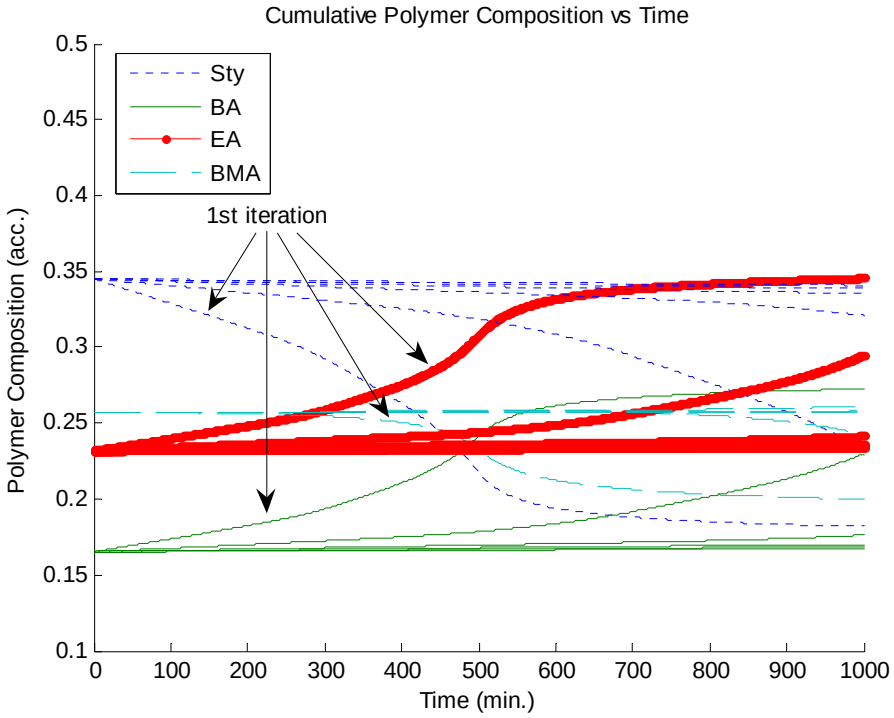

Figure 6.31: Simulation of composition control policy 2, Sty/BA/EA/BMA at 60°C $[AIBN]_0$ = 0.4 wt%

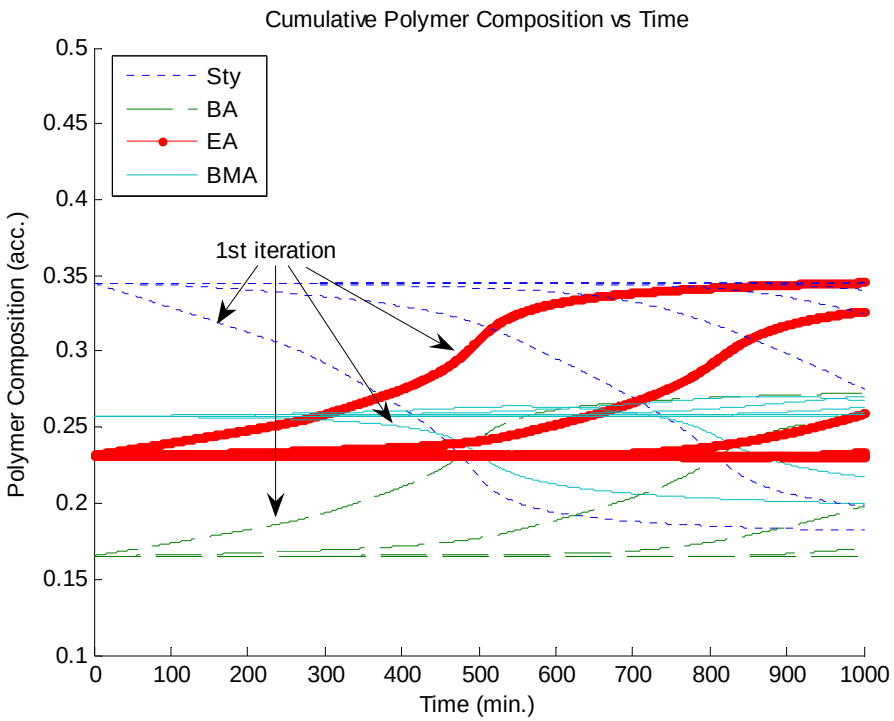

Figure 6.32: Simulation of composition control policy 3, Sty/BA/EA/BMA at 60°C $[AIBN]_0$ = 0.4 wt%

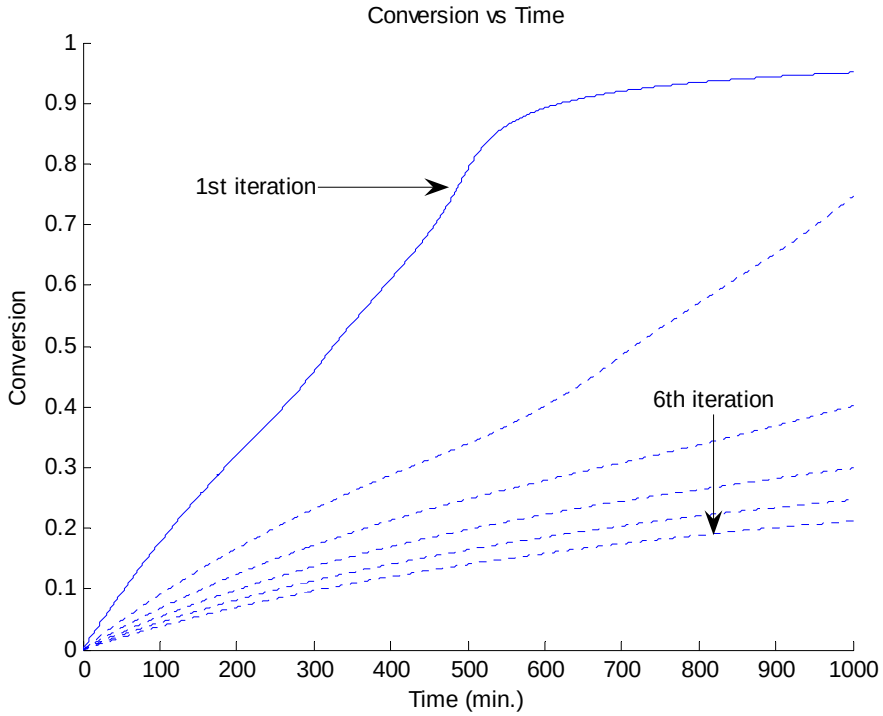

Figure 6.33: Simulation of composition control policy 2, Sty/BA/EA/BMA at 60°C $[AIBN]_0$ = 0.4 wt%

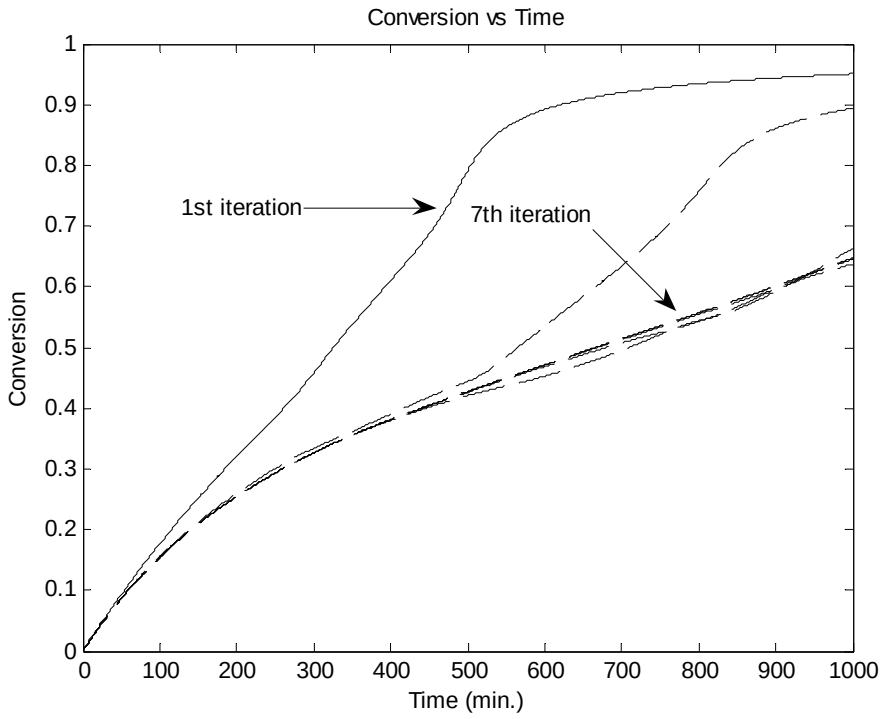

Figure 6.34: Simulation of composition control policy 3, Sty/BA/EA/BMA at 60°C $[AIBN]_0$ = 0.4 wt%

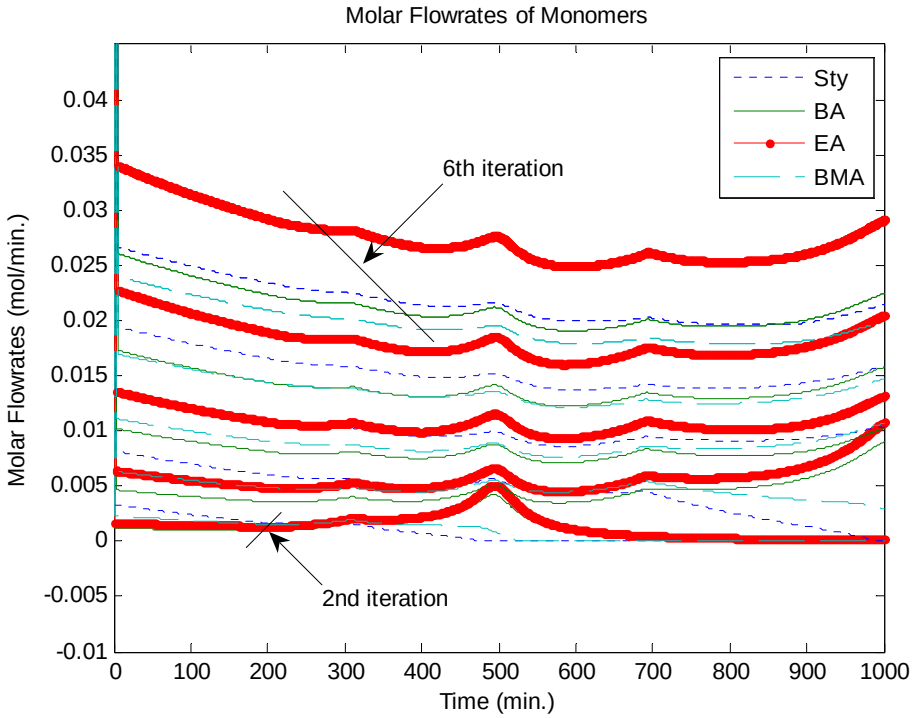

Figure 6.35: Simulation of composition control policy 2, Sty/BA/EA/BMA at 60°C $[AIBN]_0$ = 0.4 wt%

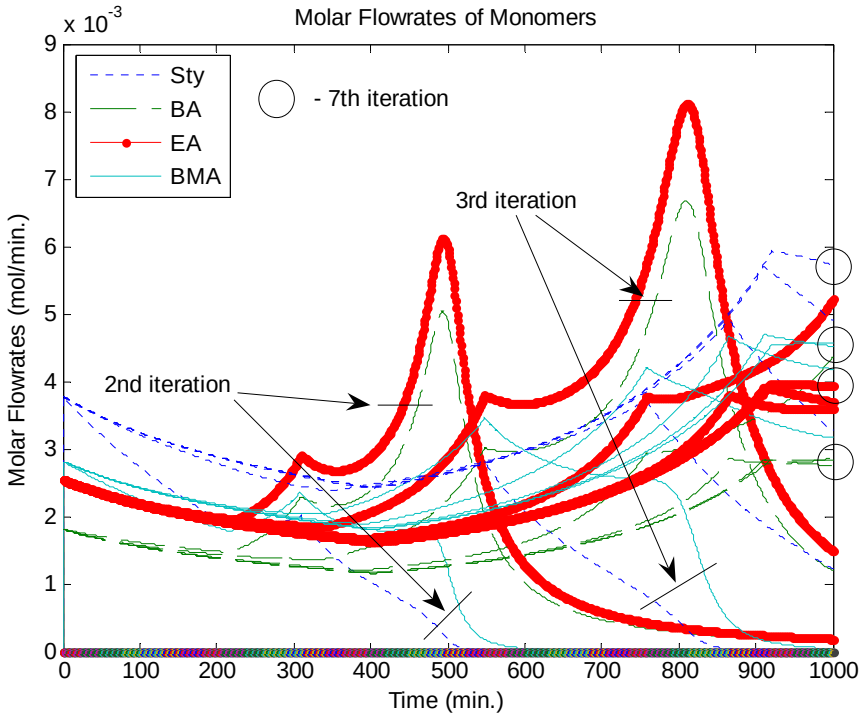

Figure 6.36: Simulation of composition control policy 3, Sty/BA/EA/BMA at 60°C $[AIBN]_0$ = 0.4 wt%

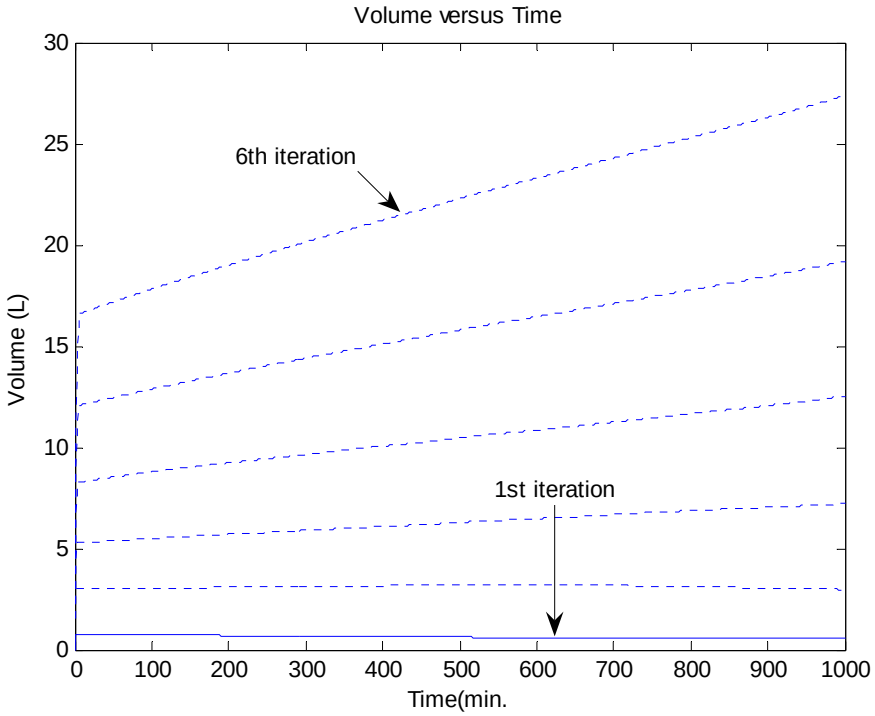

Figure 6.37: Simulation of composition control policy 2, Sty/BA/EA/BMA at 60°C $[AIBN]_0$ = 0.4 wt%

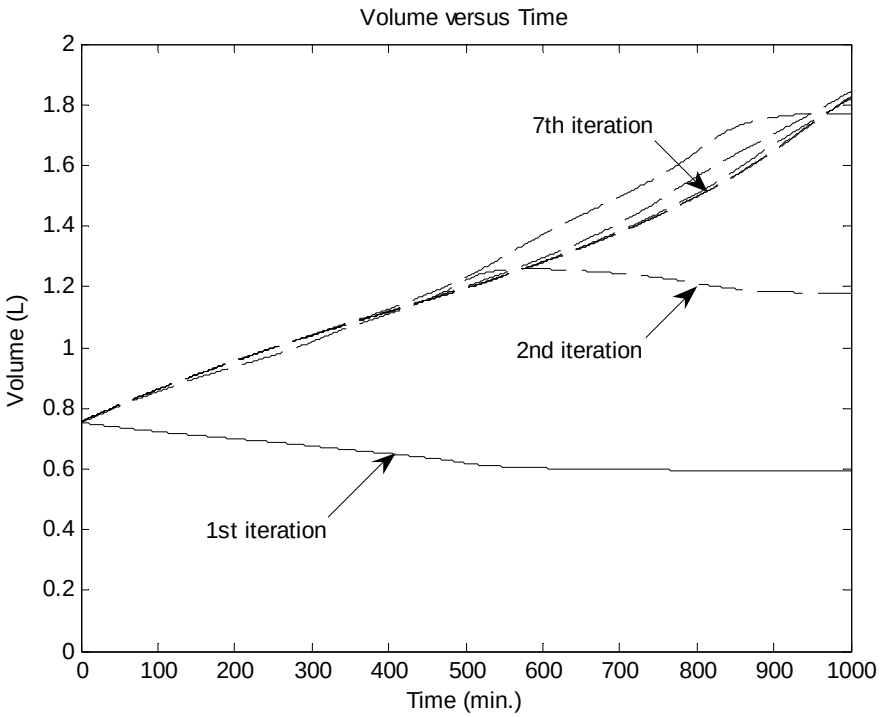

Figure 6.38: Simulation of composition control policy 3, Sty/BA/EA/BMA at 60°C $[AIBN]_0$ = 0.4 wt%

6.6. Additional Considerations/Remarks

There are many semi-batch feed policies that can be used to maintain constant co-polymer composition during polymerization. In general, these feed rates will vary with time. For practical considerations, it is of interest to know whether a co-polymer of small composition drift can be made when the two co-monomers are premixed and fed to the reactor (eliminating the need for two pumps), and also whether the premixed monomers can be fed at a constant flowrate (simplifying the reactor operation). The same questions could be asked about initiator feed rates. To maximize productivity, the choice of feed rate would be based on the heat removal capacity of the reactor. The choice of monomer concentration levels, however, would be dictated by the requirements for long chain branching and cross-linking, i.e., polymer quality. The most important consideration is practicality as some conditions like excessively high molecular weights are not feasible in reality.

Semi-batch policies are based on open-loop or off-line optimal feed rates to produce a co-polymer of constant composition. The on-line implementation, however, is related to on-line sensors and polymer reactor trajectory control. Practical implementation is discussed in section 6.7.

Quality is an important issue which differs from policy to policy. Policy 1 deals with high monomer concentrations initially as all of the slowest monomer is added at time zero. The volume of the reacting mixture is continuously increasing while the monomer concentrations are continuously decreasing. This concentration behaviour is similar to that in a batch reactor. Molecular weight and long chain branching development would therefore also be similar, with low levels of branching early in the polymerization and higher levels developing towards the end of the reaction. To minimize long chain branching, a batch or plug flow tubular reactor could be used.

Policy 2 is the only policy that is generally mentioned and implemented in the industry. This is counter-intuitive as each method has its own advantages and disadvantages, meaning no one policy is superior. The level of long chain branching and cross-linking with this policy will naturally depend on the monomer concentration levels. A common commercial practice is to maintain very low monomer concentrations so that the composition of the co-polymer produced is the same as the monomer composition in the feed. An advantage of this is that a premixed feed can be fed at a constant rate. Another advantage is that the reaction temperature can be controlled by changing the monomer feed rate. A higher feed rate would produce higher monomer concentrations, higher rate of polymerization and therefore increase the reaction temperature. This is of course assuming

that the cooling flowrate can maintain the temperature at these levels. A potential major disadvantage of this could be the very high level of long chain branching and cross-linking that results from low monomer concentrations in the reactor. Modifications to the policies that address these issues and allow for realistic implementation are discussed in section 6.7.

In all of the co-polymer composition control scenarios, styrene and butyl acrylate were the monomers selected. Different monomer systems have different reactivity ratios and therefore would react differently to control policies. The first alternative combination discussed is the co-polymerization of styrene and butyl methacrylate. These were selected because of their similar reactivity ratios: $r_{Sty\text{-}BMA} = 0.61$ and $r_{BMA\text{-}Sty} = 0.42$. The Mayo-Lewis co-polymer composition plot is shown in Figure 6.39. In this case, when styrene (monomer 1) is predominant, BMA will be the most reactive monomer. The opposite is true when styrene is less predominant. Policy 1 was executed twice for the initial styrene mole fraction of $f_{Sty0} = 0.13$ and $f_{Sty0} = 0.925$. The polymer composition results are shown in Figure 6.40 and Figure 6.41.

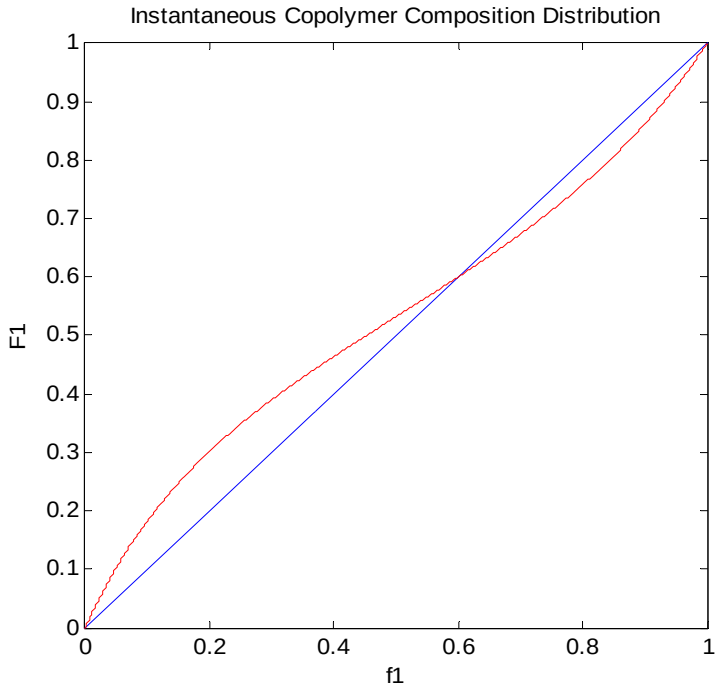

Figure 6.39: Mayo-Lewis co-polymer composition curve of styrene and butyl methacrylate

Not much composition drift was present in either simulation as the reactivity ratios are quite similar to each other. As such, more iterations were required but in the end, the composition control policy was effective nonetheless.

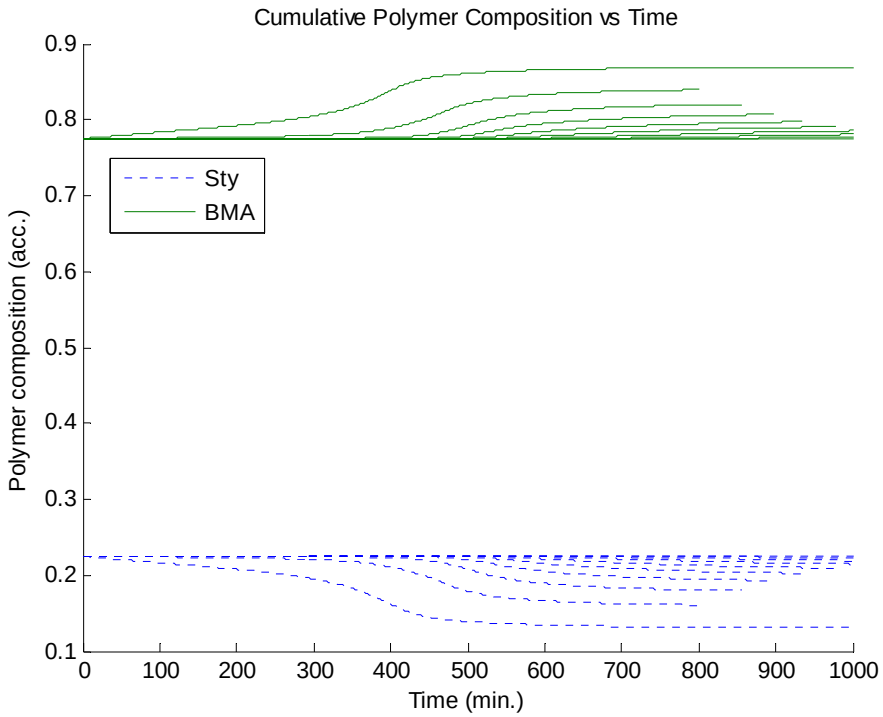

Figure 6.40: Simulation of composition control policy 1, Sty/BMA at 50°C $[AIBN]_0$ = 0.05M f_{Sty0} = 0.13

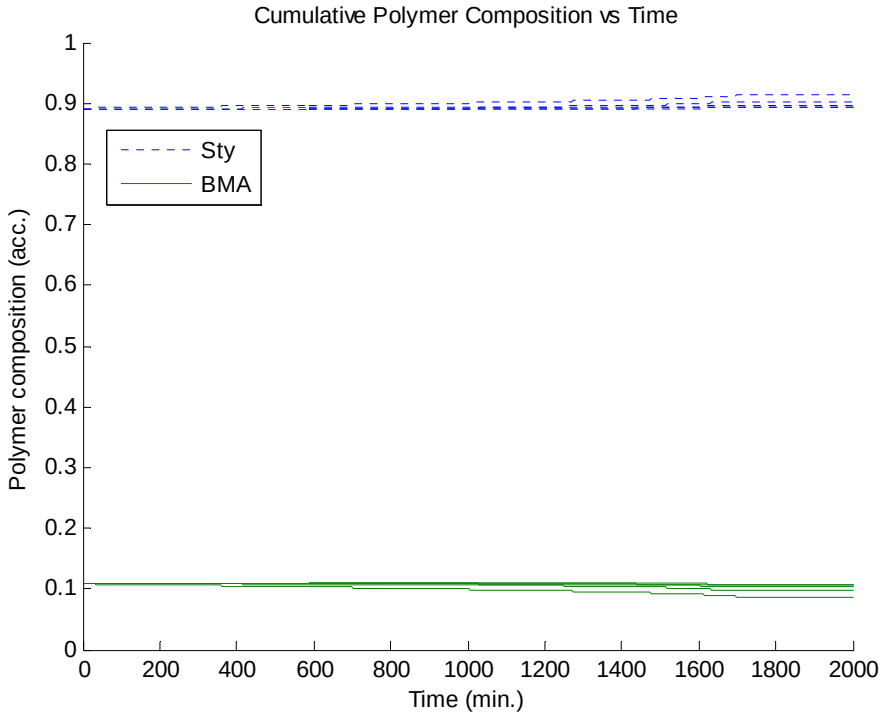

Figure 6.41: Simulation of composition control policy 1, Sty/BMA at 50°C $[AIBN]_0$ = 0.05M f_{Sty0} = 0.925

Another case that might arise is where one monomer is substantially more reactive than the other. Ethyl acrylate and butyl methacrylate is one such system. BMA is much more likely to react with the growing radical than EA regardless of the terminal monomer unit. The reactivity ratios used for this simulation come from Brandrup *et al.* (1999): $r_{EA\text{-}BMA} = 0.22$, $r_{BMA\text{-}EA} = 2.43$ (see Figure 6.42; EA refers to monomer 1). Policy 2 was used with an initial EA molar mole fraction of 0.26.

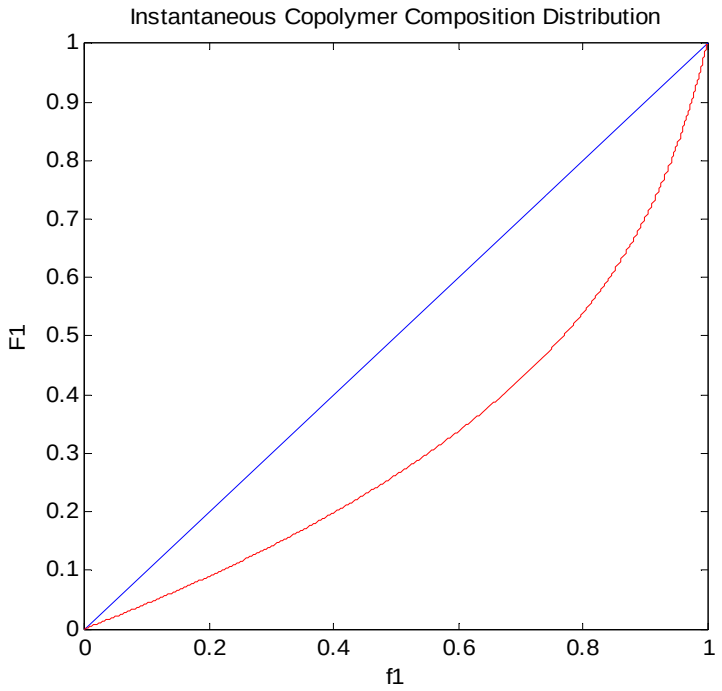

Figure 6.42: Mayo-Lewis co-polymer composition curve of ethyl acrylate and butyl methacrylate

Eight iterations using policy 2 were required in this case due to the increased complexity. With the reaction occuring at such a fast pace, large amounts of monomers were required to maintain the monomer concentration levels. As such, molecular weights shown in Figure 6.43 are at an extremely high level. The final conversion is slightly higher than the other policy 2 attempts, showing the variability that occurs with different monomer systems (Figure 6.44). Also, the monomer flowrates, shown in Figure 6.45, will create the constant polymer composition shown in Figure 6.46.

Even though only three different monomer recipes were shown in total, the model is versatile and can account for any combination of the monomers found in the database (see Appendix III or section 3.5 Database Characteristics), using either of the three composition control policies or a combination thereof.

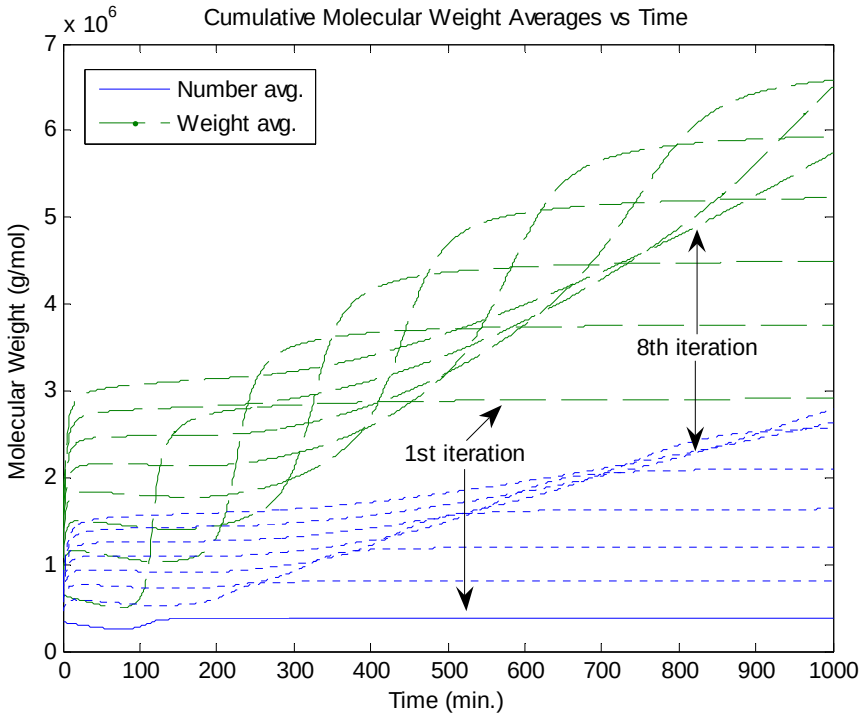

Figure 6.43: Simulation of composition control policy 2, EA/BMA at 60°C $[AIBN]_0 = 0.05M$ $f_{EA0} = 0.26$

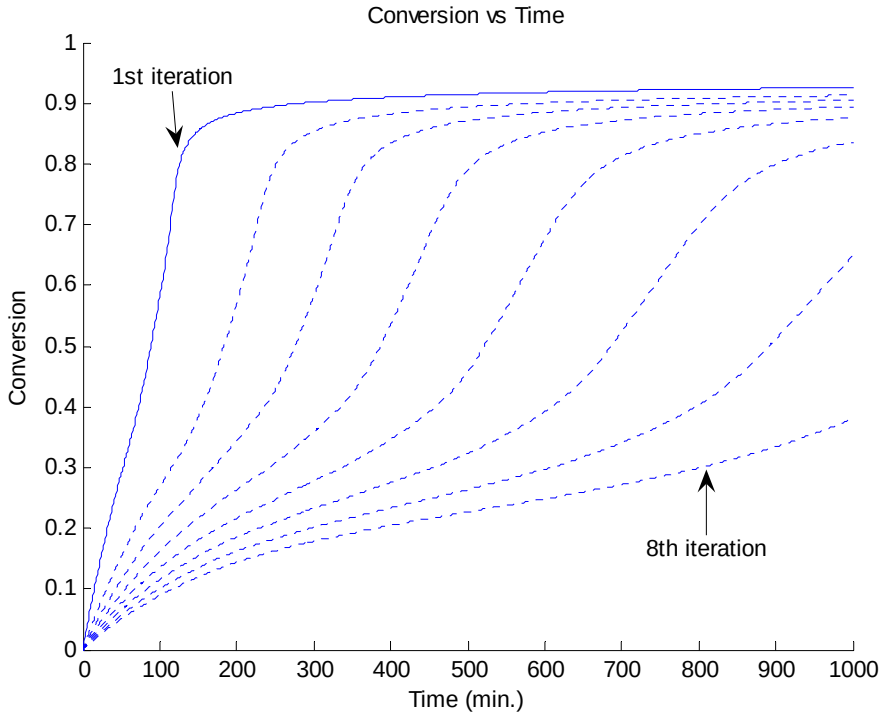

Figure 6.44: Simulation of composition control policy 2, EA/BMA at 60°C $[AIBN]_0 = 0.05M$ $f_{EA0} = 0.26$

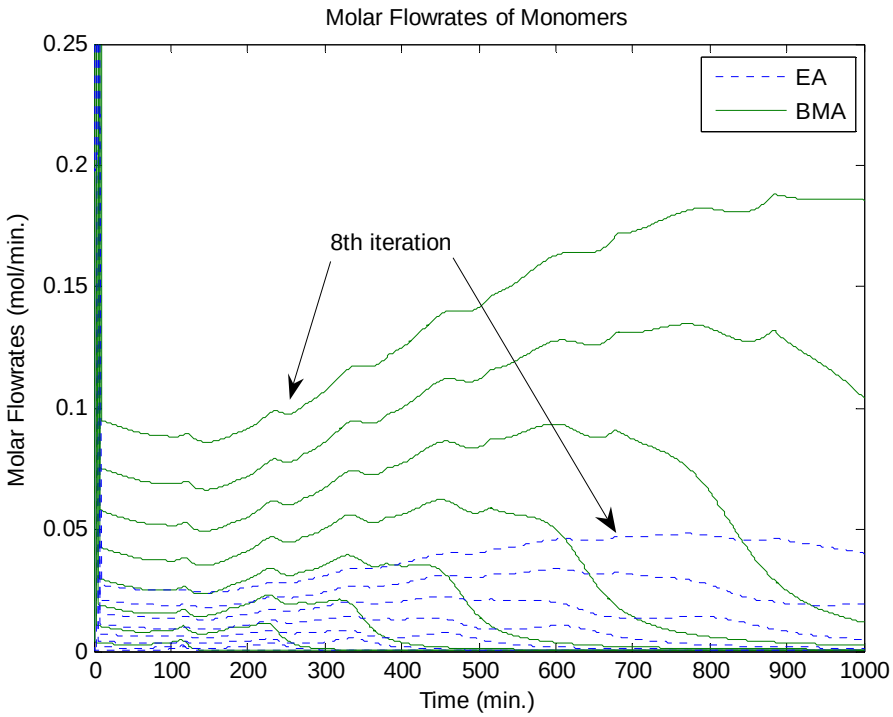

Figure 6.45: Simulation of composition control policy 2, EA/BMA at 60°C $[AIBN]_0 = 0.05M$ $f_{EA0} = 0.26$

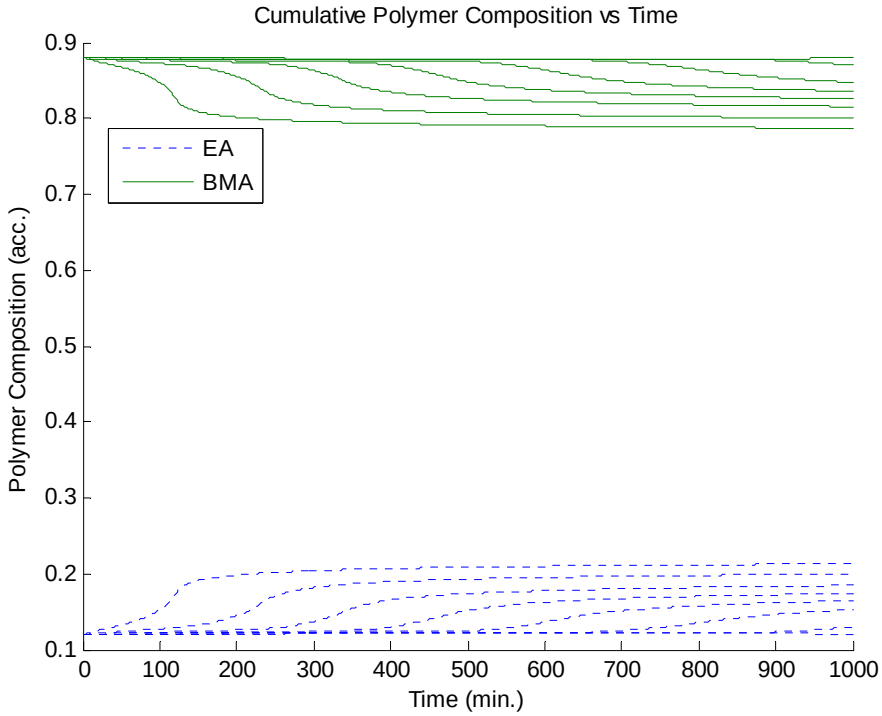

Figure 6.46: Simulation of composition control policy 2, EA/BMA at 60°C $[AIBN]_0 = 0.05M$ $f_{EA0} = 0.26$

Long chain branching and molecular weights have been discussed in the previous sections for several policies. Chain transfer agents have previously been shown to decrease the high molecular weights found in policy 2. The effect that a chain transfer agent has on long chain branching, also an issue in policy 2, is demonstrated below. Figure 6.47 shows the iterations of the average amount of tri-functional branches per chain versus time in a policy 2 simulation of styrene and BA without any CTA added. Figure 6.48, however, is the same simulation except with 1g of CTA added evenly over the 2000 minutes. The final amount of long chain branches was decreased by nearly 90% between the two polymerizations. This shows that both potential problems can simply be addressed by the use of CTA.

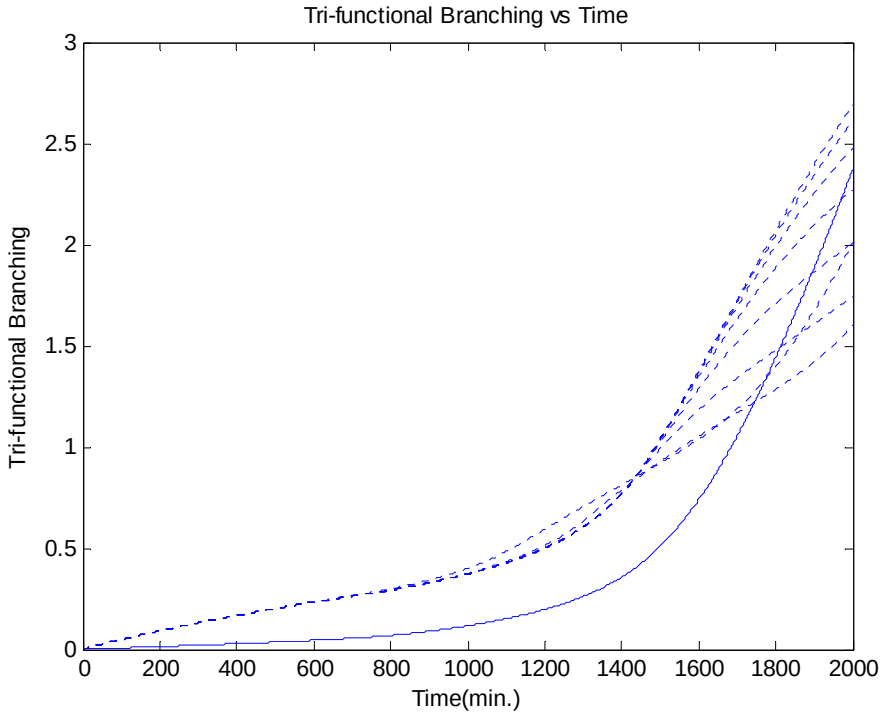

Figure 6.47: Simulation of composition control policy 2, Sty/BA at 50°C $[AIBN]_0 = 0.05M$

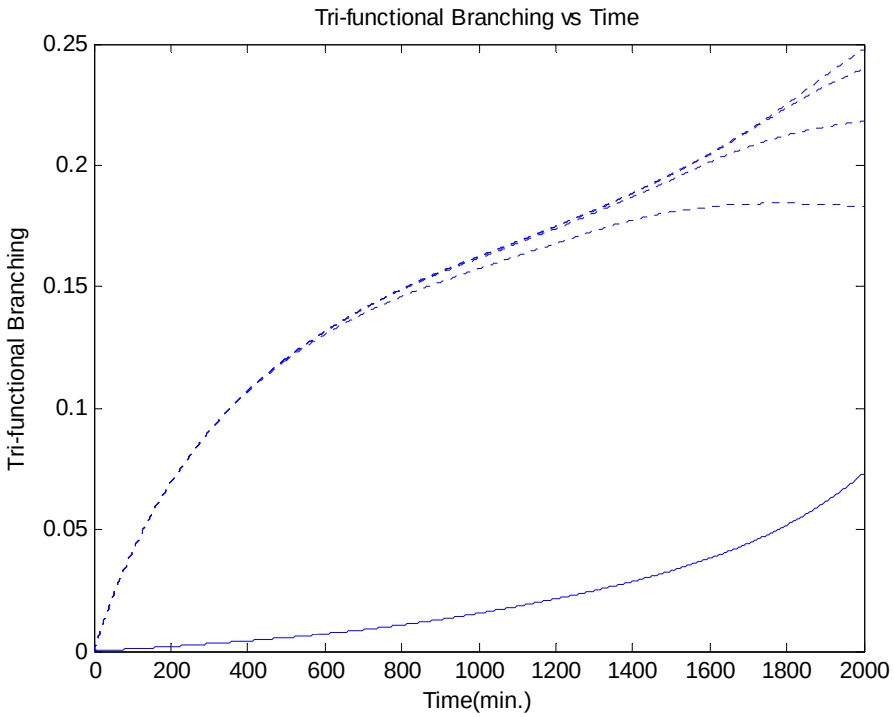

Figure 6.48: Simulation of composition control policy 2, Sty/BA at 50°C $[AIBN]_0$ = 0.05M CTA = 1g

When determining the reaction conditions, the desired monomer concentration plays a large role. In both policy 2 and policy 3, the monomer concentration remains constant. With a smaller monomer concentration, higher levels of polymer are present, increasing chain transfer, branching and potentially leading to a significant gel-effect. A larger monomer concentration is also not always advantageous (see Figure 6.49). P1 in Figure 6.49 is a stable operating point and P2 is an unstable operating point.

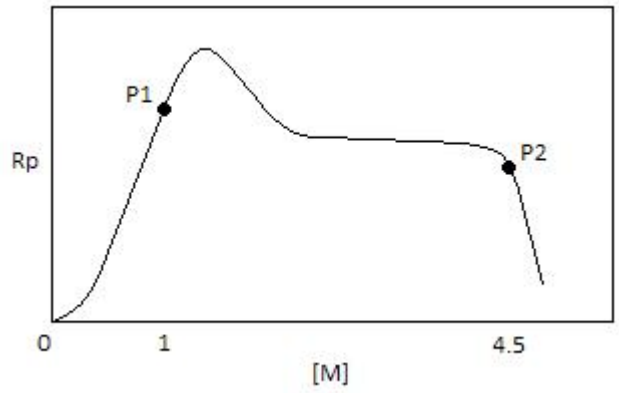

Figure 6.49: Semi-batch Co-polymerization Operating Conditions for Policy 2

Suppose there is a slight perturbation in the flowrate of the monomers to the reactor such that the monomer concentration increases beyond P1 (to the right). This immediately leads to an increase in the rate of polymerization, moving the concentration back to P1. A similar perturbation in the flowrate at P2 would lead to a decrease in Rp, moving the point yet further from its original monomer concentration. This inevitably leads to wide oscillations in the monomer concentration and gives unstable polymerizations with a potential deterioration in polymer quality. Careful consideration should be given when deciding the monomer concentrations to achieve the optimum operating condition.

A final concern that should be mentioned is the basic issue of whether the monomer flowrate solutions arrived at can actually produce uniform polymer chains. In other words, the final solution of the control policies might only work using the newly created iterative software; therefore, a simple (feasibility) test of simulating a manual flowrate similar to the final solution is required. The solution to a policy 3 simulation of styrene and BA is shown in Figure 6.50 with only the final monomer flowrates presented in the figure following, Figure 6.51. Figure 6.52 is a very basic manual attempt at the same (sub-optimal) flowrates with the polymer composition results in Figure 6.53. Very little composition drift is observed, verifying the solutions of the composition control policy and removing any concern that there might have been.

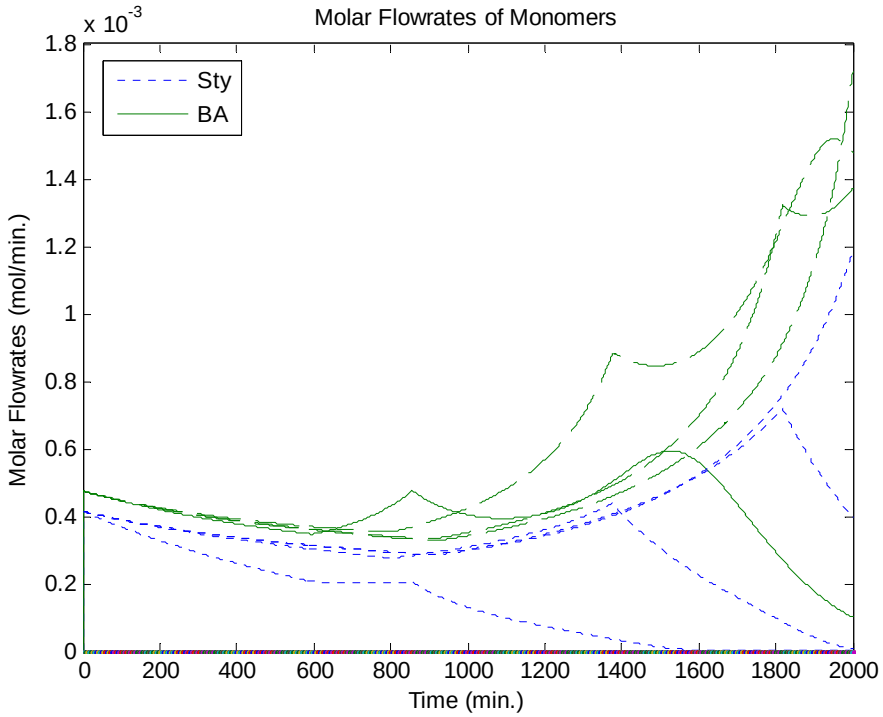

Figure 6.50: Simulation of composition control policy 3, Sty/BA at 50°C $[AIBN]_0 = 0.05M$

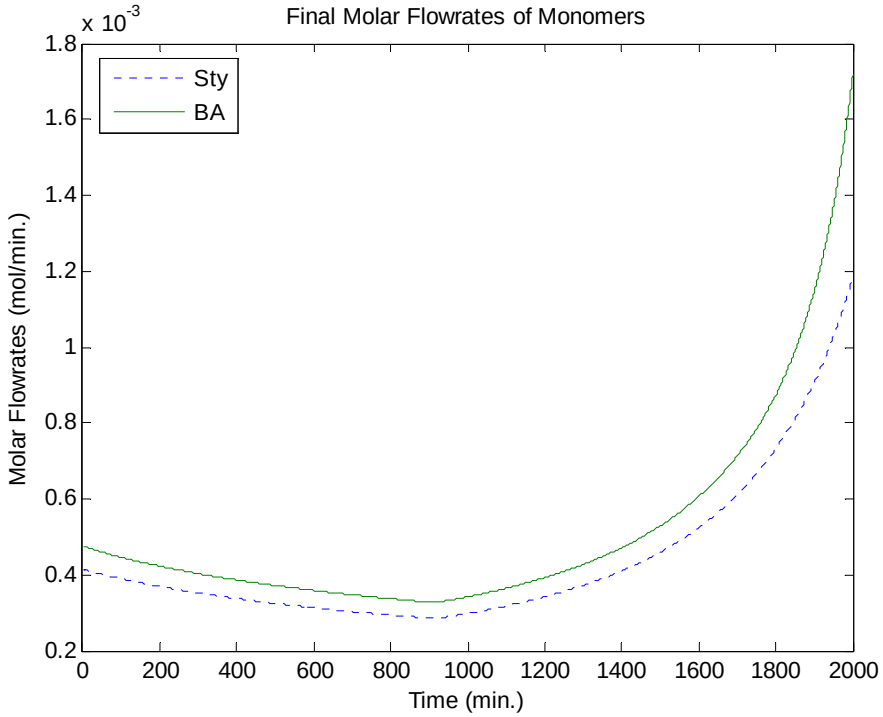

Figure 6.51: Simulation of composition control policy 3, Sty/BA at 50°C $[AIBN]_0 = 0.05M$

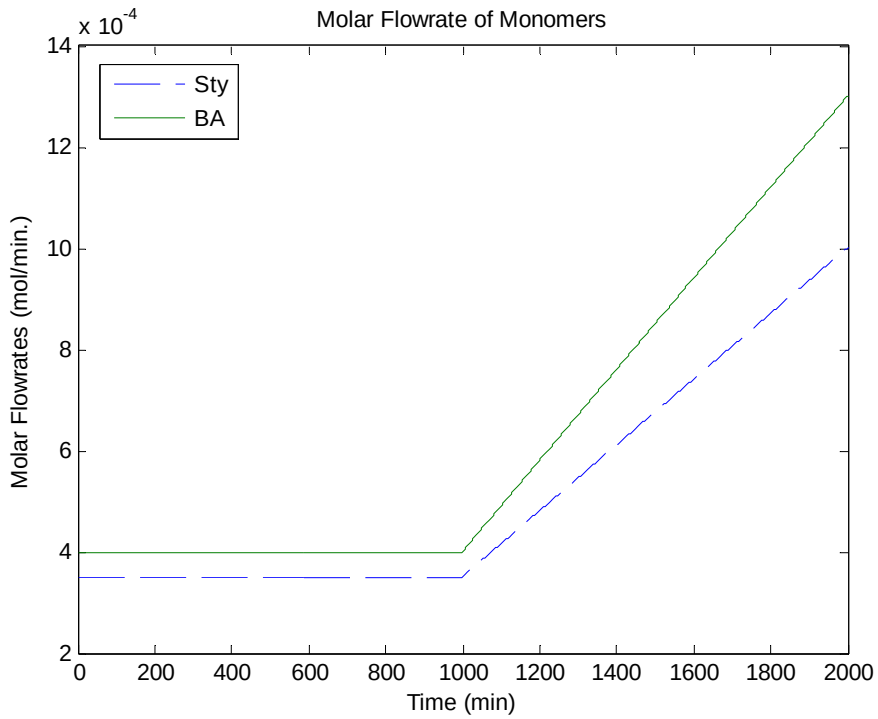

Figure 6.52: Manual simulation attempt for the co-polymerization of Sty/BA at 50°C $[AIBN]_0 = 0.05M$

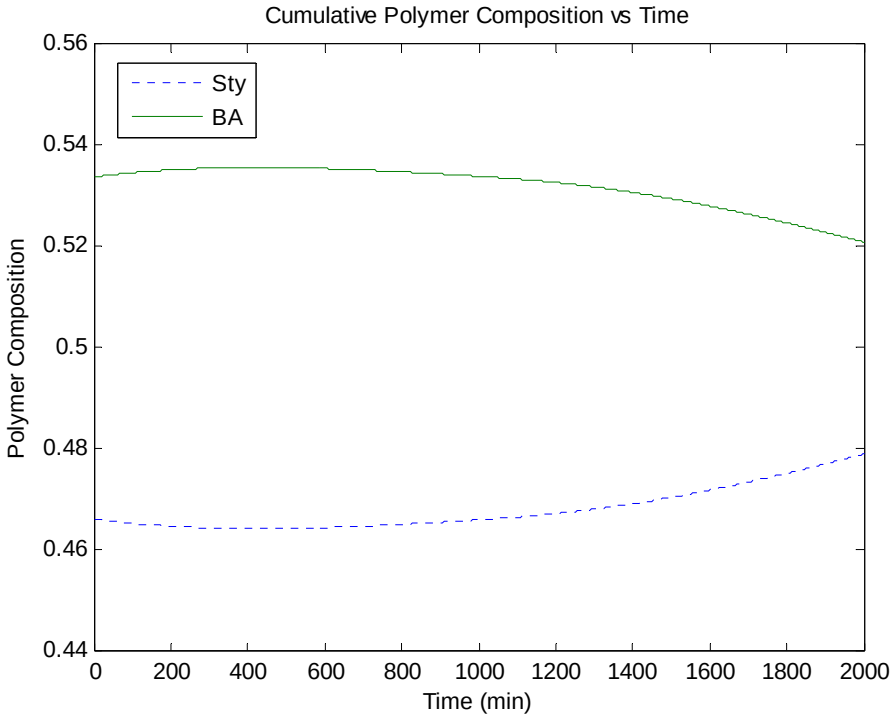

Figure 6.53: Manual simulation attempt for the co-polymerization of Sty/BA at 50°C $[AIBN]_0 = 0.05M$

6.7. Practical Implementations

Implementing these policies in an industrial setting comes with certain difficulties. Variable monomer flowrates require a pump for each monomer as well as for maintaining the reaction temperature. Also, disturbances in the feed will alter the polymer composition, requiring a control loop over the monomer flowrates. On-line polymer composition determination is unrealistic so another variable related to a change in polymer composition is required. Modifications of policies are presented below to solve these implementation issues.

6.7.1. Modified Policy 1

When $[R^*]$ is constant, N_1 decreases with time and $F_{1,in}$ increases slowly at first and then decreases with respect to time (see equation 6.34). By having $[R^*]$ increase with respect to time, a constant $F_{1,in}$ could be used to achieve the desired co-polymer with uniform composition. The bolding shown below is again used to highlight the implementation solution in an actual reactor.

$$\boldsymbol{F_{1,in} = N_1[R^*](\Phi_1 - \Phi_2)} \tag{6.30.}$$

Remember,

$$\frac{dN_1}{dt} = -N_1\Phi_2[R^*] \tag{6.32.}$$

If $\frac{dN_1}{dt} = -N_1\Phi_2[R^*] = -\Gamma_1$, then,

$$\frac{dN_2}{dt} = -N_2\Phi_2[R^*] = -\left(\frac{N_{2_0}}{N_{1_0}}\right)\Gamma_1 \tag{6.67.}$$

If Γ_1 is constant, then,

$$N_1 = N_{1_0} - \Gamma_1 t \tag{6.68.}$$

$$N_2 = N_{2_0} - \left(\frac{N_{2_0}}{N_{1_0}}\right)\Gamma_1 t = \left(\frac{N_{2_0}}{N_{1_0}}\right)(N_{1_0} - \Gamma_1 t) \tag{6.69.}$$

Let's consider now the instantaneous heat generation rate, $V\dot{Q}$:

$$V\dot{Q} = VR_{p1}(-\Delta H_{p1}) + VR_{p2}(-\Delta H_{p2}) \tag{6.70.}$$

$$= N_1\Phi_1[R^*](-\Delta H_{p1}) + N_2\Phi_2[R^*](-\Delta H_{p2}) \tag{6.71.}$$

$$= N_1 \Phi_2 [R^*] \left\{ \frac{\Phi_1}{\Phi_2} \left(-\Delta H_{p1} \right) + \left(\frac{N_{2_0}}{N_{1_0}} \right) \left(-\Delta H_{p2} \right) \right\} \qquad 6.72.$$

There are a couple of points that should be addressed about equation 6.72:

(i) Φ_2 and $\frac{\Phi_1}{\Phi_2}$ are weak functions of temperature

(ii) $\left(-\Delta H_{p1}\right)$ and $\left(-\Delta H_{p2}\right)$ are almost constant

(iii) $\left(\frac{N_{2_0}}{N_{1_0}}\right)$ is constant

Hence, as N_1 always decreases with respect to time, $\Phi_2[R^*]$ must increase in order to keep Γ_1 constant. If Γ_1 is constant, then $V\dot{Q}$ remains essentially constant. This means that a heat balance on the reactor can be used to track $V\dot{Q}$ and show whether Γ_1 is constant. Then,

$$\boldsymbol{F_{1,in} = N_1 [R^*] (\Phi_1 - \Phi_2)} \qquad 6.30.$$

$$= N_1 [R^*] \Phi_1 - \Gamma_1 \qquad 6.73.$$

$$= \Gamma_1 \left(\frac{\Phi_1}{\Phi_2} - 1 \right) \qquad 6.74.$$

Therefore, by controlling $V\dot{Q}$, both a constant monomer feed rate and constant polymer composition are achieved. Depending on the reactor set-up, there are two methods to manipulate $\Phi_2[R^*]$ such that $V\dot{Q}$ remains constant. Case I is non-isothermal polymerization and case II is an initiator flowrate.

Case I: All of the initiator is added to the reactor at time zero. In an isothermal polymerization, $\frac{dV}{dt} > 0$, and for low conversion levels (no diffusion-control), $[R^*]$ will fall with respect to time. Since Φ_1 and Φ_2 are constant, Γ_1 will also decrease with respect to time. In order to keep $F_{1,in}$ constant, one can let the reaction temperature increase with time. As the temperature increases, so do Φ_1 and Φ_2 and therefore Γ_1 as well. This will counteract the decrease in $[R^*]$ and maintain a constant monomer flowrate. The temperature is allowed to increase once a decrease in $V\dot{Q}$ is observed through the reactor energy balance. The increase in temperature required should, of course, not adversely affect polymer molecular weights.

Case II: Another way to keep $V\dot{Q}$ constant, and hence $F_{1,in}$ constant, when $[R^*]$ decreases with time, is to feed initiator in a semi-batch mode:

$$\frac{dN_I}{dt} = -k_d N_I + F_{I,in} \tag{6.75.}$$

$$[R^*] = \left(\frac{R_I}{k_t}\right)^{1/2} \tag{6.12.}$$

This case can be implemented when case I is undesirable, as it allows for isothermal polymerization. Once $V\dot{Q}$ begins to fall, an initiator feed would increase the rate of initiation and consequently increase the concentration of free radicals in the system. Both of these methods would allow for constant co-polymer composition throughout the reaction with a constant monomer flowrate.

6.7.2. Modified Policy 2

Policy 2 also has its advantages; as the monomer concentration is kept constant throughout, the rate of termination will remain more or less constant, even at high conversion. The modified policy 2 is also based around the reactor energy balance:

$$V\dot{Q} = VR_{p1}\left(-\Delta H_{p1}\right) + VR_{p2}\left(-\Delta H_{p2}\right) \tag{6.72.}$$

$$= \left\{[M_1]_0\Phi_1\left(-\Delta H_{p1}\right)V + [M_2]_0\Phi_2\left(-\Delta H_{p2}\right)V\right\}[R^*] \tag{6.76.}$$

Therefore, to maintain $V\dot{Q}$ constant, $[R^*]$ should be kept constant. As $[R^*]$ is a function of $[I]$ and k_t and k_t is relatively constant, the initiator concentration should remain constant.

$$\frac{d}{dt}\left(\frac{N_I}{V}\right) = 0 \tag{6.77.}$$

$$\frac{dN_I}{dt} = [I]_0 \frac{dV}{dt} \tag{6.78.}$$

Therefore,

$$F_{I,in} = [I]_0 \frac{dV}{dt} + k_d N_I \tag{6.79.}$$

Or,

$$\boldsymbol{F_{I,in} = [I]_0 \frac{dV}{dt} + k_d [I]_0 V} \tag{6.80.}$$

As the reaction proceeds and the volume increases, so should the initiator flowrate in order to keep $[I]$ constant and maintain a constant polymer composition. See Appendix V for a potential alternative solution for the initiator flowrate.

6.7.3. General Policy Considerations

In the previous semi-batch and modified semi-batch policies, $[R^*]$ was assumed constant or falling with respect to time. This is not realistic as the rate of termination falls drastically at high conversion in most cases causing $[R^*]$ to increase substantially. Also, $F_{1,in}$, in general, was a function of propagation rate constants, monomer concentration and $[R^*]$. Hence, in order to calculate the optimal monomer feed policy, $[R^*]$ must be specified in advance and kept at a specific constant value. This may be accomplished, as shown previously, through either an initiator feed policy or a heat production policy.

The practical implementation of monomer feed policies requires the use of on-line (and possibly off-line) measurements to be able to adjust for uncontrolled variations in recipe impurities. These impurities will affect the radical concentration and alter the polymer composition. If the monomer mole fraction was implemented as a function of conversion as opposed to time, and the conversion monitored on-line, it would help counteract the effects of disturbances and impurities in the flow.

Another method of counteracting impurities that affect $[R^*]$ is to maintain $\frac{V\dot{Q}}{F_{1,in}}$ constant. This is true for any composition control policy and offers a significant generalization of the strategies for composition control.

$$V\dot{Q} = N_1\Phi_1[R^*]\left(-\Delta H_{p1}\right) + N_2\Phi_2[R^*]\left(-\Delta H_{p2}\right) \qquad 6.71.$$

$$F_{1,in} = \left\{\frac{(\Phi_1 - \Phi_2)[R^*]}{1 - \lambda\left(\frac{N_1}{N_2}\right)}\right\} N_1 \qquad 6.81.$$

where $\lambda = \left(\frac{F_{2,in}}{F_{1,in}}\right)$.

Note, when $\lambda = 0$, equation 6.81 is identical to the monomer flowrate for policy 1 (see equation 6.30). Combining the two,

$$\frac{V\dot{Q}}{F_{1,in}} = \frac{\Phi_1(-\Delta H_{p1}) + \Phi_2(-\Delta H_{p2})\left(\frac{N_2}{N_1}\right)}{\frac{(\Phi_1 - \Phi_2)}{1 - \lambda\left(\frac{N_1}{N_2}\right)}} \qquad 6.82.$$

Equation 6.82 shows that to maintain $\left(\frac{N_1}{N_2}\right)$ constant for a single feed stream containing the monomers, one should keep $\frac{V\dot{Q}}{F_{1,in}}$ constant. So regardless of any impurities that affect $[R^*]$, the polymer composition will be uniform as long as the ratio of heat generation to monomer flowrate is kept constant (see Figure 6.54). Heat generation is directly proportional to rate of polymerization; which naturally depends on the amount of monomers in the system. Hence, without excessive analysis, one can see how this ratio, with some extra work, can be derived. The on-line measurement of $V\dot{Q}$ can thus be used to set the appropriate monomer feed rate. If the polymerization is too slow because of radical scavengers, the radical generation rate can be increased to compensate, and in parallel, the monomer flowrate can be increased to maintain the ratio $\frac{V\dot{Q}}{F_{1,in}}$ constant.

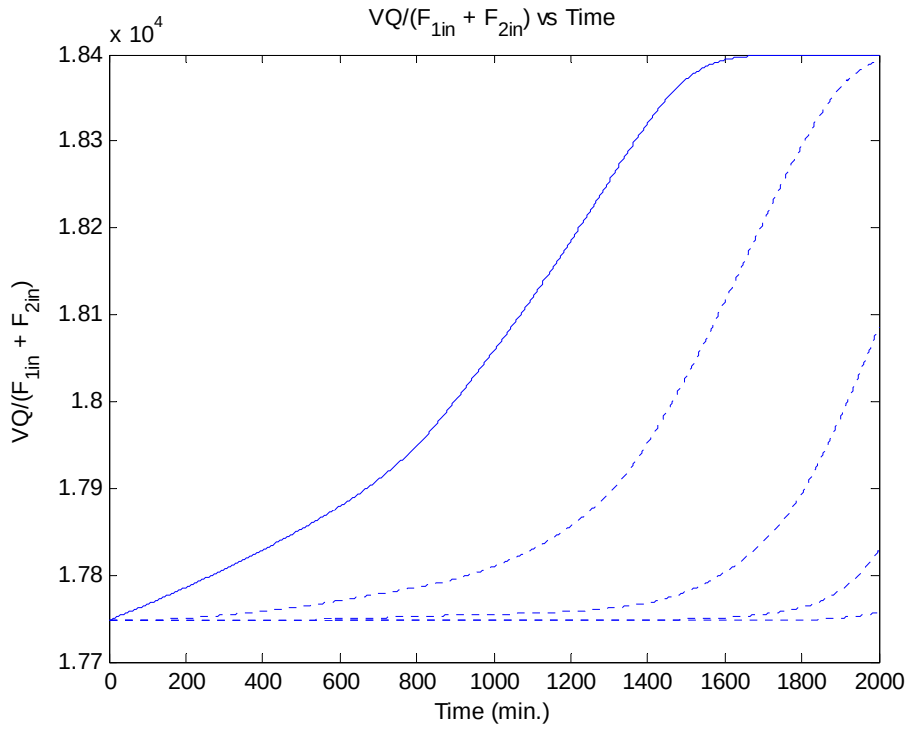

Figure 6.54: Simulation of composition control policy 3, Sty/BA at 50°C $[AIBN]_0$ = 0.05M

6.7.4. Monomer Flowrate Constraints

A concern upon implementing the ideal monomer flowrates is sensitivity. If there are constraints set by the pump capacity, reactor size, cooling ability or any other factor, it will have an effect on polymer composition.

A system with a large composition drift, EA and BMA, was simulated by policy 1 (see Figure 6.42). An initial EA mole fraction of 0.584 was chosen to further enhance the divergence. As a reminder, the reactivity ratios are $r_{EA\text{-}BMA} = 0.22$ and $r_{BMA\text{-}EA} = 2.43$ taken from Brandrup *et al.* (1999). The molar flowrates are presented in Figure 6.55. The massive composition drift attained in batch is highlighted in Figure 6.56, whereas Figure 6.57 shows the several iterations required to reach constant polymer composition. The reason the two figures show differences (as the batch simulation should be identical in both) is because Figure 6.57 is the cumulative polymer composition versus time and Figure 6.56 is versus conversion.

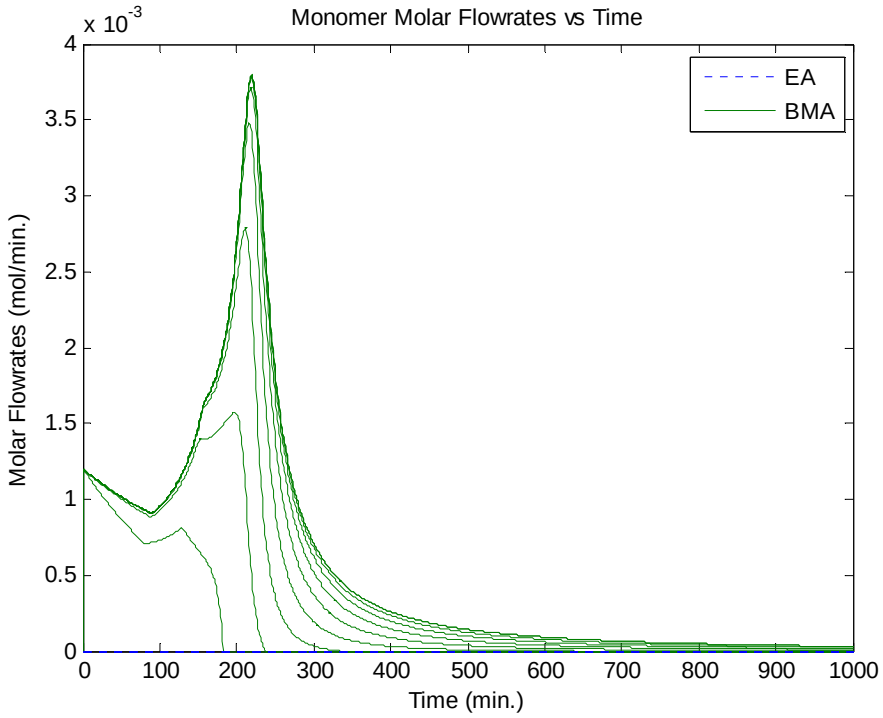

Figure 6.55: Simulation of composition control policy 1, EA/BMA at 60°C $[AIBN]_0 = 0.05M$

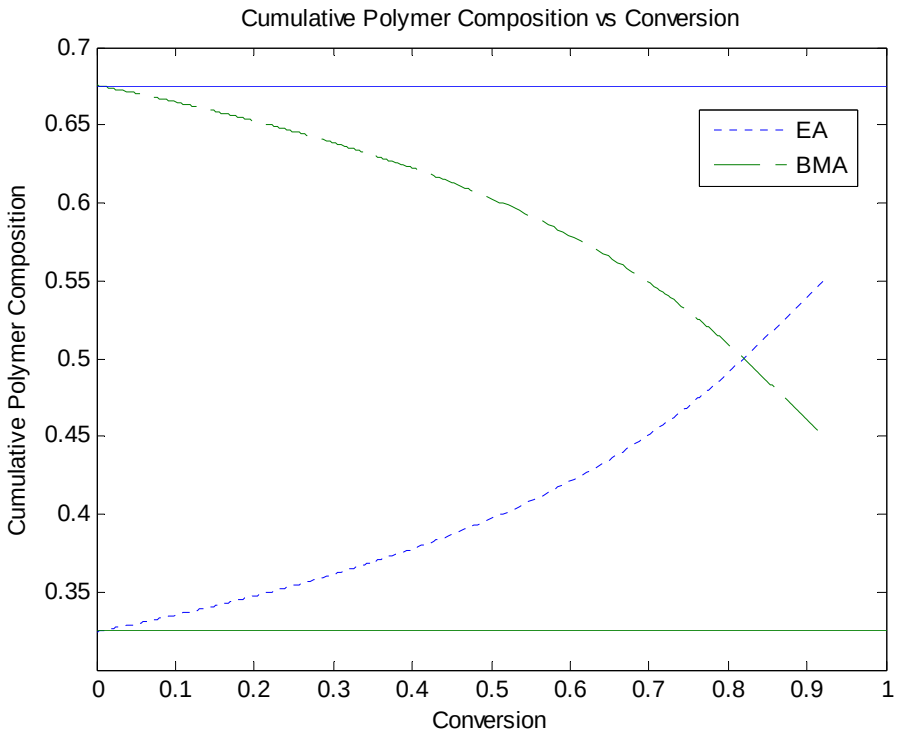

Figure 6.56: Simulation of composition control policy 1, EA/BMA at 60°C $[AIBN]_0 = 0.05M$

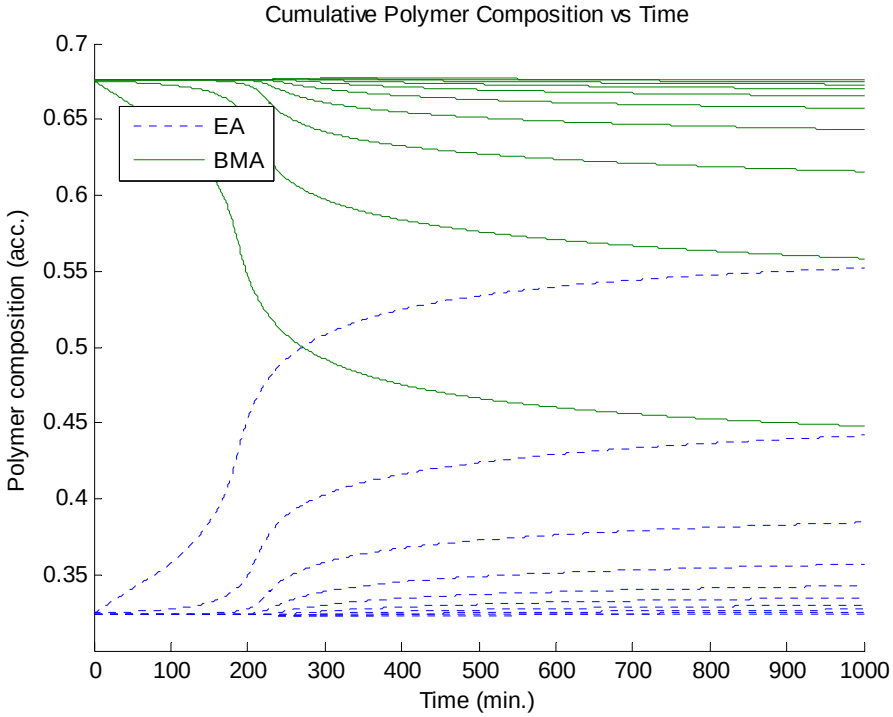

Figure 6.57: Simulation of composition control policy 1, EA/BMA at 60°C $[AIBN]_0 = 0.05M$

In order to overcome this drift, the monomer flowrate of BMA is presented in Figure 6.55. As proven in the previous section, we expect a crude manual representation to work with adequate accuracy. The sub-optimal flowrate chosen is presented in Figure 6.58 with the simulated polymer composition shown in Figure 6.59. The polymer composition remains relatively uniform even with the sub-optimal flowrate. The solid lines found in Figure 6.59 represent a constant polymer composition whereas the dashed lines represent the cumulative polymer composition attained when simulating with the sub-optimal flowrates shown.

With the same system, a maximum pumping constraint is then added to the ideal monomer flowrate, observed in Figure 6.60. Again, very little composition drift occurs (see Figure 6.61). Several other options using the same constraint are explored in Figure 6.62 through Figure 6.65, each with similar success. Sub-optimal flowrates, only slightly similar to the original proposed solution, work exceptionally well and remove almost all of the drift attained in a batch co-polymerization.

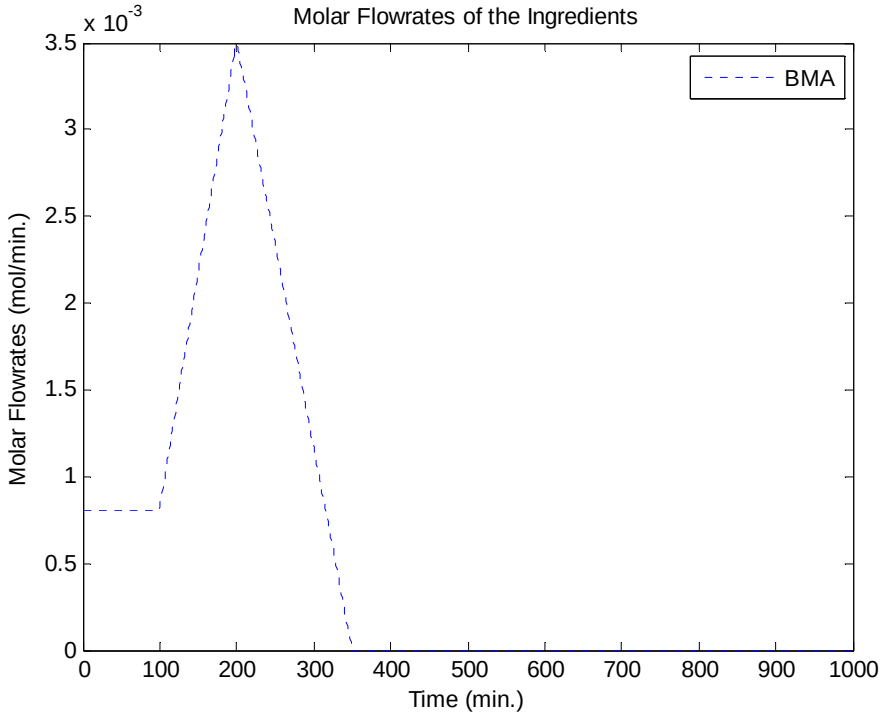

Figure 6.58: Simulation of the sub-optimal monomer flowrate used in the co-polymerization of EA/BMA

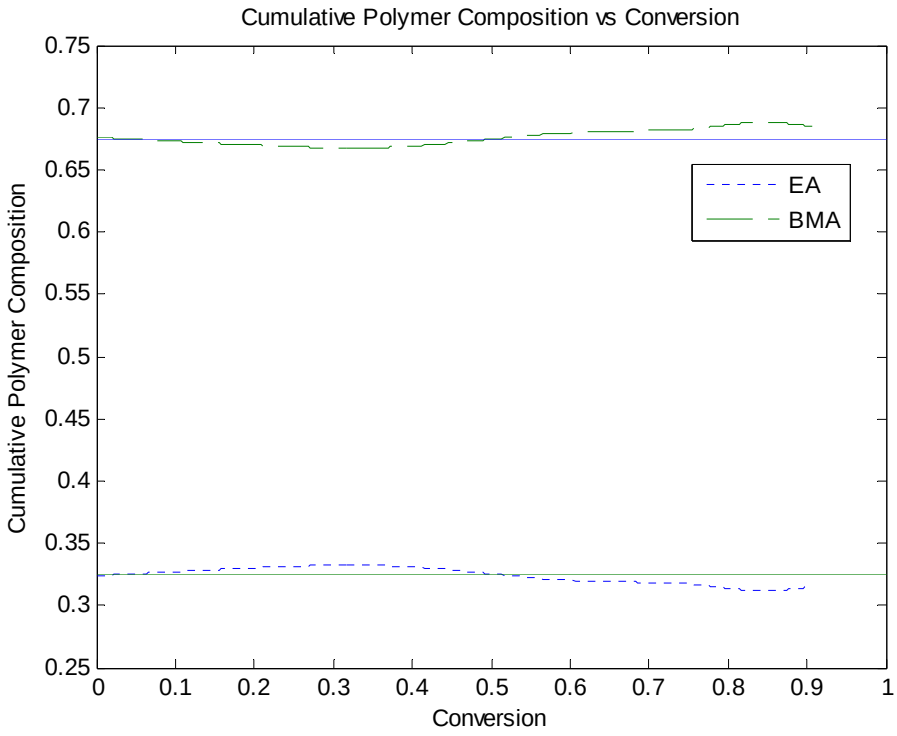

Figure 6.59: Simulation of the sub-optimal monomer flowrate used in the co-polymerization of EA/BMA

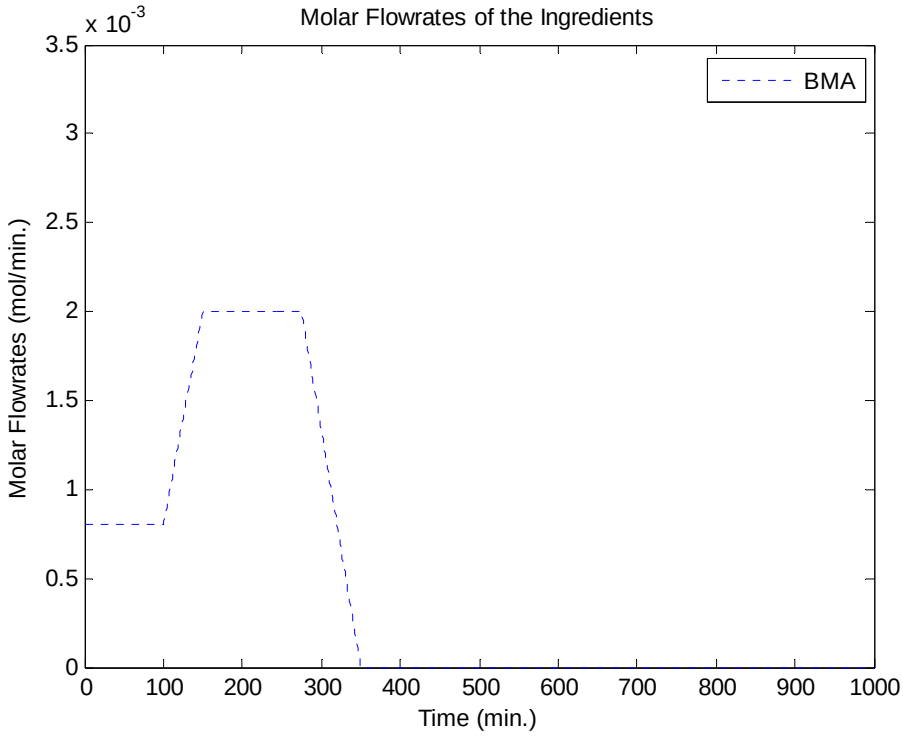

Figure 6.60: Simulation of the sub-optimal monomer flowrate with constraints

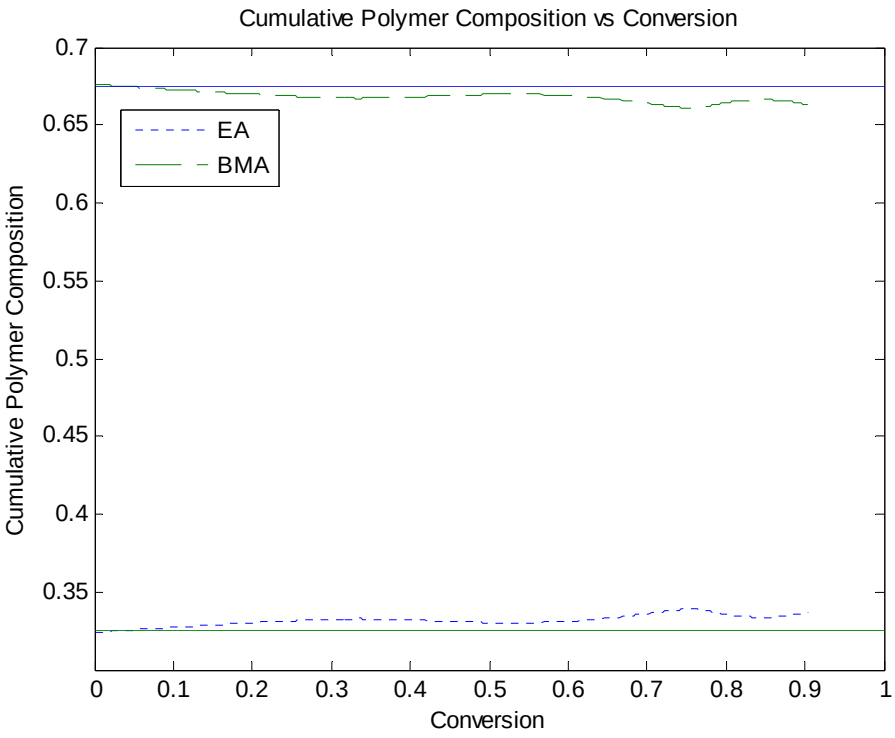

Figure 6.61: Simulation of the sub-optimal monomer flowrate with constraints

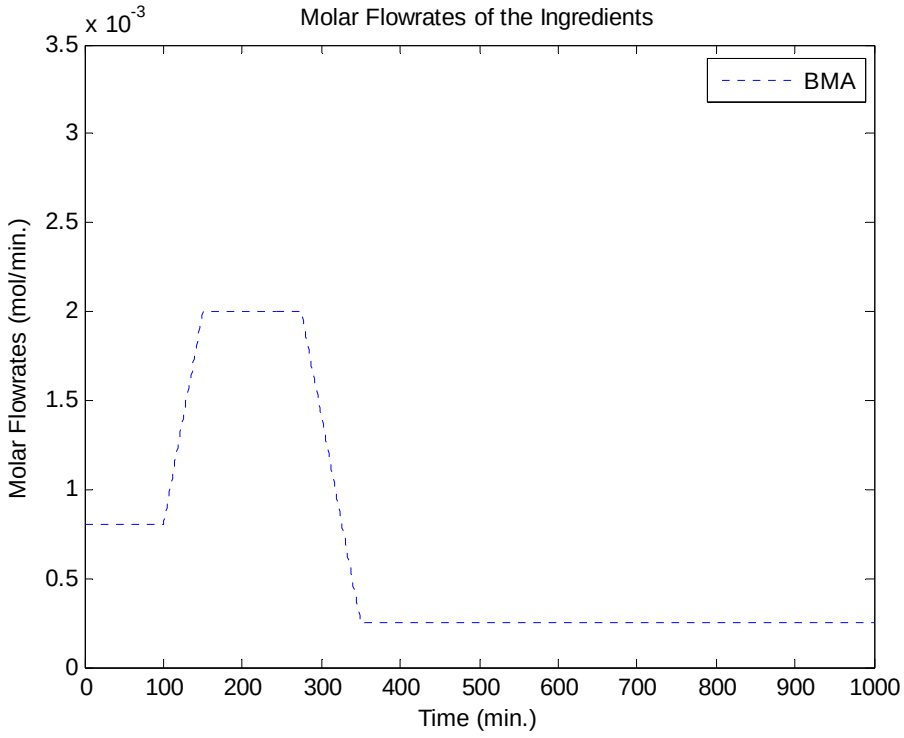

Figure 6.62: Simulation of the sub-optimal monomer flowrate with constraints

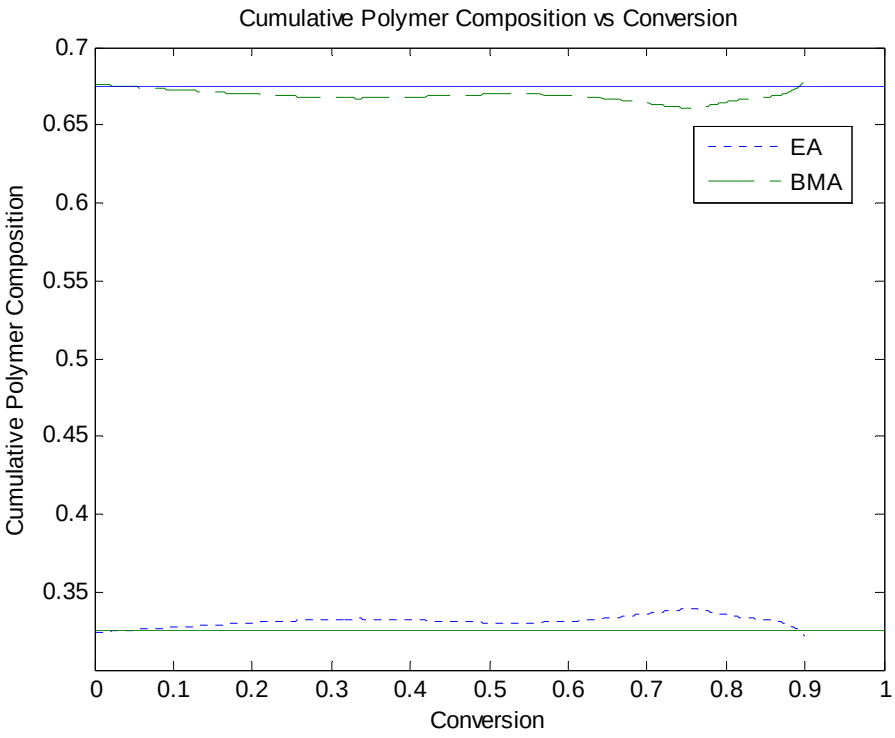

Figure 6.63: Simulation of the sub-optimal monomer flowrate with constraints

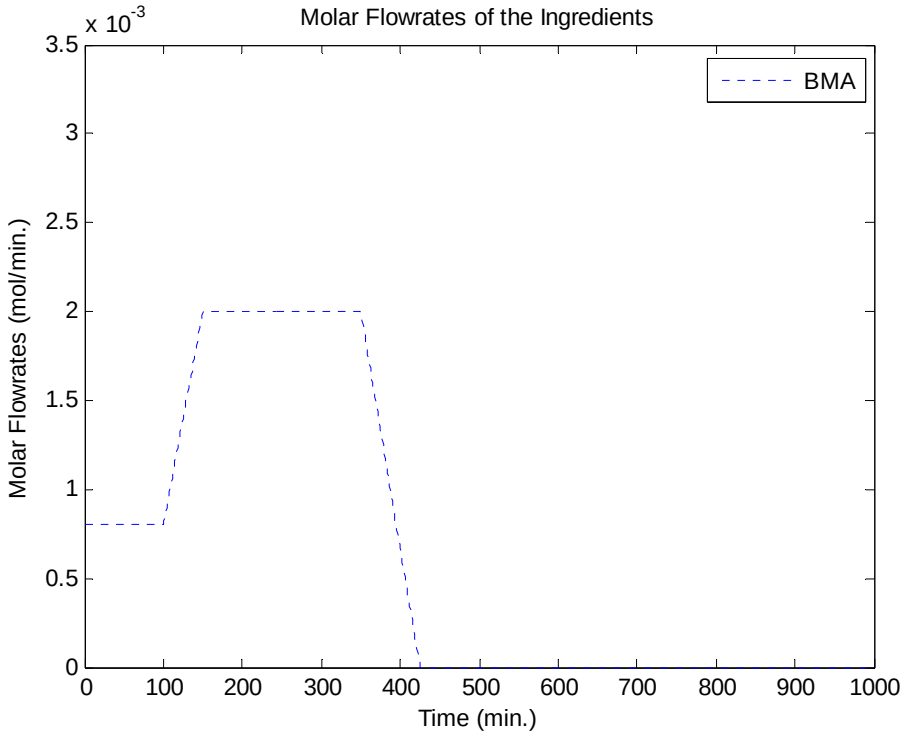

Figure 6.64: Simulation of the sub-optimal monomer flowrate with constraints

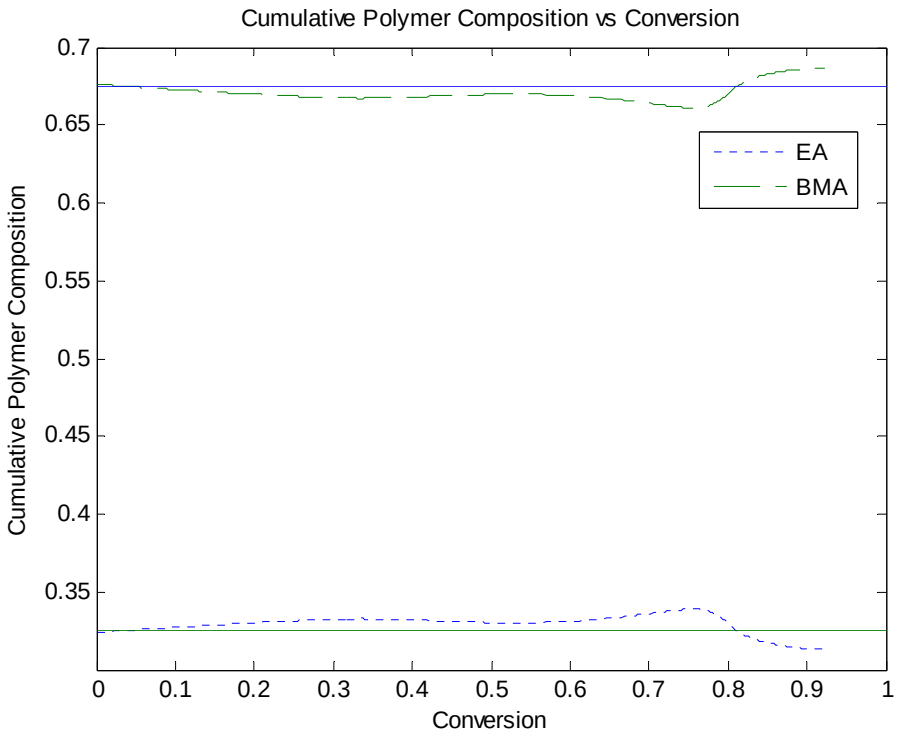

Figure 6.65: Simulation of the sub-optimal monomer flowrate with constraints

7. Conclusions and Future Steps

A multi-component free radical polymerization model was refined and extended. The generalized six-monomer model began as WATPOLY, a comprehensive simulator and database package for homo-, co- and ter-polymerizations (Gao and Penlidis, 1996; 1998 and 2000). Jung (2008) expanded the model into hexa-polymerization while adapting it to MATLAB. He also began to contribute to the database and develop the depropagation software following Kruger's probabilistic model (Kruger *et al.*, 1987). In this thesis, extensive literature searching allowed for improved depropagation parameters as per the recommendations made by Jung (2008). The results of this were demonstrated in the first five case studies of section 5. A hexa-polymerization system was simulated as the final topic in the depropagation section. With no literature available for such a large system, each of the figures plotted were discussed in detail.

The back-biting and beta-scission of butyl acrylate add-on was developed to handle up to three monomers with and without depropagation. The parameters found from Peck and Hutchinson (2004), Rantow *et al.* (2006) and Nikitin *et al.* (2007) were used to accurately model BA in various systems; the final four case studies in section 5 show the homo-, co- and ter-polymerization results.

Polymerizations with more than one initiator were simulated and various outputs were analyzed. No literature could be found with experimental data for this scenario but the pseudo-rate method employed has been shown to be quite effective in modeling multiple monomers; as such, a large amount of confidence can be placed on the multiple initiator extension to provide accurate and reliable results.

Composition control was tested in the sixth section. Three different policies, with completely different final characteristics, each produced co-, ter- and tetra-polymers with uniform composition. Applications were examined with several practical solutions for easy implementation.

Chapters 4 through 6 proved the versatility and reliability of our model. This model serves to generate better understanding of multi-component polymerizations under various conditions as well as to be an economic and educational tool for use in industry and academia.

Difficulties in creating a diverse mechanistic polymerization model arise due to the lack of literature available. Very few ter- and tetra-polymerizations have been examined against

experimental data in this thesis or in Jung (2008). Several co-polymerizations have yet to be found in literature as well. For better confidence, and increased accuracy, the relevant experiments should be conducted and compared with the model predictions. Depropagation, although improved, still has many parameters that require fine-tuning. Even though homo-depropagation is known in many cases, it is unknown which methacrylates will depropagate in co-polymerizations. As such, kinetic experiments will also be required for the determination of these parameters. Specifically, the monomer databases of AA, HEMA and GMA are not complete. In terms of acrylic acid, the database is using data for homo-polymerizations in water (Gao, 1992). The fields missing from HEMA and GMA were substituted from HEA and BMA due to logical similarity. Finally, a second complete conversion tetra-polymerization experiment would significantly test the model's ability to model multi-component systems.

References

Abdollahi M., Mehdipour-Ataei S., & Ziaee F. (2007). Using ^{1}H-NMR spectroscopy for the kinetic study of the in situ solution free-radical copolymerization of styrene and ethyl acrylate. *Journal of Applied Polymer Science*, *105*, 2588-2597.

Ahmad N., Charleux B., Farcet C., Ferguson C. J., Gaynor S. G., Hawkett B. S., Heatley F., Klumperman B., Konkolewicz D., Lovell P. A., Matyjaszewski K., & Venkatesh R. (2009). Chain transfer to polymer and branching in controlled radical polymerizations of n-butyl acrylate. *Macromolecular Rapid Communications*, *30*, 2002-2021.

Alfrey, T., & Goldfinger G. (1944). Copolymerization of systems of three and more components. *Journal of Chemical Physics*, *12*, 205-209, 322.

Alfrey, T., & Goldfinger G. (1946). Copolymerization of systems containing three components. *Journal of Chemical Physics*, *14*, 115-116.

Arai K., & Saito S. (1976). Simulation model for the rate of bulk polymerization over the complete course of reaction. *Journal of Chemical Engineering of Japan*, *9(4)*, 302-313.

Asua M., Beuermann S., Buback M., Castignolles P., Charleux B., Gilbert R. G., Hutchinson R. A., Leiza J. R., Nikitin A. N., Vairon J., & Van Herk A. M. (2004). Critically evaluated rate coefficients for free radical polymerization, 5: Propagation rate coefficient for butyl acrylate. *Macromolecular Chemistry and Physics*, *205*, 2151-2160.

Balaraman K. S., Nadkarni V. M., & Mashelkar R. A. (1986). SAN bulk copolymerization: some new insights in kinetics and microstructure. *Chemical Engineering Science*, *41(5)*, 1357-1368.

Barth J., Buback M., Hesse P., & Sergeeva T. (2009). EPR analysis of n-butyl acrylate radical polymerization. *Macromolecular Rapid Communications*, *30*, 1969-1974.

Beuermann S., Paquet D. A., McMinn J. H., & Hutchinson R. A. (1996). Determination of free radical propagation rate coefficients of butyl, 2-ethylhexyl, and dodecyl acrylates by pulsed-laser polymerization. *Macromolecules*, *29*, 4206-4215.

Beuermann S., Paquet D. A., McMinn J. H., & Hutchinson R. A. (1997). Propagation kinetics of methacrylic acid studied by pulsed-laser polymerization. *Macromolecules*, *30*, 194-197.

Beuermann S., Buback M., & Schmaltz C. (1999). Termination rate coefficients of butyl acrylate free radical homopolymerization in supercritical CO_2 and in bulk. *Industrial & Engineering Chemistry Research*, *38*, 3338-3344.

Borchardt J. K. (1982). Steric and electronic effects of alkyl substituents on reactivity ratios in copolymerization reactions of acrylates and methacrylates. *Polymer Preprints, 23(2)*, 209-211.

Borchardt J. K. (1985). Calculation of reactivity ratios and sequence distribution in copolymers from monomers ^{13}C-NMR data. *Journal of Macromolecular Science. Chemistry, A22(12)*, 1711-1733.

Bradbury J. H., & Melville H. W. (1954). The co-polymerization of styrene and butyl acrylate in benzene solution. *Proceedings of the Royal Society of London. Series A, Mathematical and Physical Sciences*, *222(1151)*, 456-470.

Brandrup J., Immergut E. H., Grulke E. A., & Bloch D. (1999). *Polymer Handbook*. 4th ed. New York: John Wiley & Sons.

Branson H., & Simha R. (1943). On the kinetics of copolymerization. *Journal of Chemical Physics*, *11(6)*, 297-298.

Brar A. S., & Dutta K. (1998). Acrylonitrile and glycidyl methacrylate copolymers: Nuclear magnetic resonance characterization. *Macromolecules*, *31*, 4695-4702.

Buback M. Degener B., & Huckestein B. (1989). Conversion dependence of free radical polymerization rate coefficients from laser-induced experiments. 1. Butyl acrylate. *Die Makromolekulare Chemie, Rapid Communications*, *10*, 311-316.

Buback M. (1990). Free radical polymerization up to high conversion. A general kinetic treatment. *Makromolekulare Chemie*, *191*, 1575-1587.

Buback M., Gilbert R. G., Hutchinson, R. A., Klumperman B., Kuchta F., Manders B. G., O'Driscoll F., Russell G. T., & Schweer J. (1995). Critically evaluated rate coefficients for free radical polymerization, 1. Propagation rate coefficient for styrene. *Macromolecular Chemistry and Physics*, *196*, 3267-3280.

Buback M., Kurz C., & Schmaltz C. (1998). Pressure dependence of propagation rate coefficients in free-radical homopolymerizations of methyl acrylate and dodecyl acrylate. *Macromolecular Chemistry and Physics*, *199*, 1721-1727.

Buback M., Klingbeil S., Sandmann J., Sderra M., Vögele H. P., Wackerbarth H., & Wittkowski L. (1999). Pressure and temperature dependence of the decomposition rate of tert-butyl peroxyacetate and of tert-butyl peroxypivalate. *Z. Physics Chemistry*, *210*, 199-221.

Buback M., Feldermann A., Barner-Kowollik B., & Lacik I. (2001). Propagation rate coefficients of acrylate-methacrylate free-radical bulk copolymerizations. *Macromolecules*, *34*, 5439-5448.

Buback M., & Junkers T. (2006). Termination kinetics of tert-butyl methacrylate and of n-butyl methacrylate free-radical bulk homopolymerizations. *Macromolecular Chemistry and Physics*, *207*, 1640-1650.

Bywater S. (1955). Photosensitized polymerization of methyl methacrylate in dilute solution above 100°C. *Transactions of the Faraday Society*, *51*, 1267-1273.

Cameron G. G., & Kerr G. P. (1967). The copolymerization behaviour of alpha-substituted methyl acrylates. *European Polymer Journal*, *3*, 1-4.

Carlsson D. J., Howard J. A., & Ingold K. U. (1966). Reactions of alkoxy radicals. II. The absolute rate constant for the combination of t-butoxy radicals. *Journal of American Chemical Society*, *88(20)*, 4725-4726.

Castignolles P. (2009). Transfer to polymer and long-chain branching in plp-sec of acrylates. *Macromolecular Rapid Communications*, *30*, 1995-2001.

Catala M., Nonn A., Pujol J. M., & Brossas J. (1986). Radical copolymerization of hydroxyethyl acrylate with alkylacrylate – Determination of the reactivity ratios. *Polymer Bulletin*, *15*, 311-315.

Chambard G., Klumperman B., & German A. L. (1999). Dependence of chemical composition of styrene/butyl acrylate copolymers on temperature and molecular weight. *Polymer*, *40*, 4459-4463.

Chan R. K. S., & Meyer V. E. (1968). Computer calculations of binary and ternary copolymerization behaviour. *Journal of Polymer Science, Polymer Symposia*, *25*, 11-21.

Chen S., Hu T., Tian Y., Chen L., & Pojman A. (2007). Facile synthesis of poly(hydroxyethyl acrylate) by frontal free-radical polymerization. *Journal of Polymer Science: Part A: Polymer Chemistry*, *45*, 873-881.

Cheong S. I., & Penlidis A. (2004). Modeling of the copolymerization, with depropagation, of alpha-methyl styrene and methyl methacrylate at an elevated temperature. *Journal of Applied Polymer Science*, *93*, 261-270.

Chow C. D. (1975). Monomer reactivity ratio and Q-e values for copolymerization of hydroxyalkyl acrylates and 2-(1-aziridinyl)ethyl methacrylate with styrene. *Journal of Polymer Science: Polymer Chemistry Edition*, *13*, 309-313.

Davis T. P., O'Driscoll K. F., Piton M. C., & Winnik M. A. (1990). Copolymerization propagation kinetics of styrene with alkyl methacrylates. *Macromolecules, 23*, 2113-2119.

Dhib R., Gao J., & Penlidis A. (2000). Simulation of free radical bulk/solution homo-polymerization using mono- and bi-functional initiators. *Polymer Reaction Engineering*, *8(4)*, 299-464.

Dionisio J. M., & O'Driscoll, K. F. (1979). High-conversion copolymerization of styrene and methyl methacrylate. *Journal of Polymer Science: Polymer Letters Edition*, *17*, 701-707.

Dubé M. A. (1989). *Co-polymerization of styrene and butyl acrylate experimental kinetics and mathematical modeling* (Doctoral dissertation) University of Waterloo, Dept. of Chemical Engineering, Waterloo, ON.

Dubé M. A., Penlidis A., & O'Driscoll K. F. (1990a). Mathematical modeling of styrene/butyl acrylate co-polymerization. *Chemical Engineering Science*, *45(8)*, 2785-2792.

Dubé M. A., Penlidis A., & O'Driscoll K. F. (1990b). A kinetic investigation of styrene/butyl acrylate copolymerization. *Canadian Journal of Chemical Engineering*, *68*, 974-987.

Dubé M. A., Rilling K., & Penlidis A. (1991). A kinetic investigation of butyl acrylate polymerization. *Journal of Applied Polymer Science*, *43*, 2137-2145.

Dubé M. A., Sanayei R. A., Penlidis A., O'Driscoll K. F., & Reilly P. M. (1991). A microcomputer program for estimation of copolymerization reactivity ratios. *Journal of Polymer Science: Part A: Polymer Chemistry*, *29*, 703-708.

Dubé M. A., & Penlidis A. (1995a). A systematic approach to the study of multi-component polymerization kinetics: butyl acrylate/methyl methacrylate/vinyl acetate example, 1. Bulk copolymerization. *Polymer*, *36(3)*, 587-598.

Dubé M. A., & Penlidis A. (1995b). A systematic approach to the study of multi-component polymerization kinetics: butyl acrylate/methyl methacrylate/vinyl acetate example, 2. Bulk (and solution) terpolymerization. *Macromolecular Chemistry and Physics*, *196*, 1102-1112.

Dubé M. A., & Penlidis A. (1996). Hierarchical data analysis of a replicate experiment in emulsion terpolymerization. *AIChE Journal*, *42(7)*, 1985-1994.

Dubé M. A., Soares J. B. P., Penlidis A., & Hamielec A. E. (1997). Mathematical modeling of multi-component chain-growth polymerizations in batch, semibatch, and continuous reactors: A review. *Industrial & Engineering Chemistry Research*, *36(4)*, 966-1015.

Dubé M. A., Hakim M., McManus N. T., & Penlidis A. (2002). Bulk and solution copolymerization of butyl acrylate/methyl methacrylate at elevated temperatures. *Macromolecular Chemistry and Physics*, *203*, 2446-2453.

Duever T. A., O'Driscoll K. F., & Reilly P. M. (1983). The use of the Error-in-Variables Method in terpolymerization. *Journal of Polymer Science: Polymer Chemistry Edition*, *21*, 2003-2010.

Englemann U., & Schmidt-Naake G. (1993). Free radical multi-component polymerization reactors and chemical composition distribution. *Makromolekulare Chemie Theory and Simulations*, *2*, 275-297.

Fernandez-Garcia M., Fernandez-Sanz M., & Madruga E. L. (2003). Free radical copolymerization of styrene with butyl acrylate. II. Elemental kinetic copolymerization step predictions from homo-polymerization data. *Journal of Polymer Science: Part A*, *42*, 130-136.

Fineman M., & Ross S. D. (1950). Linear method for determining monomer reactivity ratios in copolymerization. *Journal of Polymer Science*, *5(2)*, 259-265.

Fischer J. P. (1972). Kinetik der radikalischen copolymerization alpha-substituierter styrole mit styrol. *Die Makromolekulare Chemie*, *155*, 211-225.

Friis N., & Nyhagen L. (1973). A kinetic study of the emulsion polymerization of vinyl acetate. *Journal of Applied Polymer Science*, *17*, 2311-2327.

Fujisawa T., & Penlidis A. (2008). Copolymer composition control policies: Characteristics and applications. *Journal of Macromolecular Science, Part A: Pure and Applied Chemistry*, *45*, 115-132.

Gaddam N. B., Xavioir S. F., & Goel T. C. (1977). Copolymerization of 2-hydroxypropyl methacrylate with alkyl acrylate monomers. *Journal of Polymer Science: Polymer Chemistry Edition*, *15*, 1473-1478.

Galbraith M. N., Moad G., Solomon D. H., & Spurling T. H. (1987). Influences on the initiation and termination reactions on the molecular weight distribution and compositional heterogeneity of functional copolymers: An application of Monte Carlo Simulation. *Macromolecules*, *20*, 675-679.

Gao J. (1992). *Mathematical modeling of homo-polymerizations: Simulation package and database extensions* (Master's thesis) University of Waterloo, Dept. of Chemical Engineering, Waterloo, ON.

Gao J., & Penlidis A. (1996). A comprehensive simulator/database package for reviewing free-radical homo-polymerizations. *Journal of Macromolecular Sciences – REV. Macromolecular Chemistry and Physics*, *C36(2)*, 199-404.

Gao J., McManus N. T., & Penlidis A. (1997). Experimental and simulation studies on ethyl acrylate polymerization. *Macromolecular Chemistry and Physics*, *198*, 843-859.

Gao J., & Penlidis A. (1998). A comprehensive simulator/database package for bulk/solution free radical copolymerizations. *Journal of Macromolecular Sciences – REV. Macromolecular Chemistry and Physics*, *C38(4)*, 651-780.

Gao J., & Penlidis A. (2000). A comprehensive simulator/database package for bulk/solution free radical terpolymerizations. *Macromolecular Chemistry Physics*, *201*, 1176-1184.

Gao J., Hungenberg K. D., & Penlidis A. (2004). Process modeling and optimization of styrene polymerization. *Macromolecular Symposia*, *206*, 509-522.

Garcia-Rubio L. H., Hamielec A. E., & MacGregor J. F. (1979). Bulk polymerization of acrylonitrile. II. Model development. *Journal of Applied Polymer Science*, *23*, 1413-1429.

Garcia-Rubio L. H., Lord M. G., MacGregor J. F., & Hamielec A. E. (1985). Bulk copolymerization of styrene and acrylonitrile: Experimental kinetics and mathematical modeling. *Polymer*, *26*, 2001-2013.

Grady M. C., Simonsick W. J. & Hutchinson R. A. (2002). Studies of higher temperature polymerization of butyl methacrylate and butyl acrylate. *Macromolecular Symposia*, *182*, 149-168.

Hakim M., Verhoeven V., McManus N. T., Dubé M. A., & Penlidis A. (2000). High temperature solution polymerization of butyl acrylate and methyl methacrylate: Reactivity ratio estimation. *Journal of Applied Polymer Science*, *77*, 602-609.

Hamielec A. E., MacGregor J. F., & Penlidis A. (1987a). Comprehensive Polymer Science Encyclopedia Chapter 2. *Perhamon Press*, *3*, 17-31.

Hamielec A. E., MacGregor J. F., & Penlidis A. (1987b). Multi-component free-radical polymerization in batch, semi-batch and continuous reactors – modeling and control of chain composition, microstructure, molecular weight distribution, long chain branching and crosslinking in solution and emulsion polymerization. *Makromolekulare Chemie, Macromolecular Symposia*, *10-11*, 521-570.

Harwood H. J., & Ritchey W. M. (1964). The characterization of sequence distribution in copolymers. *Polymer Letters*, *2*, 601-607.

Harwood H. J. (1968). A FORTRAN II program for conducting sequence distribution calculations. *Journal of Polymer Science. Part C*, *25*, 37-45.

Hill D. J. T., O'Donnel J. H., & O'Sullivan P. W. (1982). Analysis of the mechanism of copolymerization of styrene and acrylonitrile. *Macromolecules*, *15*, 960-966.

Hocking M. B., & Klimchuk K. A. (1996). A refinement of the ter-polymer equation and its simple extension to two- and four-component systems. *Journal of Polymer Science: Part A: Polymer Chemistry*, *34*, 2481-2497.

Howell J. A., Izu M., & O'Driscoll K. F. (1970). Co-polymerization with depropagation III. Composition and sequence distribution from probability considerations. *Journal of Polymer Science: Part A-1*, *8*, 699-710.

Hui A. W., & Hamielec A. E. (1972). Thermal polymerization of styrene at high conversions and temperatures: An experimental study. *Journal of Applied Polymer Science*, *16*, 749-769.

Husain A., & Hamielec A. E. (1978). Thermal polymerization of styrene. *Journal of Applied Polymer Science*, *22*, 1207-1223.

Hutchinson R. A., Paquet D. A. Jr., McMinn J. H., & Fuller R. E. (1995). Measurement of free radical propagation rate coefficients for ethyl methacrylate, n-butyl methacrylate, and iso-butyl methacrylate by pulsed laser polymerization. *Macromolecules*, *28*, 4023-4028.

Hutchinson R. A., Beuermann S., Paquet D. A., & McMinn J. H. (1997). Determination of free radical propagation rate coefficients for alkyl methacrylates by pulsed-laser polymerization. *Macromolecules*, *30*, 3490-3493.

Izu M., & O'Driscoll K. F. (1970). Co-polymerization with depropagation IV. Computer simulation of copolymerization with reversibility. *Journal of Polymer Science: Part A-1*, *8*, 1675-1685.

Jianying H., Jiayan C., Jiaming Z., Yihong C., Lizong D., & Yousi Z. (2006). Some monomer reactivity ratios of styrene and (meth)acrylates in the presence of TEMPO. *Journal of Applied Polymer Science*, *100*, 3531-3535.

Johnson M., Karmo T. S., & Smith R. R. (1978). High conversion co-polymerization of styrene with methyl methacrylate. *European Polymer Journal*, *14*, 409-414.

Johnston N. W. (1973). Sequence distribution – Glass transition effects III. Alpha-methyl styrene – acrylonitrile copolymers. *Macromolecules*, *6(3)*, 453-456.

Jung W. (2008). *Mathematical modeling of free-radical six component bulk and solution polymerization* (Master's thesis) University of Waterloo, Dept. of Chemical Engineering, Waterloo, ON.

Kapur G. S., & Brar A. S. (1992). Sequence determination in vinyl acetate/alkyl methacrylate copolymers prepared by semicontinuous batch process by NMR spectroscopy. *Makromolekulare Chemie*, *193*, 1773-1781.

Keramopoulos A., & Kiparissides C. (2003). Mathematical modeling of diffusion-controlled free-radical ter-polymerization reactions. *Journal of Applied Polymer Science*, *88*, 161-176.

Kim J. D. (1994). *A kinetic study of styrene/hydroxyl ethyl acrylate co-polymerization* (Master's thesis) University of Waterloo, Dept. of Chemical Engineering, Waterloo, ON.

Kim Y., & Harwood H. J. (2002). Analysis of sequence distribution in methyl methacrylate/methyl acrylate co-polymers by ^{13}C NMR spectroscopy. *Polymer*, *43*, 3229-3237.

Koenig J. L. (1980). *Chemical Microstructure of Polymer Chains*. New York: John Wiley & Sons.

Krüger H., Bauer J., & Rübner J. (1987). Ein Modell zur Beschreibung reversible Co-polymerisationen. *Makromolekulare Chemie*, *188*, 2163-2175.

Kuindersma M. E. (1992). *On the modeling of free-radical polymerization reactions: Homo-polymerization* (Master's thesis) University of Waterloo, Dept. of Chemical Engineering, Waterloo, ON.

Kumar V. R., & Gupta S. K. (1991). Optimal parameter estimation for methyl methacrylate polymerization. *Polymer*, *32(17)*, 3233-3243.

Leamen M. J. (2005). *Kinetic investigation and modeling of multi-component polymer systems with depropagation* (Doctoral dissertation) University of Waterloo, Dept. of Chemical Engineering, Waterloo, ON.

Leamen M. J., McManus N. T., & Penlidis A. (2005). Binary copolymerization with full depropagation: A study of methyl methacrylate and alpha-methyl styrene copolymerization. *Journal of Polymer Science: Part A: Polymer Chemistry*, *43*, 3868-3877.

Leamen M. J., McManus N. T., & Penlidis A. (2006). Ter-polymerization with depropagation: Modeling the co-polymer composition of methyl methacrylate/alpha-methyl styrene/butyl acrylate system. *Chemical Engineering Science*, *61*, 7774-7785.

Li D., Grady M. C., & Hutchinson R. A. (2005). High temperature semibatch free-radical co-polymerization of butyl methacrylate and butyl acrylate. *Industrial and Engineering Chemistry Research*, *44(8)*, 2506-2517.

Li D., Li N., & Hutchinson R. A. (2006). High-temperature free radical copolymerization of styrene and butyl methacrylate with depropagation and penultimate kinetic effects. *Macromolecules*, *39*, 4366-4373.

Li D., & Hutchinson R. A. (2007). Penultimate propagation kinetics of butyl methacrylate, butyl acrylate, and styrene terpolymerization. *Macromolecular Rapid Communications*, *28*, 1213-1218.

Liu Y., Mao R., Huglin M. B., & Holmes P. A. (1995). Some aspects of the copolymerization of glyceryl methacrylate with methyl methacrylate. *Polymer*, *26*, 4287-4292.

Lord M. G. (1984). *Computer modeling of styrene and acrylonitrile bulk co-polymerization at high conversion* (Master's thesis) McMaster University, Dept. of Chemical Engineering, Hamilton, ON.

Lowry G. G. (1960). The effect of depropagation on co-polymer composition, I. General theory for one depropagating monomer. *Journal of Polymer Science*, *42*, 463-477.

Lyons R. A., Hutovic J., Piton M. C., Christie D. I., Clay P. A., Manders B. G., Kable S. H., & Gilbert R. G. (1996). Pulsed-laser polymerization measurements of the propagation rate coefficients for butyl acrylate. *Macromolecules*, *29*, 1918-1927.

Mahabadi H. K., & O'Driscoll K. F. (1978). Estimating the concentration dependence of the termination rate constant in the initial stages of free radical polymerization. *Journal of Polymer Science: Polymer Letters Edition*, *16*, 351-356.

Marten F. L., & Hamielec A. E. (1982). High-conversion diffusion-controlled polymerization of styrene I. *Journal of Applied Polymer Science*, *27*, 489-505.

Martinet F., & Guillot J. (1999). Co-polymerization with depropagation: Prediction of kinetics and properties of alpha-methyl styrene-methyl methacrylate copolymers. II. Bulk co-polymerization. *Journal of Applied Polymer Science*, *72*, 1611-1625.

Maeder S., & Gilbert R. G. (1998). Measurement of transfer constant for butyl acrylate free radical polymerization. *Macromolecules*, *31*, 4410-4418.

Matthews B., Villa C., & Pierini P. (2007). Model development in thermal styrene polymerization. *Macromolecular Symposia*, *259*, 94-101.

Mayo F. R., & Lewis F. M. (1944). A basis for comparing the behaviour of monomers in co-polymerization; The copolymerization of styrene and methyl methacrylate. *Journal of American Chemical Society*, *66*, 1594-1601.

Mayo F. R., & Walling C. (1950). Copolymerization. *Chemical Reviews (Washington D.C. USA)*, *46*, 191-287.

McCormick H. W. (1957). Ceiling temperature of alpha-methyl styrene. *Journal of Polymer Science*, *25(111)*, 488-490.

McKenna T. F., Villanueva A., & Santos A. M. (1999). Effect of solvent on the rate constants in solution polymerization. Part I. butyl acrylate. *Journal of Polymer Science: Part A: Polymer Chemistry*, *37*, 571-588.

McManus N. T., & Penlidis A. (1996). A kinetic investigation of styrene and ethyl acrylate copolymerization. *Journal of Polymer Science: Part A*, *34*, 237-248.

McManus N. T., Kim J. D. & Penlidis A. (1998). Observations on styrene-hydroxyethyl acrylate and styrene-hydroxyethyl acrylate-ethyl acrylate polymerizations. *Polymer Bulletin*, *41*, 661-668.

McManus N. T., Dubé M. A., & Penlidis A. (1999). High temperature bulk copolymerization of butyl acrylate and methyl methacrylate reactivity ratio estimation. *Polymer Reaction Engineering*, *7(1)*, 131-145.

McManus N. T., Hsieh G., & Penlidis A. (2004). Free radical terpolymerization of butyl acrylate/methyl methacrylate and alpha-methyl styrene at high temperature. *Polymer*, *45*, 5837-5845.

Merz E., Alfrey T., & Goldfinger G. (1946). Intramolecular reactions in vinyl polymers as a means of investigation of the propagation step. *Journal of Polymer Science*, *1(2)*, 75-82.

Meyer V. E., & Lowry G. G. (1965). Integral and differential binary copolymerization equations. *Journal of Polymer Science: Part A: General Papers*, *3(8)*, 2843-2851.

Moad G. & Solomon D. H. (1995). *The Chemistry of Free Radical Polymerization*. Oxford: Pergamon.

Mun G. A., Nurkeeva Z. S., Beissegul A. B., Dubalazov A. V., Urkimbaeva P. I., Park K., & Khutoryanskiy V. V. (2007). Temperature-responsive water-soluble copolymers based on hydroxyethyl acrylate and butyl acrylate. *Macromolecular Chemistry and Physics*, *208*, 979-987.

Nair A. S., & Muthana M. S. (1961). Studies on the polymerization of methacrylic esters Part I. Polymerization of n-butyl methacrylate and iso-butyl methacrylate. *Makromolekulare Chemie*, *47*, 114-127.

Nikitin A. N., Hutchinson R. A., Buback M., & Hesse P. (2007). Determination of intramolecular chain transfer and midchain radical propagation rate coefficients for butyl acrylate by pulsed laser polymerization. *Macromolecules*, *40*, 8631-8641.

Nikitin A. N., & Hutchinson R. A. (2009). Effect of intramolecular transfer to polymer on stationary free radical polymerization of alkyl acrylates, 4 – consideration of penultimate effect. *Macromolecular Rapid Communications*, *30*, 1981-1988.

Nising P., & Meyer T. (2004). Modeling of the high-temperature polymerization of methyl methacrylate. 1. Review of existing models for the description of the gel effect. *Industrial and Engineering Chemistry Research*, *43(23)*, 7220-7226.

Odian G. (1970). *Principles of Polymerization*. New York: McGraw-Hill.

O'Driscoll K. F., & Huang J. (1989). The rate of copolymerization of styrene and methyl methacrylate I. Low conversion kinetics. *European Polymer Journal*, *25(7/8)*, 629-633.

O'Driscoll K. F., & Huang J. (1990). The rate of copolymerization of styrene and methyl methacrylate II. The gel effect in copolymerization.

Otsu T., Ito T., & Imoto M. (1965). The reactivities of alkyl methacrylates in their radical polymerizations. *Polymer Letters*, *3*, 113-117.

Otsu T., Ito T., & Imoto M. (1966). Further correlations between the reactivity and the structure of alkyl acrylates and methacrylates. *Journal of Polymer Science: Part A-1*, *4*, 733-736.

Palmer D. E., McManus N. T., & Penlidis A. (2000). Copolymerization with depropagation: A study of alpha-methyl styrene and methyl methacrylate in bulk at elevated temperatures. *Journal of Polymer Science: Part A: Polymer Chemistry*, *38*, 1981-1990.

Palmer D. E., McManus N. T., & Penlidis A. (2001). Copolymerization with depropagation: A study of alpha-methyl styrene and methyl methacrylate in solution at elevated temperatures. *Journal of Polymer Science: Part A: Polymer Chemistry*, *39*, 1753-1763.

Patino-Leal H., Reilly P. M., & O'Driscoll K. F. (1980). On the estimation of reactivity ratios. *Journal of Polymer Science: Polymer Letters Edition*, *18*, 219-227.

Peck A. N. F., & Hutchinson R. A. (2004). Secondary reactions in the high temperature free radical polymerization of butyl acrylate. *Macromolecules*, *37*, 5944-5951.

Plessis C., Arzamendi G., Alberdi J. M., Van Herk A. M., Leiza J. R., & Asua J. M. (2003). Evidence of branching in poly(butyl acrylate) produced in pulsed-laser polymerization experiments. *Macromolecular Rapid Communications*, *24(2)*, 173-177.

Polic A. L., Duever T. A., & Penlidis A. (1998). Case studies and literature review on the estimation of copolymerization reactivity ratios. *Journal of Polymer Science: Part A: Polymer Chemistry*, *36*, 813-822.

Popescu D., Hoogenboom R., Keul H., & Möller M. (2010). Free radical and nitroxide mediated polymerization of hydroxyl-functional acrylates prepared via lipase-catalyzed transacylation reactions. *Journal of Polymer Science: Part A: Polymer Chemistry*, *48*, 2610-2621.

Quan C., Soroush M., Grady M. C., Hansen J. E., & Simonsick W. J. (2005). High temperature homopolymerization of ethyl acrylate and butyl acrylate: Polymer characterization. *Macromolecules*, *38*, 7619-7628.

Raghuram P. V. T., & Nandi U. S. (1967). Studies on the polymerization of ethyl acrylate. I. Kinetic studies. *Journal of Polymer Science: Part A-1*, *5*, 2005-2012.

Raghuram P. V. T., & Nandi U. S. (1970). Studies on the polymerization of ethyl acrylate. III. Effect of temperature on the solvent-transfer reaction. *Journal of Polymer Science: Part A-1*, *8*, 3079-3088.

Rantow F. S., Soroush M., Grady M. C., & Kalfas G. A. (2006). Spontaneous polymerization and chain microstructure evolution in high-temperature solution polymerization of n-butyl acrylate. *Polymer*, *47*, 1423-1435.

Reilly P. M., & Patino-Leal H. (1981). A Bayesian study of the Error-in-Variables Model. *Technometrics*, *23(3)*, 221-231.

Reilly P. M., Reilly H. V., & Keeler S. E. (1993). Algorithm AS286: Parameter estimation in the Error-in-Variables Model. *Applied Statistics*, *42(4)*, 693-701.

Rossignoli P. J., & Duever T. A. (1995). The estimation of copolymer reactivity ratios: A review and case studies using the Error-in-Variables Model and nonlinear least squares. *Polymer Reaction Engineering*, *3(4)*, 361-395.

Sahloul N. A. (2004). *A study of multi-component polymerization of styrene/ethyl acrylate/hydroxyethyl acrylate and methacrylic acid* (Doctoral dissertation) University of Waterloo, Dept. of Chemical Engineering, Waterloo, ON.

Sahloul N. A., & Penlidis A. (2004). High temperature copolymerization of styrene and ethyl acrylate: Reactivity ratio estimation in bulk and solution. *Advances in Polymer Technology*, *23(3)*, 186-195.

Sahloul N. A., & Penlidis A. (2005). Styrene and methacrylic acid monomer reactivity ratio estimation in bulk and solution at high temperatures. *Polymer-Plastics Technology and Engineering*, *44*, 771-782.

Sahloul N. A., Emwas N. A., Power W., & Penlidis A. (2005). Ethyl acrylate-hydroxyethyl acrylate and hydroxyethyl acrylate-methacrylic acid: Reactivity ratio estimation from

crosslinked polymer using high resolution magnetic angle spinning spectroscopy. *Journal of Macromolecular Science, Part A: Pure and Applied Chemistry*, *42*, 1369-1385.

Scholtens C. A., Meuldijk J., & Drinkenburg A. A. H. (2001). Production of copolymers with a predefined intermolecular chemical composition distribution by emulsion polymerization in a continuously operated reactor. *Chemical Engineering Science,* 56, 955-962.

Simha R., & Branson H. (1944). Theory of chain copolymerization reactions. *Journal of Chemical Physics*, *12(6)*, 253-267.

Skeist I. (1946). Copolymerization: the composition distribution curve. *Journal of American Chemical Society*, *68*, 1781-1784.

Stickler M. (1983). Free radical polymerization kinetics of methyl methacrylate at very high conversions. *Makromolekulare Chemie*, *184*, 2563-2579.

Stickler M., Panke D., & Hamielec A. E. (1984). Polymerization of methyl methacrylate up to high degrees of conversion: Experimental investigation of the diffusion-controlled polymerization. *Journal of Polymer Science: Polymer Chemistry Edition*, *22*, 2243-2253.

Stockmayer W. H. (1945). Distribution of chain lengths and compositions in copolymers. *Journal of Chemical Physics*, *13(6)*, 199-207.

Switata-Zeliazkow M. (1993). Microstructure of styrene-methacrylic acid and styrene-acrylic acid copolymers, 6. Relation of the glass transition temperature to the microstructure of methacrylic acid-styrene copolymers. *Makromolekulare Chemie*, *194(5)*, 1505-1511.

Tacx J. C. J. F., Ammerdorffer J. L., & German A. L. (1988). Chemical composition distribution of styrene-ethyl methacrylate copolymers studied by means of t.l.c./f.i.d.: effect of high conversion in various polymerization processes. *Polymer*, *29*, 2087-2094.

Teramachi S., Hasegawa A., & Uchiyama N. (1984). The chemical composition distribution of a high conversion sample of copoly(styrene-stat-methyl methacrylate) prepared in bulk. *Journal of Polymer Science: Polymer Letters Edition*, *22*, 71-76.

Van Herk. A. M. (2009). Historic account of the development in the understanding of the propagation kinetics of acrylate radical polymerizations. *Macromolecular Rapid Communications*, *30*, 1964-1968.

Valvassori A., & Sartori G. (1967). Present status of multi-component copolymerization theory. *Advances in Polymer Science*, *5(1)*, 28-58.

Vargün E., & Usanmaz A. (2005). Polymerization of hydroxyethyl acrylate in bulk and solution by chemical initiator and by ATRP method. *Journal of Polymer Science: Part A: Polymer Chemistry*, *43*, 3957-3965.

Vivaldo-Lima E., Hamielec A. E., & Wood P. E. (1994). Batch reactor modeling of the free radical copolymerization kinetics of styrene and divinylbenzene up to high conversions. *Polymer Reaction Engineering*, *2(1&2)*, 87-162.

Wall F. T., (1944). The structure of copolymers II. *Journal of American Chemical Society*, *66*, 2050-2057.

Walling C., & Briggs E. R. (1945). Copolymerization. III. Systems containing more than two monomers. *Journal of American Chemical Society*, *67*, 1774-1778.

Walling C. (1949). Copolymerization. XIII. Overall rates in copolymerization. Polar effects in chain initiation and termination. *Journal of American Chemical Society*, *71*, 1930-1935.

Wang W., & Hutchinson R. A. (2008a). High temperature semibatch free radical copolymerization of styrene and dodecyl methacrylate. *Macromolecular Symposia*, *261*, 64-73.

Wang W., & Hutchinson R. A. (2008b). PLP/SEC/NMR study of free radical copolymerization of styrene and glycidyl methacrylate. *Macromolecules*, *41*, 9011-9018.

Wang W., Hutchinson R. A., & Grady M. C. (2009a). Study of butyl methacrylate depropagation behaviour using batch experiments in combination with modeling. *Industrial & Engineering Chemistry Research*, *48*, 4810-4816.

Wang W., Nikitin A. N., & Hutchinson R. A. (2009b). Consideration of macromonomer reactions in n-butyl acrylate free radical polymerization. *Macromolecular Rapid Communications*, *30*, 2022-2027.

Wang W. (2010). *A comprehensive kinetic model for high temperature free radical production of styrene/methacrylate/acrylate resins* (Doctoral dissertation) Queen's University, Dept. of Chemical Engineering, Kingston, ON.

Willemse R. X. E., Van Herk A. M., Panchenko E., Junkers T., & Buback M. (2005). PLP-ESR monitoring of midchain radicals in n-butyl acrylate polymerization. *Macromolecules*, *38(12)*, 5098-5103.

Wolf A., Bandermann F., & Schwede C. (2002). Batch and continuous thermal free-radical copolymerizations of styrene with glycidyl methacrylate at high reaction temperatures. *Macromolecular Chemistry and Physics*, *203(2)*, 393-400.

Wittmer P. (1971). Copolymerization in the presence of depolymerization reactions. *Advances in Chemistry Series*, *99*, 140-174.

Xie T. Y., & Hamielec A. E. (1993). Modeling free radical copolymerization kinetics – evaluation of the pseudo-kinetic rate constant method, 2 Molecular weight calculations for copolymers with long chain branching. *Makromolekulare Chemie, Theory and Simulations*, *2(3)*, 455-483.

Zorn A., Junkers T., & Barner-Kowollik C. (2009). Synthesis of a macromonomer library from high-temperature acrylate polymerization. *Macromolecular Rapid Communications*, *30*, 2028-2035.

Appendices

Appendix I. Implementing Initiation in a Simulation Model

As shown previously, the initiation in the model for multiple initiators in multi-component polymerization is as follows:

$$f_{eff,pseudo,k} = \sum_{i=1}^{6} f_{eff,k,i} f_i \qquad 3.16.$$

$$R_I = 2 \sum_{k=1}^{m} f_{eff,pseudo,k} k_{d,pseudo,k} [I_k] \qquad 3.17.$$

$$k_{d,pseudo,k} = \sum_{i=1}^{6} k_{d,k,i} f_i \qquad 3.18.$$

$k_{d,pseudo,k}$ exists because each monomer has slightly different interactions with the initiator and this needs to be accoutned for. Here is a small excert from the code for AIBN for three different monomers. As one can see, relative to the magnitude of the numbers, there are only small differences between the monomers. After interpolation (calculating $k_{d,pseudo,k}$), the variabilities will be even less pronounced.

Initiator Code Portion for AIBN:

```
% Sty
Ad_1 = 6.33e16;
Ed_1 = 3.0719e4;
kd_1 = Ad_1 * exp(-Ed_1 / (R * T));

% BA
Ad_2 = 6.23e16;
Ed_2 = 3.0719e4;
kd_2 = Ad_2*exp(-Ed_2/(R*T));

% EA
Ad_3 = 7.78030e16;
Ed_3 = 3.07036e4;
kd_3 = Ad_3 * exp(-Ed_3 / (R * T));
```

Below is a case study showing the sensitivity of the initiator decomposition rate. dTBPO is the initiator in a BMA homo-polymerization at elevated temperatures with depropagation

present. The value used in equation A.1 is shown with the corresponding model simulation for monomer concentration versus time in Figure AI.1:

$$k_d = 7.2899 * 10^{16} \exp\left(\frac{-3.559 * 10^4}{RT}\right) \qquad \text{A.1.}$$

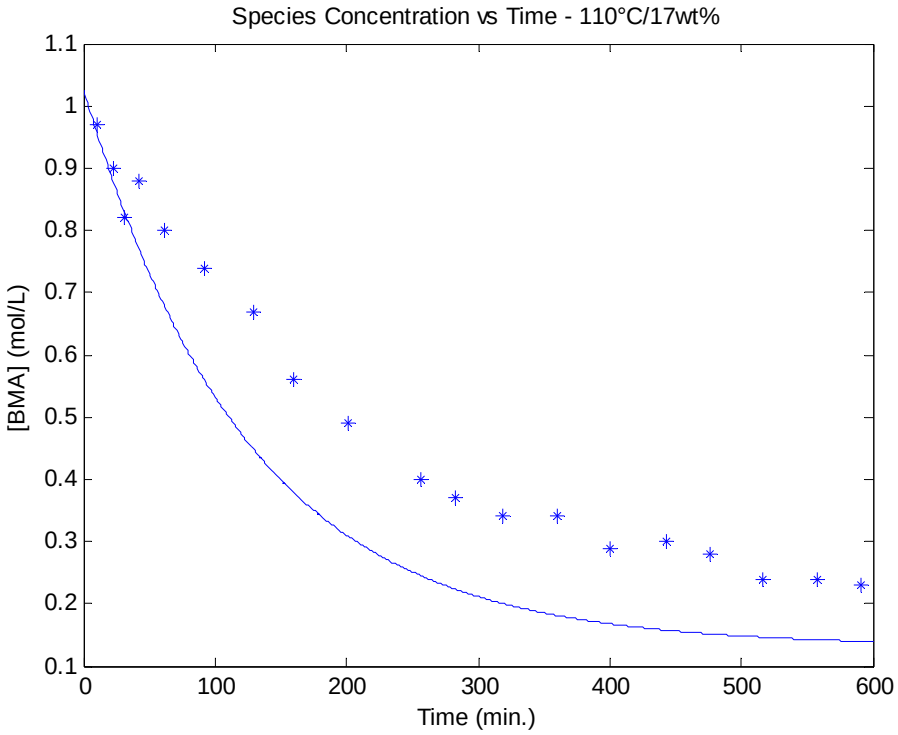

Figure AI.1: Simulation of the homo-polymerization of BMA T = 110°C $[dTBPO]_0$ = 0.17 wt% xylene = 83 wt%

After testing several troubleshooting ideas, the initiator decomposition rate constant of dTBPO for BMA was slightly modifies, as shown in equation A.2. The simulation against the same experimental data is shown in Figure AI.2.

$$k_d = 7.2899 * 10^{16} \exp\left(\frac{-3.\mathbf{6}59 * 10^4}{RT}\right) \qquad \text{A.2.}$$

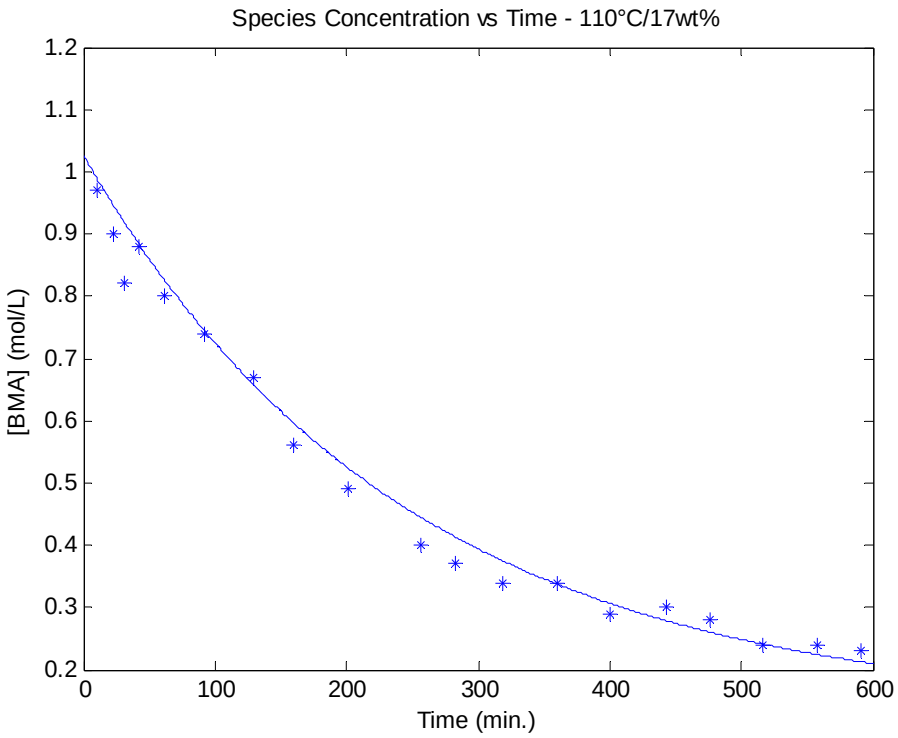

Figure AI.2: Simulation of the homo-polymerization of BMA T = 110°C $[dTBPO]_0$ = 0.17 wt% xylene = 83 wt% with modified dTBPO parameters

As one can see, even a slight change in the decomposition rate constant has a major effect on some polymerizations. Because of the sensitivity shown, a pseudo decomposition rate is required to adequately model free radical multi-component polymerization.

Appendix II. Initiator Database

This section has the kinetic data used for each of the available initiators. Certain parameters vary from monomer to monomer; the values for each monomer as well as the general value (used for any monomer not specified) are included in each of the initiator tables. Table A-6 has the arbitrary values used for the fictitious initiator mentioned in section 5.3. All of the values used below are constant and remain unchanged from simulation to simulation. Without this, there would be no confidence in the simulation package for accurate use in industry and academia. Each of the values shown was originally taken from the comprehensive WATPOLY simulator database created by Gao and Penlidis (1996, 1998 and 2000). Since then, a select few have been refined through simulation trials, sensitivity analyses or simple parameter estimation to create an enhanced mathematical model program.

Table A-1: Kinetic Database for AIBN

Parameter	Monomer	Value	Unit	Description
Mw	General	164.21	g/mol	Initiator molecular weight
k_d	Styrene	$6.33*10^{16}\exp(-3.0719*10^4/RT)$	L/min	Decomposition rate constant
	EA	$7.7803*10^{16}\exp(-3.0704*10^4/RT)$		
	General	$6.23*10^{16}\exp(-3.0704*10^4/RT)$		
f	Styrene	0.6		Initiator efficiency
	BMA	0.42		
	General	0.0247exp(-2166/RT)		
V_{fi}	Styrene	0.04	V	Critical free volume for diffusion-control
	BA	0.15		
	EA	0.825exp(-1175/RT)		
	BMA	0.09		
	General	0.6365exp(-1368.8/RT)		
C	Styrene	0.5		Rate of decrease of f
	BA	1		
	EA	1		
	General	0.685		

Table A-2: Kinetic Database for BPO

Parameter	Monomer	Value	Unit	Description
Mw	General	242.23	g/mol	Initiator molecular weight
k_d	MMA	$6.23*10^{16}\exp(-3.0704*10^4/RT)$	L/min	Decomposition rate constant
	EA	$7.7803*10^{16}\exp(-3.0704*10^4/RT)$		
	General	$6.429*10^{15}\exp(-3.01*10^4/RT)$		
f	Styrene	0.75		Initiator efficiency
	BMA	0.6		
	HEA	0.8		
	General	0.0247exp(-2166/RT)		
V_{fi}	Styrene	0.15	V	Critical free volume for diffusion-control
	BA	0.15		
	EA	0.825exp(-1175/RT)		
	BMA	0.075		
	General	0.6365exp(-1368.8/RT)		
C	Styrene	0.25		Rate of decrease of *f*
	BA	1		
	EA	1		
	General	0.685		

Table A-3: Kinetic Database for TBPA (tert-butyl peroxyacetate)

Parameter	Monomer	Value	Unit	Description
Mw	General	132.16	g/mol	Initiator molecular weight
k_d	Styrene	$4.068*10^{17}\exp(-3.52*10^4/RT)$	L/min	Decomposition rate constant
	BA	$4.068*10^{17}\exp(-3.52*10^4/RT)$		
	BMA	$4.068*10^{17}\exp(-3.52*10^4/RT)$		
	General	$1.67*10^{16}\exp(-3.29*10^4/RT)$		
f	Styrene	0.515		Initiator efficiency
	BMA	0.515		
	General	0.6		
V_{fi}	Styrene	0.015	V	Critical free volume for diffusion-control
	BMA	0.015		
	General	0.15		
C	General	1		Rate of decrease of *f*

Table A-4: Kinetic Database for TBPB (tert-butyl peroxybenzoate)

Parameter	Monomer	Value	Unit	Description
Mw	General	194.23	g/mol	Initiator molecular weight
k_d	General	$3.716*10^{16}\exp(-3.321*10^4/RT)$	L/min	Decomposition rate constant
f	Styrene	0.9		Initiator efficiency
	General	0.5		
V_{fi}	General	0.15	V	Critical free volume for diffusion-control
C	General	0.25		Rate of decrease of *f*

Table A-5: Kinetic Database for dTBPO (di-tert-butyl peroxide)

Parameter	Monomer	Value	Unit	Description
Mw	General	146.23	g/mol	Initiator molecular weight
k_d	MMA	$1.68*10^{16}\exp(-3.5*10^4/RT)$[1]	L/min	Decomposition rate constant
	General	$7.29*10^{16}\exp(-3.56*10^4/RT)$		
f	MMA	0.7		Initiator efficiency
	BA	0.3		
	General	0.5		
V_{fi}	General	0.15	V	Critical free volume for diffusion-control
C	General	0.25		Rate of decrease of *f*

[1]Nising and Meyer (2004)

Table A-6: Kinetic Database for the Fictitious Initiator

Parameter	Monomer	Value	Unit	Description
Mw	General	200	g/mol	Initiator molecular weight
k_d	General	$4*10^{16}\exp(-3*10^4/RT)$	L/min	Decomposition rate constant
f	Styrene	0.05exp(2000/RT)		Initiator efficiency
	MMA	0.02exp(2000/RT)		
	EA	0.7		
V_{fi}	Styrene	0.08	V	Critical free volume for diffusion-control
	MMA	0.15		
	EA	0.625exp(-1175/RT)		
C	Styrene	0.75		Rate of decrease of *f*
	General	1		

Appendix III. Monomer Database

The complete monomer database used in each of the simulations is shown below. The kinetic parameters that are unreferenced come from WATPOLY (Gao and Penlidis, 1997; 1998 and 2000). Again, these values are constant for each of the simulations shown in this thesis and in Jung (2008).

Note: $k_{td,ratio} = \frac{k_{td}}{k_t}$

Table A-7: Kinetic Database for Acrylic Acid

Parameter	Value	Unit	Description
Mw	72.06	g/mol	Molecular weight of the monomer
T_{gm}	189.65	K	Glass transition temp. of the monomer
T_{gp}	379	K	Glass transition temperature of the polymer
C_{pm}	502	cal/kg/K	Heat capacity of the monomer
C_{pp}	432.69	cal/kg/K	Heat capacity of the polymer
ΔH	$-1.85*10^4$	cal/mol	Heat of reaction
ρ_m	1.0776-0.001328(T-273.15)	kg/L	Density of the monomer
ρ_p	1.442	kg/L	Density of the polymer
k_p	$3.72*10^9\exp(-5600/RT)$	L/mol/min	Rate of propagation
k_t	$6*10^9$	L/mol/min	Rate of termination
$k_{td,ratio}$	0.2		Disproportionation to combination ratio
k_{fm}	$1.72*10^9\exp(-1.11*10^4/RT)$	L/mol/min	Transfer to monomer rate
k_{fp}	0	L/mol/min	Transfer to polymer rate
k_{pin}	0	L/mol/min	Internal double bond rate of propagation
k_{pte}	0	L/mol/min	Terminal double bond rate of propagation
Δ	0.001	L/g	Reaction radius for segmental diffusion
V_{fc}	3.0956exp(-1683.2/RT)	L	Critical free volume
V_{fm}	0.025	L	Free volume of the monomer
α_m	0.001	L/K	Thermal expansion coeff. of the monomer
V_{fp}	0.025	L	Free volume of the polymer
α_p	0.0048	L/K	Thermal expansion coeff. of the polymer
B	1		Rate of decrease of k_p
m	0.5		Gel-effect model parameter
n	1.75		Gel-effect model parameter
A	1.75		Rate of decrease of k_t
K_3	$5*10^6$		Onset pt. of translational diffusion-control
n_s	120		Avg. number of monomer units per chain
l_0	$6.2*10^{-8}$	cm	Length of monomer unit per chain
k_{th}	0	$L^2/mol^2/min$	Thermal (/self) initiation rate

Table A-8: Kinetic Database for Acrylonitrile

Parameter	Value	Unit	Description
Mw	53.06	g/mol	Molecular weight of the monomer
T_{gm}	190	K	Glass transition temp. of the monomer
T_{gp}	337.15	K	Glass transition temperature of the polymer
C_{pm}	430	cal/kg/K	Heat capacity of the monomer
C_{pp}	301	cal/kg/K	Heat capacity of the polymer
ΔH	$-1.781*10^4$	cal/mol	Heat of reaction
ρ_m	0.82754-0.0011(T-273.15)	kg/L	Density of the monomer
ρ_p	1.175-0.00131(T-273.15)	kg/L	Density of the polymer
k_p	$6*10^9 \exp(-7105.3/RT)$	L/mol/min	Rate of propagation
k_t	$2.5*10^{12} \exp(-3996/RT)$	L/mol/min	Rate of termination
$k_{td,ratio}$	0.08		Disproportionation to combination ratio
k_{fm}	$1.2*10^8 \exp(-1.033*10^4/RT)$	L/mol/min	Transfer to monomer rate
k_{fp}	0	L/mol/min	Transfer to polymer rate
k_{pin}	0	L/mol/min	Internal double bond rate of propagation
k_{pte}	0	L/mol/min	Terminal double bond rate of propagation
Δ	0.001	L/g	Reaction radius for segmental diffusion
V_{fc}	5.3277exp(-3059/RT)	L	Critical free volume
V_{fm}	0.025	L	Free volume of the monomer
α_m	0.001	L/K	Thermal expansion coeff. of the monomer
V_{fp}	0.025	L	Free volume of the polymer
α_p	0.0048	L/K	Thermal expansion coeff. of the polymer
B	0.5		Rate of decrease of k_p
m	0.5		Gel-effect model parameter
n	1.75		Gel-effect model parameter
A	0.95		Rate of decrease of k_t
K_3	0.8313exp(-7979.9/RT)		Onset pt. of translational diffusion-control
n_s	120		Avg. number of monomer units per chain
l_0	$6.2*10^{-8}$	cm	Length of monomer unit per chain
k_{th}	0	$L^2/mol^2/min$	Thermal (/self) initiation rate

Table A-9: Kinetic Database for Butyl Acrylate

Parameter	Value	Unit	Description
Mw	128.17	g/mol	Molecular weight of the monomer
T_{gm}	185.15	K	Glass transition temp. of the monomer
T_{gp}	218	K	Glass transition temperature of the polymer
C_{pm}	430	cal/kg/K	Heat capacity of the monomer
C_{pp}	400	cal/kg/K	Heat capacity of the polymer
ΔH	$-1.84*10^4$	cal/mol	Heat of reaction
ρ_m	0.919-0.001012(T-273.15)	kg/L	Density of the monomer
ρ_p	1.212-0.000845(T-273.15)	kg/L	Density of the polymer
k_p	$1.326*10^9\exp(-4278.1/RT)$[1]	L/mol/min	Rate of propagation
k_t	$8.04*10^{10}\exp(-1338.4/RT)$[1]	L/mol/min	Rate of termination
$k_{td,ratio}$	0.1		Disproportionation to combination ratio
k_{fm}	$9.3436*10^5\exp(-7475/RT)$	L/mol/min	Transfer to monomer rate
k_{fp}	0	L/mol/min	Transfer to polymer rate
k_{pin}	0	L/mol/min	Internal double bond rate of propagation
k_{pte}	0	L/mol/min	Terminal double bond rate of propagation
Δ	0.001	L/g	Reaction radius for segmental diffusion
V_{fc}	$0.01\exp(-1443.6/RT)$	L	Critical free volume
V_{fm}	0.025	L	Free volume of the monomer
α_m	0.001	L/K	Thermal expansion coeff. of the monomer
V_{fp}	0.025	L	Free volume of the polymer
α_p	0.0048	L/K	Thermal expansion coeff. of the polymer
B	0.5		Rate of decrease of k_p
m	0.5		Gel-effect model parameter
n	1.75		Gel-effect model parameter
A	1.31		Rate of decrease of k_t
K_3	$0.02\exp(-1.2109*10^4/RT)$		Onset pt. of translational diffusion-control
n_s	200		Avg. number of monomer units per chain
l_0	$6.54*10^{-8}$	cm	Length of monomer unit per chain
k_{th}	$4.96*10^4\exp(-17483/RT)$[1]	$L^2/mol^2/min$	Thermal (/self) initiation rate
k_p^{tert}	$3594\exp(-127.6/RT)$[2]	L/mol/min	Rate of propagation of tertiary radicals
$k_t^{tert\text{-}ert}$	$8.04*10^{10}\exp(-1338.4/RT)$[3]	L/mol/min	Rate of termination of tertiary radicals
$k_t^{sec\text{-}tert}$	$8.04*10^{10}\exp(-1338.4/RT)$[3]	L/mol/min	Termination of tertiary and secondary rad.
k_{bb}	$2.32*10^8\exp(-4568/RT)$[2]	/min	Rate of backbiting
k_β	$1.73*10^{19}\exp(-34860/RT)$[2]	/min	Rate of beta-scission
k_{fm}^{tert}	$1.2*10^7\exp(-1.10*10^4/RT)$[1]	L/mol/min	Transfer to monomer for tertiary radicals

[1]Nikitin *et al.* (2007) [2]Rantow *et al.* (2006) [3]Peck and Hutchinson (2004)

Table A-10: Kinetic Database for Butyl Methacrylate

Parameter	Value	Unit	Description
Mw	142.191	g/mol	Molecular weight of the monomer
T_{gm}	224.2	K	Glass transition temp. of the monomer
T_{gp}	293	K	Glass transition temperature of the polymer
C_{pm}	420	cal/kg/K	Heat capacity of the monomer
C_{pp}	401.914	cal/kg/K	Heat capacity of the polymer
ΔH	-18.373	cal/mol	Heat of reaction
ρ_m	0.911-0.000886(T-273.15)	kg/L	Density of the monomer
ρ_p	1.19-0.000807(T-273.15)	kg/L	Density of the polymer
k_p	$2.064*10^8\exp(-5574.2/RT)$	L/mol/min	Rate of propagation
k_t	$2.352*10^9\exp(-701/RT)$	L/mol/min	Rate of termination
$k_{td,ratio}$	0.65		Disproportionation to combination ratio
k_{fm}	$3.0795*10^5\exp(-8322.5/RT)$	L/mol/min	Transfer to monomer rate
k_{fp}	0	L/mol/min	Transfer to polymer rate
k_{pin}	0	L/mol/min	Internal double bond rate of propagation
k_{pte}	0	L/mol/min	Terminal double bond rate of propagation
Δ	0.001	L/g	Reaction radius for segmental diffusion
V_{fc}	0.06	L	Critical free volume
V_{fm}	0.025	L	Free volume of the monomer
α_m	0.001	L/K	Thermal expansion coeff. of the monomer
V_{fp}	0.025	L	Free volume of the polymer
α_p	0.0048	L/K	Thermal expansion coeff. of the polymer
B	1		Rate of decrease of k_p
m	0.5		Gel-effect model parameter
n	1.75		Gel-effect model parameter
A	1.02		Rate of decrease of k_t
K_3	$5.8*10^6$		Onset pt. of translational diffusion-control
n_s	126		Avg. number of monomer units per chain
l_0	$6.2*10^{-8}$	cm	Length of monomer unit per chain
k_{th}	0	$L^2/mol^2/min$	Thermal (/self) initiation rate

Table A-11: Kinetic Database for Ethyl Acrylate

Parameter	Value	Unit	Description
Mw	101.12	g/mol	Molecular weight of the monomer
T_{gm}	167.1	K	Glass transition temp. of the monomer
T_{gp}	249	K	Glass transition temperature of the polymer
C_{pm}	429.4	cal/kg/K	Heat capacity of the monomer
C_{pp}	437.5	cal/kg/K	Heat capacity of the polymer
ΔH	$-1.927*10^4$	cal/mol	Heat of reaction
ρ_m	0.949-0.00128(T-273.15)	kg/L	Density of the monomer
ρ_p	1.11	kg/L	Density of the polymer
k_p	$3*10^{10}\exp(-8002.9/RT)$	L/mol/min	Rate of propagation
k_t	$1.046*10^{10}\exp(-2950.4/RT)$	L/mol/min	Rate of termination
$k_{td,ratio}$	$191.6\exp(-3817.75/RT)$		Disproportionation to combination ratio
k_{fm}	$1.487*10^{12}\exp(-17543/RT)$	L/mol/min	Transfer to monomer rate
k_{fp}	0	L/mol/min	Transfer to polymer rate
k_{pin}	0	L/mol/min	Internal double bond rate of propagation
k_{pte}	0	L/mol/min	Terminal double bond rate of propagation
Δ	0.001	L/g	Reaction radius for segmental diffusion
V_{fc}	$0.2865\exp(-984.94/RT)$	L	Critical free volume
V_{fm}	0.025	L	Free volume of the monomer
α_m	0.001	L/K	Thermal expansion coeff. of the monomer
V_{fp}	0.025	L	Free volume of the polymer
α_p	0.0048	L/K	Thermal expansion coeff. of the polymer
B	1		Rate of decrease of k_p
m	0.5		Gel-effect model parameter
n	1.75		Gel-effect model parameter
A	1.552		Rate of decrease of k_t
K_3	$43.68\exp(-7921.83/RT)$		Onset pt. of translational diffusion-control
n_s	100		Avg. number of monomer units per chain
l_0	$5.8*10^{-8}$	cm	Length of monomer unit per chain
k_{th}	0	$L^2/mol^2/min$	Thermal (/self) initiation rate

Table A-12: Kinetic Database for Glycidyl Methacrylate

Parameter	Value	Unit	Description
Mw	142.16	g/mol	Molecular weight of the monomer
T_{gm}	185.15	K	Glass transition temp. of the monomer
T_{gp}	347	K	Glass transition temperature of the polymer
C_{pm}	429.397	cal/kg/K	Heat capacity of the monomer
C_{pp}	437.5	cal/kg/K	Heat capacity of the polymer
ΔH	-13.74	cal/mol	Heat of reaction
ρ_m	1.09-0.00104(T-273.15)	kg/L	Density of the monomer
ρ_p	$1.13-7.07*10^{-4}$(T-273.15)	kg/L	Density of the polymer
k_p	$3.0455*10^{8}\exp(-5473/RT)$[1]	L/mol/min	Rate of propagation
k_t	$6.6*10^{10}\exp(-2465.87/RT)^2$	L/mol/min	Rate of termination
$k_{td,ratio}$	0.65		Disproportionation to combination ratio
k_{fm}	$9360\exp(-5207.9/RT)^2$	L/mol/min	Transfer to monomer rate
k_{fp}	0	L/mol/min	Transfer to polymer rate
k_{pin}	0	L/mol/min	Internal double bond rate of propagation
k_{pte}	0	L/mol/min	Terminal double bond rate of propagation
Δ	0.001	L/g	Reaction radius for segmental diffusion
V_{fc}	0.07	L	Critical free volume
V_{fm}	0.025	L	Free volume of the monomer
α_m	0.001	L/K	Thermal expansion coeff. of the monomer
V_{fp}	0.025	L	Free volume of the polymer
α_p	0.0048	L/K	Thermal expansion coeff. of the polymer
B	1		Rate of decrease of k_p
m	0.5		Gel-effect model parameter
n	1.75		Gel-effect model parameter
A	1.02		Rate of decrease of k_t
K_3	$5.8*10^{6}$		Onset pt. of translational diffusion-control
n_s	126		Avg. number of monomer units per chain
l_0	$6.2*10^{-8}$	cm	Length of monomer unit per chain
k_{th}	0	$L^2/mol^2/min$	Thermal (/self) initiation rate

[1]Wang and Hutchinson (2008b) [2]Wang (2010)

Table A-13: Kinetic Database for Hydroxyethyl Acrylate

Parameter	Value	Unit	Description
Mw	116.12	g/mol	Molecular weight of the monomer
T_{gm}	185.15	K	Glass transition temp. of the monomer
T_{gp}	258	K	Glass transition temperature of the polymer
C_{pm}	429.397	cal/kg/K	Heat capacity of the monomer
C_{pp}	437.5	cal/kg/K	Heat capacity of the polymer
ΔH	$-1.84*10^4$	cal/mol	Heat of reaction
ρ_m	1.011-0.001012(T-273.15)	kg/L	Density of the monomer
ρ_p	1.041-0.000845(T-273.15)	kg/L	Density of the polymer
k_p	$6.487*10^8 \exp(-6706.2/RT)$[1]	L/mol/min	Rate of propagation
k_t	$2.63*10^{11} \exp(-6639.5/RT)$[1]	L/mol/min	Rate of termination
$k_{td,ratio}$	$191.61 \exp(-3817.8/RT)$		Disproportionation to combination ratio
k_{fm}	$9.3436*10^5 \exp(-7475.1/RT)$	L/mol/min	Transfer to monomer rate
k_{fp}	0	L/mol/min	Transfer to polymer rate
k_{pin}	0	L/mol/min	Internal double bond rate of propagation
k_{pte}	0	L/mol/min	Terminal double bond rate of propagation
Δ	0.001	L/g	Reaction radius for segmental diffusion
V_{fc}	$\exp(-2100/RT)$[1]	L	Critical free volume
V_{fm}	0.0275	L	Free volume of the monomer
α_m	0.0011	L/K	Thermal expansion coeff. of the monomer
V_{fp}	0.0275	L	Free volume of the polymer
α_p	0.000528	L/K	Thermal expansion coeff. of the polymer
B	1		Rate of decrease of k_p
m	0.5		Gel-effect model parameter
n	1.75		Gel-effect model parameter
A	3.5		Rate of decrease of k_t
K_3	$4*10^{-5} \exp(-1.447*10^4/RT)$[1]		Onset pt. of translational diffusion-control
n_s	126		Avg. number of monomer units per chain
l_0	$6.2*10^{-8}$	cm	Length of monomer unit per chain
k_{th}	0	$L^2/mol^2/min$	Thermal (/self) initiation rate

[1]Refined through sensitivity analysis based on the work by Kim (1994)

Table A-14: Kinetic Database for Hydroxyethyl Methacrylate

Parameter	Value	Unit	Description
Mw	130.14	g/mol	Molecular weight of the monomer
T_{gm}	185.15	K	Glass transition temp. of the monomer
T_{gp}	381.15	K	Glass transition temperature of the polymer
C_{pm}	429.397	cal/kg/K	Heat capacity of the monomer
C_{pp}	437.5	cal/kg/K	Heat capacity of the polymer
ΔH	$-1.84*10^4$	cal/mol	Heat of reaction
ρ_m	1.092-0.00098(T-273.15)[1]	kg/L	Density of the monomer
ρ_p	1.041-0.000845(T-273.15)	kg/L	Density of the polymer
k_p	$4.325*10^8\exp(-6706.2/RT)$	L/mol/min	Rate of propagation
k_t	$2.631*10^{11}\exp(-6639.5/RT)$	L/mol/min	Rate of termination
$k_{td,ratio}$	$191.61\exp(-3817.8/RT)$		Disproportionation to combination ratio
k_{fm}	$9.3436*10^5\exp(-7475.1/RT)$	L/mol/min	Transfer to monomer rate
k_{fp}	1500	L/mol/min	Transfer to polymer rate
k_{pin}	0	L/mol/min	Internal double bond rate of propagation
k_{pte}	0	L/mol/min	Terminal double bond rate of propagation
Δ	0.001	L/g	Reaction radius for segmental diffusion
V_{fc}	$\exp(-2100/RT)$	L	Critical free volume
V_{fm}	0.0275	L	Free volume of the monomer
α_m	0.0011	L/K	Thermal expansion coeff. of the monomer
V_{fp}	0.0275	L	Free volume of the polymer
α_p	0.000528	L/K	Thermal expansion coeff. of the polymer
B	1		Rate of decrease of k_p
m	0.5		Gel-effect model parameter
n	1.75		Gel-effect model parameter
A	3.5		Rate of decrease of k_t
K_3	$4*10^{-5}\exp(-1.447*10^4/RT)$		Onset pt. of translational diffusion-control
n_s	126		Avg. number of monomer units per chain
l_0	$6.2*10^{-8}$	cm	Length of monomer unit per chain
k_{th}	0	$L^2/mol^2/min$	Thermal (/self) initiation rate

[1]Buback *et al.* (1998)

Table A-15: Kinetic Database for Methacrylic Acid

Parameter	Value	Unit	Description
Mw	86.1	g/mol	Molecular weight of the monomer
T_{gm}	188.532	K	Glass transition temp. of the monomer
T_{gp}	501	K	Glass transition temperature of the polymer
C_{pm}	502.39	cal/kg/K	Heat capacity of the monomer
C_{pp}	432.69	cal/kg/K	Heat capacity of the polymer
ΔH	$-1.352*10^4$	cal/mol	Heat of reaction
ρ_m	1.019-0.0004(T-273.15)	kg/L	Density of the monomer
ρ_p	1.014-0.00078(T-273.15)	kg/L	Density of the polymer
k_p	$4.4979*10^8 exp(-4379.3/RT)$	L/mol/min	Rate of propagation
k_t	$2.78*10^9 exp(-430.57/RT)$	L/mol/min	Rate of termination
$k_{td,ratio}$	0.3		Disproportionation to combination ratio
k_{fm}	$1.717*10^9 exp(-11117/RT)$	L/mol/min	Transfer to monomer rate
k_{fp}	0	L/mol/min	Transfer to polymer rate
k_{pin}	0	L/mol/min	Internal double bond rate of propagation
k_{pte}	0	L/mol/min	Terminal double bond rate of propagation
Δ	0.001	L/g	Reaction radius for segmental diffusion
V_{fc}	3.095exp(-1683.2/RT)	L	Critical free volume
V_{fm}	0.025	L	Free volume of the monomer
α_m	0.001	L/K	Thermal expansion coeff. of the monomer
V_{fp}	0.025	L	Free volume of the polymer
α_p	0.00048	L/K	Thermal expansion coeff. of the polymer
B	1		Rate of decrease of k_p
m	0.5		Gel-effect model parameter
n	1.75		Gel-effect model parameter
A	1.65		Rate of decrease of k_t
K_3	$5*10^6$		Onset pt. of translational diffusion-control
n_s	126		Avg. number of monomer units per chain
l_0	$6.2*10^{-8}$	cm	Length of monomer unit per chain
k_{th}	$4.5*10^6 exp(-2.745*10^4/RT)$	$L^2/mol^2/min$	Thermal (/self) initiation rate

Table A-16: Kinetic Database for Methyl Methacrylate

Parameter	Value	Unit	Description
Mw	100.12	g/mol	Molecular weight of the monomer
T_{gm}	167.1	K	Glass transition temp. of the monomer
T_{gp}	378	K	Glass transition temperature of the polymer
C_{pm}	411.1	cal/kg/K	Heat capacity of the monomer
C_{pp}	400	cal/kg/K	Heat capacity of the polymer
ΔH	$-1.381*10^4$	cal/mol	Heat of reaction
ρ_m	0.9665-0.001164(T-273.15)	kg/L	Density of the monomer
ρ_p	1.195-0.00033(T-273.15)	kg/L	Density of the polymer
k_p	$2.952*10^7 \exp(-4353/RT)$	L/mol/min	Rate of propagation
k_t	$5.88*10^9 \exp(-701/RT)$	L/mol/min	Rate of termination
$k_{td,ratio}$	$1.6093\exp(-440.12/RT)$		Disproportionation to combination ratio
k_{fm}	$9.3435*10^4 \exp(-7475/RT)$	L/mol/min	Transfer to monomer rate
k_{fp}	0	L/mol/min	Transfer to polymer rate
k_{pin}	0	L/mol/min	Internal double bond rate of propagation
k_{pte}	0	L/mol/min	Terminal double bond rate of propagation
Δ	0.001	L/g	Reaction radius for segmental diffusion
V_{fc}	$0.7408\exp(-1589.6/RT)$	L	Critical free volume
V_{fm}	0.025	L	Free volume of the monomer
α_m	0.001	L/K	Thermal expansion coeff. of the monomer
V_{fp}	0.025	L	Free volume of the polymer
α_p	0.00048	L/K	Thermal expansion coeff. of the polymer
B	1		Rate of decrease of k_p
m	0.5		Gel-effect model parameter
n	1.75		Gel-effect model parameter
A	1.11		Rate of decrease of k_t
K_3	$0.563\exp(-8900/RT)$		Onset pt. of translational diffusion-control
n_s	47		Avg. number of monomer units per chain
l_0	$6.9*10^{-8}$	cm	Length of monomer unit per chain
k_{th}	$2.26*10^{-6} \exp(-6578/RT)$	$L^2/mol^2/min$	Thermal (/self) initiation rate

Table A-17: Kinetic Database for α-methyl Styrene

Parameter	Value	Unit	Description
Mw	118.18	g/mol	Molecular weight of the monomer
T_{gm}	150.15	K	Glass transition temp. of the monomer
T_{gp}	449.15	K	Glass transition temperature of the polymer
C_{pm}	400	cal/kg/K	Heat capacity of the monomer
C_{pp}	400	cal/kg/K	Heat capacity of the polymer
ΔH	$-1.7*10^4$	cal/mol	Heat of reaction
ρ_m	0.875-0.000918(T-273.15)	kg/L	Density of the monomer
ρ_p	1.15-0.000918(T-273.15)	kg/L	Density of the polymer
k_p	$3.54*10^8\exp(-8870/RT)$[1]	L/mol/min	Rate of propagation
k_t	$1.38*10^{10}\exp(-2100/RT)$[1]	L/mol/min	Rate of termination
$k_{td,ratio}$	0.07		Disproportionation to combination ratio
k_{fm}	$3.3615*10^9\exp(-15177/RT)$	L/mol/min	Transfer to monomer rate
k_{fp}	0	L/mol/min	Transfer to polymer rate
k_{pin}	0	L/mol/min	Internal double bond rate of propagation
k_{pte}	0	L/mol/min	Terminal double bond rate of propagation
Δ	0.0001	L/g	Reaction radius for segmental diffusion
V_{fc}	1.2exp(-2220/RT)	L	Critical free volume
V_{fm}	0.025	L	Free volume of the monomer
α_m	0.001	L/K	Thermal expansion coeff. of the monomer
V_{fp}	0.025	L	Free volume of the polymer
α_p	0.00048	L/K	Thermal expansion coeff. of the polymer
B	0.5		Rate of decrease of k_p
m	0.5		Gel-effect model parameter
n	1.75		Gel-effect model parameter
A	0.55		Rate of decrease of k_t
K_3	10^{10}		Onset pt. of translational diffusion-control
n_s	120		Avg. number of monomer units per chain
l_0	$5*10^{-8}$	cm	Length of monomer unit per chain
k_{th}	0	$L^2/mol^2/min$	Thermal (/self) initiation rate

[1] Carlsson *et al.* (1966)

Table A-18: Kinetic Database for Styrene

Parameter	Value	Unit	Description
Mw	104.12	g/mol	Molecular weight of the monomer
T_{gm}	185	K	Glass transition temp. of the monomer
T_{gp}	378	K	Glass transition temperature of the polymer
C_{pm}	430	cal/kg/K	Heat capacity of the monomer
C_{pp}	400	cal/kg/K	Heat capacity of the polymer
ΔH	$-1.7*10^4$	cal/mol	Heat of reaction
ρ_m	0.924-0.000918(T-273.15)	kg/L	Density of the monomer
ρ_p	1.084-0.000605(T-273.15)	kg/L	Density of the polymer
k_p	$1.302*10^9 exp(-7759.2/RT)$ [1]	L/mol/min	Rate of propagation
k_t	$4.92*10^{11} exp(-3471.3/RT)$ [1]	L/mol/min	Rate of termination
$k_{td,ratio}$	0.01		Disproportionation to combination ratio
k_{fm}	$1.386*10^8 exp(-12670/RT)^2$	L/mol/min	Transfer to monomer rate
k_{fp}	0	L/mol/min	Transfer to polymer rate
k_{pin}	0	L/mol/min	Internal double bond rate of propagation
k_{pte}	0	L/mol/min	Terminal double bond rate of propagation
Δ	0.001	L/g	Reaction radius for segmental diffusion
V_{fc}	0.31105exp(-1671.8/RT)	L	Critical free volume
V_{fm}	0.025	L	Free volume of the monomer
α_m	0.001	L/K	Thermal expansion coeff. of the monomer
V_{fp}	0.025	L	Free volume of the polymer
α_p	0.00048	L/K	Thermal expansion coeff. of the polymer
B	1		Rate of decrease of k_p
m	0.5		Gel-effect model parameter
n	1.75		Gel-effect model parameter
A	0.348		Rate of decrease of k_t
K_3	$9.44exp(-3832.9/RT)^3$ [3]		Onset pt. of translational diffusion-control
n_s	173		Avg. number of monomer units per chain
l_0	$7.4*10^{-8}$	cm	Length of monomer unit per chain
k_{th}	$1.35*10^7 exp(-27450/RT)^2$ [2]	$L^2/mol^2/min$	Thermal (/self) initiation rate

[1]Mahabadi and O'Driscoll (1978)

[2]Hui and Hamielec (1972)

[3]Marten and Hamielec (1982)

Table A-19: Kinetic Database for Vinyl Acetate

Parameter	Value	Unit	Description
Mw	86.09	g/mol	Molecular weight of the monomer
T_{gm}	109.15	K	Glass transition temp. of the monomer
T_{gp}	303	K	Glass transition temperature of the polymer
C_{pm}	471.6	cal/kg/K	Heat capacity of the monomer
C_{pp}	318.1	cal/kg/K	Heat capacity of the polymer
ΔH	$-2.0895*10^{4}$	cal/mol	Heat of reaction
ρ_m	0.9574-0.00127(T-273.15)	kg/L	Density of the monomer
ρ_p	1.2145-0.000875(T-273.15)	kg/L	Density of the polymer
k_p	$7.8*10^{10}\exp(-8403.5/RT)$	L/mol/min	Rate of propagation
k_t	$9.84*10^{11}\exp(-3401.4/RT)$	L/mol/min	Rate of termination
$k_{td,ratio}$	0		Disproportionation to combination ratio
k_{fm}	$1.117*10^{7}\exp(-9895/RT)$	L/mol/min	Transfer to monomer rate
k_{fp}	$4.255*10^{6}\exp(-8947/RT)$	L/mol/min	Transfer to polymer rate
k_{pin}	0	L/mol/min	Internal double bond rate of propagation
k_{pte}	$2.7289*10^{7}\exp(-5509.9/RT)$	L/mol/min	Terminal double bond rate of propagation
Δ	0.0001	L/g	Reaction radius for segmental diffusion
V_{fc}	0.06	L	Critical free volume
V_{fm}	0.025	L	Free volume of the monomer
α_m	0.001	L/K	Thermal expansion coeff. of the monomer
V_{fp}	0.025	L	Free volume of the polymer
α_p	0.00048	L/K	Thermal expansion coeff. of the polymer
B	1		Rate of decrease of k_p
m	0.5		Gel-effect model parameter
n	1.75		Gel-effect model parameter
A	0.8		Rate of decrease of k_t
K_3	3.1866exp(-7065.6/RT)		Onset pt. of translational diffusion-control
n_s	100		Avg. number of monomer units per chain
l_0	$7.5*10^{-8}$	cm	Length of monomer unit per chain
k_{th}	$2*10^{-10}$	$L^2/mol^2/min$	Thermal (/self) initiation rate

Appendix IV. Chain Transfer Agent and Solvent Databases

The remaining databases can be found here with all the kinetic parameters coming from WATPOLY (Gao and Penlidis, 1997; 1998 and 2000).

Table A-20: Kinetic Database for Xylene

Parameter	Monomer	Value	Unit	Description
Mw	General	106.16	g/mol	Molecular weight of the solvent
T_g	General	187.4	K	Glass transition temperature
C_p	General	420	cal/kg/K	Heat capacity
ρ_s	General	0.868	kg/L	Density of the solvent
k_{fs}	Styrene	$0.0001*k_{pSty}$	L/mol/min	Chain transfer to solvent
	BA	$17.6exp(-3870/T)*k_{pBA}$		
	BMA	$5.55exp(-4590/T)*k_{pBMA}$		
	General	$1.373*10^5exp(-4353/RT)$		
V_{fs}	General	0.025	L	Free volume of solvent
α_s	General	0.001	L/K	Thermal expansion coefficient

Table A-21: Kinetic Database for Toluene

Parameter	Monomer	Value	Unit	Description
Mw	General	92.14	g/mol	Molecular weight of the solvent
T_g	General	113	K	Glass transition temperature
C_p	General	404.8	cal/kg/K	Heat capacity
ρ_s	General	$0.883-9.16*10^{-4}(T-273.15)$	kg/L	Density of the solvent
k_{fs}	General	$1.237*10^7exp(-1.14*10^4/RT)$	L/mol/min	Chain transfer to solvent
V_{fs}	General	0.025	L	Free volume of solvent
α_s	General	0.001	L/K	Thermal expansion coefficient

Table A-22: Kinetic Database for Benzene

Parameter	Monomer	Value	Unit	Description
Mw	General	78.12	g/mol	Molecular weight of the solvent
T_g	General	171	K	Glass transition temperature
C_p	General	414.7	cal/kg/K	Heat capacity
ρ_s	General	0.876	kg/L	Density of the solvent
k_{fs}	Styrene	$1.237*10^7\exp(-1.14*10^4/RT)$	L/mol/min	Chain transfer to solvent
	BMA	$3261\exp(-5574/RT)$		
	General	$1.373*10^5\exp(-4353/RT)$		
V_{fs}	General	0.025	L	Free volume of solvent
α_s	General	0.001	L/K	Thermal expansion coefficient

Table A-23: Kinetic Database for Ethyl Acetate

Parameter	Monomer	Value	Unit	Description
Mw	General	88.12	g/mol	Molecular weight of the solvent
T_g	General	181	K	Glass transition temperature
C_p	General	460.7	cal/kg/K	Heat capacity
ρ_s	General	0.928-0.00138*(T-273.15)	kg/L	Density of the solvent
k_{fs}	BA	$3.93*10^{16}\exp(-2.4*10^4/RT)$	L/mol/min	Chain transfer to solvent
	General	$1.373*10^5\exp(-4353/RT)$		
V_{fs}	General	0.025	L	Free volume of solvent
α_s	Styrene	0.00081	L/K	Thermal expansion coefficient
	General	0.001		

Table A-24: Kinetic Database for Carbon Tetra-chloride

Parameter	Monomer	Value	Unit	Description
Mw	General	153.82	g/mol	Molecular weight of the CTA
k_{fCTA}	Styrene	$1.736*10^7\exp(-7759/RT)$	L/mol/min	Chain transfer to CTA
	AA	$7085\exp(-4353/RT)$		
	General	1*105		

Table A-25: Kinetic Database for Octanethiol

Parameter	Monomer	Value	Unit	Description
Mw	General	146.3	g/mol	Molecular weight of the CTA
k_{fCTA}	EA	$3*10^{11}exp(-7128/RT)$	L/mol/min	Chain transfer to CTA
	General	$7.124*10^{10}exp(-7128/RT)$		

Table A-26: Kinetic Database for Dodecanethiol

Parameter	Monomer	Value	Unit	Description
Mw	General	202.2	g/mol	Molecular weight of the CTA
k_{fCTA}	EA	$1.167*10^{10}exp(-7759/RT)$	L/mol/min	Chain transfer to CTA
	General	$2.718*10^{12}exp(-1.3*10^{4}/RT)$		

Appendix V. Alternative Solution for Composition Control Policy 2

The following solution might be equivalent to the solution presented in section 6 for policy 2. Due to time constraints, it has not been verified.

$$N_1 = N_{1_0}\exp(At) \tag{A.3.}$$

$$N_2 = N_{2_0}\exp(At) \tag{A.4.}$$

$$\boldsymbol{F_{1,in} = (A + \Phi_1)N_{1_0}\exp(At)} \tag{A.5.}$$

$$\boldsymbol{F_{2,in} = (A + \Phi_2)N_{2_0}\exp(At)} \tag{A.6.}$$

$$V = V_0\exp(At) \tag{A.7.}$$

$$A = \frac{f_{1_0}\Phi_1[R^*] + f_{2_0}\Phi_2[R^*]}{\frac{V_0\rho}{MW(N_{1_0} + N_{2_0})} - 1} \tag{A.8.}$$

where $V_0\rho$ is the initial mass of the 'heel' (monomers, solvent and polymer).

Again, the molecular weights and densities of the monomers are assumed equal. Also, continuing from equation 6.80 (under the modified policy 2 section):

$$F_{I,in} = [I]_0\frac{dV}{dt} + k_d[I]_0V \tag{6.80.}$$

$$= [I]_0\frac{dV}{dt} + k_d\left(\frac{N_{I_0}}{V_0}\right)V \tag{A.9.}$$

$$= [I]_0\frac{dV}{dt} + k_d\left(\frac{N_{I_0}}{V_0}\right)V_0\exp(At) \tag{A.10.}$$

Therefore,

$$\boldsymbol{F_{I,in} = [I]_0\frac{dV}{dt} + k_dN_{I_0}\exp(At)} \tag{A.11.}$$

These solutions simplify the originals found in section 6. Investigation into how accurate they are could be quite beneficial.

Appendix VI. User Manual Excerpt and Overall Summary

The user manual deals with the following topics:

Model Features and Output Profiles
Model Structure
Instructions on How to Run the Simulator
Simulation Example
and
Troubleshooting Typical Errors

An excerpt from 'Instructions on How to Run the Simulator' is shown below:

Before running the model, make sure to do the following:

- Set current directory where the function files are located, usually Source Code Dorschner.

- Activate the monomer/ingredient species participating in polymerization.

Example: Sty (m_1)/BA (m_2) bulk co-polymerization with AIBN (no CTA and inhibitor)

1. Open the overall database file (parameters.m).
2. Activate and assign the monomer kinetic database files, such as Stydata.m and BAdata.m, to m_1 and m_2, respectively. Any monomer files can be assigned to m_3 to m_6; these do not affect the calculations as the amounts are zero. In order to comment out one monomer and comment in another, use control - t and control – r, respectively.
3. Activate and assign the initiator kinetic database file (AIBNdata.m, in this case) and deactivate the others.
4. Open AIBNdata.m (in this case) and match the initiator kinetic parameters, k_{d1}, k_{d2}, etc. in the file with m_1 and m_2. Again, the parameters for m_3 through m_6 have no effect. You can ignore those parameters.

5. The co-polymer parameters in parameters.m, such as reactivity ratios r_{12} and r_{21}, cross-termination rate constant k_{t12}, and glass transition temperature T_{gp12}, should also be chosen to match m_1 and m_2.
6. Activate solvent/CTA/inhibitor database files, if present in the recipe, completing steps 3 and 4 for each additive present.

- For semi-batch simulations, the monomer and ingredient flow profiles (moles/min. vs. time) should be prepared in the corresponding flowprogram file. If the file is unknown, it can be found directly after the parameter load section in the main executable file. (Approximately line 58 in hexapolymerization_semibatch.m). Note: the feed end time must match the reaction time plus one. In the above example, the index counter in the flowprogram file should run from 1 to 2501.

- For temperature programming, a temperature profile (°C vs. time) should be prepared and assigned in the main file. First, the temprogram file must be commented out and then set appropriately. This can generally be found directly before the first iteration of the for loop, approximately at line 810 in hexapolymerization.m. Remember to set the index to one plus the final reaction time. Also, after the numerical calculation portion of the code, the parameters must be loaded again at the new temperature. This means commenting out the 'if temperature programming is available' portion within the for loop (~line 1050 in hexapolymerization.m).

- Finally, choose/activate 'plot' source codes for output profiles of interest. This can be done at the end of the main executable file by commenting out the desired figures.